



Structural and Biophysical Insights into T Cell
Receptor Recognition of Lengthy Antigens
Presented by Major Histocompatibility Complex
Class I Molecules

by

Yu-Chih Liu

Bachelor of Biomedical Science (Hons)

Protein Crystallography Unit
Department of Biochemistry and Molecular Biology
Faculty of Medicine, Nursing and Health Sciences
Monash University

Submitted to fulfil the requirements for the degree of

Doctor of Philosophy

Copyright Notices

Notice 1

Under the Copyright Act 1968, this thesis must be used only under the normal conditions of scholarly fair dealing. In particular no results or conclusions should be extracted from it, nor should it be copied or closely paraphrased in whole or in part without the written consent of the author. Proper written acknowledgement should be made for any assistance obtained from this thesis.

Notice 2

I certify that I have made all reasonable efforts to secure copyright permissions for third-party content included in this thesis and have not knowingly added copyright content to my work without the owner's permission.

Table of Contents

Acknowledgements.....	17
Abbreviations.....	18
1 Chapter 1 Introduction	19
1.1 Major Histocompatibility Complex molecules.....	21
1.1.1 Roles of MHC-Ia polymorphism in cellular immunity	23
1.1.2 Antigen processing and presentation by the MHC-I molecules.....	24
1.1.3 Crystal structures of MHC-I molecules and the antigen-binding cleft.....	27
1.1.4 Peptide-binding pockets and MHC-Ia supertypes	29
1.2 The $\alpha\beta$ T Cell Receptor (TCR).....	32
1.2.1 Genetic diversity of $\alpha\beta$ T cell receptors	32
1.2.2 T cell development: The thymic selection.....	35
1.2.3 The structure of $\alpha\beta$ T cell receptor	36
1.3 Rules of TCR-pMHC engagement	38
1.3.1 The binding kinetics of TCR-pMHC-I complexes	41
1.3.2 Early insights from the murine TCR-pMHC-I complexes: TCR recognition of disparate peptide ligands	43
1.3.3 TCR recognition of altered ligand: Insights from the Human Leukocyte Antigen (HLA)-A*2 system.....	48
1.3.4 Impact of buried MHC polymorphism on TCR recognition	53
1.3.5 Structural evidence of inherent TCR-MHC interactions.....	57
1.3.6 Structural basis of TCR bias.....	61
1.3.7 Structural insights into T cell allorecognition and self-tolerance.....	64
1.4 Conformational changes upon TCR-pMHC-I ligation	70
1.5 TCR recognition of lengthy antigens presented by MHC molecules	71
1.5.1 Structure of lengthy antigen bound to MHC class I molecule	72
1.5.2 Structural mechanism and insights into lengthy peptide-MHC recognition by the TCR	74
1.6 Research leading up to this project.....	79
1.6.1 Structural and biophysical investigations into TCR recognition towards a super- bulged pHLA molecule	79
1.6.2 The role of antigen flexibility in TCR cross-recognition	80
1.6.3 Research Project Aims	82
2 Materials and Methods.....	83
2.1 Molecular cloning of expression vectors	83

2.2	Production and purification of the HLA-B*35 molecules	84
2.3	Production and purification of recombinant TCRs	85
2.4	Production, biotinylation and tetramerization of pHLA-B*35:08	86
2.5	Thermal stability experiments	86
2.6	Surface Plasmon Resonance	87
2.7	Crystallisation and data collection	87
2.8	Structural determination and refinement	88
2.9	Structural analysis.....	88
3	Results: The energetic basis of TCR recognition towards a bulged viral antigen bound to a HLA molecule.....	90
4	Results: Divergent T cell receptor recognition modes towards a bulged epitope presented by a HLA molecule	105
5	Results: A molecular basis for the interplay between T cells, viral mutants and HLA micropolymorphism.....	129
6	Discussion	151
6.1	TCR recognition towards lengthy antigen	152
6.2	The energetic basis of biased TCR repertoire.....	154
6.3	TCR binding strategies towards super-bulged pMHC landscapes	155
6.4	TCR recognition of altered pHLA landscape	159
6.4.1	TCR recognition of polymorphic HLA landscapes	160
6.4.2	Impacts of altered peptide ligand (APL) presentation.....	161
6.4.3	TCR recognition of APL	162
6.4.4	Insights into TCR allorecognition	163
6.5	Insights into the paradigm of MHC restriction	165
6.6	Future directions	167
6.7	Conclusions.....	169
7	References.....	171

Publication Arising From This Thesis

Chapter	Publication title	Journal	Year	Page number
3	The energetic basis of TCR recognition towards a bulged viral antigen bound to human leukocyte antigen	Journal of Biological Chemistry	2012	90-104
4	Divergent T cell receptor recognition modes towards a bulged epitope presented by a human leukocyte antigen	Journal of Biological Chemistry	2013	105-128
5	A molecular basis for the interplay between T cells, viral mutants and human leukocyte antigen micropolymorphism	Journal of Biological Chemistry	2014	129-150

List of Figures

Figure 1 The immunological synapse.	20
Figure 2 A schematic of the antigen-processing pathway.	26
Figure 3 Crystal Structures of MHC- class I and class II molecules	28
Figure 4 Antigen-binding pockets of the MHC-class I molecule.	30
Figure 5 Structural overview of the $\alpha\beta$ T cell receptor.	33
Figure 6 Somatic recombination of the $\alpha\beta$ T cell receptor.	34
Figure 7 Crystal structure of the 2C T cell receptor.	37
Figure 8 The two-step binding model.	41
Figure 9 The 2C TCR recognises disparate ligands via the flexible CDR3 α loop.	45
Figure 10 Binding specificity and degeneracy of the BM3.3 TCR.	47
Figure 11 The cross-reactivity of the A6 TCR is depicted with different mechanisms.	50
Figure 12 TCR recognition of altered peptide ligand.	52
Figure 13 The binding of TCRs towards polymorphic MHC-I molecules.	55
Figure 14 TCR recognition of buried polymorphism in the HLA-B*57 system.	57
Figure 15 Structural insights into MHC-restricted recognition.	60
Figure 16 Structural basis of immunodominant TCR recognition.	63
Figure 17 Alternative binding and molecular mimicry modes of TCR allorecognition.	66
Figure 18 Divergent TCR docking footprints towards a viral HLA-B*8-FLR target.	69
Figure 19 Lengthy epitopes presented by MHC molecules.	73
Figure 20 Diagonal docking orientation of the SB27 TCR towards the HLA-B*35:08- LPEP.	75
Figure 21 TCR recognition modes towards lengthy antigens presented by MHC-I molecules.	76

List of Tables

Table 1 Polymorphisms within HLA-Class I molecules.	22
Table 2 HLA class Ia supertypes and their binding specificity at the B and F pockets.	31
Table 3 Summary of unique TCR-pMHC-I complexes determined until the end 2014	40
Table 4 Crystal structures of lengthy antigens bound to MHC-I molecules.....	72
Table 5 T cell receptor repertoires arising from HLA-B*35:08+ individuals restricted to the LPEP antigen.	79

Abstract

Cytotoxic T cells represent an important line of defence in the vertebrate immune system to combat against intracellular abnormality such as viral and bacterial infections, as well as cellular transformation. In order to perform these functions effectively, cytotoxic T cells express $\alpha\beta$ T cell receptors ($\alpha\beta$ TCRs) on their cell surface, which allow them to specifically engage and differentiate self, altered self and foreign antigens on the surface of targeted cells. Intriguingly, such recognition is genetically restricted to antigen presentation by the host Major Histocompatibility Complex class I (MHC-I) molecules, which typically bind to short peptide fragments between 8 to 10 amino acids in length. Longer antigens on the other hand, have also been shown to represent potential targets for cytotoxic T cells, although it is not fully understood how TCRs can accommodate these peptide-MHC-I landscapes. Contrasting TCR specificity, TCRs also simultaneously exhibit remarkable ability to cross-react onto different targets. This binding degeneracy forms an essential part of the protective immunity, and allows TCRs to effectively recognise a diverse range of antigens that is presented to the host. Understanding the dual specificity of TCR (specificity versus degeneracy) is important, as it not only plays central roles in protective immunity but also contributes to clinical manifestation such as graft rejection and graft-versus-host diseases during organ transplantation.

Using X-ray crystallography and Surface Plasmon Resonance (SPR) approaches as main techniques, my thesis set out to explore the underlying basis of simultaneous TCR specificity and cross-reactivity in the context of lengthy antigens (>10 amino acids) derived from a ubiquitous human pathogen, Epstein-Barr Virus (EBV). These antigens, when bound to closely related Human Leukocyte Antigen (HLA, MHC in human) molecules, HLA-B*35:08 and HLA-B*35:01, exhibit a range of non-canonical structural features, either bulging away from the antigen-binding platform or displaying marked conformational mobility. The structures presented in this thesis demonstrated that, in response to a super-bulged and rigid peptide antigen, two distinct TCR binding mechanisms could be employed. Namely, via the use of differing gene usages, TCRs can either engage and focus structurally and energetically onto the bulged antigen or, opt to bypass such a prominent feature by adopting an extreme docking orientation. These differences in the structural footprints

in turn, allow TCRs to “see” or “ignore” subtle variations on the MHC landscape, and subsequently determine whether the TCR is MHC-restricted or cross-reactive. In addition to these findings, I also investigated the mechanism utilized by a TCR to accommodate lengthy and mobile antigen. Here, TCR recognition occurred via induced-fit of the antigen itself, which allows the optimal co-recognition of peptide and HLA landscapes to be achieved. Subtle sequence variations, such as HLA polymorphism or viral variants for instance, can modulate the shape and dynamic of the MHC bound antigen, which indirectly fine-tune TCR recognition and the subsequent biological responses.

Taken together, these discoveries have not only provided novel kinetic and structural insights into lengthy detection by cytotoxic T cells, but also contributed towards our current understanding into the multifaceted nature of T-cell mediated cellular immune responses.

General Declaration

In accordance with Monash University Doctorate Regulation 17 Doctor of Philosophy and Research Master's regulations the following declarations are made:

I hereby declare that this thesis contains no material which has been accepted for the award of any other degree or diploma at any university or equivalent institution and that, to the best of my knowledge and belief, this thesis contains no material previously published or written by another person, except where due reference is made in the text of the thesis.

This thesis includes two original papers published in peer reviewed journals and one unpublished publications. The core theme of the thesis is the structural and biophysical insights into T cell receptor recognition of lengthy antigens presented by MHC class I molecules. The ideas, development and writing up of all the papers in the thesis were the principal responsibility of myself, the candidate, working within the department of Biochemistry and Molecular Biology, Monash University under the supervision of Professor Jamie Rossjohn and Dr. Stephanie Gras.

The inclusion of co-authors reflects the fact that the work came from active collaboration between researchers and acknowledges input into team-based research.

In the case of chapters three, four and five my contribution to the work involved the following:

Thesis chapter	Publication title	Publication status	Nature and extent of candidate's contribution
3	The energetic basis of TCR recognition towards a bulged viral antigen bound to human leukocyte antigen	Published in 2012	Cloning, expression, refolding purification and crystallisation of recombinant proteins. Mutagenesis of TCR and HLA variants. Structural data collection, processing, solution and refinements. SPR and thermal stability experiments for the paper. Tetramer staining and cellular experiments. Data analysis, presentation and manuscript preparation.
4	Divergent T cell receptor recognition modes towards a bulged epitope presented by a human leukocyte antigen	Published in 2013	Cloning, expression, refolding purification and crystallisation of the SB47 and CA5 ternary complexes. Structural data collection, processing, solution and refinements. Performed SPR experiment between the TCRs and HLA variants. Data analysis, presentation and manuscript preparation.
5	A molecular basis for the interplay between T cells, viral mutants and human leukocyte antigen micropolyorphism	Published in 2014	Expression, refolding, purification and crystallisation of pHLA-I variants and the TK3 TCR. Thermal stability experiment on pHLA variants. Structural data collection, processing,

			solution and refinements. Conducted SPR experiment between the TCRs and HLA variants. Data analysis, presentation and manuscript preparation.
--	--	--	---

I have / have not (circle that which applies) renumbered sections of submitted or published papers in order to generate a consistent presentation within the thesis.

Signed:

Date:

Declaration for Thesis Chapter Three

Declaration by candidate

In the case of Chapter Three, the nature and extent of my contribution to the work was the following:

Nature of contribution	Extent of contribution (%)
Cloning, expression, refolding purification and crystallisation of recombinant proteins. Mutagenesis on TCR and HLA constructs. Preparation of pHLA tetramers and cellular assays. Structural data collection, processing, solution and refinements. SPR and thermal stability experiments for the paper. Data analysis, presentation and manuscript preparation.	50%

The following co-authors contributed to the work. Co-authors who are students at Monash University must also indicate the extent of their contribution in percentage terms:

Name	Nature of contribution	Extent of contribution (%) for student co-authors only
Zhenjun Chen	Cell culture, FACs experiment and data interpretation (Tetramer staining).	N/A
Scott R. Burrows	Conception, direction, data interpretation and manuscript preparation.	N/A
Anthony W. Purcell	Conception, direction, data interpretation and manuscript Conception.	N/A
James McCluskey	Conception, direction, data interpretation and manuscript preparation.	N/A
Jamie Rossjohn	Supervision, conception, direction, data interpretation and manuscript preparation.	N/A
Stephanie Gras	Supervision, conception, direction, data interpretation and manuscript preparation.	N/A

Candidate's Signature

	Date
--	-------------

Declaration by co-authors

The undersigned hereby certify that:

- (1) the above declaration correctly reflects the nature and extent of the candidate's contribution to this work, and the nature of the contribution of each of the co-authors.
- (2) they meet the criteria for authorship in that they have participated in the conception, execution, or interpretation, of at least that part of the publication in their field of expertise;
- (3) they take public responsibility for their part of the publication, except for the responsible author who accepts overall responsibility for the publication;
- (4) there are no other authors of the publication according to these criteria;
- (5) potential conflicts of interest have been disclosed to (a) granting bodies, (b) the editor or publisher of journals or other publications, and (c) the head of the responsible academic unit; and

(6) the original data are stored at the following location(s) and will be held for at least five years from the date indicated below:

Location(s)

Department of Biochemistry and Molecular Biology, Monash University, Clayton 3800, Australia.
Departments of Microbiology & Immunology and Biochemistry and Molecular Biology and Bio21 Molecular Science and Biotechnology Institute, University of Melbourne, Parkville 3010, Australia.
Queensland Institute of Medical Research and Australian Centre for Vaccine Development, Brisbane 4006, Australia.

[Please note that the location(s) must be institutional in nature, and should be indicated here as a department, centre or institute, with specific campus identification where relevant.]

Zhenjun Chen

Scott R. Burrows

Anthony W. Purcell

James McCluskey

Jamie Rossjohn

Stephanie Gras

		Date 26.9.14
		26.9.14
		26/9/14
		10/11/2014
		1/10/2014
		26/9/14

Declaration for Thesis Chapter Four

Declaration by candidate

In the case of Chapter Four, the nature and extent of my contribution to the work was the following:

Nature of contribution	Extent of contribution (%)
Cloning, expression, refolding purification and crystallisation of the SB47 and CA5 ternary complexes. Structural data collection, processing, solution and refinements. SPR experiment between the TCRs and HLA variants. Data analysis, presentation and manuscript preparation.	50%

The following co-authors contributed to the work. Co-authors who are students at Monash University must also indicate the extent of their contribution in percentage terms:

Name	Nature of contribution	Extent of contribution (%) for student co-authors only
John J. Miles	Cellular experiment, data interpretation and manuscript preparation.	N/A
Michelle A. Neller	Cellular experiment, data interpretation and manuscript preparation.	N/A
Emma Gostick	Cellular experiment, data interpretation and manuscript preparation.	N/A
David A. Price	Cellular experiment, data interpretation and manuscript preparation.	N/A
Anthony W. Purcell	Conception, data interpretation and manuscript preparation.	N/A
James McCluskey	Conception, direction, data interpretation and manuscript preparation.	N/A
Scott R. Burrows	Supervision, conception, direction, data interpretation and manuscript preparation.	N/A
Jamie Rossjohn	Supervision, conception, direction, data interpretation and manuscript preparation.	N/A
Stephanie Gras	Supervision, conception, direction, data collection, interpretation and manuscript preparation.	N/A

Candidate's Signature

	Date
--	-------------

Declaration by co-authors

The undersigned hereby certify that:

- (7) the above declaration correctly reflects the nature and extent of the candidate's contribution to this work, and the nature of the contribution of each of the co-authors.
- (8) they meet the criteria for authorship in that they have participated in the conception, execution, or interpretation, of at least that part of the publication in their field of expertise;

- (9) they take public responsibility for their part of the publication, except for the responsible author who accepts overall responsibility for the publication;
- (10) there are no other authors of the publication according to these criteria;
- (11) potential conflicts of interest have been disclosed to (a) granting bodies, (b) the editor or publisher of journals or other publications, and (c) the head of the responsible academic unit; and
- (12) the original data are stored at the following location(s) and will be held for at least five years from the date indicated below:

Location(s)

Department of Biochemistry and Molecular Biology, School of Biomedical Sciences, Monash University, Clayton, 3800, Australia.
 Queensland Institute of Medical Research and Australian Centre for Vaccine Development, Brisbane, 4006, Australia.
 Institute of Infection and Immunity, Cardiff University School of Medicine, Heath Park, Cardiff CF14 4XN, Wales, UK.
 Human Immunology Section, Vaccine Research Center, National Institute of Allergy and Infectious Diseases, National Institutes of Health, Bethesda, MD 20892, USA.
 Department of Microbiology and Immunology, University of Melbourne, Parkville, 3010.

[Please note that the location(s) must be institutional in nature, and should be indicated here as a department, centre or institute, with specific campus identification where relevant.]

John J. Miles

Michelle A. Neller

Emma Gostick

David A. Price

Anthony W. Purcell

James McCluskey

Scott R. Burrows

Jamie Rossjohn

Stephanie Gras

	Date 26/10/14
	26.09.14
	1/10/14
	28 SEP 14
	26/9/14
	10/11/2014
	26.9.14
	1/10/2014
	26/9/14

Declaration for Thesis Chapter Five

Declaration by candidate

In the case of Chapter Five, the nature and extent of my contribution to the work was the following:

Nature of contribution	Extent of contribution (%)
Cloning, expression, refolding, purification and crystallisation of TK3 TCR and pHLA-I complexes. Thermal stability assay for pHLA variants. Structural data collection, processing, solution and refinements. SPR experiment and kinetic analysis. Data analysis, presentation and manuscript preparation.	50%

The following co-authors contributed to the work. Co-authors who are students at Monash University must also indicate the extent of their contribution in percentage terms:

Name	Nature of contribution	Extent of contribution (%) for student co-authors only
ZhenJun Chen	Cellular experiment, data interpretation and manuscript preparation.	N/A
Michelle A. Neller	Cellular experiment, data interpretation and manuscript preparation.	N/A
John J. Miles	Cellular experiment, data interpretation and manuscript preparation.	N/A
Anthony W. Purcell	Conception, direction, data interpretation and manuscript preparation.	N/A
James McCluskey	Conception, direction, data interpretation and manuscript preparation.	N/A
Scott R. Burrows	Supervision, conception, direction, data interpretation and manuscript preparation.	N/A
Jamie Rossjohn	Supervision, conception, direction, data interpretation and manuscript preparation.	N/A
Stephanie Gras	Supervision, conception, direction, data interpretation and manuscript preparation.	N/A

Candidate's
Signature

	Date
--	-------------

Declaration by co-authors

The undersigned hereby certify that:

- (13) the above declaration correctly reflects the nature and extent of the candidate's contribution to this work, and the nature of the contribution of each of the co-authors.
- (14) they meet the criteria for authorship in that they have participated in the conception, execution, or interpretation, of at least that part of the publication in their field of expertise;
- (15) they take public responsibility for their part of the publication, except for the responsible author who accepts overall responsibility for the publication;

- (16) there are no other authors of the publication according to these criteria;
- (17) potential conflicts of interest have been disclosed to (a) granting bodies, (b) the editor or publisher of journals or other publications, and (c) the head of the responsible academic unit; and
- (18) the original data are stored at the following location(s) and will be held for at least five years from the date indicated below:

Location(s)	Department of Biochemistry and Molecular Biology, School of Biomedical Sciences, Monash University, Clayton, 3800, Australia. Queensland Institute of Medical Research and Australian Centre for Vaccine Development, Brisbane, 4006, Australia. Institute of Infection and Immunity, Cardiff University School of Medicine, Heath Park, Cardiff CF14 4XN, Wales, UK. Department of Microbiology and Immunology, University of Melbourne, Parkville, 3010.
--------------------	---

[Please note that the location(s) must be institutional in nature, and should be indicated here as a department, centre or institute, with specific campus identification where relevant.]

ZhenJun Chen	[REDACTED]	Date 26.09.14
Michelle A. Neller	[REDACTED]	26.09.14
John J. Miles	[REDACTED]	15/10/14
Anthony W. Purcell	[REDACTED]	26/9/14
James McCluskey	[REDACTED]	10/11/2014
Scott R. Burrows	[REDACTED]	26.9.14
Jamie Rossjohn	[REDACTED]	1/10/2014
Stephanie Gras	[REDACTED]	26/9/14

Acknowledgements

The success of my doctoral thesis would not be possible without the help and kindness of many people around me. Above all, I would firstly like to thank Professor Jamie Rossjohn for providing me with an opportunity to study and work in his laboratory. Professor Rossjohn is a strong mentor who has constantly offered me professional insights, not only in relation to project directions but also towards the development of analytic skills, which forms an integral part of my PhD progression. Secondly, I would like to express my gratitude to my co-supervisor, Dr. Stephanie Gras, who has been extremely helpful in terms of laboratory skills and scientific knowledge, particularly with her expertise in crystallography and SPR techniques. Furthermore, I would also like to acknowledge both my supervisors (Jamie and Stephanie), for their generosity in supporting me financially to attend various conferences and training programs throughout my candidature. In addition, thanks also extended to all Rossjohn lab members, who have helped me and provided support along this journey. This thesis also involved strong collaborations with local, interstate and international members from the University of Melbourne, University of Queensland, as well as Cardiff University. As such, I would like to take this opportunity and acknowledge their hard work and contributions to various projects associated with my doctoral degree. Particularly, I would like to thank Professor Jim McCluskey for giving me with an opportunity to expand my skill sets towards functional and cellular studies under the guidance of Dr. Zhenjun Chen.

Outside of the laboratory, I would like to thank my friend Kylie, Jason, Adrian, Ray, and Wun for organizing various activities during weekends and holidays when they are needed the most. I also want to express my gratitude towards Larry and Jun, who often joined me during lunchtime to have a short break from work. Last but not least, I thank my family for their understanding and support towards my education, as well as my partner Sze Nee, who has always been there for me throughout stressful, frustrating and emotional moments. Finally, whilst it has been difficult to express my appreciation in words, I hope what I have achieved would make all of you proud and your efforts worthwhile.

Abbreviations

Altered peptide ligand	APL
Antigen Presenting Cell	APC
β -2 Microglobulin	β_2m
Complementarity-Determining Region	CDR
Cytotoxic T Lymphocyte	CTL
Endoplasmic Reticulum	ER
Epstein-Barr virus	EBV
<i>Escherichia coli</i>	<i>E.coli</i>
Histocompatibility 2 antigen	H2
Histocompatibility-2	H-2
Human cytomegalovirus	HCMV
Human Immunodeficiency Virus	HIV
Human Leukocyte Antigen	HLA
Human Leukocyte antigen class I	HLA-I
Hydrogen Bond	H-Bond
Immunoglobulin	Ig
kDa	kilodalton
Major Histocompatibility Complex	MHC
Mb	Megabase
MHC class Ia molecules	MHC-Ia
MHC class Ib molecules	MHC-Ib
MHC class II molecules	MHC-II
Nature Killer	NK
Peptide	p
Peptide Loading Complex	PLC
Peptide of 11 residues in length	11mer
Peptide of 13 residues in length	13mer
Peptide-Major Histocompatibility Complex class I	pMHC-I
Peptide-Human Leukocyte Antigen Complex class I	pHLA-I
Protein Data Bank	PDB
Surface Plasmon Resonance	SPR
$\alpha\beta$ T cell receptor	$\alpha\beta$ TCR
TCR α -chain	TRA
TCR β -chain	TRB
Transport Associated with Antigen Processing	TAP
Van der Waals	VDW

1 Chapter 1 Introduction

The humoral and cellular immune responses are the two main lines of adaptive immunity in vertebrate to combat against foreign pathogens. Cytotoxic T cells in particular, belong to the cellular arm of immunity and play a pivotal role in eliminating virally infected cells and cancerous cells. As an important step for cytotoxic T cell-mediated responses, antigens are required to be presented by a self-derived molecule known as the Major Histocompatibility Complex (MHC) molecule (Davis and Bjorkman, 1988; Rosenthal and Shevach, 1973; Zinkernagel and Doherty, 1974). The targeted antigen-MHC complexes are then recognised by T cell receptors (TCRs) express on the surface of T cells. In this context, intracellular proteins, including self, altered self, and foreign, are constantly degraded into short peptide fragments via the proteasome machinery, allowing the cellular content to be sampled. These peptide (p) antigens are subsequently translocated and loaded onto the MHC molecules in the endoplasmic reticulum (ER) before peptide-MHC (pMHC) complexes migrate to the cell surface for immuno-surveillance by T cells. Interestingly, T cell receptors themselves do not contain any signalling domains, and therefore the recruitment of other co-receptors including CD4/CD8 and CD3 are crucial for the downstream signalling outcome post TCR-pMHC engagement. These receptors work connectively in a micro-environment termed the immunological synapse (**Figure 1**) (Grakoui et al., 1999; Monks et al., 1998), and only with the appropriate formation of this synapse, the effector function of the T cells can then be initiated to trigger cytokine secretion, targeted cell lysis as well as T-cell proliferation (Appay and Rowland-Jones, 2004).

Despite the complexity of the T-cell mediated immunity, effectively it is the formation of productive TCR-pMHC complex that initiates this whole process. Understanding the fundamental basis of TCR-pMHC specificity is hence an area of intense interest. Via the use of X-ray crystallography technique, many structural studies have been carried out to investigate the specific atomic details underpinning TCR-pMHC interactions. However, the exact mechanism how TCRs engage their target pMHCs remains elusive, as the mode of TCR recognition often varies significantly between the various systems investigated. This structural "inconsistency" is attributed partly to differences between the specific TCR sequences, the nature of

MHC subtypes and polymorphisms, as well as the particular ligands examined. Thus, how TCRs exhibit simultaneous specificity to distinguish self from foreign pMHCs while maintaining inherent cross-reactivity to cope with the vast number of potential foreign antigens is not fully understood.

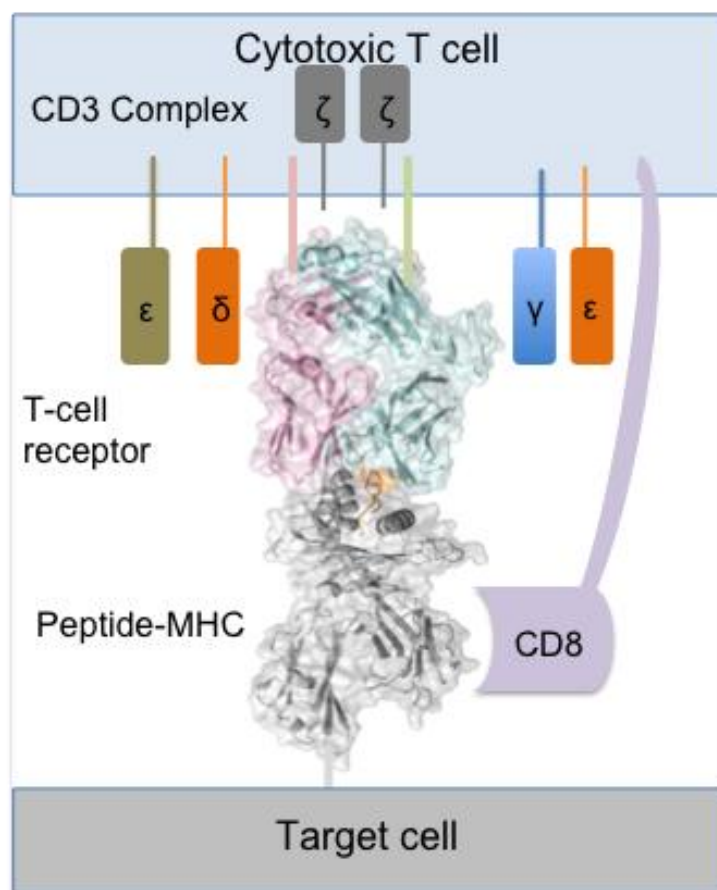


Figure 1 The immunological synapse.

The specific binding event between the T-cell receptor (α in pink and β in blue) and the peptide-MHC complex is essential for the activation of T cells and its effector function. This interaction is stabilized by co-receptors such as the CD8 (light purple) and CD3 complexes that are required to initiate the signaling cascade. Figure adapted from Clements and colleagues (Clements et al., 2006) (PDB used: 2AK4).

The main focus of my research project is to examine how T cells, via their TCRs, engage antigens of non-canonical length (>10 amino acids) compared to the typical length of 8-10 amino acids for MHC-I restricted antigen presentation. These antigens, when presented by polymorphic class I MHC molecules, protrude away from the antigen-binding platform, and in some cases, exhibit variable degree of antigen mobility. It is unclear however, how TCRs can overcome such structurally distinct landscapes while maintaining simultaneous specificity and cross-reactivity. I

presented here, the structural and biophysical examinations of different lengthy antigens recognised by their cognate TCRs, and the impact of MHC micropolymorphism on TCR-pMHC-I interactions. To introduce my research topic, this following section summarises our current knowledge on MHC-I molecules, TCRs and insights arising from the interaction between these two components.

1.1 Major Histocompatibility Complex molecules

Major Histocompatibility Complex (MHC) molecules in humans are also known as human leukocyte antigen (HLA) molecules as they were discovered originally from the surface of human white blood cells. These molecules are encoded from a collection of genes, spanning more than 3.5M base pairs on chromosome 6 at 6p21.3 in humans (Beck and Trowsdale, 2000; Mungall et al., 2003). Among the genes that encode MHC molecules, they are broadly classified into two main categories with distinctive immunological roles. These include the MHC class I (MHC-I) and MHC class II (MHC-II) molecules.

MHC-I molecules are expressed ubiquitously in all nucleated cells in the body, and they can be further subdivided into the “classical” MHC-Ia and the “non-classical” MHC-Ib families. These MHC-I molecules comprise a 45k Dalton (kDa) heavy chain that is non-covalently associated with a soluble, 12kDa β 2-microglobulin (β 2m) subunit, derived independently on chromosome 15 of the human genome (Strominger et al., 1976; York and Rock, 1996). In general, MHC-Ia molecules function to present peptide antigens for recognition by the CD8+ T cells and thus, are central for the control of intracellular abnormality such as microbial infection or cellular transformation. MHC-Ia molecules also play a role in natural killer cell biology, which is achieved via their recognition by the killer cell immunoglobulin-like receptors (KIRs) expressed on the surface of natural killer cells (Archbold et al., 2006; Borbulevych et al., 2007; Gunther et al., 2010). In humans, MHC-Ia proteins arise from three highly polymorphic regions of the genome, including HLA-A, HLA-B and HLA-C (**Table 1**). In the murine system, MHC-Ia proteins are encoded from the H-2 (Histocompatibility-2) genes, consisting of H-2K, H-2D and H-2L derived from chromosome 17. Depending on the specific cell types, MHC-Ia molecules are expressed in high abundance, and can display than 200,000 copies on the cell surface (Parham and Ohta, 1996). Notably, the expression of different MHC-Ia molecules is

co-dominant, and therefore in the case of heterozygosity, a total number of six different MHC-Ia molecules in an individual would be available for antigen presentation.

In contrast to the highly polymorphic nature of MHC-Ia, MHC-Ib molecules only display limited genetic diversity (**Table 1**). MHC-Ib molecules comprise the HLA-E, HLA-F and HLA-G in humans, and H-2M3 and Qa1^b in mice. Due to the limited diversity, MHC-Ib proteins have relatively restricted antigen presentation capability, and some MHC-Ib proteins also exhibit limited tissue distribution (such as liver, skin and placenta). The role of MHC-Ib molecules is important in both innate and adaptive immune responses. For example, HLA-G has been shown to associate with maternal tolerance of the fetus (Brodsky et al., 1979b; Parham et al., 1979a) as well as regulating natural killer cell activity (Munz et al., 1997; Strominger et al., 1979), whilst HLA-E molecules has been demonstrated to present microbial antigens to stimulate cytotoxic T cells (Parham et al., 1979b; Rodgers and Cook, 2005; Sullivan et al., 2006).

Table 1 Polymorphisms within HLA-Class I molecules.

Figures abstracted from IMGT/HLA database (Robinson et al., 2013).

Gene	<i>HLA-Class Ia</i>			<i>HLA-Class Ib</i>		
	A	B	C	E	F	G
Alleles	2,188	2,862	1,746	11	22	50
Protein	1,571	2,156	1,252	3	4	16
Null	107	95	45	0	0	2

The MHC genes also encode MHC-II molecules, which are heterodimers formed by a 34kDa α chain and a 29kDa β chain that are non-covalently linked. These components derived from the HLA-DR, HLA-DP, HLA-DQ genes in humans, as well as H-2A and H-2E in mice. Unlike the class I family, MHC-II molecules are expressed only on specialized antigen presenting cells (APC) such as B cells, macrophages and dendritic cells (Watts, 1997). They are also capable of presenting longer peptide antigens than the MHC-I molecules (Engelhard, 1994). The primary function of MHC-II is to present extracellular peptides via the exogenous pathway for CD4⁺ (helper) T cells recognition, which ultimately leads to the production of antibody and cytokines secretion.

Pertinent to my research topic are the MHC-class Ia molecules and their recognition by cytotoxic T cells and thus, only MHC class Ia molecules will be discussed further.

1.1.1 Roles of MHC-Ia polymorphism in cellular immunity

Given that the function of MHC class Ia molecules is to present diverse peptide repertoire for T cell immuno-surveillance, it is therefore not surprising that MHC-Ia molecules are extremely polymorphic, comprising more than 6,000 alleles identified to date (Robinson et al., 2013). MHC polymorphisms may vary as little as single amino acid (termed micropolymorphism) or as many as more than 30 amino acid differences between MHC alleles. In fact, polymorphisms in MHC-Ia play a vital role in protective immunity, and the “heterozygous advantage theory” has been previously proposed (Doherty and Zinkernagel, 1975), which is supported by disease resistances that are associated with specific MHC allotypes. For instance, individuals expressing HLA-B*27 and HLA-B*57 are known to display a slower disease progression during the course of human immunodeficiency virus (HIV) infection (Goulder et al., 1997; Hendel et al., 1999; Kaslow et al., 1996; Magierowska et al., 1999). Similarly, HLA-B*53 also represents a protective allele in western Africa against cerebral malaria infection (Hill et al., 1992).

In contrast to the enormous diversity of the HLA and its protective roles in humans, the total number of HLA genes carried by a given individual remains relatively small. Indeed, whilst HLA polymorphisms can confer survival advantages as described previously, they are also associated with disease susceptibility. For example, HLA-A genes are linked to the Alzheimer’s disease (HLA-A*2) and IgA deficiency (HLA-A*1) (Ambrus et al., 1977; Ballerini et al., 1999; Combarros et al., 1998; Mohammadi et al., 2010; Payami et al., 1997), whilst HLA-B gene, such as HLA-B*27, is associated with susceptibility towards the Ankylosing spondylitis and acute anterior uveitis (Breur-Vriesendorp et al., 1987; Fernandez-Sueiro et al., 2004; Gouveia et al., 2012). In addition, specific HLA molecules are also known to cause various adverse drug reactions (Lancet et al., 1979). For instance, the drug-induced hypersensitivity in Human Immunodeficiency virus type I (HIV-I) patients treated with abacavir, is uniquely associated with HLA-B*57:01, but not the closely related HLA-B*57:02, HLA-B*57:03 or HLA-B*58:01, which differed from HLA-B*57:01 by only two or three amino acids (Brodsky et al., 1979a). The underlying mechanism of abacavir-

mediated drug hypersensitivity has been recently reported. In this study, it was found that small molecules such as abacavir can bind to MHC molecule (HLA-B*5701) and indirectly modify the repertoire of the bound self antigens. As a result, the drug-modified self peptide-HLA repertoire is recognised by the immune cells as "foreign", and manifest clinically in abacavir hypersensitivity syndrome (Illing et al., 2012; Lawrence and Colman, 1993). This study not only provides novel insights into drug-mediated hypersensitivity, but also highlights the role of HLA polymorphisms in contributing towards this process (more examples of HLA polymorphism and its impact on T cell recognition are discussed later). Last but not least, excessive HLA allotypes carried by individuals would also ultimately alter the fine-balance of T cell maturation step during development in the thymus (discussed later) and drastically reduce the availability of periphery T cells for immuno-surveillance. As such, a high degree of HLA polymorphisms is maintained to increase the survivability on a population level, whereas individuals only carry a small subset of HLA alleles to retain sufficient immuno-surveillance.

1.1.2 Antigen processing and presentation by the MHC-I molecules

In order for MHC-I molecules to function, peptide antigens must be processed and loaded within the cells prior to their recognition by T-cells on the cell surface. This is a complex process involving a number of chaperones and a multi-subunit machinery, called the peptide-loading complex (PLC) in the Endoplasmic Reticulum (ER) (Blum et al., 2013; Cresswell et al., 2005). Firstly, intracellular proteins, including self and foreign, are polyubiquitinated and targeted for degradation via the proteasome into fragments typically between 5 to 20 amino acids long (**Figure 2**) (Stevanovic, 2005). Most of these peptides are rapidly eliminated by the cytosolic peptidase while a small fraction is able to escape from this process and be transported into the ER via the transporter associated with antigen processing (TAP) for antigen presentation.

The TAP-dependent peptide translocation has a general preference of transporting peptide antigens with 9-11 amino acids in length. This is in contrast to antigens containing a proline at position 2 (P2) in their primary sequences, which are less effectively transported via TAP (Androlewicz and Cresswell, 1996; Momburg et al., 1994). Once the antigens are within the ER, longer antigens expressing an extended N-terminal precursor sequence are further trimmed by the ER aminopeptidase to yield

small antigenic fragments typically between 8-10 amino acids for loading onto the MHC-I (Saric et al., 2002; Serwold et al., 2002). Although this mechanism was once thought to represent a “molecular ruler” governing the optimal peptide lengths for MHC-I loading (Wenzel et al., 1994), it is now clear that longer antigens can also be transported and loaded onto MHC-I (Burrows et al., 2006).

The formation of empty MHC-I on the other hand, begins with newly synthesized MHC-I heavy chains that being retained in the ER by a transmembrane chaperone known as calnexin (**Figure 2**) (Diedrich et al., 2001). This interaction initiates the folding procedure, and allows the β_2m light chain to be recruited to the MHC-I heavy chain for stability. Upon the association of MHC-I heavy chain and β_2m , calnexin is displaced, and the mono-glycosylated N-linked glycan on the MHC-I heavy chain allows the empty MHC-I- β_2m complex to be further stabilised by a soluble chaperone called calreticulin (Wearsch et al., 2011). This empty form of the MHC-I is further incorporated into a larger assembly, the peptide loading complex (PLC), consisting of the ERp57, tapasin and TAP, before the peptide is loaded. Upon loading of the peptide onto MHC-I, the whole pMHC-I complex can then migrate to the cell surface via the secretory pathway for T cell recognition.

It is known that tapasin's prior association with TAP functions to facilitate the transportation and loading of antigens onto MHC-I molecules (Zarling et al., 2003). In fact, the association of TAP and tapasin is crucial for effective peptide loading for a number of MHC-I alleles such as HLA-B*27:09 (Peh et al., 1998) and HLA-B*44:02 (Williams et al., 2002). This is further supported by the marked reduction of pMHC surface expression observed in tapasin-deficient cells compared to tapasin-positive cells (Garbi et al., 2000; Grandea et al., 2000; Howarth et al., 2004; Sadasivan et al., 1996; Williams et al., 2002), although it is also known that some MHC-I molecules including HLA-B*27:05, HLA-B*1510 and HLA-B*44:05, are capable of presenting antigens in the absence of tapasin (Peh et al., 1998). More recently, the role of tapasin has been further explored as the structure of tapasin bound to ERp57 became available. In the tapasin-ERp57 structure solved by Dong *et al*, tapasin formed a heterodimer with ERp57 by interacting with its two catalytic domains (Dong et al., 2009). This heterodimer is considered to play important roles not only to promote PLC assembly, but also to stabilize the empty MHC-I molecules for peptide loading

(Wearsch and Cresswell, 2007). In addition, the authors also proposed that a conserved patch on tapasin might act to stabilize the empty MHC-I molecules by interacting with the MHC-I α 2-helix. As such, the interaction between empty MHC-I and tapasin-ERp57 dimer were hypothesized to play crucial role in maintaining the MHC-I molecule in its peptide-receptive conformation (Dong et al., 2009). This study represents a major steppingstone towards the molecular basis of PLC functions and peptide loading of MHC-I molecules.

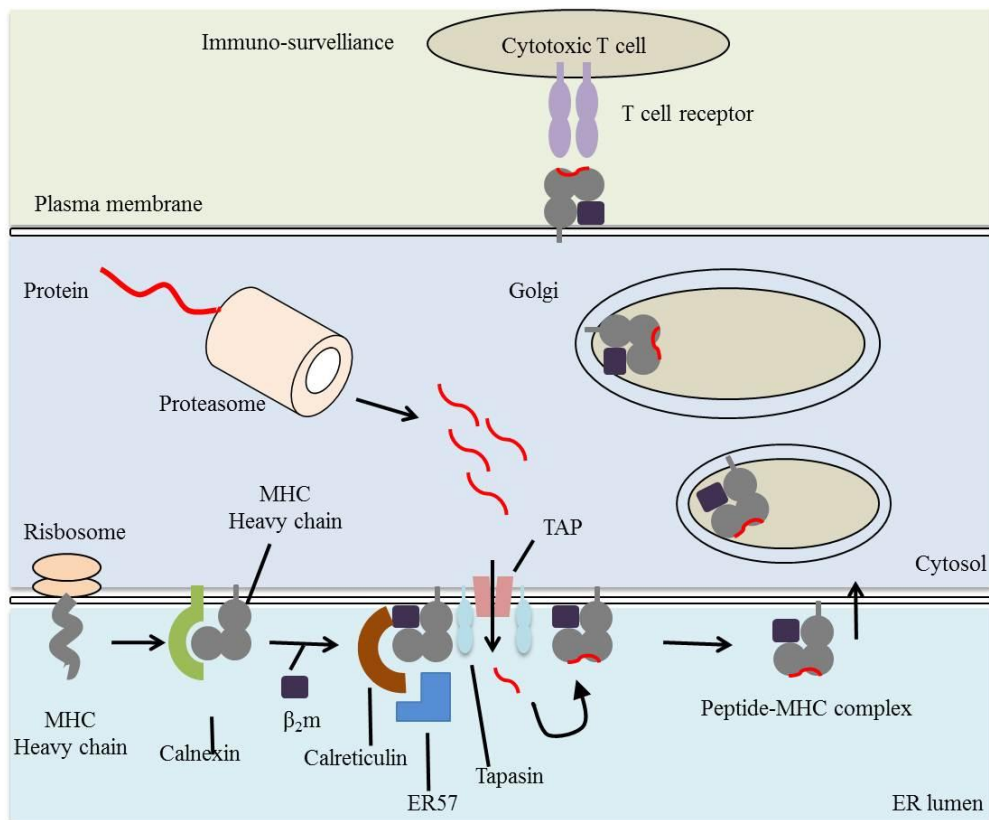


Figure 2 A schematic of the antigen-processing pathway.

The loading of peptides onto the MHC-I molecules involves in the formation of a large protein assembly known as the peptide loading complex (PLC) in the ER lumen. Peptide antigens that derived from cytosolic degradation of proteins are transported into the ER lumen via TAP before being loaded on to MHC molecules. The peptide-MHC complexes are then secreted to the cell surface for T cell surveillance. Figure adapted from Cresswell and colleagues (Cresswell et al., 2005).

1.1.3 Crystal structures of MHC-I molecules and the antigen-binding cleft

The first crystal structure of the MHC class I molecule was determined by Bjorkman *et al* in 1987 to a resolution of 3.5 Å (Bjorkman et al., 1987a, b; Bjorkman et al., 1985). In order to solve this structure, the hydrophilic portion of HLA-A*2 was extracted via papain digestion from the surface of lymphoblastoid cells, as this extracellular portion formed a stable structure independent of the membrane region. Despite the resolution limit, clear electron density was observed, covering residue 1-271 of the HLA-A*2 heavy chain as well as the β_2m subunit. Notably, three distinct domains were observed within the HLA-A*2 heavy chain, including the $\alpha 1$ (residue 1-92), $\alpha 2$ (93-182) and $\alpha 3$ (183-271) domains. The $\alpha 3$ domain, alongside with the β_2m subunit, were found to pack closely and both adopted typical immunoglobulin (Ig) – like folds (**Figure 3a**). Perhaps most importantly, the structure of the HLA-A*02:01 also unmasked a specialized architecture formed by the $\alpha 1$ - and $\alpha 2$ -helices where peptide antigens were bound (Bjorkman et al., 1987a). The Antigen (Ag)-binding cleft was approximately 25 Å long and 10 Å wide, formed by the $\alpha 1$ - and $\alpha 2$ -helices that sat above an eight-stranded anti-parallel β sheet platform (**Figures 3b** and **3c**). This Ag-binding cleft was further stabilized by its association with the $\alpha 3$ domain as well as the β_2m subunit. Importantly, the size of this groove is constrained due to the tight closures of the $\alpha 1$ - and $\alpha 2$ -helices at both N- and C-terminal ends of the bound antigen, and thus peptides between 8-10 amino acids were considered optimal for MHC-I presentation. This feature is in contrast with the open ended antigen-binding platform observed in MHC-II (**Figure 3d**), which allows longer antigens to protrude at both ends and therefore to be presented.

Within the Ag-binding cleft of HLA-A*02:01, continuous electron density was observed, and illustrated its role in antigen presentation. However, due to the heterogeneity of the antigen that might be presented and co-crystallised from the sample preparation, the precise amino acid sequence of the bound antigens were unknown. Importantly, the availability of the HLA-A*02:01 structure also allowed HLA polymorphisms to be mapped onto the model (Bjorkman et al., 1987a, b), which showed that polymorphisms are generally clustered within the Ag-binding cleft and highlights their role in enabling antigen presentation

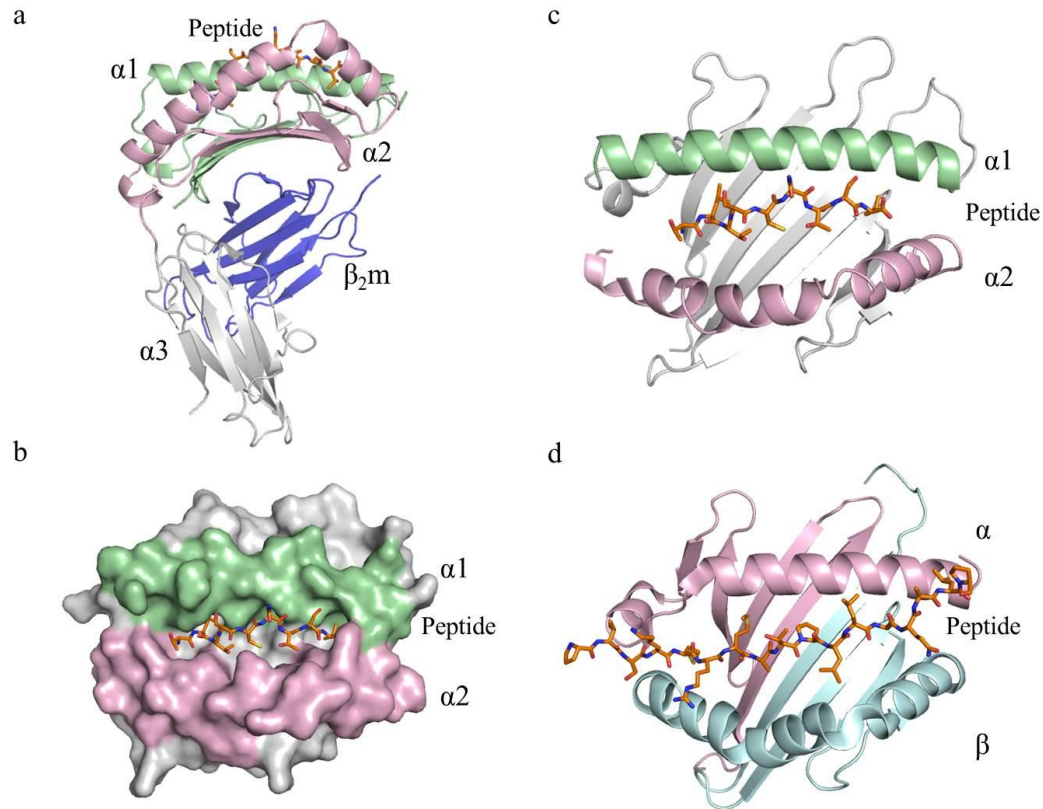


Figure 3 Crystal Structures of MHC- class I and class II molecules

(a) Side view of the HLA-A*02:01 heavy chain ($\alpha 1$ domain in green, $\alpha 2$ in pink and $\alpha 3$ in grey) that is non-covalently associated with the $\beta 2$ -microglobulin (blue) presenting a peptide antigen (orange). (b) Surface representation of the HLA-A*02:01 Ag-binding cleft (top view), formed by the $\alpha 1$ - (green), $\alpha 2$ - (light pink) helices that sandwiching the peptide (orange stick) as well as a β sheet floor (grey). Structural representations of the MHC-I and MHC-II antigen-binding clefts are shown in (c) and (d) respectively. The α and β chains of MHC-II are coloured in pink and cyan. PDB used: 1HHG for MHC-I (Madden et al., 1993) and 3PDO for MHC-II (Gunther et al., 2010).

Crystal structures of the HLA-B*27 at 2.1 Å resolution and HLA-Aw68 at 3.0 Å bound to endogenous peptides provided first insights into the antigen conformation within the Ag-binding cleft (Madden et al., 1991, 1992). Interestingly, although these structures were obtained from a mixed population of self-derived antigens bound to the HLA molecule, the electron density for the antigen was unambiguous at several positions, particularly those buried within the Ag-binding cleft. Thus, it was proposed that antigens are typically tethered N- and C- terminally to the Ag-binding cleft via a series of conserve bonding networks with the HLA residues (refer to **Figure 4** using HLA-B*35 as an example), whilst the central region of these heterogeneous antigens adopt an “extended conformation”.

Since these early structural discoveries, Garbozic and colleagues have established new methods to produce pMHC complexes (Garboczi et al., 1992). This is achieved via the expression of MHC-I and β_2m chains as inclusion bodies in *Escherichia coli* (*E. coli*) cells, followed by a refolding procedure in the presence of synthetic peptides. This approach was designed to resolve the issues of antigen heterogeneity arising from intact cell extraction. In fact, with this advancement, researchers are now able to investigate the structures of MHC-I bound to specific peptides of interest and begin to address various immunological questions associated.

1.1.4 Peptide-binding pockets and MHC-Ia supertypes

In 1989, Garrett and colleagues introduced the concept of peptide-binding pockets for MHC-Ia molecules as the structure of the HLA-Aw68 became available (Garrett et al., 1989). In this study, the authors compared the structure of HLA-Aw68 to HLA-A*2 that was available at the time. Strikingly, whilst the two HLA molecules differed by 11 amino acids, many of these residues were clustered within the Ag-binding cleft, and formed a negatively charged “pocket” in the HLA-Aw68 structure. As a result, the peptide density bound to this specialized pocket also differed between the HLA-A*2 and HLA-Aw68 structures. These observations illustrated that the diverse biochemical properties of the peptide-binding pocket contributed by polymorphisms can influence and select the antigen repertoire that a given HLA can present. Similar observation has also been reported in the crystal structures of HLA-B*27, demonstrating peptide side chains were constrained at various anchoring positions due to the extensive peptide contact with the HLA antigen-binding pockets (Madden et al., 1992).

Based on the MHC-Ia structures available, researchers have identified six pockets within the Ag-binding cleft that allow antigens to be anchored to MHC-I (Garrett et al., 1989; Saper et al., 1991). These pockets comprise different “binding motifs” that can vary between HLA allotypes and hence govern the selection of peptide repertoires based on the antigen’s side chain sizes, charges, hydrophobicity and other biophysical properties. These six pockets are termed from A to F, spanning across from the N- to C-terminal part of the bound peptide (**Figure 4a**). Of these six pockets, it is considered that peptides are anchored primarily to the B and F pockets, which

correspond to the second (P2) and the C-terminal (P Ω) position of the bound peptide, although evidences of secondary anchoring points have also been reported (Kjer-Nielsen et al., 2002a; Li and Bouvier, 2004).

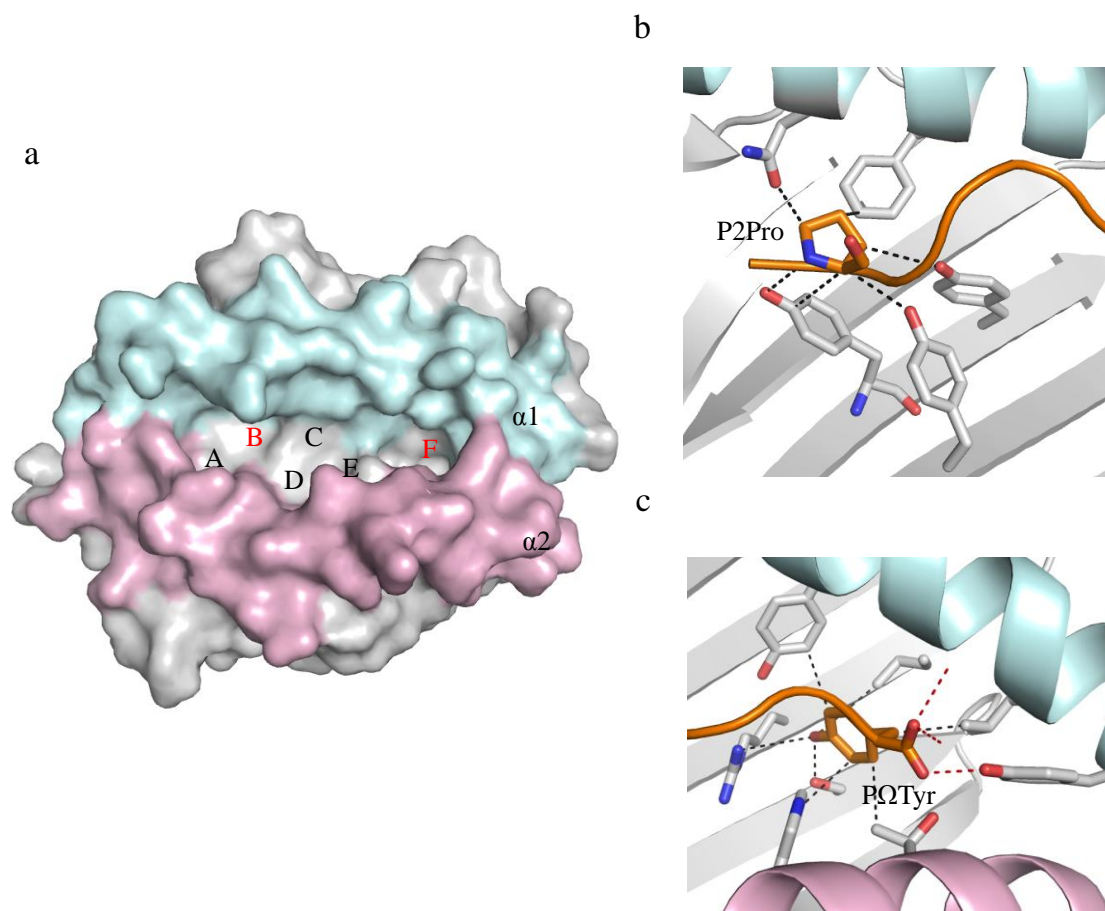


Figure 4 Antigen-binding pockets of the MHC-class I molecule.

(a) Six antigen-binding pockets (termed A to F) are illustrated with the surface representation of the HLA-B*35 structure. The MHC-I $\alpha 1$ -helix is shown in cyan and the $\alpha 2$ -helix is coloured in pink. Peptide-MHC interactions within the B and F pockets are highlighted in (b) and (c) respectively. Van der Waals (VDW) contacts are shown as black dash lines and H-bonds are shown in red. PDB used: 2H6P (Archbold et al., 2006).

Based on the biophysical properties of the B and F pockets that select different peptide repertoires at the P2 and P Ω positions, class I HLA molecules were originally grouped into nine families, termed supertypes, firstly proposed by Sette and Sidney (Sette and Sidney, 1999). Following on from the expansion of our knowledge in Ag-binding pockets, this idea was further revisited by the same group, resulting in a total number of twelve distinct supertype families (**Table 2**) (Sidney et al., 2008). For instance, the HLA-B*35 allotype that is examined in this thesis arises from the HLA-

B*7 supertype as it prefers a proline at the P2 of the peptide to occupy the B pocket as well as an aromatic residue at the C-terminal end such as phenylalanine or tyrosine (Table 2, Figures 4b and 4c).

Table 2 HLA class Ia supertypes and their binding specificity at the B and F pockets.

HLA Supertype	B pocket specificity	F pocket specificity
A*1	Small and aliphatic	Aromatic and large hydrophobic
A1*, A*3	Small and aliphatic	Aromatic and basic
A1*, A*24	Small, aliphatic and aromatic	Aromatic and large hydrophobic
A*2	Small and aliphatic	Aromatic and large hydrophobic
A*3	Small and aliphatic	Basic
A*24	Aromatic and aliphatic	Aromatic, aliphatic and hydrophobic
B*7	Proline	Aromatic, aliphatic and hydrophobic
B*8	Undefined	Aromatic, aliphatic and hydrophobic
B*27	Basic	Aromatic, aliphatic, basic and hydrophobic
B*44	Acidic	Aromatic, aliphatic and hydrophobic
B*58	Small	Aromatic, aliphatic and hydrophobic
B*62	Aliphatic	Aromatic, aliphatic and hydrophobic

Table adapted from and Sidney and colleagues (Sidney et al., 2008). The table summarises the nature of the peptide residues that are compatible for binding to the B and F pockets of HLA supertypes.

Understanding the binding specificity of subtypes alongside with studying allele frequency within different populations can provide useful information for therapeutic development such as peptide vaccine. For instance, this information, in theory, would effectively reduce the number of peptides that is required to vaccinate a targeted population, as well as facilitating the development of computational programs to predict promiscuous antigens towards particular HLA type (Brusic et al., 2002; Guan et al., 2003). However, it should also be noted that such predictions are inaccurate, as subtle allelic variations in HLA-I can also drastically impact on the stability and structural conformation of the presented antigen (Purcell et al., 2007). Furthermore, even the same peptide can be used to elicit protective immune responses in individuals with differing HLA allotypes, the profile of antigen presentation and the

subsequent recognition by T cells can vary significantly. Thus, exactly how differing HLA molecules fine-tune and manipulate antigen presentation thereby impacting on TCR recognition, awaits more experimental insights.

1.2 The $\alpha\beta$ T Cell Receptor (TCR)

1.2.1 Genetic diversity of $\alpha\beta$ T cell receptors

There are two types of T cell receptor, $\alpha\beta$ and $\gamma\delta$. The $\alpha\beta$ T cell receptor, which is the main focus of this thesis, represents the major population of TCRs. These TCRs are heterodimers, formed by the α and β chains, originating from the human TCR α -chain (TRA) genes on chromosome 14 and the TCR β -chain (TRB) genes on chromosome 7 respectively (Chothia et al., 1988; Davis and Bjorkman, 1988; Lefranc, 2011). Both TCR α and β chains comprise a variable domain, a constant domain, an extracellular stalk region, a transmembrane region and a short cytoplasmic tail. The two TCR chains are covalently linked together by a disulfide bond between the stalk regions, and tethered to the cell surface via the transmembrane domains (**Figure 5**). Notably, the short cytosolic tails of TCRs do not contain any signalling domain and hence are unable to trigger intracellular signalling cascades. As such, the recruitment of co-receptors such as CD3 complexes is thought to be essential for the initiation of its effector function although the atomic detail of this signal transduction is not elucidated.

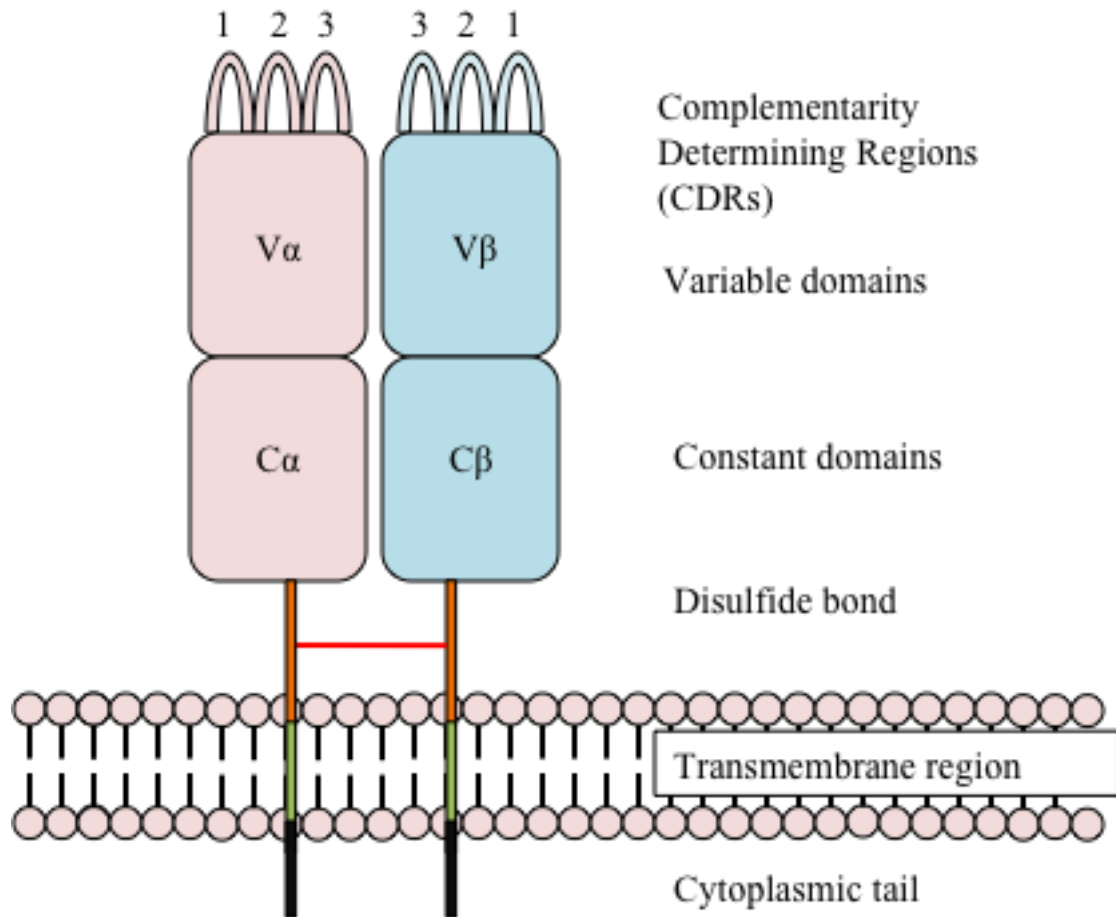


Figure 5 Structural overview of the $\alpha\beta$ T cell receptor.

The $\alpha\beta$ TCR consists of the variable (V) and constant domains (C) in the extracellular region, a stalk region (orange) that is linked by a disulfide bond (red), a transmembrane region (green), as well as a short cytoplasmic tail (black). Three Complementary Determining Regions (CDR loops) are presented in the variable domains of each chain, conferring the binding specificity of a given TCR.

TCRs comprise extremely diverse sequences in order to recognise the vast number of antigens that they might encounter. This diversity is achieved via a genetic recombination event that is similar to the generation of B cell antigen receptors (Tonegawa, 1983). The TCR α and β chains are derived from somatic gene recombination of the variable (V), diversity (D, only exist in TCR β chain), joining (J) and C (constant) gene segments (**Figure 6**). The sequence complexity is further maximized via randomized nucleotide insertions, deletions or mutations within the V-(D)-J junctional region, known as the N region. Within the TCR architecture, the binding specificity is determined via three hypervariable regions on each TCR chains. These regions are located within the variable domains, termed the complementarity-determining region 1, 2 and 3 (CDR1/2/3). Notably, the CDR1 and CDR2 regions are derived from the respective TRAV/TRBV genes, whereas the CDR3 loops are

encoded from the junctional gene regions (V-(N)-J for the CDR3 α , or V-(N)-D(N)-J for the CDR3 β loop), and thus encompass the greatest sequence diversity. Collectively, TCR diversity in humans is attributed to the availability of 54 V α genes, 61 J α genes, 67 V β genes, 2 D β genes, 14 J β genes segments, as well as the randomized N regions (Cabaniols et al., 2001; Lefranc, 2011).

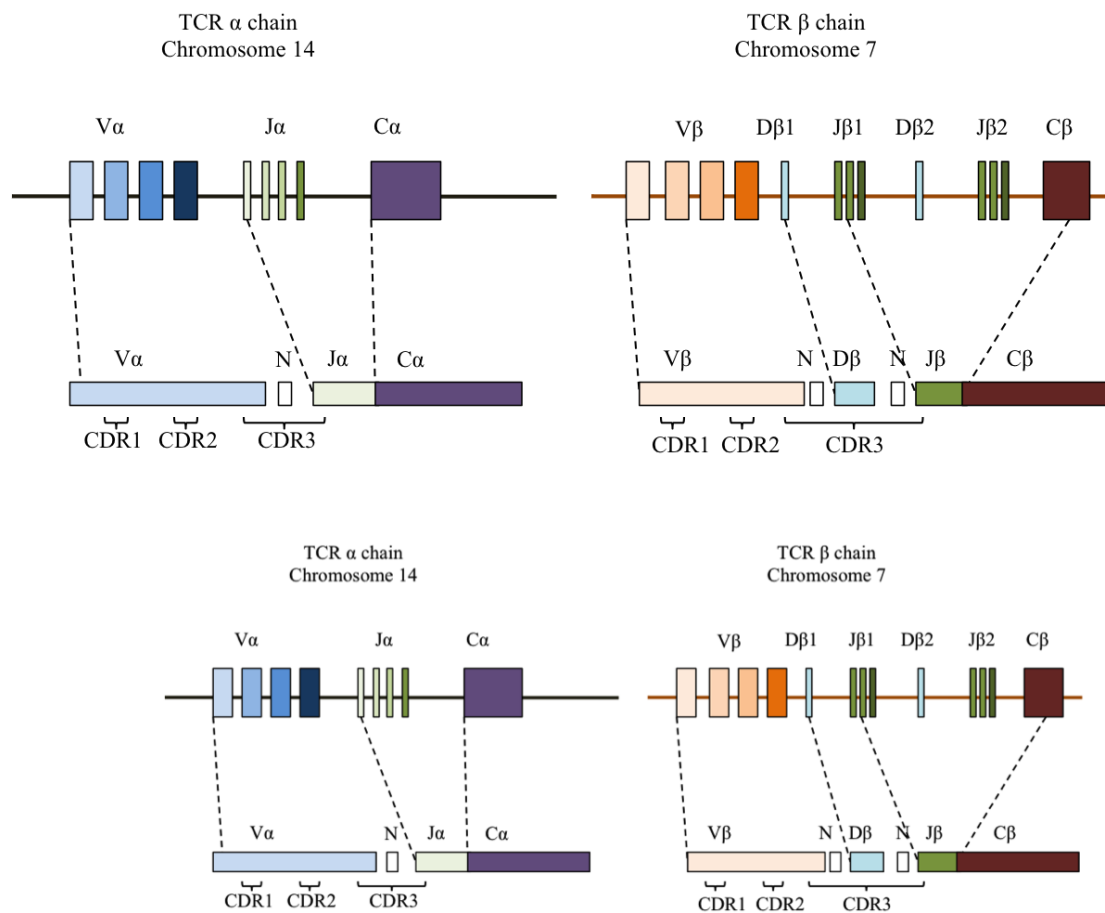


Figure 6 Somatic recombination of the $\alpha\beta$ T cell receptor.

TCRs are generated via the genetic recombination of different variable (V), junctional (J) and diversity (D, only found in β chain) genes. This diversity is further maximized at the junctional region where non-templated insertion or deletion occurred. As such, the variable gene segments determine the sequences of CDR1 and CDR2 loops whereas the CDR3 loops are derived from the V-(N)-J region in the V α chain or V-(N)-D(N)-J segment in the V β chain. Figure adapted from Turner and colleagues (Turner et al., 2006).

1.2.2 T cell development: The thymic selection

In humans, it is estimated that individuals can carry between 10^{12} to 10^{15} unique TCRs in theory from the genetic recombination of TCR genes (Davis and Bjorkman, 1988). However, preliminary estimation from the human peripheral T cells *in vivo* indicated that the actual number is only approximately 2.5×10^7 TCRs (Arstila et al., 1999). This difference is attributed to T cell maturation steps in the thymus where they undergo a selection process known as the “thymic selection”.

The thymic selection involves the presentation of self-derived pMHC complexes to the double positive (CD4+ and CD8+) immature T cells. This encompasses two processes, positive and negative selections (Gascoigne et al., 2001; Viret and Janeway, 1999). Firstly, positive selection occurs in the thymic cortex, enabling thymocytes to interact with epithelia cells in the context of self-pMHC. This process selects thymocytes that bind to pMHC complexes with adequate binding affinity to mature, and allows the selected thymocytes to turn into either CD8+ or CD4+ T cell. Conversely, thymocytes that express TCRs with no obvious pMHC binding capacity will receive no surviving signal, and hence be removed and neglected at this point (Sebzda et al., 1999). The second part of the thymic selection (negative selection) takes place in the thymic medulla and functions to eradicate thymocytes that react against self-pMHC complexes (termed self-reactive) in order to prevent auto-reactivity. During this stage, thymocytes that interact too strongly with the self-pMHC from antigen presenting cells (APC) will receive an apoptotic signal and undergo programmed cell death. Indeed, using three transgenic mouse strains expressing unique MHC-I-restricted TCRs, an apparent affinity of $\sim 6 \mu\text{M}$ has been determined to represent the threshold for this negative selecting process (Naeher et al., 2007). As such, the combined outcome of positive and negative selection would ideally only allow non-alloreactive thymocytes that preserve inherent pMHC binding property to mature and enter the peripheral circulation (Gascoigne et al., 2001).

1.2.3 The structure of $\alpha\beta$ T cell receptor

The first structural insights of TCR arise from the crystallisation of monomeric TCR chains in 1995 (Bentley et al., 1995; Fields et al., 1995). These studies revealed that both the TCR α and β chains adopt typical immunoglobulin folds, comprising a pair of anti-parallel sheets within the respective constant and variable domains. Shortly after these findings, Garcia *et al* determined the first heterodimeric form of the murine TCR (named 2C) in 1996 (Garcia et al., 1996). Within the C α domain of the 2C TCR, the back (a, b, e, and d strands) and top (c, f and g strands) anti-parallel β sheets were loosely packed against each other. This structural feature was considered to partly contribute to the instability of the TCR α chain in cells. On the other hand, the two variable domains of the 2C TCR structurally resembled to that of the antibody light chains (**Figure 7a**). All six hypervariable regions of the 2C TCR (termed complementarity-determining regions, CDRs) arranged into loop structures and pointed distally from the constant regions (**Figures 7a and 7b**). The binding surface of the 2C TCR was relatively “flat” due to the lack of large protruding side chains, with the exception of a hydrophobic cavity formed by the two CDR3 loops. Thus, it was also considered that this flat binding surface would allow the 2C TCR to come into close proximity with the pMHC-I upon ligation. Based on these findings, alongside with other subsequent TCR structures determined, it was also noted that the first and second TCR hypervariable regions (CDR1 and CDR2) are typically arranged into one of three or four "canonical" conformations in their free states. These conformations are well-defined, and appear to be conserve even after ligand binding (Al-Lazikani et al., 2000), although examples of CDR1/2 rearrangement post pMHC-I engagement have also been reported (Gras et al., 2012b; Kjer-Nielsen et al., 2002b; Kjer-Nielsen et al., 2003).

In additional to the weak binding affinity between TCR-pMHC-I interactions, one of the major hurdles to examine TCR-pMHC interactions is the production of $\alpha\beta$ TCR as the extracellular domains are only weakly associated via non-covalent interactions. The 2C TCR described earlier was originally isolated from *Drosophila melanogaster* cells, which includes only the extracellular fragments of the α (residue 1-213) and β (residue 1-247) chains (Garcia et al., 1996). Since then, protocols have been developed to refold TCRs from inclusion bodies extracted from *Escherichia coli*

expression system, similar to that of the MHC refolding strategy (Garboczi et al., 1992). Furthermore, a number of different molecular approaches have been introduced to improve the proper pairing and yield of TCR refold. These methods include the use of artificial linkers, engineered cysteine pairs between the two TCR chains, single chain construct, C-terminal zippers, as well as mouse-human hybrid (detailed summary is reviewed by Ely *et al*) (Ely et al., 2005). Alternative TCR expression systems such as eukaryotic cells have also been described (Garcia et al., 1999), although promising, this approach can potentially display significant problem for crystallisation work due to the heterogeneity of N-linked glycosylation sites. Nevertheless, a universal protocol that reliably generates heterodimeric TCRs for structural work remains a major challenge for the field.

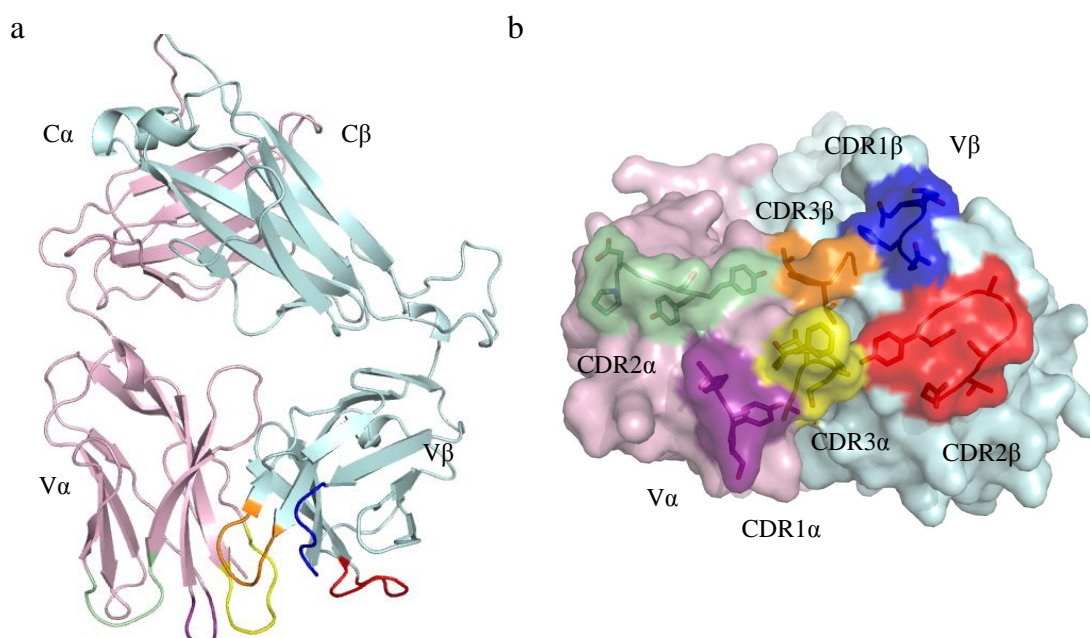


Figure 7 Crystal structure of the 2C T cell receptor.

(a) Cartoon representation of the TCR constant (C) and variable (V) domains. The α chain is coloured in pink and β chain in cyan. Three hypervariable regions that located at the end of the variable domains adopt distinct loop conformations and confer TCR with binding specificity for the pMHC ligand. (b) Surface representation of the 2C CDR loops that are solvent exposed. Both figures are coloured as follow: CDR1 α , purple; CDR2 α , green; CDR3 α , yellow; CDR1 β , blue; CDR2 β , red; CDR3 β , orange. PDB used: 1TCR (Garcia et al., 1996).

1.3 Rules of TCR-pMHC engagement

The function of TCRs is to provide ongoing surveillances to the pMHC molecules that are presented on the cell surface in the body. However, one of the major challenges to understand the molecular basis of this process is the remarkable specificity that TCR exhibit to discriminate foreign antigens, as well as its inherent ability to simultaneously cross-react onto different ligands either during the thymic selection or peripheral immunosurveillance. Indeed, this dual specificity is not only central in antiviral immunity, but also manifest clinically in the setting of organ transplantation where T cells can discriminate the allogeneic pMHC ligand as “foreign” and rejects the donor organ. In this context, since the first three-dimensional crystal structure of the TCR-pMHC-I complex solved in 1996 (Garboczi et al., 1996), a total number of 30 unique ternary complexes has been determined to date. Despite the expansion of structural information available, these structures are solved within a limited subset of MHC-I subtypes. In fact, the murine ternary complexes are determined from three MHC-I subtypes (H-2K^b, H-2L^d and H-2D^b), whilst the human complexes are examined only in the context of HLA-A*2, HLA-B*8, HLA-B*35, HLA-B*44 and more recently, the HLA-B*27, HLA-B*57 and HLA-B*24 systems (**Table 3**). Thus, it remains difficult to illustrate a common rule for TCR-pMHC-I engagement as such generalization could be potentially biased towards particular alleles. In fact, many of the “rules” that were originally proposed, have been disproven as we discover more about TCR-pMHC-I interactions.

For example, early discoveries suggest that TCRs often bind to MHC-I molecules in diagonal docking orientation, defined by the centres of mass of both TCR chains and their relative positioning along the peptide axis (refer to **Figure 9**). This docking mode determines the locations of both variable domains so that the V α domain is situated on top of the α 1-helix of MHC-I and close to the peptide N terminus, whereas the V β domain is located above the α 2-helix, proximal to the peptide C terminus (Garboczi et al., 1996; Garcia et al., 1996). Of note, this “canonical” docking orientation also allows TCRs to typically interact more extensively to the MHC surface (MHC-centric) via the germ-line derived CDR1 and CDR2 loops, whereas the relatively limited TCR-peptide contacts are mediated predominantly via the CDR3 loops. Furthermore, comparison between the free and liganded TCR structures have also revealed that remarkable conformational changes are often associated within the

CDR3 loops to enable antigen recognition (Garcia et al., 1998; Kjer-Nielsen et al., 2003; Reiser et al., 2002). The structural plasticity of TCRs is further mirrored by the thermodynamic signature of TCR-pMHC interaction, which is enthalpically driven and entropically unfavourable (Boniface et al., 1999; Krosgaard et al., 2003; Willcox et al., 1999). However, based on structural and biophysical information determined to date, it is now obvious that TCRs can also engage MHC-I molecules via an orthogonal docking mode (Tynan et al., 2005b). Furthermore, CDR1/2 loops often interact with the peptide, whilst CDR3 loops frequently mediate contact with the MHC surface (Burrows et al., 2010; Gras et al., 2009a; Tynan et al., 2005b). It has also been demonstrated by Ely and colleagues that a favourable entropy could also contribute towards TCR-pMHC-I binding (Ely et al., 2006).

The availability of the structural and biophysical investigations on TCR-pMHC-I systems (**Table 3**) has provided fundamental insights into TCR recognition of pMHC-I ligands. Nonetheless, identifying a universal mechanism that governs TCR binding specificity and degeneracy remains challenging as we only begin to understand the many different ways TCRs interact with their target ligands. Some of these investigations, both structural and biophysical, as well as their associated immunological implication are summarized in the following section.

Table 3 Summary of unique TCR-pMHC-I complexes determined until the end 2014

PDB	Human/ Mouse	TCR	TRAV	TRBV	MHC-I	Antigen source	Sequence	Kd (μ M)	Reference
2OI9	M	2C	9-4	13-2	H-2L ^d	Synthetic peptide	QLSPFPFDL	2	(Colf et al., 2007)
1G6R	M	2C	9-4	13-2	H-2K ^b	Synthetic peptide	SIYRYYGL	54	(Degano et al., 2000)
1FO0	M	scBM3.3	16D/DV11*01	1*01	H-2K ^b	Self peptide	INFDFTI	2.6	(Reiser et al., 2000)
2OL3	M	scBM3.3	16D/DV11*01	1*01	H-2K ^z bm ⁸	Synthetic peptide	SQYYYNSL	112	(Mazza et al., 2007)
1KJ2	M	scKB5-C20	14-1*01	1*01	H-2K ^b	Self-peptide	KVITFIDL	100	(Reiser et al., 2002)
3PQY	M	6218	21/DV12*02	29*01	H-2D ^b	Influenza	SSLENFRAYV	ND	(Day et al., 2011)
1AO7	H	A6	12-2*02	6-5*01	HLA-A*2	HTLV	LLFGYPVYV	0.9	(Garboczi et al., 1996)
1BD2	H	B7	29/DV5*01	6-5*01	HLA-A*2	HTLV	LLFGYPVYV	ND	(Ding et al., 1998)
3GSN	H	RA14	24*01	6-5*01	HLA-A*2	HCMV	NLVPMVATV	27	(Gras et al., 2009b)
3HG1	H	CD8	12-2*01	30*01	HLA-A*2	Melanoma	ELAGIGILTV	18	(Cole et al., 2009)
3O4L	H	AS01	5*01	20-1*01	HLA-A*2	EBV	GLCTLVAML	8.1	(Miles et al., 2010)
1LP9	H	AHIII 12.2	12D-2*01	13-3*01	HLA-A*2	Self-peptide	ALWGGFFPVL	11.3	(Buslepp et al., 2003)
2BNQ	H	1G4	21*01	6-5*01	HLA-A*2	Self-peptide	SILMWITQV	5.7	(Chen et al., 2005)
3UTS	H	1E6	12-3*01	12-4*01	HLA-A*2	Self-peptide	ALWGPDPAAA	278	(Bulek et al., 2012)
3QDM	H	DMF4	35*01	10-3*01	HLA-A*2	Melanoma	ELAGIGILTV	170	(Borbulevych et al., 2011)
3QDJ	H	DMF5	12-2*01	6-4*01	HLA-A*2	Melanoma	AAGIGILTV	40	(Borbulevych et al., 2011)
1OGA	H	JM22	27*01	19*01	HLA-A*2	Influenza	GILGFVFTL	5.6	(Stewart-Jones et al., 2003)
1MI5	H	LC13	26-2*01	7-8*01	HLA-B*8	EBV	FLRGRAYGL	8.9	(Kjer-Nielsen et al., 2003)
3FFC	H	CF34	14/DV4*01	11-2*03	HLA-B*8	EBV	FLRGRAYGL	8.9	(Gras et al., 2009a)
3SJV	H	RL42	12-1*01	6-2*01	HLA-B*8	EBV	FLRGRAYGL	31	(Gras et al., 2012b)
3KPS	H	LC13	26-2*01	7-8*01	HLA-B*44:05	Self-peptide	EEYLQAFY	49	(Macdonald et al., 2009)
3DXA	H	DM1	26-1*02	7-9*01	HLA-B*44:05	EBV	EENLLDFVRF	0.3	(Archbold et al., 2009)
2AK4	H	SB27	19*01	6-1*01	HLA-B*35:08	EBV	LPEPLPQGQLTAY	9.9	(Tynan et al., 2005b)
4JRY	H	SB47	39*01	5-6*01	HLA-B*35:08	EBV	LPEPLPQGQLTAY	25.0	(Liu et al., 2013)
4JRX	H	CA5	19*01	6-1*01	HLA-B*35:08	EBV	LPEPLPQGQLTAY	3.7	(Liu et al., 2013)
2NX5	H	ELS4	1-2*01	10-3*01	HLA-B*35:01	EBV	EPLPQGQLTAY	ND	(Tynan et al., 2007)
3MV7	H	TK3	20*01	9*01	HLA-B*35:01	EBV	HPVGEADYFEY	2.2	(Gras et al., 2010)
2YPL	H	AGA1	5*01	19*01	HLA-B*57:01	HIV-1	KAFSPEVIPMF	0.6	(Stewart-Jones et al., 2012)
4G8G	H	C12C	14*01	6-5*01	HLA-B*27:05	HIV-1	KRWIILGLNK	4.6	(Ladell et al., 2013)
3VXM	H	C1-28	8-3*01	4-1*01	HLA-A*24:02	HIV-1	RFPLTFGWCF	21.1	(Shimizu et al., 2013)

Table adapted and modified from a recent review by Gras and colleagues (Gras et al., 2012a).

1.3.1 The binding kinetics of TCR-pMHC-I complexes

TCRs typically bind pMHC-I ligands within the μM affinity range (1-100 μM) (Davis et al., 1998; Gras et al., 2012a; Rudolph et al., 2006). This relatively weak interaction is characterized by a slow association rate and a fast dissociation rate. The slow association phase consists of two kinetically independent processes. Firstly, the TCR approaches the pMHC-I target via a fast, diffusion-controlled association, followed by a slower association step that reflects the conformational adjustments within the binding interface (**Figure 8**) (Schamel and Reth, 2007). Finally, the stable TCR-pMHC-I complex is rapidly dissociated, in order to allow TCR to effectively survey the vast number of ligands presented by the immune system.

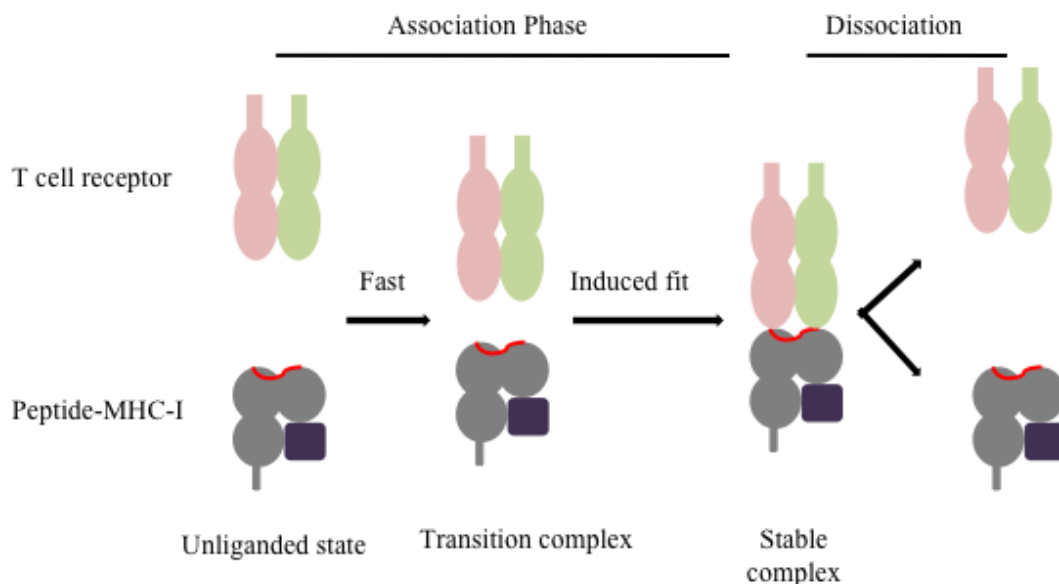


Figure 8 The two-step binding model.

Cartoon representation of the two-step binding model. The heterodimers of T cell receptor are shown in green and pink. The heavy chain and light chain of MHC molecule is coloured in grey and purple respectively, whereas the peptide antigen is shown in red.

The two-step model proposed by Wu and colleagues suggests that the initiation of TCR-pMHC interaction is driven by germ-line encoded interaction formed between the CDR1/2 loops and MHC helices, whereas the CDR3 loops only participate during the second association step to allow optimal scanning of the bound peptide (Wu et al., 2002). This idea of subdividing TCR-pMHC interactions into a peptide-independent and a peptide-dependent step was experimentally supported by the impact of alanine-mutagenesis on the MHC class II molecule, I-E^k and its recognition

by the 2B4 TCR (Wu et al., 2002). This finding also coincides with the observations that CDR3 loops typically display the greatest plasticity that allows them to accommodate different peptide landscapes. However, the two-step model remains controversial, as many structural studies have demonstrated that CDR1 and CDR2 loops can contribute minimally to MHC binding, and the CDR3 loops often contacts MHC residues (Borg et al., 2005; Burrows et al., 2010; Gras et al., 2009a). Furthermore, biophysical examinations on the A6 and B7 TCR systems have also revealed that CDR3 loops that contact the peptide can also participate markedly in both transition states (Davis-Harrison et al., 2007), which again, does not align fully with the original two-step model. Regardless, it is thought that TCR-pMHC-I interaction involves an intermediate transition step before the formation of stable TCR-pMHC complex, despite the driving force underpinning this process can vary.

To understand the relationship between T cell activation and TCR-pMHC-I interactions, biophysical studies have been carried out by many research groups. These initial studies showed that a rough correlation could be drawn with respect to the stability (half-life, derived from off-rate) of the TCR-pMHC complex and the strength of T cell stimulation (Ding et al., 1999; Rudolph and Wilson, 2002) despite exceptions were also noted. Krogsgaard and colleagues further refined this concept by demonstrating that changes in heat capacity, which reflect conformational changes and structural flexibility, should also be taken into account (Krogsgaard and Davis, 2005; Krogsgaard et al., 2003). More recently, there is a growing appreciation on the 2D affinity measurement that helps to better understand T-cell responsiveness to different ligands. Unlike the traditional approaches that determine TCR-pMHC interactions using recombinant proteins that interact freely in a 3D environment, the 2D affinity measurements (either mechanical-based or fluorescent-based) are performed using live T cells against pMHC complexes on APC or planar lipid bilayers. Thus, in the context of 2D affinity measurement, the impacts of other biological molecules, such as CD3 and coreceptors (CD4 or CD8) that are known to associate with TCR-pMHC complexes, are also taken into account. This is in contrast to the 3D approach (mainly SPR), where the affinity is largely determined by the sequence and specificity of TCRs [refer to Zhu *et al.* for a summary of the 2D methods (Zhu et al., 2013)]. Using the 2D approaches, the kinetic constants appear to correlate more accurately with the biological responses associated with T-cell

recognition (Adams et al., 2011; Huang et al., 2010; Huppa et al., 2010; Sabatino et al., 2011). These findings are in contrast to the 3D kinetic measurements where often, only the half-life of the TCR-pMHC interactions is considered. Moreover, unlike the kinetic constants obtained from the 3D experiments, the 2D kinetic measurements have demonstrated a broader range of rapid on rates, alongside with a significantly faster off rate (Adams et al., 2011; Huppa et al., 2010). These findings highlight the key differences between the 2D and 3D TCR-pMHC interactions, as well as open up new and exciting directions for future research in the field.

1.3.2 Early insights from the murine TCR-pMHC-I complexes: TCR recognition of disparate peptide ligands

Moving to the structural perspective of TCR-pMHC-I interactions, the first murine TCR-pMHC-I complex described was the 2C TCR bound to H-2K^b presenting a self-antigen (termed dEV8), derived from mitochondrial NADH ubiquinone oxidoreductase complex (Garcia et al., 1998). In this system, the H-2K^b-dEV8 acted as a weak agonist for the positive selection of the 2C TCR. Structurally, the 2C TCR adopted a diagonal mode onto the H-2K^b surface with its CDR1 and CDR2 loops located above and contacted primarily with the two MHC helices (**Figure 9a**). Notably, TCR-peptide contacts were mediated predominantly via the CDR3 α loop, allowing the optimal “scanning” of this antigen to be conducted via this hypervariable region.

To understand how the 2C TCR responds to a different ligand that gives rise to an altered signalling response, Degano *et al* investigated the 2C TCR in complex with a synthetic super-agonist, SYIR, presented by the same H-2K^b molecule (Degano et al., 2000). The overall structure of 2C-H-2K^b-SYIR was similar to that of the 2C-H-2K^b-dEV8 complex in that the TCR also sat atop of the Ag-binding cleft in a diagonal docking orientation. However, differences between the two complexes were noted, particularly at the P4 peptide positions where the side chains differed between the dEV8 and SYIR antigens. Namely, the P4Arg side chain of the SYIR peptide displaced significantly and mediated new contacts with the CDR3 β loops (**Figure 9b**) compared to the P4Lys of the dEV8 peptide. In fact, whilst both peptide variants still interacted with their respective CDR3 α loops, the newly formed peptide-CDR3 β

contacts were unique to the 2C-H-2K^b-SYIR complex. Thus, the overall shape complementarity (sc) of the TCR-pMHC-I binding interface was improved slightly in the 2C-H-2K^b-SYIR complex (sc=0.47), and the total number of TCR contacts to the P4 peptide position was also increased (15 contacts) compared to that of the 2C-H-2K^b-dEV8 complex (sc=0.46, 9 contacts to P4 peptide position). Collectively, these subtle structural differences provided an explanation for the improved cellular response associated with the SYIR super-agonist (Degano et al., 2000).

In order to explore the residues that are important for the 2C TCR recognition, an alanine mutagenesis approach was used, and the impact of TCR mutations was tested using Enzyme-linked immuno sorbent assay (ELISA). A range of 2C TCR tetramers (including wildtype and mutants) were initially tested against the allogeneic pMHC ligands, H-2L^d-QL9 (structure discussed later) (Manning et al., 1998), and subsequently the super-agonist ligand, H-2K^b-SIYR (Lee et al., 2000). Interestingly, of the 41 TCR residues selected, 16 residues were shown to be important for 2C TCR recognition towards both ligands. These residues mainly correspond to the germline encoded CDR1 and CDR2 loops that interacted with the surface of MHC-I surface in the crystal structures (Lee et al., 2000). Thus, the 2C system demonstrates that TCR-MHC contacts govern the binding energetics for TCR-pMHC-I interaction.

Another murine TCR-pMHC-I system that has been investigated was the KB5-C20 TCR, which comprises an unexpectedly long CDR3 β loop (13 residues) compared to the 2C TCR (6 residues) described earlier. Due to the extreme length of the CDR3 β , it was hypothesized that either the KB5-C20 TCR or the pMHC-I would have to undergo conformation readjustment in order to achieve a canonical TCR-pMHC-I docking orientation. To test this concept, Resier and colleagues determined the structure of the KB5-C20 TCR in complex with the H-2K^b presenting an octapeptide, and compare this to the unliganded KB5-C20 TCR structure (Housset et al., 1997; Reiser et al., 2003). This structural comparison demonstrated that most of the KB5-C20 CDR loops remained structurally conserved upon TCR-pMHC-I ligation, with an exception for the CDR3 β loop that underwent a remarkable conformational change of approximately 15 Å (**Figure 9c**). However, it is important to note that the CDR3 β loop of the KB5-C20 TCR in its unliganded form was involved in crystal contact, and its structure might not necessarily represents its biological conformation. Regardless,

the remarkable conformational rearrangement associated with the CDR3 β loop allowed the KB5-C20 TCR to interact with the MHC-I ligand via a canonical docking orientation. This study highlights the role of CDR flexibility in enabling TCR recognition.

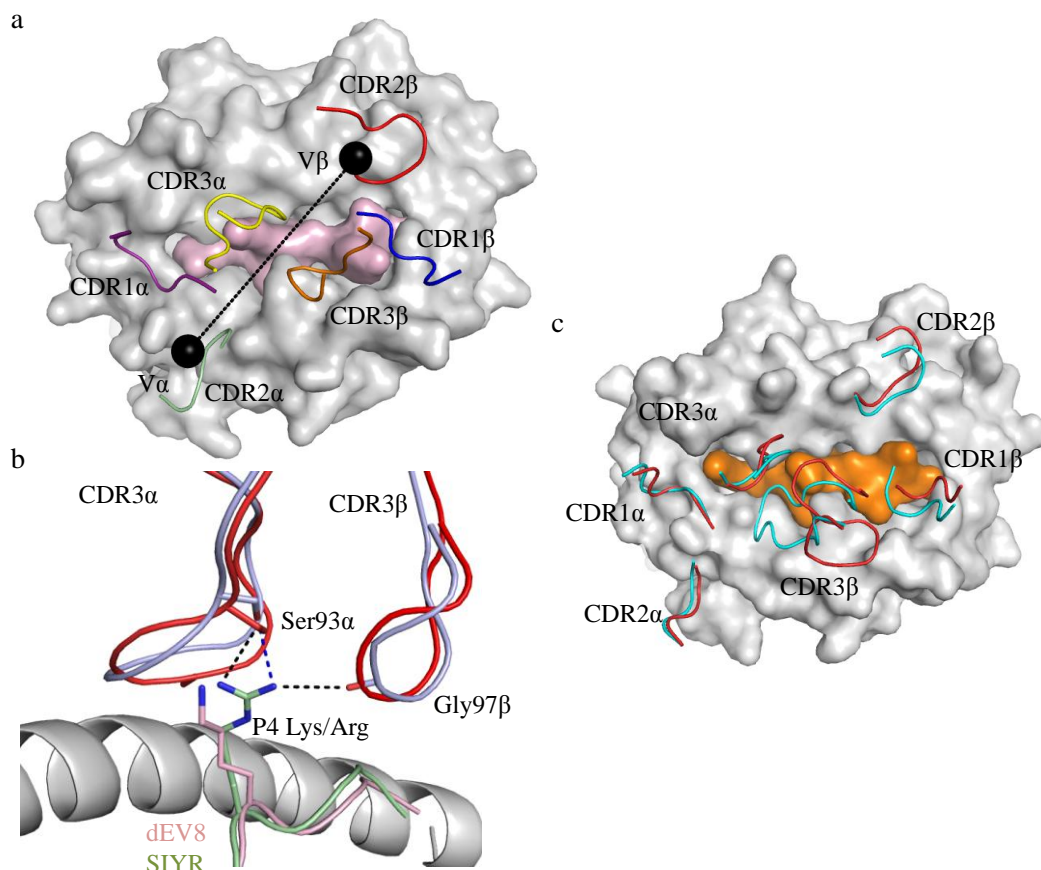


Figure 9 The 2C TCR recognises disparate ligands via the flexible CDR3 α loop.

(a) Diagonal docking orientation of the 2C TCR onto the surface of its target pMHC-I ligand, H-2K^b-dEV8. The CDR loops are coloured as depicted in Figure 8. The centre of mass for the TCR variable domains is shown as black sphere. (b) The 2C TCR cross-recognises the self dEV8 peptide (pink) and the super-agonist SYIR ligand (green) via the rearrangement of the CDR3 α loop as well as the formation of new contacts with the CDR3 β . The CDR loops in the 2C-H-2K^b-dEV8 and 2C-H-2K^b-SIYR complexes are coloured in red and blue respectively. VDW contacts are represented as black dash lines whereas H-bonds are in blue. PDB used: 2CKB (2C-H-2K^b-dEV8) (Garcia et al., 1998) and 1G6R (2C-H-2K^b-SIYR) (Degano et al., 2000). (c) Structural comparison between the unliganded (cyan) and liganded (red) forms of the TCR. The MHC-I is surface is shown in grey and the peptide is coloured in orange. PDB used: 1KJ2 for the KB5-C20 TCR-pMHC-I complex (Reiser et al., 2003) and 1KB5 for the unliganded KB5-C20 TCR (Housset et al., 1997).

The single chain construct of the murine BM3.3 TCR (scBM3.3) represents another system to examine immuno-recognition of different pMHC-I ligands. The BM3.3

TCR has been investigated in the context of three pMHC-I molecules. These include the H-2K^b bound to a viral VSV8 peptide (RGYVYQGL), a self-peptide (INFDNTI, pBM1), as well as a synthetic pBM8 (SQYYNSL) peptide presented by the H-2K^{bm8} molecule (Mazza et al., 2007; Reiser et al., 2003; Reiser et al., 2000). Since H-2K^{bm8} is an allele of the H-2K^b family, which comprises four buried substitutions (Y22F, M23I, E24S and D30N) within the antigen-binding groove, the BM3.3 TCR-pMHC-I system is therefore ideal to investigate how single TCR cross-reacts with diverse peptide antigens sharing minimal similarity in their primary sequences. In this context, structural examinations showed that the BM3.3 TCR docked onto all pMHC-I surfaces similarly, and interacted with the respective antigens primarily via both CDR3 loops. It was also noted that the CDR3 α loop that contacted the P4 peptide position, exhibited the greatest conformational differences between the three ternary complexes (**Figure 10a**). This finding correlated with the fact that the BM3.3 TCR can tolerate the antigen substitution at the P4 position. As such, the authors proposed that the adaptability of the BM3.3 TCR to accommodate different antigens at P4 side chain arises from structural flexibility of the BM3.3 CDR3 α loop. Conversely, the BM3.3 TCR has been shown to be extremely sensitive to substitutions at the P6 position of the peptide. Close structural inspections at this peptide position showed that this coincided with the lack of CDR3 β malleability that interacted with the P6 peptide position (**Figure 10b**). Collectively, studies of BM3.3 TCR-MHC-I complexes highlighted how a single TCR (BM3.3) can simultaneously exhibit binding specificity (towards P6 of the peptide) and degeneracy (P4) via the modulation of CDR3 loops flexibility and rigidity.

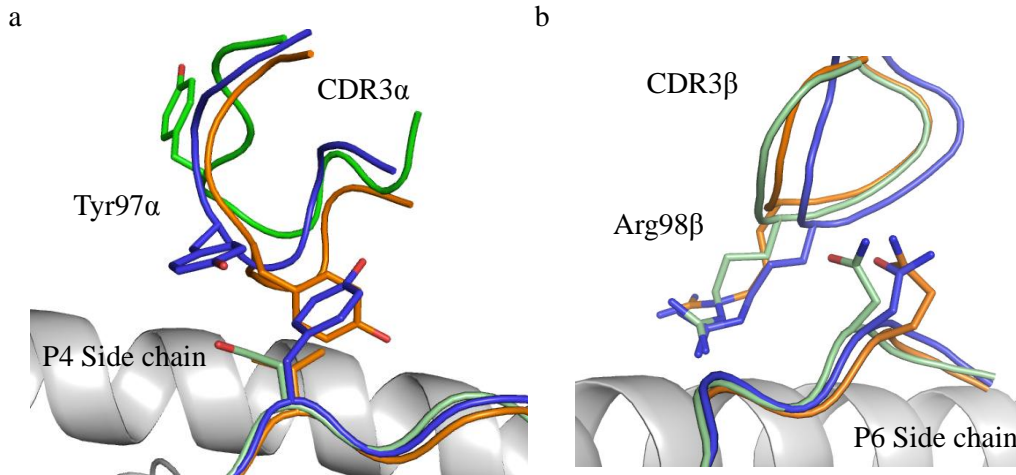


Figure 10 Binding specificity and degeneracy of the BM3.3 TCR.

Superimposition of the BM3.3-H-2K^b-pBM1, BM3.3-H-2K^b-VSV8 and BM3.3-H-2K^{bm8}-pBM8 ternary complexes with main focuses on the P4 (a) and P6 (b) peptide positions. In both figures, the MHC-I $\alpha 1$ -helix is coloured in grey and represented as cartoon, whilst the different peptides along with the corresponding CDR3 loops are coloured as follow: pBM1 in green, VSV8 in orange and pBM8 in blue. PDB used: 1FO0 (BM3.3-H-2K^b-pBM1) (Reiser et al., 2000), 1NAM (BM3.3-H-2K^b-VSV8) (Reiser et al., 2003) and 2OL3 (BM3.3-H-2K^{bm8}-pBM8) (Mazza et al., 2007).

1.3.3 TCR recognition of altered ligand: Insights from the Human Leukocyte Antigen (HLA)-A*2 system

Of the 30 unique TCR-pMHC-I structures solved to date, 11 were derived from antigens presented by the HLA-A*2 (**Table 3**). Notably, all the available TCR-HLA-A*2 structures were restricted to only one allomorph, the HLA-A*02:01, and in a number of systems, the same TCR was also examined in complex with a range of different peptide ligands. As such, studying the HLA-A*2 system provides us with an ideal opportunity to investigate how a given TCR can recognise different altered peptide ligands (APL) while maintain simultaneous binding specificity and degeneracy. These findings are discussed in the following section.

The A6 TCR bound to HLA-A*2 presenting a human T-cell lymphotropic virus peptide (LLFGYPVYV, termed Tax) was the first human TCR-pMHC-I structure described (Garboczi et al., 1996). In this structure, the A6 TCR engaged HLA-A*2-Tax via a diagonal docking orientation that allowed both CDR3 loops to interact primarily with the viral determinant, whereas the TCR-HLA contacts are primarily mediated via the CDR1 α and 2 α loops. The energetic landscape of the A6-HLA-A*2-Tax has also been investigated via alanine mutagenesis, Surface Plasmon Resonance (SPR), as well as cellular approaches (Baker et al., 2001). Notably, of the 15 TCR contacted HLA-A*2 residues, only three amino acids (R65, K66 and A69) were found to be important for the functional recognition of the A6 TCR. This is in contrast to the peptide substitution data, which showed that 3 out of the 7 non-anchoring Tax substitutions abolished TCR recognition (Hausmann et al., 1999). As such, the authors concluded that the TCR-peptide contacts dominated the energetic of the A6-HLA-A*2-Tax binding interface.

Since these initial studies on A6-HLA-A*2-Tax, a number of different Tax peptide variants (including P6A, V7R, Y8A and Y5K) have been established by Ding *et al* (Ding et al., 1999) and Gagnon *et al* (Gagnon et al., 2006). Structural investigations into these ternary complexes indicated that the A6 TCR engaged all HLA-A*2-Tax variants via a highly conserved binding mode. Limited structural adjustments were observed primarily between the CDR3 β loops of the respective complexes in order for the A6 TCR to accommodate variations in the Tax peptide sequence (**Figure 11a**).

These HLA-A*2-Tax studies demonstrated how a single TCR (A6) can accommodate antigenic variations via minimal rearrangements in the CDR3 loops that are typically directed towards the antigen in a “canonical” TCR docking orientation.

In 1998, Ding and colleagues solved the ternary structure of HLA-A*2-Tax in complex with another TCR, the B7 TCR (Ding et al., 1998). In comparison to the A6 TCR, the B7 TCR comprised a shared TRBV6-5*01 gene usage, but encompassed a markedly different CDR3 β loop, as well as an alternate V α chain (TRVA29-5*01 for the B7 TCR and TRAV12-2*02 for the A6 TCR). The structure of the B7-HLA-A*2-Tax complex revealed that the B7 TCR also docked onto HLA-A*2-Tax in a diagonal manner similar to that of the A6 ternary complex (**Figure 11b**). Notably, whilst the V α chain of the B7 aligned closely in comparison to the A6 TCR with only minor differences between the respective CDR2 α loops, the V β chain of B7 TCR was positioned substantially different compared to the A6 complex (~5 Å displacement). This observation was unexpected given that both TCRs utilised the same TRBV chain, and there was only one shared V β residue that contacts the HLA-A*2 in both ternary complexes. The authors proposed that these structural variations were attributed to the impact of TCR pairing between the V α and V β chains (Ding et al., 1998). This study demonstrates how a single pHLA-I target can be recognised by divergent TCRs, and provides a structural explanation for the altered specificity associated with the A6 and B7 TCRs.

Contrasting to the single residue substitution of the Tax peptide, Borbulevych *et al* recently described another antigen that A6 TCR cross-recognised in the context of HLA-A*2 (Borbulevych et al., 2009). The Telp1 antigen (MLWGYLQYV) that derived from *Saccharomyces cerevisiae*, was originally identified by a database screening approach targeting Tax-like peptides carrying the recognition motifs for the A6 TCR. Interestingly, although the conformation of the Telp1 bound to HLA-A*2 formed an ideal structural mimic to that of the Tax peptide in the binary structure, the binding interfaces between the two ternary complexes differed substantially upon the binding of the A6 TCR (Borbulevych et al., 2009). Namely, the Telp1 antigen underwent significant conformational readjustments, especially at the P5Y and P7Q peptide positions (**Figure 11c**). These movements were further accompanied by an unexpected displacement of 6.9 Å within the hinge region (Ala150-Val152) of HLA-

A*2 α 2-helix (**Figure 11d**). Similarly, the conformation of the A6 CDR3 β loop also differed between the two ternary complexes (Tax and Telp1) in order to avoid steric clash with altered P5Y peptide conformation. As such, whilst the cross-reactivity of A6 TCR towards Tax peptide variants is depicted mainly by a shared binding mode with minor readjustments in the CDR3 β loop, its binding degeneracy towards the Telp1 peptide is governed by the structural dynamics of the TCR, MHC, as well as the peptide determinant.

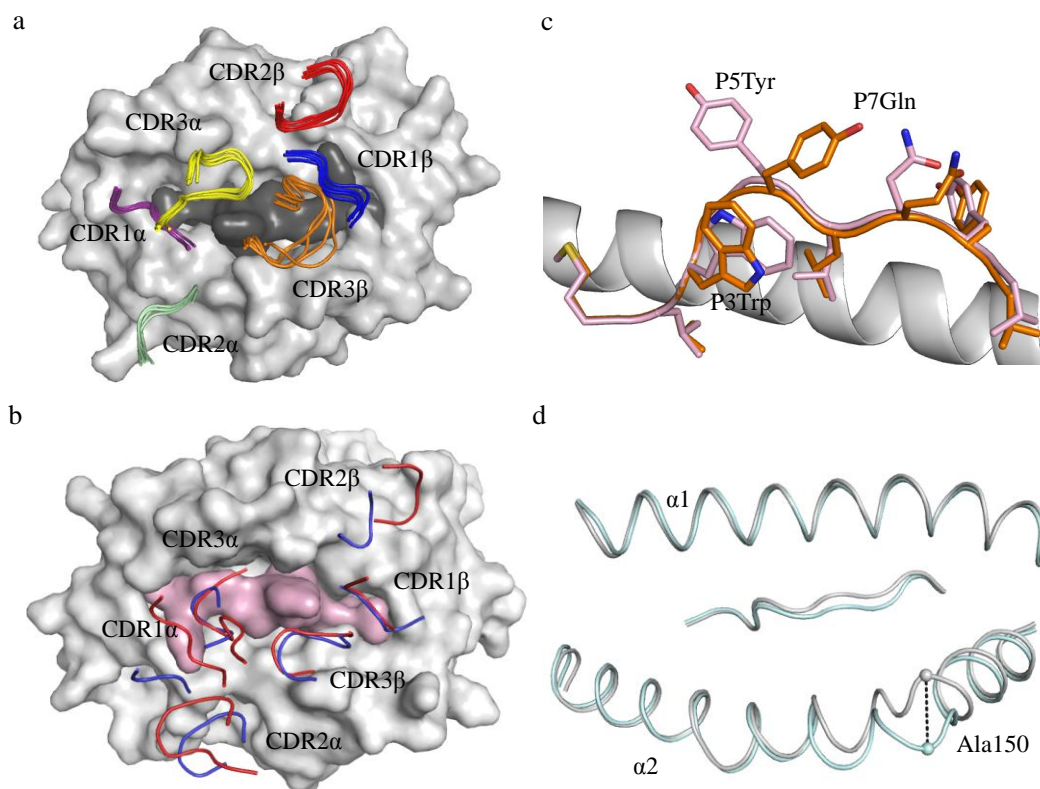


Figure 11 The cross-reactivity of the A6 TCR is depicted with different mechanisms.

(a) The A6 TCR accommodates Tax peptide variants (Tax in black) primarily via a conserved binding mode with subtle structural rearrangements in the CDR3 β loop (orange). PDB used: 1AO7 (Tax) (Garboczi et al., 1996), 1QRN (Tax-P6A), 1QSE (Tax-P7R), 1QSF (Tax-P8A), 2GJ3 (Tax-Y5K) (Ding et al., 1999). The CDR loops are coloured as depicted in Figure 8. (b) Structural comparison between the B7 (blue) and the A6 (red) CDR loops that interact with the HLA-A*2-Tax. The surface representation of the HLA-A*2 is shown in white and the Tax peptide is coloured in pink. PDB used: 1AO6 for the A6 complex (Garboczi et al., 1996) and 1BD2 for the B7 complex (Ding et al., 1998). (c) Superimposition of the Telp1 antigen conformations from the pMHC binary complex (pink) and the TCR-pMHC-I ternary complex (orange). (d) Using Ala150 as a reference point, the hinge region of HLA-A*2 α 2-helix is markedly displaced upon A6 TCR ligation (cyan to grey). PDB used in (c) and (d): 3H7B (HLA-A*2-Telp1 binary) and 3H9S (ternary complex) (Borbulevych et al., 2009).

In addition to the exposed peptide residue modifications, antigen carrying buried substitutions can also have substantial impact on TCR recognition, albeit it is less obvious how TCRs can recognise these differences. Towards this end, Chen and colleagues described the structures of 1G4 TCR bound to a tumor antigen (SLLMWITQC, NY-ESO-1) presented by the HLA-A*2, and compared that to an anchor-modified peptide counterpart carrying substitution at the P9 position (Cysteine to Valine) (Chen et al., 2005). In this system, although the two binary structures of the two pHLA-I variants were similar, and the 1G4 TCR were also directed towards the P4M and P5W peptide positions in both ternary complexes, subtle differences were noted. Namely, the P9V antigen substitution caused its side chain to sit further inside the F pocket of HLA-A*2 with a significantly larger buried surface area (190 \AA^2 for P9V and 160 \AA^2 for P9C) and an improved shape complementarity ($sc=0.81$ for P9V and $sc=0.72$ for P9C). This impact further propagated through the peptide main chains, causing P6 to P8 of the antigen to also sit lower within the Ag-binding cleft (**Figure 12a**). As such, the 1G4 TCR in the P9V ternary complex adopted a slightly tilted docking orientation ($\sim 0.9^\circ$) compared to that of the P9C ternary complex, and mediated more focused interactions with position 155 of the HLA. These subtle changes resulted in an slightly improved shape complementarity ($sc=0.73$ for the P9V complex and $sc=0.71$ for the P9C complex) at the TCR-pMHC binding interface, as well as additional H-bonds formed between the 1G4 TCR and the Q155 of the HLA-A*2 (only present in the P9V variant), thereby providing a structural explanation for the heightened immunogenicity associated with the anchor-modified variant.

Recently, Borbulevych *et al* examined TCR binding degeneracy by solving the crystal structures of two distinct TCRs (DMF4 and DMF5) bound to an overlapping nonamer ($^{26}\text{EAAGIGILTV}^{35}$) and decamer ($^{27}\text{AAGIGILTV}^{35}$) melanoma antigens (MART-1) presented by HLA-A*2 (Borbulevych et al., 2011). The cross-reactivity of the DMF4 (TRAV35*01, TRBV10-3*01) TCR was triggered by two major events. Firstly, upon the ligation of DMF4 TCR, the nonamer antigen altered its conformation to mimic that of the decamer epitope (**Figure 12b**). However, substantial differences between the two DMF4 ternary complexes were noted, particularly between the N-terminal regions of the respective antigens. Thus, the DMF4 TCR adopted two alternative docking modes towards the nonamer and decamer pHLA-A*2 ligands with an

approximately 15° rotation. These changes in docking orientation resulted in the repositioning of five CDR loops (r.m.s.d. of 5.1 Å between the two TCR variable domains), whilst the limited interactions between the CDR3β loop and the C-terminal part of the antigen were maintained (**Figure 12c**). As such, minimal shared contacts between the two DMF4 ternary complexes were observed. In marked contrast to the DMF4 ternary structures, the binding degeneracy of the DMF5 TCR (TRAV12-2*01, TRBV6-4*01) was rather straightforward. Upon DMF5 TCR binding, the nonamer antigen also shifted itself to mimic the decamer peptide, thereby allowing the DMF5 TCR to interact with both ligands identically (**Figure 12d**) (Borbulevych et al., 2011).

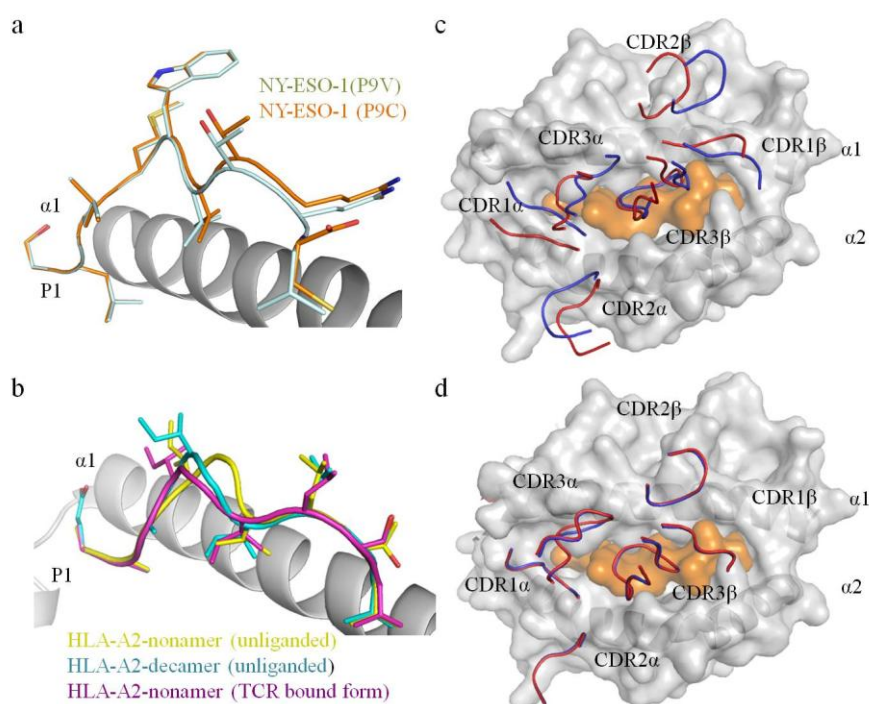


Figure 12 TCR recognition of altered peptide ligand.

(a) Structural comparison between the NY-ESO-1-P9V (green) and the NY-ESO-1-P9C (orange) peptides from the respectively TCR-pMHC-I complexes. Subtle differences are located near the peptide C-terminal end. PDB used: 2BNQ (1G4-HLA-A*2-NY-ESO-1-P9V) and 2BNR (1G4-HLA-A*2-NY-ESO-1-P9C) (Chen et al., 2005). (b) The nonamer peptide bound to HLA-A*2 changes its conformation upon DMF4 TCR ligation (yellow to purple) to mimic that of the decamer antigen (cyan). PDB used: 2GUO (HLA-A*2-nonamer), 2GT9 (HLA-A*2-decamer) (Borbulevych et al., 2007) and 3QEQ (DMF4-HLA-A*2-nonamer) (Borbulevych et al., 2011). (c) Alternative docking orientations of the DMF4 TCR bound to HLA-A*2 presenting the nonamer and decamer peptides are shown. The CDR loops of the nonamer and decamer complexes are shown in red and blue respectively. PDB used: 3QEQ (nonamer) and 3QDM (decamer) (Borbulevych et al., 2011). (d) The CDR loops of the DMF5 TCR bound to HLA-A*2-nonamer (red) and HLA-A*2-decamer (blue) are shown. PDB used: 3QDJ (nonamer complex) and 3QDG (decamer complex) (Borbulevych et al., 2011).

Taken together, studying the HLA-A*2 system showed that TCR binding degeneracy towards antigenic variants are depicted via a number of different mechanisms. These range from a shared docking and binding mode to substantial movements in the CDR loops, peptide and MHC landscapes. Indeed, it is obvious that, depending on the particular antigen investigated, as well as the characteristics of the TCRs, individual components within the binding interface of the TCR-pMHC can adapt significantly in order to achieve optimal binding.

1.3.4 Impact of buried MHC polymorphism on TCR recognition

The highly polymorphic HLA-A, HLA-B, HLA-C in humans, as well as H-2K, H-2D and H-2L in mice, allow them to present diverse range of peptide antigens for T cell recognition. As previously outlined, polymorphisms are generally located within the antigen-binding cleft, and hence altering its biophysical property towards the presented peptides. Interestingly, whilst many of these polymorphic residues are inaccessible for direct TCR contact, they can nevertheless impact on TCR recognition. Structural insights into how buried polymorphisms are detected by TCRs have been examined by comparing the binary structures of the pMHC-I as well as different TCR-pMHC-I complexes.

The murine 2C TCR has been reported to interact with a self-ligand (dEV8) bound to both the H-2K^b and a naturally occurring variant, H-2K^{bm3} that exhibited only two amino acid substitutions (D77S and K89A) within the MHC-I heavy chain. Interestingly, whilst the H-2K^b-dEV8 acted as a weak agonist during the positive selection for the 2C TCR, the same dEV8 bound to H-2K^{bm3} was able to trigger negative selection (Sha et al., 1990). To explore the impact of polymorphism in this system, Luz and colleagues determined the structures of the H-2K^{bm3} in its unliganded and TCR bound states, and compared that to the H-2K^b counterparts (Luz et al., 2002). These structures revealed that, the Asp77 (in H-2K^b) to Ser77 substitution that confers H-2K^{bm3} with its reactivity, was able to induce a local rearrangement of the MHC-I bound peptide, and caused its main chain to shift towards the α 1-helix of the Ag-binding cleft (**Figure 13a**). This movement resulted in the formation of new hydrogen bonds, van der Waals interactions, as well as improving the shape complementarity associated with the 2C and H-2K^{bm3}-dEV8 binding interface (shape

complementarity improved from 0.48 to 0.59 for the α chain and 0.43 to 0.72 for the β chain). Accordingly, these observations demonstrated how subtle polymorphisms could lead to changes in the TCR-pMHC binding interface, which ultimately gives rise to distinct biological outcomes.

Studies on the human HLA-B*44 system also explored the impact of buried HLA polymorphisms on TCR recognition. For example, Archbold and colleagues investigated the immuno-recognition of an Epstein-Barr viral (EBV) determinant (EENLLDFVRF) bound to three HLA-B*44 variants, HLA B*44:02, HLA-B*44:03 and HLA-B*44:05, which differed each other by only one or two buried polymorphic residues at position 116 and/or 156 (HLA-B*44:02: Asp116, Asp156; HLA-B*44:03: Asp116, Leu156; HLA-B*44:05: Tyr116, Asp156) (Archbold et al., 2009). Notably, the DM1 TCR, which derived from HLA-B*44:05+ donor, interacted with HLA-B*44:05-EENL more than 10-fold stronger than that of the HLA-B*44:02 and HLA-B*44:03, highlighting its fine-specificity towards the polymorphic HLA landscape. To understand the structural basis of this HLA-restricted recognition, Archbold and colleagues determined and compared the binary structures of all three HLA-B*44 allomorphs bound to the EENL antigen (**Figure 13a**). Strikingly, whilst all polymorphic residues were buried within the antigen-binding cleft, the conformation of the bound antigen was significantly impacted. In particular, the central part of the EENL antigen that protruded away from the Ag-binding cleft in all three binary structures deviated substantially not only in the overall conformation but also flexibility (Archbold et al., 2009). This observation was most pronounced in the binary structure of HLA-B*44:05-EENL, whose antigen conformation shifted towards the α 2-helix by approximately 3.4 Å compared to that of the HLA-B*44:02 (**Figure 13b**), and exhibited flexible P6 and P7 antigen side chains. To further investigate how the DM1 TCR discriminates these antigen differences, the co-crystal structure of DM1-HLA-B*44:05-EENL was determined. Notably, upon binding of the DM1 TCR, the central region of the EENL antigen was bent towards the α 1-helix, and allowed the CDR1 β , CDR3 α and CDR3 β loops to interact with P3-7 and P9 of the peptide (**Figure 13c**) (Archbold et al., 2009). This TCR-induced peptide rearrangements was considered to play critical role for DM1 TCR recognition as the central region of the EENL peptide was highly mobile in the binary structure of the HLA-B*44:05-EENL complex. In contrast, the DM1 TCR interacted weakly with :-

B*44:02-EENL and HLA-B*44:03-EENL, which coincided with the limited antigen flexibility associated with the EENL antigens in respective binary structures. As such, the HLA-B*44 system demonstrated how HLA polymorphisms can fine-tune T cell responses by altering the dynamic and conformation of the presented antigen which indirectly facilitate or disturb TCR recognition.

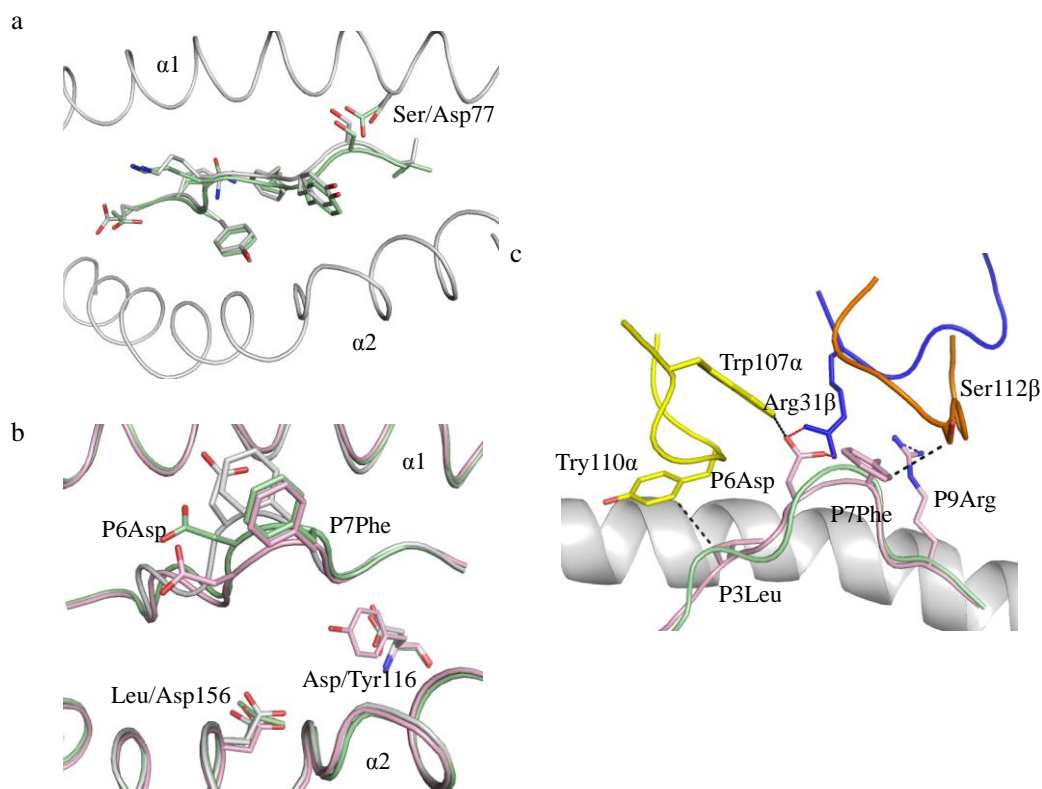


Figure 13 The binding of TCRs towards polymorphic MHC-I molecules.

(a) The polymorphic Ser77 substitution in H-2K^{bm3} (grey) induces a local peptide rearrangement towards the α 1-helix that in turn impacts on 2C TCR recognition. The 2C-H-2K^b-dEV8 complex is superimposed in green for comparison. PDB used: 1MWA (2C-H-2K^{bm3}-dEV8) (Luz et al., 2002) and 2CKB (2C-H-2K^b-dEV8) (Garcia et al., 1998). (b) The EENLLDFVRF antigen displays different conformations and flexibility depending on the specific HLA-B*44 allomorph that it is presented (HLA-B*44:02: grey, HLA-B*44:03: green, HLA-B*44:05: light pink). PDB used: 3DX6 (HLA-B*44:02), 3DX7 (HLA-B*44:03) and 3DX8 (HLA-B*44:05) (Archbold et al., 2009). (c) The EENL antigen bound to HLA-B*44:05 changes its conformation upon binding of the DM1 TCR (green to pink). The CDR3 α (yellow), CDR1 β (blue) and CDR3 β loops (orange) of the DM1 TCR are shown. VDW contacts are represented as black dash lines and salt bridge interactions are coloured in red. PDB used: 3DX8 (binary) and 3DXA (ternary) (Archbold et al., 2009).

The impact of buried MHC polymorphism has also been recently explored in the context of HLA-B*57. In this system, Stewart-Jones and colleague investigated the AG1 TCR that was frequently utilised in response to the KF11 antigen (HIV-I epitope) when presented by HLA-B*57:01 (Asp114/Ser116) but not the closely

related HLA-B*57:03 (Asn114 / Tyr116). To understand the differential recognition of AG1 TCR towards these two allotypes, the authors determined the crystal structures of the HLA-B*57:03-KF11 in its free and TCR liganded forms, and compare that to the HLA-B*57:01-KF11 (Stewart-Jones et al., 2005). Structurally, the HLA-B*57:03-KF11 complex demonstrated that the central stretch of the KF11 antigen (P4-P9) protruded away from the antigen-binding cleft, forming a prominent structural feature for TCR recognition. Upon AG1 TCR binding, this central stretch was crumpled towards the α 2-helix of HLA-B*57:03. This conformational change was further accommodated by the P9Pro of the peptide that rotated approximately 15° into the antigen-binding cleft, the repositioning of the polymorphic Tyr116 (HLA-B*57:03), as well as the exclusion of two water molecules from the peptide-HLA-I interface (**Figure 14a**). On the other hand, whilst the authors were unable to determine the structure of the AG1-HLA-B*57:01-KF11, the binary complex of HLA-B*57:01 was highly superimposable to that of the HLA-B*57:03, suggesting a common mode for AG1 recognition (Stewart-Jones et al., 2012). Nevertheless, the polymorphic Ser116 of HLA-B*57:01 was considerably more favourable for the AG1 recognition due to its smaller side chain compared to the Tyr116 of HLA-B*57:03. In fact, the additional space associated with the polymorphic Ser116 was thought to be more favorable in accommodating the structural change of the P9Pro upon AG1 TCR binding (**Figure 14b**). This hypothesis was further supported by the associated kinetic experiments, as the AGA1 TCR showed a fivefold increased dissociation towards B*57:03-KF11 compared to B*57:01-KF11. Thus, whilst polymorphism between the two HLA-B*57 allotypes was structurally concealed in this system, its interplay with the water molecules, as well as the roles in accommodating the peptide readjustment associated with TCR binding, can drastically impact on the kinetics and specificity of TCR.

Other examples of buried MHC-I polymorphism have also been implicated in the HLA-B*44 system that contributes to TCR allorecognition, as well as the HLA-B*35 system that presents a range of lengthy antigens in anti-viral immune responses. These findings are discussed later in the relevant sections.

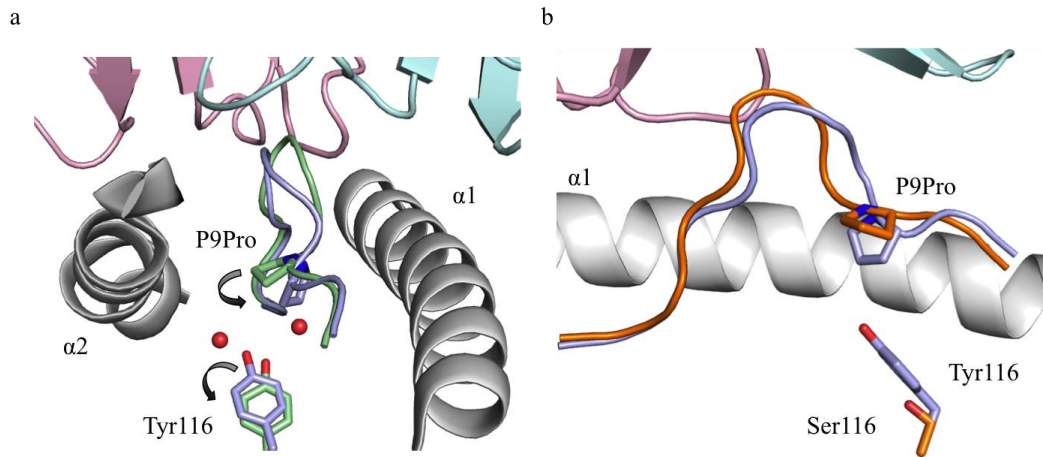


Figure 14 TCR recognition of buried polymorphism in the HLA-B*57 system.

(a) Structural representation of the unliganded HLA-B*57:03 (white) bound to the KF11 antigen (green) and the AG1-HLA-B*57:03-KF11 complex. For the AG1 complex, the TCR is coloured in pink and cyan, and the KF11 peptide is shown in blue. Two water molecules (red spheres) are excluded from the binding interface post AG1 TCR binding. (b) Structural superimposition between the AG-HLA-B*57:03-KF11 complex (peptide in blue) and the HLA-B*57:01-KF11 (peptide in orange). The polymorphic HLA residue 116 in both structures is shown as stick (Ser116 for the HLA-B*57:01 in red and Tyr116 of the HLA-B*57:03 in white). PDB used: 2BVO (HLA-B*57:03-KF11) (Stewart-Jones et al., 2005), 2YPL (AG1-HLA-B*57:03-KF11) and 2YPK (HLA-B*57:01-KF11) (Stewart-Jones et al., 2012).

1.3.5 Structural evidence of inherent TCR-MHC interactions

Whilst TCRs are designed to see a potentially infinite number of antigens, they nevertheless recognise them in the context of self-MHC molecules, a phenomenon known as “MHC restriction”, first described by Nobel Prize winners, Doherty and Zinkernagel (Zinkernagel and Doherty, 1974). Indeed, the fact that TCRs generally display a roughly conserved docking mode, whereby the CDR1 and CDR2 loops contact the MHC helices and the CDR3 loops interact with the peptide landscape, has led to the speculation that TCRs preserve inherent binding properties to MHC surfaces, mediated by the germline-encoded sequences and interactions. Garcia and colleagues further refined this original concept by proposing that individual MHC allotypes are co-evolved with the respective TCR variable regions in a pair-wise manner (Garcia et al., 2009). In this model, the elements of MHC restriction are governed not only by the MHC allotype but also the specific variable regions of the TCR. As such, the TCR docking orientation is defined by the germ-line derived CDR1 and CDR2 loops as well as the corresponding MHC contacts. In fact, by

examining four different TCRs sharing the same V β chain (V β 8.2) and their interactions with the murine class II (I-A) molecules, Feng and colleagues were able to identify conserved TCR-MHC interactions mediated by the respective germline-encoded CDR1 β and CDR2 β loops (Feng et al., 2007). Namely, Asn31 β , Tyr48 β and Glu56 β from all V β 8.2 ternary complexes were found in a similar position that interacted with Glu61, Gln57 and Lys39 of the I-A α 1-helix (**Figure 15a**). Alongside with mutagenesis approach, these TCR regions (CDR1 β and CDR2 β) were further illustrated to play crucial roles for I-A recognition in two of the selected V β 8.2 TCR systems (Feng et al., 2007). Moreover, analysis of 9 TCRs carrying V β 8-like V β chains further revealed that 46Y, 48Y and 54E from the TCR CDR2 β loop often interacted with conserved residues (39K, 57Q, 60L, and 64A) on the α 1-helix of MHC-II (Marrack et al., 2008). The conserved TCR-MHC contacts have also been noted for TCR V α chains (Dai et al., 2008; Marrack et al., 2008). Similarly, the “codon” interaction can also be examined in the context of class I MHC molecules. For instance, the murine 2C TCRs with randomized sequences in the non-germline encoded CDR3 α regions has resulted in an identical bonding network between key germline-encoded CDR loops and the corresponding H-2L^d molecule (**Figure 15b**) (Jones et al., 2008). These studies highlight the roles of germline-encoded CDR loops in determining TCR docking orientations.

The “codon” theory has also been challenged by a number of structural observations. For example, four TCRs expressing TRBV6-5*01 (A6, 1G4, RA14 and B7 TCRs) bound to the same HLA-A*2 molecule have illustrated a range of V β docking orientations (**Figure 15c**) (Chen et al., 2005; Ding et al., 1998; Garboczi et al., 1996; Gras et al., 2009b). Similar findings have also been noted from the murine BM3.3 and KB5-C20 TCRs that both expressed TRBV1*01 and interacted with the H-2K^b molecule differently (Reiser et al., 2003; Reiser et al., 2002). Furthermore, the DMF5 TCR and CD8 TCR that derived from the TRAV12-2*01 gene, adopted completely different footprints onto the HLA-A*2 surface with no conserved TCR-MHC contact (**Figure 15d**) (Borbulevych et al., 2011; Cole et al., 2009). More recently, it has also been shown that the pairing of different V α chains can also influence how a single V β interacted with the MHC (Stadinski et al., 2011). Last but not least, a number of TCR-pMHC-I interactions have demonstrated the peptide-centric nature of TCR

recognition that clearly contradicted the MHC-centric view proposed by the “codon” theory. For instance, the human LC13 TCR-HLA-B*8-FLR interaction was energetically driven by the non-germline encoded CDR3 loops that interacts with both the peptide and the MHC-I molecule (Borg et al., 2005; Kjer-Nielsen et al., 2003). Furthermore, the SB27 TCR bound to a lengthy pHLA-I molecule (more details in section 1.5.2) has also been shown to exhibit a highly peptide-focussed mode of TCR recognition (Tynan et al., 2005b). In particular, of the minimal HLA contacts that were observed in this system, three HLA residues (65, 69 and 155) were proposed to serve as minimal elements governing MHC restriction. The term “restriction triad” was given accordingly (Tynan et al., 2005b). However, subsequent mutagenesis work from Burrows and colleagues has illustrated that different TCRs may have varied degrees of dependency towards the restriction triad (Burrows et al., 2010) and in fact, recent structural study on the murine 6218 TCR has shown that TCRs can interact with pMHC-I without making contacts to all restriction triad residues (Day et al., 2011). It is unclear however, whether or not the restriction triad can play a more significant role during process of thymic selection. Regardless, understanding the inherent properties of TCR bias towards MHC (MHC restriction) will advance our knowledge in fundamental immunology and ultimately allowing the prediction of TCR docking. However, it appears that the ability of TCR to see antigens in a MHC-restricted manner remains surprisingly subtle. Indeed, while the germline-encoded interaction might provide a simplistic solution to the underlying basis of MHC restriction, variations between different TCR chain pairing and peptide sequences can also have profound impact in editing the interaction and therefore mask the key elements governing MHC restriction.

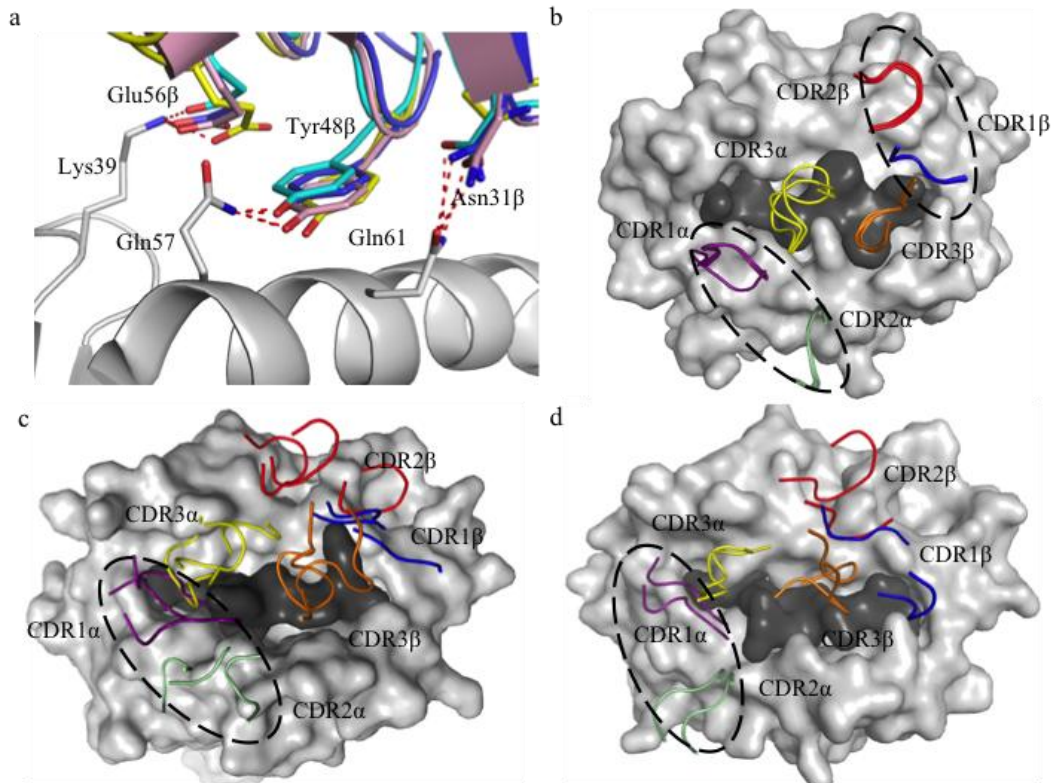


Figure 15 Structural insights into MHC-restricted recognition.

(a) Four V β 8.2 TCRs (D10 in yellow, 1934.4 in pink, C119 in cyan and 172.1 in blue) interacts with a MHC class II molecule (I-A) via germline-encoded CDR1 β and CDR2 β loops to form conserved interactions with the MHC α 1-helix (grey). PDB used: 1D9K (D10) (Archbold et al., 2006), 2PXY (1934.4), 2Z31(C119) (Feng et al., 2007) and 1U3H (172.1) (Borbulevych et al., 2007). (b) Mutants of the 2C TCR that carry randomized CDR3 α loop sequence exhibit a shared docking mode onto the H-2L^d surface. PDB used: 2OI9 (Colf et al., 2007), 3E2H, and 3E3Q (Jones et al., 2008). (c) Four TRAV6-5*01 TCRs (A6, 1G4, RA14 and B7) place their germline-encoded CDR1 α and CDR2 α loops differently onto the HLA-A*2 molecule. PDB used: 3HG1(CD8) (Cole et al., 2009), 3GSN (R14) (Gras et al., 2009b), 1AO7(A6) (Garboczi et al., 1996) and 1BD2 (B7) (Ding et al., 1998). (d) Two TRAV12-2*01 TCRs (DMF5 and CD8) show divergent V α docking orientations onto HLA-A*2. PDB used: 3QDJ (DMF5) (Borbulevych et al., 2011) and 2BNQ (CD8) (Chen et al., 2005). The CDR loops in figure b, c and d are coloured purple (CDR1 α), green (CDR2 α), yellow (CDR3 α), blue (CDR1 β), red (CDR2 β) and orange (CDR3 β). The surfaces of all MHCs are shown in grey. The shared TCR variable regions in figures b, c and d are circled with black dash lines. Peptides are coloured in black.

1.3.6 Structural basis of TCR bias

Despite the vast diversity of human periphery TCR repertoire ($\sim 10^7$) that is presented in the immune system (Arstila et al., 1999), CTL responses towards a given determinant can often display a biased profile in TCR gene selection (Acha-Orbea et al., 1988; Babbe et al., 2000; Baker et al., 2002; Price et al., 2005; Torres-Nagel et al., 1997; Turner and Carbone, 1998), a phenomenon known as TCR bias. As proposed by Turner *et al*, TCR bias, which is defined by the repetitive selection of TCR repertoire in unrelated individuals, can be categorized into three types (Turner et al., 2006). The Type I TCR bias is classified by the selection of shared TRAV and/or TRBV genes with variability in the CDR3 loops. Type II bias is characterized by the conservation of TRAV and/or TRBV genes alongside with repetitive selection of certain motifs within the CDR3 loops. Finally, Type III bias, which is the least common TCR bias, represents the repetitive TRAV and/or TRBV selection, as well as conservation in the CDR3 loops arising from identical genetic transcript or redundant codons. This clonal selection of TCR chains in unrelated individuals is also referred as “public”, contrasting to the “private” TCR repertoire where different TCR repertoires are used in unrelated individuals towards the same pHLA target. Functionally, the bias in TCR genetic selection implies that certain motifs or sequences within the TCR might play important roles contributing to the binding specificity of its target pMHC ligand. In fact, structural studies, alongside with associated mutagenesis and retrogenic approaches have begun to shed lights into the underlying basis of this process.

Kjer-Nelsen et al provided the first structural insight of TCR bias when they examined a “public” (Type III TCR bias) anti-viral response in HLA-B*8 positive individuals towards an EBV viral determinant (FLRGRAYGL, FLR) (Kjer-Nielsen et al., 2003). In this system, the CTL response in different individuals was not only biased towards the selection of TCR $V\alpha$ (TRAV26-2*01) and $V\beta$ (TRBV7-8*01) chains, but also conserved within the non-germline derived CDR3 loops (Argaet et al., 1994; Callan et al., 1998). To gain an understanding of such a biased CTL response, the crystal structure the public TCR (termed LC13) bound to HLA-B*8-FLR was determined. In this ternary structure, all six CDR loops were involved in

contacting the HLA surface. TCR-peptide interactions in this system were mediated predominantly via the CDR3 β loop, as well as the CDR1 α and CDR3 α loops to a lesser extent. Of note, the P7Tyr side chain of the FLR peptide pointed into a central cavity of the LC13 TCR, serving as a focal point for TCR recognition (**Figure 16a**). Associated mutagenesis on LC13 TCR further demonstrated that both CDR3 loops that interacted with the peptide (and HLA to a lesser extent) principally conferred to the binding energetic. The CDR1 loops on the other hand, appeared to play more critical roles in stabilizing the conformation of the CDR3 loops post pMHC-I engagement (Borg et al., 2005). The underlying basis for the biased selection in the LC13 system appears to be attributed to the non-germline encoded CDR3-mediated interactions.

The anti-influenza CTL response in HLA-A*2 positive individuals been shown to direct predominantly towards the MP₅₈₋₆₆ antigen (GILGFVFTL) that derived from the influenza viral matrix protein (Gotch et al., 1987; Morrison et al., 1992). In particular, the TCR repertoire in this system was characterized by a dominant selection of the TRBV19*1 gene, as well as a highly conserved ⁹⁸RS⁹⁹ motif in the non-germline derived CDR3 β loop (Type II TCR bias) (Lehner et al., 1995; Moss et al., 1991). To establish the underlying basis of this bias selection, Stewart-Jones *et al* determined the structure of the immunodominant TCR (termed JM22) in complex with HLA-A*2-MP₅₈₋₆₆ (Stewart-Jones et al., 2003). Intriguingly, whilst TCRs typically interact with exposed side chains from the MHC bound antigen, the binary structure of the HLA-A*2-MP₅₈₋₆₆ on its own was relatively “featureless” as the side chains of the MP₅₈₋₆₆ epitope were mostly buried (Madden et al., 1993). Thus, to overcome this unusual pHLA-I landscape, the JM22 TCR adopted an orthogonal docking mode, which enabled the insertion of the ⁹⁸RS⁹⁹ (V β) side chains into the Ag-binding cleft of HLA-A*2 (**Figure 16b**). It is therefore considered that the bias TCR repertoire observed in the JM22 system is dictated by the unprecedented binding mechanism, driven by the featureless pHLA landscape. In fact, mutagenesis study on the JM22 TCR has further supported this idea, where the energetic hot spots of the JM22 TCR were found to locate within in the V β domain, spanning across all three CDR loops (Ishizuka et al., 2008). The V β -orientated energetic profiles, which enabled the JM22 TCR to contact both helices of the HLA-A*2 and the peptide,

provides the underlying basis for the bias V β gene selection in this system (Ishizuka et al., 2008).

The murine 6218 TCR represents another example to study TCR bias towards an anti-influenza immune response in H-2D^b mice. TCR bias in this system was characterized by the preferential selection of the TRBV29*01 gene as well as a CDR3 β loop that was six amino acids in length (Turner et al., 2003). Day and colleagues solved the crystal structure of the 6218 TCR bound to the H-2D^b presenting an influenza epitope (PA₂₂₄), and revealed that the interaction between the CDR3 β loop and the peptide was achieved primarily via its backbone (Figure 16c) (Day et al., 2011). Thus, although the length of the CDR3 β loop was restricted, the amino acid sequence in this region varied between CTL clones. Using a retrogenic approach that induced the expression the H-2D^b-PA₂₂₄ specific TRAV TCR chain, the authors further concluded that the biased TCR repertoire was also attributed to the preferential TRBV pairing (Day et al., 2011).

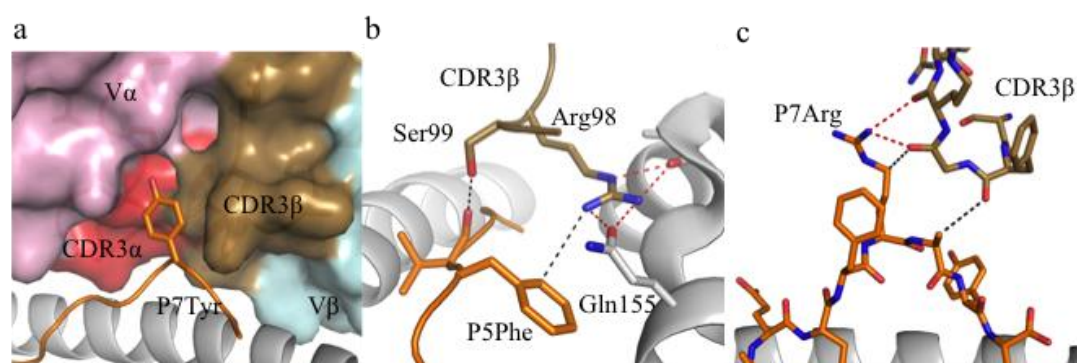


Figure 16 Structural basis of immunodominant TCR recognition.

(a) The side chain of the P7Tyr points into a central cavity formed by the LC13 CDR3 α and CDR3 β loops which serves as a focal point for antigen recognition. PDB used: 1MI5 (Kjer-Nielsen et al., 2003). (b) The CDR3 β loop of JM22 TCR comprises a ⁹⁸RS⁹⁹ motif that inserts into the Ag-binding cleft and facilitates the recognition of a “featureless” pHLA landscape. PDB used: 2VLK (Ishizuka et al., 2008). (c) The CDR3 β of 6218 TCR interacts with the peptide mainly via backbone-mediated interactions. PDB used: 3PQY (Day et al., 2011). All peptides are coloured in orange, CDR3 α in red and CDR3 β in sand.

More recently, Coles and colleagues determined the structure of the public MEL5 TCR (biased TRAV12-2*01 usage) in complex with HLA-A*2 presenting a melanoma antigen (MART-1). This study revealed that the germline-encoded CDR1 α and CDR2 α loops dominated the peptide contacts at the TCR-pHLA-I binding interface, highlighting the potential role of this “innate” recognition in driving

the biased TCR gene usage (Cole et al., 2009). In marked contrast, the structural study of the C12C TCR (biased TRBV6-5*01 usage) in complex with HLA-B*27:05-KK10 has demonstrated only suboptimal interactions between the CDR1/2 β loops and the pHLA-I landscape. (Ladell et al., 2013). This conflicting evidence shows that although TCR bias might be partly driven by the structural requirement that enables pHLA-I recognition, other factors including the preferential TCR pairing, the frequency of the naïve precursor, the effectiveness of the antigen presentation as well as the shaping of TCR repertoire during the thymic selection, can also contribute towards this process. Understanding the driving force that underpins TCR bias is a key step towards therapeutics development, as a more diverse TCR repertoire would be potentially more advantageous in response to subtle antigen variations.

1.3.7 Structural insights into T cell allorecognition and self-tolerance

Despite TCR-pMHC-I interaction being genetically restricted to self-MHC molecules as a result of the thymic selection, up to 10% of T cells can violate the rule of MHC restriction and interact with “foreign” MHC, a phenomenon known as allorecognition (Ely et al., 2008; Felix et al., 2007; Gras et al., 2011; Sherman and Chattopadhyay, 1993). Although allorecognition is irrelevant to the host protective immune responses, it can nevertheless manifest in a clinical setting during organ transplantation. For instance, T cells from HLA-mismatched bone marrow transplantation can alloreact with the recipient’s tissue and contribute to graft-versus-host diseases (Afzali et al., 2007; Keever et al., 1994). Similarly, protective T cells derived from the host can also trigger an alloresponse against the donor’s organ and results in graft rejection (Brehm et al., 2010; Jurcevic et al., 2001; Sayegh, 1999). As such, understanding the molecular basis governing allorecognition is an area of intense interest.

There are two historical models that describe the basis for T cell allorecognition. The HLA-centric model suggests that alloreactivity is triggered by TCR recognition towards polymorphic residues on the MHC surface (Bavan, 1984; Elliott and Eisen, 1990; Smith et al., 1997). In contrast, the peptide-centric model proposes that TCRs form interactions with conserved features of the MHC surface (molecular mimicry) and distinguish differences between the peptides as “foreign” (Matzinger and Bevan, 1977). To date, despite many examples of T cell allorecognition having been reported (Archbold et al., 2008; Lawrence and Colman, 1993), there are only two MHC-I

systems where the structures of the TCR bound to the self and allogeneic ligands were both determined. These examples, namely the murine 2C TCR and the human LC13 TCR system, have provided first structural insights underscoring T cell allorecognition in the context of MHC-I, although it has also been shown that MHC-II restricted TCR can also alloreact with MHC-I molecules using a semi-conserved TCR docking orientation, and distinguishes the ligands via the flexibility of the CDR3 loops, as well as alternating the relative position of the V α and V β domains (Yin et al., 2011).

In the murine system, the 2C TCR was determined in complex with the self H-2K^b molecule presenting a positively selected ligand (EQYKFYSV, dEV8) (Garcia et al., 1998), as well as the allogeneic MHC-I (H-2L^d) bound to the QL9 (QLSPFPFDL) ligand that resulted in the negative selection of this TCR (Colf et al., 2007). These two pMHC ligands differ substantially not only in the peptide sequences but also 31 substitutions between the α 1 and α 2 domains of the respective MHC-I molecules. Given these differences, the 2C TCR utilized markedly shifted docking mechanisms onto these two pMHC-I surfaces with only four shared MHC-I positions contacted by the TCR, including MHC-I residues 65, 76, 79 and 158 (**Figure 17a**). Furthermore, alongside with associated mutagenesis data (Lee et al., 2000; Manning et al., 1998), the 2C system suggests limited role of molecular mimicry and highlights the importance of TCR-MHC interactions in driving T-cell allorecognition.

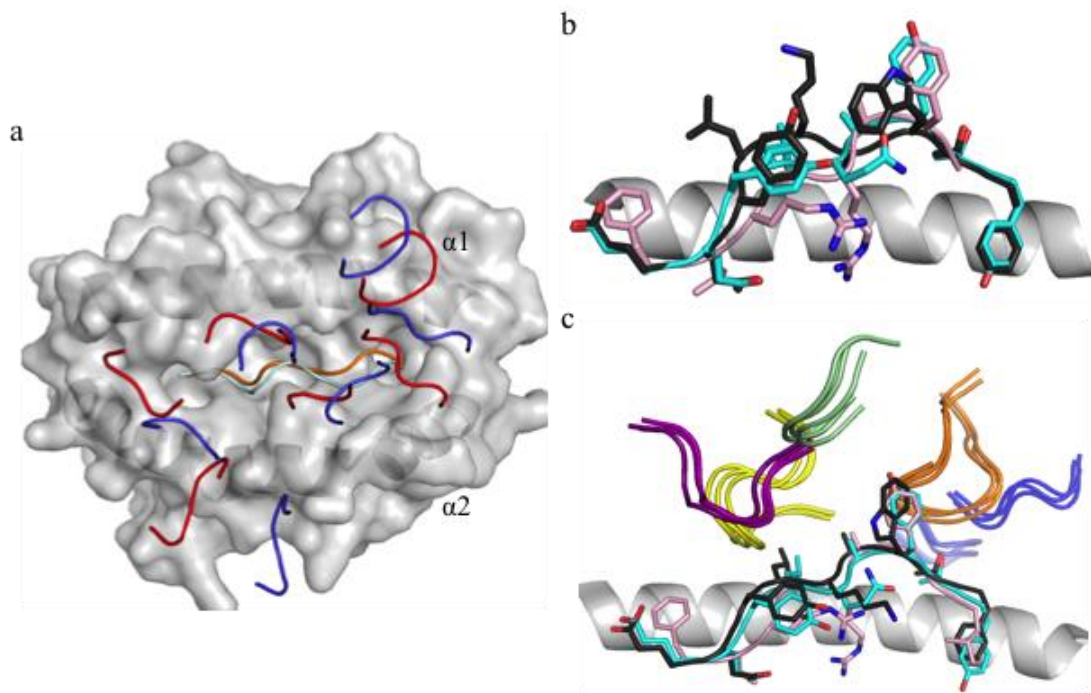


Figure 17 Alternative binding and molecular mimicry modes of TCR allorecognition.

(a) The murine 2C TCR cross-reacts onto the H-2K^b (2C CDR loops in red) and H-2L^d (CDR loops in blue) via alternative TCR docking orientations. PDB used: 2CKB (Garcia et al., 1998), 2OI9 (Colf et al., 2007). (b) Structural comparison between the unliganded FLR antigen (pink), the mimotope (black) and the allotope (cyan) that bound to HLA-I molecules. PDB used: 1M05 (Kjer-Nielsen et al., 2002a), 3KPP and 3KPQ (Macdonald et al., 2009). (c) The mimotope (black) and allotope (cyan) form structural mimics to the viral FLR (pink) which in turn allows the LC13 TCR to engage all three pHLA landscapes via a shared docking orientation. The LC13 CDR loops are coloured purple (CDR1 α), green (CDR2 α), yellow (CDR3 α), blue (CDR1 β), red (CDR2 β) and orange (CDR3 β). PDB used: 3KPR, 3KBS (Macdonald et al., 2009) and 1MI5 (Kjer-Nielsen et al., 2003).

On the other hand, the structure of human LC13 TCR was originally determined in complex with an EBV viral determinant (termed FLR) presented by HLA-B*8 (Kjer-Nielsen et al., 2003). Recently, using a peptide library screening in insect cells as well as bioinformatics approaches, Macdonald and colleagues identified a mimotope (EEYLKAWTF) and an allo-peptide (EEYLQAFTY) derived from the ATP binding cassette protein in the context of HLA-B*44:05 which caused allorecognition by the LC13 CTL (Macdonald et al., 2009). Due to the alloreactivity of LC13 towards HLA-B*44, this TCR is absent in HLA-B*8+/B*44+ individuals, as a result of negative selection, in order to avoid auto-reactivity (Burrows et al., 1997; Burrows et al., 1995). To understand how LC13 TCR alloreacts onto HLA-B*44:05, Macdonald and

colleagues determined the co-crystal structures of the allogeneic LC13-HLA-B*44:05-mimotope and LC13- HLA-B*44:05-allotope complexes and compared them to that of the cognate LC13-HLA-B*8-FLR ternary structure (Kjer-Nielsen et al., 2003; Macdonald et al., 2009). Interestingly, in contrast to the divergent binding modes observed in the murine 2C-H-2K^b/L^d system, alloreactivity of the LC13 TCR was achieved using a similar binding footprint where the mimotope and allotope both form structural mimics to that of the viral FLR peptide (**Figures 17b** and **17c**). In particular, this structural mimic of the antigen was facilitated, in the context of the mimotope, via a substantial peptide conformational change upon TCR ligation. As such, allorecognition in the human LC13 TCR system is depicted by a molecular mimicry mechanism, which involves in the structural reconfiguration of the bound antigen. This is further supported by the fact that the LC13 T cells did not alloreact onto HLA-B*44:03 due to the disfavoured polymorphic substitution (Leu156) that impacted on the plasticity of the allotope (Macdonald et al., 2009). Accordingly, the role of the antigen-induced fit in enabling TCR-pHLA-I recognition is also highlighted in this study.

Contrasting to the public TCR repertoire in HLA-B*8+/B*44- individuals against the FLR antigen (bound to HLA-B*8), the TCR repertoire in HLA-B*8+/B*44+ individuals towards the same pHLA target is more diverse. To understand how these different TCRs respond to the viral HLA-B*8-FLR complex whilst being able to discriminate HLA-B*44 and pass the negative selection process, Gras and colleagues determined the structure of a prototypical TCR (named CF34, comprising TRAV14*01 and TRBV11-2*03), derived from HLA-B*8+/B*44+ individual bound to HLA-B*8-FLR and compared that to the LC13-HLA-B*8-FLR structure (Gras et al., 2009a). Intriguingly, unlike the LC13 TCR that focused on the P7Tyr of the FLR antigen (Kjer-Nielsen et al., 2003), the CF34 TCR docked N-terminally towards the Ag-binding cleft and contacted P1 of the bound peptide (**Figures 18a** and **18b**). This alternative docking mode enabled the CF34 TCR to contact MHC residues (Thr163 and Trp167) that are different between HLA-B*8 and HLA-B*44 (**Figure 18c**) and hence able to distinguish the two allotypes. More recently, Gras and colleagues investigated another private TCR [termed RL42 (TRAV12-2*01 and TRBV6-2*01), derived from HLA-B*8+/B*44+ individual] that is also specific for the recognition of HLA-B*8-FLR. The structure of RL42 ternary complex demonstrated a central TCR

docking mode, which allowed the TCR to interact with both P1 and P7 of the FLR peptides (**Figure 18d**) (Gras et al., 2012b). Using alanine mutagenesis scanning approach on the HLA-B*8, the authors further investigated and compared the energetic landscapes between the three HLA-B*8-FLR-restricted TCRs. This approaches illustrated that, the energetic landscapes of the HLA-B*8 in the three TCR-pHLA-I complexes were found to locate neighbouring to the respective peptide hot spots (Gras et al., 2012b). This observation prompted the authors to conclude that the driving force between these three TCRs and the HLA-B*8-FLR relied primarily on the antigen itself (main glue), whilst the surrounding HLA residues only acted as supporting adhesive. Collectively, these findings show how three different TCRs (LC13, CF34 and RL42), derived from different HLA background, respond to a common viral-determinant using alternative docking mechanisms via the peptide-centricity of TCRs. These differences in docking in turn allow TCRs to cross-react (such as LC13) or distinguish (CF34, RL42) different HLA molecules, and hence provide structural insights into T cell allorecognition and self-tolerance.

In summary, TCR allorecognition is an unintended consequence of the inherent TCR binding degeneracy. Based on the limited number of structural studies available, both molecular mimicry and alternative TCR binding mechanisms have been proposed to underpin this process, it remains unclear which of these governs TCR allorecognition in general. As such, TCR repertoires are shaped based on the host genetic background to utilize differing binding motifs and structural footprints in order to provide protective immunity. Nevertheless, identifying the peptide ligand that is responsible for T cell allorecognition remains a major bottleneck for the field due to the vast number of self-antigens that might be presented by MHC-I. Thus, exactly how many different ways can TCR alloreact with disparate ligands, and how self-tolerance is maintained to avoid auto-reactivity, awaits further experimental insights.

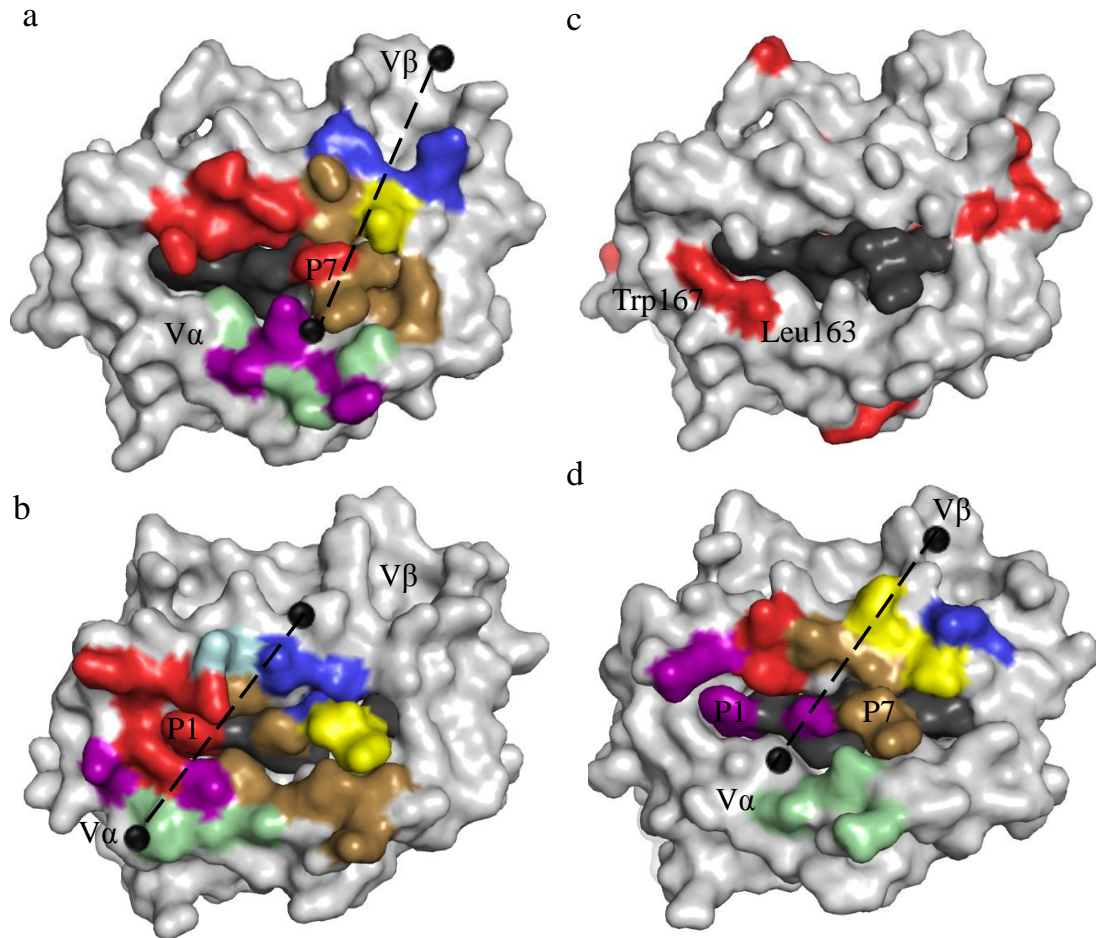


Figure 18 Divergent TCR docking footprints towards a viral HLA-B*8-FLR target.

(a) The LC13 TCR docks C-terminally onto the Ag-binding cleft and focuses on the P7 position of the FLR peptide. PDB used: 1MI5 (Kjer-Nielsen et al., 2003). (b) The CF34 TCR engages N-terminally and interacts with the P1 position of the antigen. PDB used: 3FFC (Gras et al., 2009a). (c) Structural comparison between the HLA-B*8 and HLA-B*44:05. Polymorphic residues are coloured in red. PDB used: 1MI5 (Kjer-Nielsen et al., 2003). (d) The RL42 adopts a central binding mode onto the viral HLA-B*8-FLR complex whilst contact both P1 and P7 of the peptide. PDB used: 3SJV (Gras et al., 2012b). Surface representations of the HLA molecules and peptides in all four figures are coloured in white and grey respectively. In figure (a), (b) and (d), the MHC residues are coloured based on their interactions with their respective TCR contacts; CDR1 α , purple; CDR2 α , green; CDR3 α , red; CDR1 β , yellow; CDR2 β , blue; CDR3 β , sand. The docking orientations of the respective TCRs are shown in black spheres and dash lines.

1.4 Conformational changes upon TCR-pMHC-I ligation

Unlike the lock and key mechanism for many protein interactions, the binding between the TCR and its pMHC-I target is characterized by its adaptability at the binding interface. This “plasticity” was typically described mainly within the TCR CDR loops, providing the structural basis for TCR binding degeneracy. However, there is also a growing appreciation on the role of pMHC-I flexibility that also contributes towards this process.

Understanding the conformational changes that take place upon TCR-pMHC-I engagement can be examined by comparing the structures of the individual component in their free and liganded states. For instance, comparing the murine 2C TCR in its unbound and its pMHC-I-bound states has revealed significant movements within three out of six CDR loops (CDR1 α , CDR3 α and CDR3 β) to allow close contact with the pMHC. The pMHC ligand on the other hand, remained structurally unchanged upon TCR binding in this system (Garcia et al., 1996; Garcia et al., 1999). Similarly, four out of six CDR loops (CDR1 α , CDR2 α and both CDR3 loops) from the human LC13 TCR also underwent conformational adjustments to enhance the complementarity of the binding interface (Kjer-Nielsen et al., 2002b; Kjer-Nielsen et al., 2003). Furthermore, TCR plasticity can also be examined by comparing its structural conformations bound to different pMHC-I ligands. For instance, the murine BM3.3 TCR that interacted with three antigenic pMHC-I landscapes has illustrated remarkable movements associated with the CDR3 β loop in order to accommodate altered pMHC-I landscapes (Mazza et al., 2007; Reiser et al., 2003; Reiser et al., 2000; Reiser et al., 2002).

In addition to the TCR malleability, pMHC flexibility also plays important roles in TCR-pMHC-I interaction. For instance, the Tax peptide bound to HLA-A*2 was “squished” into the Ag-binding groove upon A6 TCR binding (Garboczi et al., 1996). A similar, but more pronounced impact was evidenced by the “bulldozing” of the EPLP peptide upon ligation to the ELS4 TCR (discussed later) (Tynan et al., 2007). The recognition of the Telp1 peptide by the A6 TCR was also depicted by unexpected conformational readjustments in both the peptide and MHC-I (Borbulevych et al., 2009). Similarly, the nonamer MART-1 antigen also changed its conformation upon

binding to both the DMF4 and DMF5 TCRs (Borbulevych et al., 2011). Last but not least, this induced fit mechanism of the pMHC-I has also been reported to underpin T-cell allorecognition (Macdonald et al., 2009).

Collectively, conformational rigidity and plasticity serve as a key towards the binding specificity and degeneracy of the TCR-pMHC interaction. This adaptability can be attributed to the “moulding” of the CDR loops and/or the malleability of the pMHC ligands, allowing the optimal formation of stable TCR-pMHC-I interaction and the subsequent activation of T cells.

1.5 TCR recognition of lengthy antigens presented by MHC molecules

The presentation of antigens by MHC-I molecules is typically restricted to peptide length of 8-10 amino acids, partly due to the rigid closure of MHC-I Ag-binding cleft as well as the biased antigen-processing pathway that was described previously (section 1.1). However, at least 5% of the naturally presented self-peptide repertoire by MHC-I molecules comprises antigens longer than 10 amino acids (Hickman et al., 2004). Indeed, antigens comprising a proline at the amino terminal sequence are less likely to be transported via TAP (Androlewicz and Cresswell, 1996). This potentially implies that only peptides with a proline distally to the N-terminal end would be translocated via TAP into the ER. Furthermore, due to the unique backbone structure of proline residue, the ER aminopeptidase is also less efficient in trimming the proline-containing antigen (Androlewicz and Cresswell, 1996). Thus, the combination of these parameters can potentially result in the accumulation of relatively long peptide fragments in the ER, containing an X-Pro-X_n motif in their primary sequences. Whilst some MHC-I molecules are less likely to bind to these longer antigens as they require secondary peptide anchors which typically locates at the central part of the peptide (such as HLA-B*8 and HLA-B*14), a number of different MHC alleles are evolved to salvage such indigestible peptides by selecting a proline as the N-terminal anchor (P2 of the peptide that binds to the B pocket). These MHCs includes the HLA-B*7 supertype (**Table 2**) in human for instance, and specifically the HLA-B*35 allotype that is the focus of this thesis.

1.5.1 Structure of lengthy antigen bound to MHC class I molecule

To date, in contrast to our expanded knowledge on MHC-I presenting short peptide fragments, structural studies of lengthy antigen bound to MHC-I are relatively under-appreciated. In this context, there are currently only 17 unique MHC-I structures presenting antigens longer than 10 amino acids across different species and MHC-I alleles (**Table 4**). The first structural insight of lengthy antigen presentation by MHC-I came from the work done by Speir and colleagues (Speir et al., 2001). This crystal structure was determined to a resolution of 2.55 Å, consisting of a 13mer antigen derived from mitochondrial ATPase6 bound to the rat's MHC-I molecule, RT1-A^a. Strikingly, this structure showed that, although the N- and C-terminal anchors of the antigen were tethered similar to short peptides bound to MHC-I, the central region of the antigen adopted two completely distinct conformations with clear and unambiguous electron densities, protruding away from the Ag-binding cleft (**Figure 19a**). In these two conformations, the peptide was elevated approximately 13 Å and 15 Å above the MHC groove respectively. These observations not only demonstrate the “super-bulged” nature of lengthy antigen presented by MHC-I, but also illustrate the flexible nature of the lengthy antigen.

PDB code	Antigen length	MHC-I	Peptide conformation	Reference
1JPF	11mer	H-2D ^b	Ordered	(Ciatto et al., 2001)
1ZSD	11mer	HLA-B*35:01	Ordered	(Miles et al., 2005)
2BVO	11mer	HLA-B*57:03	Ordered	(Stewart-Jones et al., 2005)
2FYY	11mer	HLA-B*35:01	Flexible	(Miles et al., 2006)
2NW3	11mer	HLA-B*35:08	Flexible	(Tynan et al., 2007)
2HJK	11mer	HLA-B*57:03	Ordered	(Gillespie et al., 2006)
2XFX	11mer	N01301 (Cattle)	Ordered	(Macdonald et al., 2010)
2YF1	11mer	B21 (Chicken)	Ordered	(Koch et al., 2007)
2YPK	11mer	HLA-B*57:03	Ordered	(Stewart-Jones et al., 2012)
3BW9	12mer	HLA-B*35:08	Ordered, Helical	(Wynn et al., 2008)
1ED3	13mer	RT1-Aa	2 Conformations	(Speir et al., 2001)
1XH3	14mer	HLA-B*35:01	Flexible	(Probst-Kepper et al., 2004)
3LN4	16mer	HLA-B*41:03	Flexible	(Bade-Doding et al., 2011)
3LN5	11mer	HLA-B*41:04	Ordered	(Bade-Doding et al., 2011)
1ZHK	13mer	HLA-B*35:01	Ordered	(Tynan et al., 2005a)
3RWD	11mer	B*17 (Monkey)	Ordered	(Wu et al., 2011)
3VCL	11mer	HLA-B*07:02	Ordered	(Brennan et al., 2012)

Table 4 Crystal structures of lengthy antigens bound to MHC-I molecules.

Similar observations have also been noted in the HLA system. For instance, Bade-Doding and colleagues described the crystal structure of a 16mer antigen bound to HLA-B*41:03 (Bade-Doding et al., 2011). Unlike to the two alternate conformers seen in the RT1-A^a structure, the central region between P4 to P13 of the epitope was completely disordered and the electron density was absent (**Figure 19b**). On the other hand, the structure of a 13mer viral antigen (termed LPEP) bound to HLA-B*35:08 has illustrated a rigid and super-bulged peptide conformation, attributed partly by the proline-rich sequence within peptide (**Figure 19c**) (Tynan et al., 2005a). Although the mechanism governing antigen flexibility in these cases were unclear, factors such as the primary peptide sequence as well as inter-residue interactions are thought to constraint antigen mobility (Theodossis et al., 2010). Regardless, these atypical features of the MHC-restricted lengthy antigen presentation are considered to impose significant challenge for TCR engagement, and exactly what structure TCRs can adopt to “see” these structurally challenging targets while maintaining fine specificity towards the MHC-I landscapes remains to be elucidated.

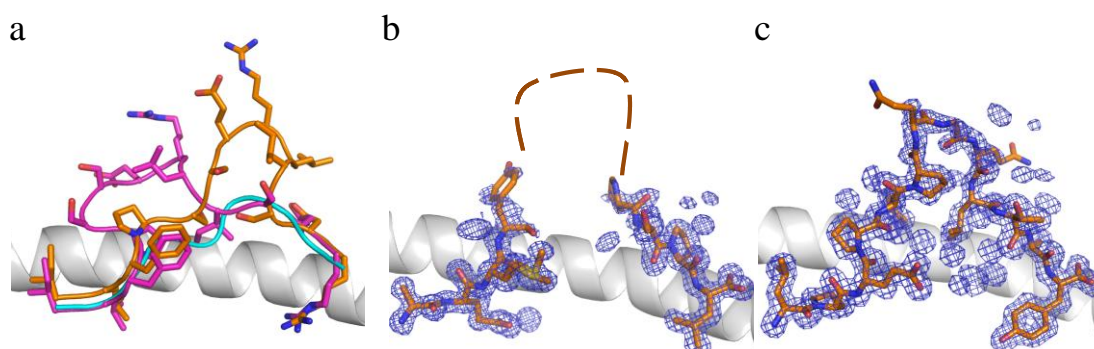


Figure 19 Lengthy epitopes presented by MHC molecules.

(a) The Rat’s MHC class I molecule (grey) presenting a 13mer peptide antigens revealed two alternative peptide conformations (orange and purple) that bulged away from the antigen-binding cleft. A 9mer antigen presented by HLA-B*8 is shown in cyan for comparison. PDB used: 1ED3 (RT1-A^a-13mer) (Speir et al., 2001) and 1MI5 (HLA-B*8-9mer) (Kjer-Nielsen et al., 2002a). (b) A 16mer epitope presented by HLA-B*41:03 demonstrated the flexible nature of the central peptide region. PDB used: 3LN4 (Bade-Doding et al., 2011). (c) A rigid and super-bulged peptide conformation was observed in the HLA-B*35:08-LPEP complex. PDB used: 1ZHK (Tynan et al., 2005a). Electron densities for (b) and (c) are generated from the 2Fo-Fc map.

1.5.2 Structural mechanism and insights into lengthy peptide-MHC recognition by the TCR

To date, of the 30 unique TCR-pMHC-I structures available, only three were determined in the context of longer antigens (excluding structures arising from this thesis). These studies arise exclusively from the human system, investigating T-cell mediated immune responses via the presentation of HLA-B*35 allotypes bound to antigens derived from a ubiquitous human pathogen, the Epstein-Barr Virus (EBV). Notably, among these TCR-pHLA-I systems, the binary structures of the pHLA complexes were also determined, enabling the visualization of conformational changes that take place upon TCR ligation.

To gain an understanding of TCR recognition towards longer antigenic targets, Tynan *et al* investigated CTL responses against a 13mer antigen (named LPEP) derived from the immunogenic lytic antigen BZLF1 (⁵²LPEPLPQGQLTAY⁶⁴) bound to HLA-B*35:08. The crystal structure of the immunodominant TCR (termed SB27) comprising a "public" V α chain (TRAV19*01) alongside with a biased V β (TRBV6-1*01) chain was determined in complex with HLA-B*35:08-LPEP (Tynan et al., 2005b). Interestingly, in the ternary complex structure, the SB27 TCR was able to dock onto the HLA-B*35:08-LPEP surface centrally and directly onto the bulged region of the LPEP antigen. It was also noted that the docking angle of SB27 TCR was orthogonal (**Figure 20**), contrasting to the canonical (diagonal) orientation for most TCR-pMHC-I systems determined at the time (Rudolph et al., 2006). When comparing the unliganded and liganded structures of the HLA-B*35:08-LPEP, there was no major structural movement associated with the LPEP peptide (**Figure 21a**). Indeed, due the rigid and bulged peptide landscape, the SB27 TCR mediated extensive contacts with the peptide primarily via the CDR3 α and the germline derived CDR1 β loop, whilst struggling to interact with the HLA surface. Thus, the SB27 TCR focused significantly more on the peptide (~45% BSA) than most other TCR-pMHC-I structures determined (typically ~20% BSA) (Godfrey et al., 2008; Rudolph and Wilson, 2002).

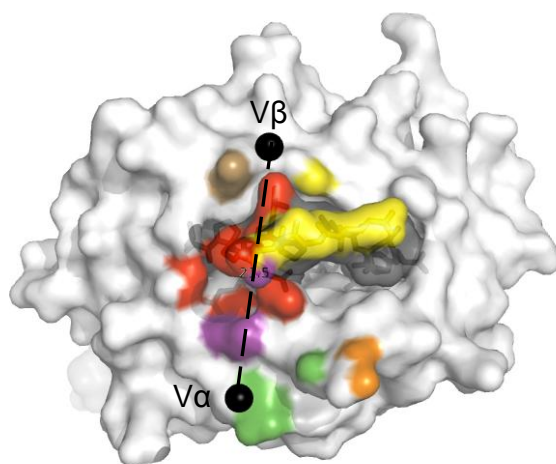


Figure 20 Diagonal docking orientation of the SB27 TCR towards the HLA-B*35:08-LPEP.

Structural footprint of the SB27 TCR on HLA-B*35:08-LPEP (white) is shown. The orthogonal docking orientation of the SB27 TCR is illustrated with the centre masses of the respective TCR variable domains (black spheres). MHC residues are coloured based on their contacts with the CDR loops (CDR1 α ; purple, CDR2 α ; green, CDR3 α ; red, CDR1 β ; yellow, CDR2 β ; sand and CDR3 β ; orange). PDB used: 2AK4 (Tynan et al., 2005b).

Another interesting observation in the SB27 system is that, although the SB27 only interacted minimally with the MHC, it can distinguish micropolymorphism of the HLA. That is, the SB27 TCR recognised the LPEP epitope bound to HLA-B*35:08 (Arg156), and differentiated the closely related allomorph, HLA-B*35:01 (Leu156), presenting the same antigen (Tynan et al., 2005b). Thus, HLA-B*35:01+ individuals responded weakly to the 13mer LPEP antigen, and the SB27 TCR also showed approximately 3.5-fold lower binding affinity towards the HLA-B*35:01-LPEP compared to HLA-B*35:08-LPEP (Tynan et al., 2005a). Structurally, although the single amino acid substitution between HLA-B*35:08 and HLA-B*35:01 did not act as a direct contacting point for SB27 recognition, but caused a rigid body shift around the hinge region of the α 2-helix between the HLA-B*35:01/08 binary structures (**Figure 21b**). This shift was considered, and recently demonstrated (by publications arising from this thesis), to dictate the fine HLA specificity of SB27, as most of the TCR-MHC contacts located within this region are critically important for the interaction (Liu et al., 2012). Collectively, the SB27 system demonstrated for the first time, how a TCR interacts with a “featured” pHLA landscape via an antigen-centric mode of binding, as well as providing insights into the fine-specificity of MHC restriction.

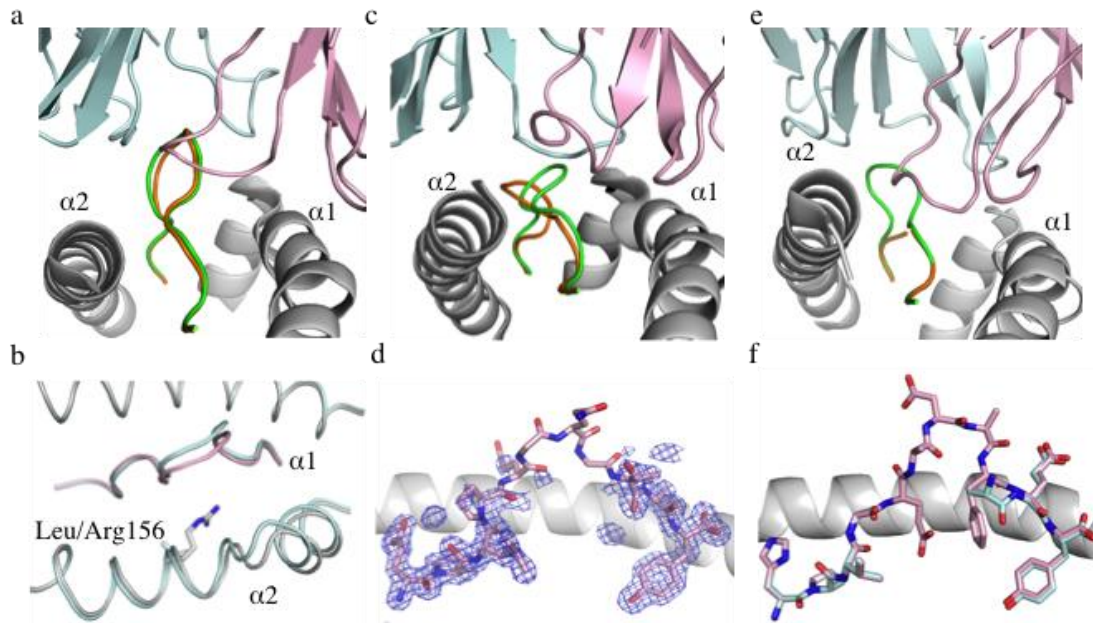


Figure 21 TCR recognition modes towards lengthy antigens presented by MHC-I molecules.

(a) The rigid LPEP peptide (orange and green) bound to HLA-B*35:08 (grey) remains structurally intact upon SB27 TCR binding (cyan and pink). PDB used: 1ZHL (binary complex) (Tynan et al., 2005a) and 2AK4 (ternary complex) (Tynan et al., 2005b). (b) Micropolymorphism of the HLA-B*35 causes a shift on the α 2-helix of HLA-B*35:01/08-LPEP. PDB used: 1ZHK (HLA-B*35:01) and 1ZHL (HLA-B*35:08) (Tynan et al., 2005a). (c) The ELS4 TCR “bulldozing” a 11mer epitope (green to orange) presented by HLA-B*35:01. PDB used: 1ZSD (binary complex) (Miles et al., 2005) and 2NX5 (ternary) (Tynan et al., 2007). (d) The EPLP peptide became flexible when presented by HLA-B*35:08. PDB used: 2NW3 (Tynan et al., 2007). (e) The flexible 11mer HPVG antigen is stabilized (orange to green) upon binding to the TK3 TCR. PDB used: 2FYU (binary) (Miles et al., 2006) and 3MV7 (ternary) (Gras et al., 2010). (f) The conformation of the HPVG peptide exhibits different flexibility when bound to HLA-B*35:08 (pink) and HLA-B*35:01 (cyan). PDB used: 2FYU (HLA-B*35:01) and 2FZ3 (HLA-B*35:08) (Miles et al., 2006).

To further investigate TCR binding strategy towards lengthy antigens, Tynan and colleagues determined the structure of the ELS4 TCR bound to HLA-B*35:01 presenting a 11mer viral epitope (termed EPLP, TRAV1-2*1 and TRBV10-3*01) (Tynan et al., 2007). The EPLP antigen ($^{54}\text{EPLPQGQLTAY}^{64}$) is an N-terminally truncated version of the 13mer LPEP antigen described earlier (Green et al., 2004). The binary structure of the HLA-B*35:01-EPLP demonstrated a bulged peptide conformation with unambiguous electron density (Miles et al., 2005). Strikingly, upon ELS4 ligation, residue 5 to residue 9 of the antigen was flattened as a result of the TCR central docking mode (**Figure 21c**). This mechanism is markedly in contrast to typical TCR-pMHC-I interactions where the plasticity of TCR CDR loops allows

them to mould around the pMHC-I ligand to achieve optimal binding. In fact, comparing the unliganded and liganded forms of the ELS4 TCR structures showed that only limited movement within the CDR3 α loop was observed, which was flexible and only partly resolved in its unliganded status. Thus, unlike the peptide-centric mode that governed the SB27 ternary complex, via “bulldozing” of the antigen, the ELS4 TCR was able to interact closely with both helices of the HLA-B*35:01 surface as well as P1 and P5 to P8 of the antigen to a lesser extent (Tynan et al., 2007).

Similar to the fine HLA specificity observed in SB27 system, the ELS4 TCR also exhibited remarkable HLA specificity towards the self-derived HLA-B*35:01, and responded weakly to the HLA-B*35:08 presenting the EPLP antigen (Tynan et al., 2007). To explore the underlying basis for such discrimination, Tynan and colleagues solved the structure of the EPLP bound to HLA-B*35:08 and compared it to that of the HLA-B*35:01-EPLP. Interestingly, unlike the rigid EPLP conformation bound to HLA-B*35:01, the central region of the antigen (P5 to P8) was mobile when presented by HLA-B*35:08 (**Figure 21d**). It was therefore considered that this difference in antigen flexibility, as well as the bulky polymorphic Arg156 side chain of the HLA-B*35:08, could act to potentially disturb the “bulldozing” of the peptide, which is important of ELS4 TCR recognition. As such, the ELS4 ternary complex illustrated a mechanism whereby TCR recognition is underpinned by the plasticity of MHC-bound epitope. This study also provides an alternative view for TCR fine-specificity towards MHC-I-restricted antigen recognition.

More recently, Gras *et al* has described the third system of TCR binding to a lengthy pHLA-I target. This study was initially established to understand the impact of TCR polymorphism and its functional impact, but nevertheless provided structural insights into longer epitope recognition. The TK3 TCR that was investigated, recognises a 11mer EBV viral antigen (HPVGEADYFEY, HPVVG) restricted to HLA-B*35:01 (Gras et al., 2010; Miles et al., 2006). Although the central region (P5 to P8) of the HPVVG peptide conformation was highly mobile in the binary structure of HLA-B*35:01-HPVVG, upon TK3 ligation, the HPVVG peptide was stabilized and bent towards the α 2-helix of the HLA-B*35:01 (**Figure 21e**). As a result, the TK3 TCR was able to contact both the peptide (42% of BSA) and the HLA surface (52% of BSA) (Gras et al., 2010). Due to the mobile HPVVG conformation in the HLA-

B*35:01-HPVG structure, it is not possible to visualize the conformational changes that took place upon TK3 binding. However, it is important to note that the TK3 TCR cross-reacted only weakly onto the rigid HPVG conformation presented by HLA-B*35:08 (**Figure 21f**). Therefore, contrasting to the ELS4 system, these observations suggest that antigen flexibility may also serve to facilitate TCR recognition, although the underlying mechanism governing TK3 recognition towards the HLA-B*35:08-HPVG is not fully explored.

My thesis describes two unique examples of TCRs bound to a super-bulged pHLA-I target. These structures have unmasked novel mechanisms that TCRs can adopt to overcome an atypical pMHC landscape, as well as shed lights into the fine-specificity of MHC restriction. These results are described and discussed in Chapter 4.

1.6 Research leading up to this project

Prior to the initiation of this project, a collaboration between the University of Melbourne, Queensland institute of Medical Research (QIMR), Cardiff University and Monash University was formed to investigate protective immune responses in HLA-B*35 positive individuals towards a ubiquitous human pathogen, the Epstein-Barr Virus.

1.6.1 Structural and biophysical investigations into TCR recognition towards a super-bulged pHLA molecule

In 2004, Professor Scott Burrows' group described a 13mer epitope derived from the lytic protein (BZLF1) of the Epstein-Barr virus that expresses a P2 proline and a C-terminal tyrosine motif in its primary sequence (⁵²LPEPLPQGQLTAY⁶⁴, LPEP) (Green et al., 2004). This antigen was presented by HLA-B*35:08 naturally via the compatible anchoring residues within the respective B and F pockets. Of note, the LPEP epitope was significantly longer than the canonical length of MHC-I bound peptide (8 to 10 amino acid long). In fact, the 13mer LPEP antigen represented the longest HLA-I restricted epitope identified at the time.

Table 5 T cell receptor repertoires arising from HLA-B*35:08+ individuals restricted to the LPEP antigen.

<i>CTL</i>	<i>TRAV</i>	<i>VJ</i>	<i>TRAJ</i>	<i>TRBV</i>	<i>VDJ</i>	<i>TRBJ</i>
SB27	19*01	CALSGFYNTDKLIF	34	6-1*01	CASPGLAGEYEQYF	2-7
CA5	19*01	CALSGFYNTDKLIF	34	6-1*01	CASPGETEAF	1-1
*SB47	39*01	CAVGGGSNYQLIW	33	5-6*01	CASSRTGSTYEQYF	2-7
SB9	19*01	CALSGFYNTDKLIF	34	7-2*01	CASSIGTGGSQPQHF	1-5
SB32	19*01	CALSGFYNTDKLIF	34	5-6*01	CASSKLGTSSEETQYF	2-5

* The genetic recombination of the SB47 TCR was re-confirmed. The SB47 TCR α chain shown here is different from the TRAV16*01/TRAJ56 described in the original literature. CTL clones under investigation in this thesis are highlighted in bold. [Table adapted and modified from Tynan and colleagues (Tynan et al., 2005a)].

To further investigate how HLA-B*35:08+ individuals respond to this viral determinant, CTL responses towards HLA-B*35:08-LPEP were examined. Strikingly, TCR repertoire analysis in two unrelated individuals showed that a biased V α usage of TRAV19*01/TRAJ34 gene was preferred, including a highly conserved N-region

in the CDR3 α loop that comprised a ⁹⁴Gly-Phe⁹⁵ binding motifs (CALSGFYNTDKLIF). The pairing of the respective V β chains on the other hand appeared to be more diverse, including the use of TRBV6-1*01, TRBV5-6*01 or TRBV7-2*01 chains, as well as differing CDR3 β loops (**Table 5**).

To understand the structural basis of immuno-recognition towards this unusually long antigen, members of the Rossjohn lab determined the crystal structure of the HLA-B*35:08-LPEP in its unliganded form, and sequentially in complex with the immunodominant TCR (termed SB27) (Tynan et al., 2005a; Tynan et al., 2005b). The binary structure of the HLA-B*35:08-LPEP revealed that the LPEP peptide formed a super-bulged conformation, which in turn drove a peptide-centric mode of recognition by the SB27 TCR. Nevertheless, the SB27 TCR was highly specific towards the HLA surface as it discriminated a single buried polymorphic variation between HLA-B*35:08 and HLA-B*35:01 (Arg156 and Leu156 respectively) (Tynan et al., 2005a; Tynan et al., 2005b).

Whilst the structure of the SB27-HLA-B*35:08-LPEP complex provides an interesting snapshot of how a TCR overcomes a structurally challenging pHLA-I landscape, due to the lack of biophysical examinations, the energetic basis governing lengthy antigen recognition by TCR, remains to be elucidated. Further, it also remained unclear, how differing TCR architectures, such as the CA5 (TRAV-19*01-TRAJ34, TRBV6*01-TRBJ-1-1), and perhaps more interestingly, the SB47 TCR that utilize a completely different V α -V β combination (TRAV39*01-TRAJ33, TRBV5-6*01-TRJB2-7), can impact on the specificity of antigen recognition.

1.6.2 The role of antigen flexibility in TCR cross-recognition

This part of my thesis arises from another system that investigated the CTL response towards a lengthy (11mer) EBV viral determinant (termed HPVG) that originates from residue 407 to 417 of the Epstein-Barr Virus Nuclear Antigen 1 (EBNA-1) protein in HLA-B*35 positive individuals (Blake et al., 1997; Lee et al., 2004; Miles et al., 2006; Tellam et al., 2004). In 2006, Miles and colleagues examined the CTL responses in HLA-B*35:01 and HLA-B*35:08 positive individuals and showed that a biased TCR repertoire was used to mount an immune response towards the HPVG antigen. Namely, regardless of the specific allotype (HLA-B*35:08/01) individual

exhibited, the TCR repertoire was highly restricted to the expression of the TRBV9*01 gene segment, alongside with varying sequences in the CDR3 β loop. The pairing of the TRAV gene on the other hand, was dependent on the particular allotype individual contained (Miles et al., 2006). In this context, the selection of the V α chain was dominated by TRAV20*01 in HLA-B*35:01+ individuals, whereas the TRAV29*01 gene segment was preferred in HLA-B*35:08+ individuals.

To understand how micropolymorphism can drive the different selections of TCR repertoires, crystal structures of the HPV β G antigen bound to HLA-B*35:01 and HLA-B*35:08 were determined to 1.5 Å and 1.9 Å resolution respectively (Miles et al., 2006). Whilst the differences between the two HLA allomorphs lied deeply within the Ag-binding cleft (position 156), the HPV β G conformation differed significantly between the two binary complexes. In particular, the HPV β G peptide in HLA-B*35:08 formed a typical super-bulged and rigid peptide conformation, whereas this same antigen was partially disordered when presented by the HLA-B*35:01 (refer to **Figure 20f**). As such, these differences in antigen mobility were thought to play important roles governing MHC-restricted TCR recognition in this system.

Another interesting observation arising from this study was that, the TK3 CTL that derived from HLA-B*35:01 positive individual, was able to cross-react towards HLA-B*35:08 presenting HPV β G, albeit less efficiently (Miles et al., 2006). Recently, members of the Rossjohn lab determined the structure of the TK3 TCR bound to the HLA-B*35:01-HPV β G, and provided the first insights how this antigen is detected by the immune system (Gras et al., 2010). Alongside with associated SPR data (and unpublished data), a remarkable binding degeneracy was demonstrated with the TK3 TCR. Indeed, the TK3 TCR was able to cross-recognise three naturally occurring HPV β G variants, presented by either HLA-B*35:08 or HLA-B*35:01, although these antigen variants appeared to be less potent than the cognate HPV β G bound to HLA-B*35:01. These antigens included the HPV β G-D5 (HPV β GDADYFEY) variant that dominates infection in the Chinese population (Wang et al., 2002; Zhang et al., 2004), the HPV β G-A4 (HPV β GAEADYFEY) variants from type 2 EBV viral strain (Dolan et al., 2006), as well as the HPV β G-Q5 (HPV β GQADYFEY) variants that was described in type 1 EBV isolates (Bell et al., 2008; Snudden et al., 1995). Taken together, the TK3 system represents an ideal system to examine TCR binding degeneracy in the

setting of lengthy antigens, and allows us to explore the underlying basis governing MHC-restricted recognition in protective immuno-recognition against a range of viral variants.

1.6.3 Research Project Aims

The research project of my thesis aims to explore the simultaneous binding specificity and degeneracy of TCR-pMHC-I interaction in the context of lengthy epitopes, derived from a range of different EBV viral determinants. On the basis of this, my project employs X-ray crystallography techniques, along with biophysical and cellular investigations, to understand the structural, functional and energetic basis governing TCR recognition towards lengthy antigens presented by MHC-I molecules.

My specific aims are:

1. To explore the energetic landscape of between the SB27-HLA-B*35:08-LPEP interaction via the use of alanine mutagenesis and affinity measurement (Surface Plasmon Resonance, SPR).
2. To obtain the crystal structures of the CA5 and SB47 TCRs bound to the “super-bulged” HLA-B*35:08-LPEP complex, and examine their fine-specificity towards the pHLA target via SPR.
3. To determine the binary and ternary structures of various HLA-B*35:01/08-HPVG variants bound to TK3 TCR, and investigate the underlying basis for TK3 cross-reactivity.

2 Materials and Methods

This thesis involves the biophysical and structural examinations of a range of TCR-pMHC complexes, including the SB27, SB47 and CA5 TCRs bound to HLA-B*35:01/08 presenting the LPEP variants, as well as the TK3 TCR that interacts with the HLA-B*35:01/08 bound to four HPVG peptide variants. Most of the methods and techniques are highlighted in the material and method sections of the corresponding publications. Thus, this section will cover a brief summary of the key experimental procedures that are involved.

2.1 Molecular cloning of expression vectors

Heavy chains of the HLA-B*35:08 and HLA-B*35:01, the human β 2m, and both chains of the SB27 TCR were developed previously in the laboratory by Tynan *et al* (Tynan *et al.*, 2005b). Similarly, α and β chains of the TK3 TCR were constructed by Gras *et al* (Gras *et al.*, 2010). On the other hand, the CA5 and SB47 TCR chains were synthesized, codon-optimized and purchased from Genescript (USA) for the *Escherichia coli* (*E.coli*) expression system. To clone all TCR chains into the pET30 expression vector, synthetic genes fragments from the supplied plasmid (pUC57) were excised via endonuclease digestions with commercially available restriction enzymes (New England Biolabs). This cleavage process was performed with buffers supplied by the manufacture at 37°C for two hours in order to reach completion. DNA fragments were separated on the basis of electrophoresis on a 1% agarose gel before being gel-purified using a DNA purification kit (Promega Corporation). Individual TCR genes were sequentially ligated into the pET30 vector via a T7 ligase overnight at 4°C. Plasmids containing the desired TCR genes were confirmed via DNA sequencing facility at the Monash University (Micromon). Notably, all TCR constructs described in this thesis were engineered with a disulfide linkage (Avidex system) between the two constant domains (TRAC48 to TRBC57) in order to assist the refolding procedure (Boulter *et al.*, 2003).

For alanine scanning mutagenesis studies, mutants of the HLA-B*35:08 and SB27 TCR were generated via the site-directed mutagenesis protocols (QuikChange, Stratagene). Briefly, approximately 30 ng of the DNA template was mixed with

synthetic oligonucleotides (GeneWorks), dNTP (2.5 mM final concentration), 2.5 units of Pfu DNA polymerase, and the supplied reaction buffer. This mixture was subjected to 18 Polymerase Chain Reaction (PCR) cycles to allow adequate DNA products to be produced. The parental DNA template was removed using the restriction enzyme digestion with the DpnI (New England Biolabs) for 2 hours at 37 °C. Plasmids were transformed into the XL1 blue strain *E.Coli* competent cells and colonies carrying the desired mutations were selected based on sequencing results (Micromon, Monash University).

2.2 Production and purification of the HLA-B*35 molecules

The expression of HLA-B*35:01/08 heavy chains and β 2m subunit were carried out in BL21 (DE3) *E.coli* competent cells. Following on a standard 5-hour isopropyl β -D-1-thiogalactopyranoside (IPTG)-induced expression, cells were lysed via the addition of lysozyme, and the inclusion bodies were extracted via repetitive washing and centrifugation steps with the wash buffer (10 mM Tris-HCl, pH 8, 5%-TRITON-X100). Pellets of inclusion bodies were solubilized in urea buffer containing 10 mM Tris-HCl, pH 8, 8 M urea, 1 mM dithiothreitol (DTT) and 0.2 mM phenylmethanesulfonylfluoride (PMSF). The purity and quantity of the inclusion body preparation was assessed via a 15% sulfate polyacrylamide gel electrophoresis (SDS-PAGE) using standard bovine serum albumin (BSA) solutions with known concentrations.

The production of MHC variants followed the refolding protocol that was previously established by Garbozi *et al* (Garboczi et al., 1992). Typically, 30 mg of the HLA heavy chain and 15 mg of the β 2m proteins were co-injected into a refolding solution (100 mM Tris-HCl, pH 8, 2 mM Ethylenediaminetetraacetic acid (EDTA), 400 mM L-Arginine, 0.5 mM oxidized Glutathione and 5 mM reduced Glutathione) alongside with 10 mg of the synthetic peptides that was pre-dissolved in 100% dimethyl sulfoxide (DMSO). This refolding mixture was left at 4°C with constant stirring for two days, and the HLA heavy chain was re-injected at 12 and 24 hours post the initial injection. After 48 hours of the refolding step, the protein mixture was dialyzed against 15 L of Tris-HCl buffer (10 mM Tris-HCl, pH 8) three times daily to allow effective removal of urea from the buffer.

To purify the properly folded pHLA, protein sample was loaded by gravity onto a Diethylaminoethyl cellulose (DEAE) column that was pre-equilibrated in 10 mM Tris-HCl, pH 8 at 4°C. The protein was then eluted with buffer containing 10 mM Tris-HCl, pH 8 and 150 mM NaCl. The eluted protein sample was then concentrated to <4 ml and loaded onto a size-exclusion chromatography column (16/60 Superdex 200, Amersham Pharmacia, Uppsala, Sweden). Fractions containing folded pHLA, as judged by the 15% SDS-PAGE, were pooled, concentrated and subjected to a HiTrap Q (anion exchange) purification step. A NaCl gradient (0 to 1 M) with the buffer containing 10 mM Tris-HCl, pH 8 was used to elute pHLA complex from the HiTrapQ column. The final purity was analysed by SDS-PAGE. To ensure the purified pMHC-I complexes were properly folded, samples were tested by binding against the conformational specific antibody, W6/32 (Parham et al., 1979a).

2.3 Production and purification of recombinant TCRs

The production of the TCR is similar to that of the HLA molecules described above with minor adjustments. Namely, 50 mg of the TCR α and β chains were injected into the refolding buffer with the addition of urea (5 M final concentration). Both TCR chains were re-injected (50 mg of each) 12 hours post the initial injection, and the samples was dialyzed and loaded onto the DEAE column accordingly. To elute the protein from DEAE, buffer containing 10 mM Tris-HCl, pH 8 and 400 mM NaCl was used. After DEAE purification, the TCR sample was applied onto a size-exclusion purification step before being subjected to an additional hydrophobic interaction column (HIC) in order to remove unfolded proteins from the sample. The HIC chromatography was conducted in buffer containing 10 mM Tris-HCl and 0.8 M ammonium sulphate. Properly folded TCR was obtained in the flow-through and buffer-exchanged into 10 mM Tris-HCl before a final HiTrapQ purification step was conducted. The purity and quality of the TCR sample was measured by 15% SDS-PAGE under reducing and non-reducing conditions. The conformational integrity of the refolded TCR was tested using the conformational specific antibody, 12H8 (Borg et al., 2005).

2.4 Production, biotinylation and tetramerization of pHLA-B*35:08

To generate pHLA-B*35:08 tetramers for the cellular experiment (described in chapter 3), heavy chains of different HLA-B*35:08 variants were cloned to include an additional C-terminal BirA tag in pET30 expression vector. The expression, refold and purification of the HLA-B*35:08-BirA variants were performed identically to that of the untagged constructs. To biotinylate the samples, properly folded HLA-B*35:08-BirA variants were firstly desalted and buffer exchanged into 10 mM Tris-HCl, pH 8 before concentrating to 0.5-1 mg/ml protein concentration. The process of HLA-B*35:08-BirA biotinylation was conducted at room temperature overnight, by incubating 1 mg of the protein sample with 2.5 μ g of the BirA enzyme in a buffer containing 50 mM bicine pH, 8.3, 10 mM adenosine triphosphate (ATP), 10 mM MgOAc and 50 mM d-biotin. Excessive free biotin and reaction buffer were removed sequentially by buffer exchanging into 10 mM Tris-HCl, pH 8. The efficiency of sample biotinylation was calculated based on a pull-down experiment using commercially available Streptavidin sepharose beads (GE Heathcare), judging from the ratio of unbound and bound samples on a SDS-PAGE.

In order to produce pHLA tetramers, 15 μ l of the commercially available Streptavidin-PE (Invitrogen) was added repetitively to 100 μ g biotinylated HLA-B*35:08-BirA at an interval of every 10 minutes (a total amount of 150 μ l Streptavidin-PE was added). Excessive pHLA and unbound Streptavidin-PE were removed via buffer exchange using a 100 KDa cut-off concentrator. The quality of the tetramers was assessed and compared by native gel electrophoresis. All tetramer-staining experiments were performed and analysed as described in the Chapter 3 under material and method section with the help from our collaborator, Dr. Zhenjun Chen at the University of Melbourne.

2.5 Thermal stability experiments

Thermal stability experiments for the pHLA variants were performed using a Real Time detection instrument (Corbett RotorGene 300). Briefly, all protein samples were prepared in TBS buffer (10 mM Tris-HCl, pH 8, 150 mM NaCl) and tested in replicates at two different concentrations, 1 and 0.5 μ M. Using an excitation wavelength of 530 nm and an emission wavelength at 555 nm, a final concentration

of 10X fluorescence dye (Sypro orange) was added to the pHLA samples in order to monitor the process of protein unfolding. The temperature of the sample was increased steadily from 30°C to 90°C at a speed of 1°C/min, and changes in fluorescent intensity were recorded accordingly. To determine the thermal melting temperatures (T_m) of all protein samples, changes of fluorescent signals were normalized from 0 to 100% and the T_m value was determined based on the temperature where half (50%) of the maximum signal changes were observed.

2.6 Surface Plasmon Resonance

All Surface Plasmon resonance experiments were conducted via a BIA3000 instrument at 25°C with HBS buffer containing 10 mM HEPES, pH 7.4, 150 mM NaCl, 0.005% P20, and 1% bovine serum albumin supplement to avoid non-specific binding. The 12H8 conformational specific anti-body (Borg et al., 2005) produced by our collaborator from the McCluskey laboratory at University of Melbourne was covalently coupled to a research grade CM5 sensorchip via standard amine coupling methods. For individual experiment, approximately 200-400 response units (RU) of the different TCRs were passed over and captured onto independent flow cells, whilst the first flow cell was always left uncoupled as a negative control. Different HLA-B*35 variants, ranging between 200 μ M to 0.78 μ M were injected onto all flow cells at a speed of 30 μ l/min, and the final response were calculated from subtraction of the control flow cell. All experiments were conducted at least in duplicates and the surface of the TCR bound 12H8 sensorchip was regenerated between each analyte injection with Actisep (Sterogene). Finally, to analyse the result, sensorgrams were exported to BIAevaluation program version 3.0 and fitted with a 1:1 Langmuir binding model with the addition of drifting baseline parameter when required.

2.7 Crystallisation and data collection

All crystallisation trials were performed using the vapor-diffusion technique at 20°C. In this context, crystals of HLA-B*35:08 variants were obtained at 5 mg/ml protein concentration with the reservoir solution (0.2 M sodium citrate, pH 5.6, 0.2 M ammonium acetate, and 16-18% polyethylene glycol (PEG) 4000) at a 1:1 drop ratio. Similarly, the CA5 TCR-pHLA-I complex crystallized at 9 mg/ml protein concentration in a reservoir solution containing 0.2 M potassium iodide, 0.1 M

sodium cacodylate, pH 6.7, and 16% PEG 3350. Crystals of the TK3 TCR-pHLA-I variants were obtained in at 6 mg/ml protein concentration in a reservoir solution comprising 0.2 M lithium sulphate, 0.1 M sodium citrate (pH 5.6), and 18% PEG3350 with cross-seeding techniques from the TK3-HLA-B*35:01-HPVG crystals. For the SB47 ternary complex, crystallisation trial was initially conducted in a 96-well format using the “Crystalmation” facility at Monash University with commercially available screening kits. Subsequent crystal production and optimization was achieved using a 24-well tissue culture Linbro® plate. Crystals were harvested and flash-frozen with reservoir solution containing increased PEG concentration (typically 30%) as cryoprotectant before being exposed to X-ray radiation source at the Australian synchrotron, Clayton. Data were collected either via the ADSC-Quantum 210 CCD detector on MX1 beamline or ADSC-Quantum 315r CCD on MX2 beamline at 100K.

2.8 Structural determination and refinement

All datasets were integrated with the XDS program, scaled with XSCALE software (Kabsch, 2010) or SCALA in the CCP4 suit (Winn et al., 2011). Structures were solved via molecular replacement with PHASER (McCoy et al., 2007), using the HLA-B*35:01/08 without the peptide (for HLA), the SB27 or TK3 TCR (for TCR) as search models. Manual building of structures was performed with COOT (Emsley and Cowtan, 2004), while the maximum-likelihood refinement was conducted using PHENIX (Adams et al., 2002) and Buster (Bricogne G., 2011). All structures were validated via the protein data bank validation server (<http://www.rcsb.org/pdb/home/home.do>). Graphic representations were generated using PyMol (DeLano Scientific).

2.9 Structural analysis

Structural analyses for all projects were carried out using the CCP4 suit (Winn et al., 2011). The contacts table was generated using the CONTACT program, with a distance cutoff of 4 Å for VDW interactions, 3.5 Å for H-bonds and 5 Å for the presence of salt bridges. The buried surface area for all complexes was calculated using AREAIMOL (Lee and Richards, 1971). The B factor of the protein was calculated using Baverage, and the r.m.s.d. values between different PDB models were measured via SUPERPOSE (Krissinel and Henrick, 2004). The centre masses of

the TCR V α and V β domains were determined using AREAIMOL in order to measure the docking angle relative to the long peptide axis of the pHLA complex.

3 Results: The energetic basis of TCR recognition towards a bulged viral antigen bound to a HLA molecule

Structural and biophysical investigations into TCR-pMHC-I interactions have focused primarily on peptide length of 8-10 amino acids, a typical length for MHC-I restricted epitope. However, lengthy peptides (>10aa) can often bind to MHC-I and manifest in both protective and aberrant cellular immunity. In this context, the SB27 TCR that arises from HLA-B*35:08+ individual described previously, represents a well-established example to demonstrate anti-viral immune responses against a super-bulged EBV viral determinant (LPEP). Notably, the structure of SB27 TCR-pHLA-I complex has illustrated the characteristics that were unusual for typical TCR-pMHC-I interactions reported to date (Rudolph et al., 2006). In particular, the SB27 TCR docked orthogonally onto HLA-B*35:08 whilst made limited contacts with the HLA surface. Despite limited TCR-HLA contacts, SB27 TCR showed remarkable specificity towards HLA-B*35:08 and finely distinguished the closely related HLA-B*35:01.

Using the published SB27-HLA-B*35:08-LPEP structure as a guide, my work published in the *Journal of Biological Chemistry* (Liu et al., 2012), employed an alanine mutagenesis approach in conjunction with surface plasmon resonance technique, to investigate the energetic basis governing this TCR-pHLA-I interaction, alongside with associated cellular data (tetramer staining), this study showed that, similar to the peptide-focused nature of the SB27 ternary complex, the binding energetic rested heavily around the ascending part of the peptide as well as the corresponding TCR-contacting residues. In contrast, HLA residues contributed minimally to the binding interface, with only two critical hot spots (>5-fold reduction in affinity) located exclusively on the α 2-helix of HLA-B*35:08 (refer to **Figure 4** and **Table 2** of this journal). Collectively, these findings represent the first energetic mapping of TCR-pMHC-I interaction in the context of lengthy antigen. These results also illustrate that lengthy epitope presentation by MHC-I can drive the focus of TCR recognition towards the peptide antigen which in turn, impact on the selection, function and fine specificity of T-cells.

The Energetic Basis Underpinning T-cell Receptor Recognition of a Super-bulged Peptide Bound to a Major Histocompatibility Complex Class I Molecule^{*,§}

Received for publication, January 19, 2012. Published, JBC Papers in Press, February 16, 2012. DOI 10.1074/jbc.M112.344689

Yu Chih Liu[‡], Zhenjun Chen[§], Scott R. Burrows^{¶1}, Anthony W. Purcell^{||2}, James McCluskey[§], Jamie Rossjohn^{†3,4}, and Stephanie Gras^{‡4,5}

From the [‡]Department of Biochemistry and Molecular Biology, Monash University, Clayton, 3800, the Departments of [§]Microbiology & Immunology and ^{||}Biochemistry and Molecular Biology and Bio21 Molecular Science and Biotechnology Institute, University of Melbourne, Parkville, 3010, and the [¶]Queensland Institute of Medical Research and Australian Centre for Vaccine Development, Brisbane 4006, Australia

Background: T-cell receptor (TCR) recognition of a lengthy peptide-human leukocyte antigen (HLA) complex indicates a peptide-centric mode of interaction.

Results: The energetic landscape of this interaction is centered on the peptide and peptide-contacting residues.

Conclusion: Lengthy peptides drive a more peptide-focused mode of TCR recognition.

Significance: This is the first description of the energetic landscape underpinning TCR recognition of lengthy HLA-restricted peptides.

Although the major histocompatibility complex class I (MHC-I) molecules typically bind short peptide (p) fragments (8–10 amino acids in length), longer, “bulged” peptides are often presented by MHC-I. Such bulged pMHC-I complexes represent challenges for T-cell receptor (TCR) ligation, although the general principles underscoring the interaction between TCRs and bulged pMHC-I complexes are unclear. To address this, we have explored the energetic basis of how an immunodominant TCR (termed SB27) binds to a 13-amino acid viral peptide (LPEPLPQGQLTAY) complexed to human leukocyte antigen (HLA) B*3508. Using the crystal structure of the SB27 TCR-HLA B*3508^{LPEP} complex as a guide, we undertook a comprehensive alanine-scanning mutagenesis approach at the TCR-pMHC-I interface and examined the effect of the mutations by biophysical (affinity measurements) and cellular approaches (tetramer staining). Although the structural footprint on HLA B*3508 was small, the energetic footprint was even smaller in that only two HLA B*3508 residues were critical for the TCR interaction. Instead, the energetic basis of this TCR-pMHC-I interaction was attributed to peptide-mediated interactions in which the complementarity determining region 3 α and germline-encoded complementarity determining region 1 β loops of the SB27 TCR played the principal role. Our findings highlight

the peptide-centricity of TCR ligation toward a bulged pMHC-I complex.

The specificity of cytotoxic T-cells is characterized by the surface expression of the $\alpha\beta$ T-cell receptor (TCR),⁶ which recognizes peptide fragments (typically between 8 and 10 amino acids in length) presented by class I major histocompatibility complex (MHC-I) molecules on target cells. The antigen-recognition site of the TCR is comprised of six complementarity-determining regions (CDRs), three each from the TCR α and β chains, of which the CDR1 and -2 loops are germline encoded, whereas the CDR3 loops can be comprised of germline-encoded and non-germline-encoded regions. The rearrangement of TCR gene elements yields a potential 10¹⁵ different TCRs in humans, which after undergoing positive and negative selection represent a mature T-cell repertoire of $\sim 10^8$ different TCRs (1). Typically, the antigenic peptide is tethered within the antigen (Ag)-binding cleft of the MHC molecule, whereupon a few of the surface-exposed amino acids represent potential TCR contact points (2). Accordingly, relative to the short peptide, the polymorphic MHC-I heavy chain dominates the interactions with the TCR (3). Successful peptide-MHC (pMHC) engagement by the TCR is an obligate requirement for thymic selection and for the recognition of foreign Ags in the periphery, which subsequently leads to a series of effector functions. Accordingly, understanding the factors that dictate the nature of the TCR-pMHC engagement is an area of intense interest. However, generalizations regarding the nature of this interaction are compounded by the extensive human leukocyte antigen (HLA) polymorphism and the diverse T-cell repertoire.

* This work was supported in part by the Australian National Health and Medical Research Council (NHMRC) and the Australian Research Council.

§ This article contains supplemental Tables S1 and S2 and Fig. S1.

¹ NHMRC Principal Research Fellow.

² NHMRC Senior Research Fellow.

³ Australia fellow of the NHMRC. To whom correspondence may be addressed. E-mail: jamie.rossjohn@monash.edu.

⁴ Joint senior authors.

⁵ Supported by a Senior Fellowship from Monash University. To whom correspondence may be addressed: Bldg. 76, Ground Floor, Rm. G12, Dept. of Biochemistry & Molecular Biology, School of Biomedical Sciences, Monash University, Clayton, Vic 3800, Australia. Tel.: 613-99029227 and 99029236; E-mail: Stephanie.gras@monash.edu.

⁶ The abbreviations used are: TCR, T-cell receptor; MHC-I, major histocompatibility complex class I; CDR, complementarity determining region; Ag, antigen; MF, mean fluorescence; HLA, human leukocyte antigen; SPR, surface plasmon resonance; VDW, van der Waals.

Peptide Focused TCR Recognition

Structural studies have shown that the TCR can engage the pMHC-I surface in a wide range of docking modes (4). Nevertheless, a conserved docking mode between the TCR-pMHC-I is observed, in which the V α and V β domains are positioned over the MHC α 2- and α 1-helices, respectively, suggesting some hidden basis in TCR-pMHC engagement that may be attributable to signaling outcome (5, 6). Whether this hidden logic is underpinned by germline-encoded TCR-MHC recognition remains an area of intense investigation (7–11). The insight gleaned from TCR-pMHC-I structural studies have been bolstered significantly by associated biophysical, thermodynamic, and mutational studies, which have shown that the relative energetic contributions from the CDR loops can vary between different TCR-pMHC systems (7, 12–19). To date, most of the structural/mutagenesis studies have focused on TCR recognition of short peptides (8–10 amino acids), whereas it is known that ~5–10% of the repertoire of peptides bound to MHC-I can be longer than 10 amino acids in length (20, 21).

Indeed, there is a growing understanding of the role longer MHC-I-restricted peptides play in immunity, where these longer determinants can form targets for MHC-restricted cytotoxic T-cells in tumor immunity and viral immunity (8, 22–24). The size limitation of peptides binding to MHC-I is, in part, defined by the hydrogen bonding network at the N- and C-terminal ends of the Ag binding cleft. As such, longer peptides generally bulge centrally from the Ag-binding cleft. Some of these long bulging MHC-I peptides display substantial mobility, whereas others assume a more rigid conformation, and thus they may be considered to potentially represent challenges for TCR ligation. Indeed, biased (immunodominant) TCR usage has been found as a mechanism for the adaptive immune system to deal with such challenging MHC-restricted viral peptides (11, 25). For example, biased TCR usage was observed against a flexible 11-mer peptide (EPLPQGQLTAY) (26) and a rigid 13-mer peptide (LPEPLPQGQLTAY, termed “LPEP”) (27) restricted to HLA B*3501 and HLA B*3508, respectively. The flexible 11-mer determinant was flattened upon TCR ligation, enabling the TCR to make substantial contacts with HLA B*3501 (28). In contrast, in recognizing the rigid 13-mer peptide, the prototypical biased TCR (termed SB27) made extensive peptide contacts but limited contacts with HLA B*3508 (29). As such, the SB27 TCR made noticeably fewer contacts with the MHC in comparison to TCRs interacting with canonical length (8–10-mer) epitopes. Given this observation, we aimed to explore the energetic basis of the SB27 TCR-HLA B*3508^{LPEP} interaction. How important are the TCR-MHC contacts in comparison to the TCR-peptide interactions? Our data show that longer peptides drive peptide-focused TCR recognition.

EXPERIMENTAL PROCEDURES

Generation of SB27 TCR and HLA B*3508 Mutants—Collectively, 28 single alanine mutants and 2 glycine substitutions (if the C β atoms only were involved in the contact) were made on either the SB27 TCR or HLA B*3508. These mutants were generated via site-directed mutagenesis techniques (QuikChange; Stratagene) with DNA templates that were previously described (8).

Protein Expression and Purification—Individual chains of the SB27 TCR, HLA B*3508 and the β ₂-microglobulin were expressed as inclusion bodies in BL21(DE3) *Escherichia coli* cells, followed by refolding procedures as previously described (29). Post-refolding samples were dialyzed against 10 mM Tris-HCl, pH 8, twice daily and further purified through anion exchange chromatography and size-exclusion chromatography. The purity and the molecular weight of the samples were assessed with SDS-PAGE.

Surface Plasmon Resonance—Using a BIAcore 3000 instrument, all surface plasmon resonance (SPR) experiments were measured at 25 °C with a buffer containing 10 mM HEPES, pH 7.4, 150 mM NaCl, 0.005% surfactant P20, and 1% bovine serum albumin to avoid nonspecific binding. With a research grade CM5 sensorchip, a conformational specific monoclonal antibody (12H8) (12) was amine-coupled onto the surface to capture properly folded wild type or mutated SB27 TCR. Typically, one of the four flow cells was left empty without coupling any TCR (the control), whereas the other three flow cells were used to capture SB27 TCR (and mutants) to ~200–400 response units. Serial dilutions of HLA B*3508^{LPEP} (or variants thereof) ranging between 0.78 and 200 μ M were prepared and injected into the flow cells individually and the antibody surface was regenerated with Actisep (Sterogene) between each injection. All experiments were performed in duplicates and the kinetic constants were determined by the BIAevaluation program (version 3.1) using 1:1 Langmuir binding models with the addition of a drifting baseline parameter.

Thermal Stability Assay—Thermal stability assays of HLA B*3508^{LPEP} variants were performed with the Real Time Detection instrument (Corbett RotorGene 300). Briefly, all pHLA samples were prepared at two concentrations (5 and 10 μ M) in 10 mM Tris-HCl, pH 8, and 150 mM NaCl buffer. The fluorescent dye Sypro orange were added to the sample to enable monitoring of the protein unfolding process. Samples were heated from 30 to 95 °C at the rate of 1 °C/min and the changes in fluorescent intensity were recorded accordingly with the excitation wavelength of 530 nm and the emission wavelength at 555 nm. The results are summarized in supplemental Table S1.

Crystallization of pHLA and Structure Determination—Crystals of selected HLA B*3508^{LPEP} variants were obtained by the hanging-drop, vapor-diffusion method at 20 °C. Protein samples at 5 mg/ml concentration were mixed with the reservoir solution (0.1 M sodium citrate, pH 5.6, 16% polyethylene glycol (PEG) 4000, and 0.2 M ammonium acetate) at a 1:1 ratio. Microseeding techniques were applied to allow the formation of crystals with optimal size. Crystals of pHLA variants were soaked with reservoir solution containing an increased percentage of PEG 4000 (30%) followed by flash freezing in liquid nitrogen. All data were collected at the Australian synchrotron, Clayton, with an ADSC-Quantum 210 CCD on MX1 and an ADSC-Quantum 315r CCD on MX2 detector (at 100 K). The datasets were processed with XDS software (30), scaled with XSCALE and the structures were solved by molecular replacement using PHASER (31) and the published HLA B*3508^{LPEP} structure (PDB code 1ZHK (27)) minus the peptide as a search model. Manual building of all pHLA variants were performed with COOT (32) and further refined using maximum-likeli-

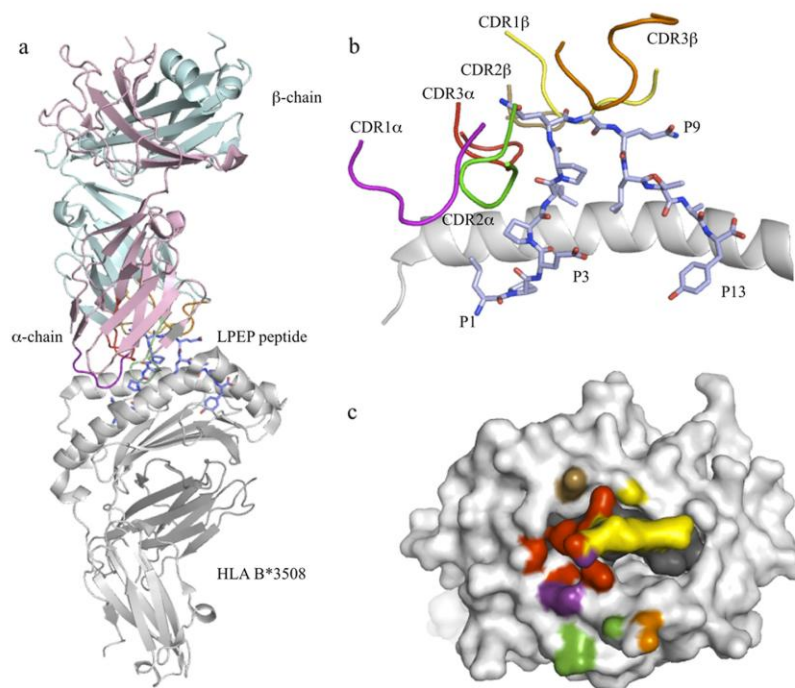


FIGURE 1. **Overview of the SB27 TCR interaction with the HLA B*3508^{LPEP}.** *a*, the SB27 TCR is represented in schematic with the α -chain in pink, the β -chain in blue, the CDR1, -2, and -3 α are purple, green, and red, and the CDR1, -2, and -3 β colored in yellow, brown, and orange, respectively. The HLA B*3508 is represented as a white schematic and the β_2 -microglobulin in gray, with the LPEP peptide in blue stick. *b*, close-up of the SB27 CDR loops interacting with the bulged LPEP peptide (blue stick), with the CDR loops colored accordingly to panel *a*. *c*, peptide centric structural footprint of the SB27 TCR on the HLA B*3508^{LPEP} surface (white), the atoms of the HLA B*3508 and LPEP peptide involved in the interaction are colored by the CDR loops contacted accordingly to panel *a*.

hood refinement with PHENIX (33) and the structural representation showed in all figures were generated using PyMOL (30). The final models have been validated and submitted using the Protein Data Base validation web site and the final refinement statistics and PDB accession codes are summarized in supplemental Table S2.

Retroviral Transduction into SKW3 Cells—The transduction of the SKW3 cell lines was carried out as previously described (8). In brief, 4 μ g of pMIG plasmid containing SB27 or LC13 TCR (used as control) was mixed with two retroviral packaging vectors DNA (2 μ g of each pPAM-E and pVSV-g) and FuGENE-6. The mixture was used to co-transfect a total number of 10^6 293T epithelial cells. The transfected 293T cells were cultured further for 5 days and all virus-containing supernatants were harvested and replaced twice daily to transduce SKW3 cells with the addition of 6 μ g/ml of Polybrene. After 3–5 days of transduction, the surface expression level of TCRs on the SKW3 cells was monitored using FACS. TCR positive cells were enriched, and cloned, with a BD FACSAria cell sorter.

Fluorescence-activated Cell Sorting (FACS) and Tetramer Binding Assay— 10^5 SKW3-SB27 cells and the positive control SKW3-LC13 cells were stained with the anti-CD3 antibody (OKT3) on ice for 30 min or with peptide-loaded HLA class I-multimers (HLA B*3508^{LPEP}-PE tetramer) at 26 °C for 45 min. After washing twice with FACS buffer (phosphate-buffered saline containing 2% fetal calf serum and 0.02% azide), the

cells were run through a FACS-calibur or FACS-Aria with Cell-QuestPro and analyzed with FlowJo. For cell sorting experiments, the desired number of cells was stained similarly and all steps were carried out aseptically in a Bio-hazardous hood and filter-sterile reagents. Tetramer binding was measured by the increase of the mean fluorescence (MF) of tetramer staining. The TCR expression level was normalized with tight gating on the expression of green fluorescent protein (GFP), which correlated well with TCR expression levels in the transfected cells.

RESULTS

Experimental Rationale—To define the underlying energetic basis of the interaction between SB27 TCR and HLA B*3508^{LPEP}, we undertook an alanine scanning approach on both the SB27 TCR and HLA B*3508^{LPEP}. We analyzed the effect of the mutations on the affinity of the interaction using surface plasmon resonance (SPR), and furthermore, the effect of the HLA B*3508 mutants were investigated via cell surface staining using tetrameric versions of the mutants. Given the structure of the SB27 TCR-HLA B*3508^{LPEP} complex had been solved (29) (Fig. 1), we were able to rationalize the SB27 TCR and HLA B*3508^{LPEP} residues selected for mutational analysis. Solvent-exposed SB27 TCR residues whose side chains interacted with HLA B*3508^{LPEP} were selected for substitution to alanine. Similarly, HLA B*3508 residues, as well as those from the viral peptide, were selected for substitution if their side

Peptide Focused TCR Recognition

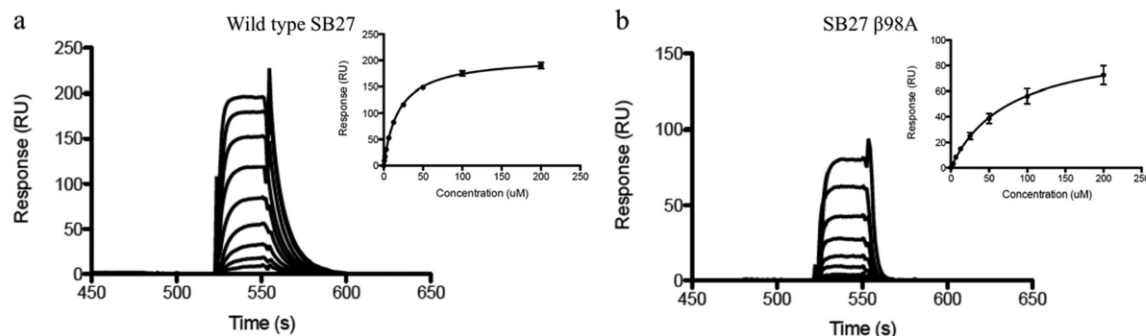


FIGURE 2. **Surface plasmon resonance experiment of SB27 TCR variants binding to HLA B*3508^{LPEP}.** Kinetic rate constant measurements of the SB27 TCR (a) and SB27- β Ala⁹⁸ TCR (b), binding to a concentration series of HLA B*3508^{LPEP} complex; inset, equilibrium concentration versus response relationship. The experiments have been conducted in duplicate and the error bars are shown for each data point (mean \pm S.E.).

chains made contact with the SB27 TCR. In total, the effect of 34 mutations was investigated (18 from the TCR, 10 from HLA B*3508, and 6 from the LPEP peptide), thereby permitting a comprehensive understanding of the energetic basis of this interaction.

SB27 TCR Mutations—The cytotoxic T-cell response to the HLA B*3508^{LPEP} epitope exhibited biased α -chain usage, with the SB27 TCR representing an archetypal clonotype of this T-cell repertoire (34) (encoded by the *TRAV19*01*, *TRAJ34*01*, *TRBV6-1*01*, and *TRBJ2-7*01* genes (35)). The SB27 TCR docked orthogonally across the Ag-binding cleft to accommodate the bulged epitope (Fig. 1a), in which the V α chain leaned toward the α 2-helix, whereas the V β chain formed few contacts with HLA B*3508, and interacted more extensively with the peptide (29). In brief, the CDR1 α , CDR2 α , and CDR3 α loops provided the main contacts with HLA B*3508 (Fig. 1, b and c), whereas the CDR1 β loop played a prominent role in interacting with the peptide, thereby underscoring the differing roles underpinning the biased V α and V β usage in the SB27 TCR.

In total, 18 (17 alanine and β S31G) mutants were generated within the α and β chains of SB27, which included β Asn⁶⁶ as a negative control (this residue was not involved in binding to HLA B*3508^{LPEP}). The residues that were mutated within the various CDR loops were: CDR1 α , α Thr²⁹ and α Tyr³¹; CDR2 α , α Asn⁵⁰ and α Phe⁵²; CDR3 α , α Ser⁹³, α Phe⁹⁵, α Tyr⁹⁶, and α Asn⁹⁷; CDR1 β , β Asn²⁸, β His²⁹, β Asn³⁰, β Ser³¹, β Tyr³³; CDR2 β , β Ser⁵¹; CDR3 β , β Pro⁹⁵, β Leu⁹⁸, and β Glu¹⁰¹ and the framework residue β Asn⁶⁶. We mutated, expressed, refolded, and purified all mutants and, to ensure the structural integrity of these mutants, we compared their biochemical characteristics and reactivity toward a conformationally specific TCR mAb (PDB 12H8) (12). All mutants behaved similarly to the wild type SB27 TCR (data not shown), thereby ensuring the conformational integrity of the targeted mutants.

First, we measured the affinity and kinetic rate constants of the wild-type (WT) SB27 TCR-HLA B*3508^{LPEP} interaction. The SB27 TCR bound HLA B*3508^{LPEP} with a $K_{d,eq}$ of $18.7 \pm 0.4 \mu\text{M}$, an on rate (K_{on}) of $6.56 \times 10^4 \text{ M s}^{-1}$; and a dissociation constant (K_{off}) of 0.12 s^{-1} , values that were consistent with previous measurements (29) (Fig. 2a, Table 1). Although these WT $K_{d,eq}$ measurements were reproducible on two separate

occasions and using two separate batches of WT SB27 TCR, all the SB27 TCR mutants (example shown in Fig. 2b) were, nevertheless, analyzed in the same experiment, in duplicate and relative to the same batch of WT SB27 TCR. This was to ensure that all the $K_{d,eq}$ values were comparable and relative to one another (see Table 1). SB27 TCR mutations that caused less than a 3-fold loss in the affinity of the interaction with HLA B*3508^{LPEP} compared with WT SB27 TCR were considered to have no major effect; a 3–5-fold effect as moderate, and anything greater than 5-fold as critical to the energetics of the interaction.

CDR1 α Loop—The CDR1 α loop is situated above the α 2-helix of HLA B*3508, forming interactions with a single HLA residue as well as the peptide antigen. Two mutants were investigated within this loop; namely α Thr²⁹, which contacted Ala¹⁵⁸, and α Tyr³¹, which contacted the peptide P7-Gln. Neither the α T29A nor α Y31A mutants impacted on the affinity of the interaction, indicating that the germline-encoded CDR1 α loop played a marginal role toward Ag recognition.

CDR2 α Loop—The CDR2 α loop contains two residues (α Asn⁵⁰ and α Phe⁵²) that contact the α 2-helix of HLA B*3508 (Fig. 3a). α Asn⁵⁰ hydrogen bonds (H-bonds) exclusively to Glu¹⁵⁴, and the corresponding α N50A mutant had a critical impact on the affinity of the interaction (Table 1). α Phe⁵² formed van der Waals (VDW) contacts with three HLA B*3508 residues (Glu¹⁵⁴, Arg¹⁵⁷, and Ala¹⁵⁸) and the α F52A mutation abrogated HLA B*3508^{LPEP} recognition. Accordingly, the mutational data showed that the CDR2 α played a critical role in the interaction with the HLA B*3508^{LPEP} complex.

CDR3 α Loop—The CDR3 α loop of SB27 TCR contains four residues that bind to HLA B*3508^{LPEP} via side chain-mediated interactions (Fig. 3b), namely α Ser⁹³ from the V α gene, α Phe⁹⁵ from the non-germline-encoded region and α Tyr⁹⁶ and α Asn⁹⁷ from the J α gene. The CDR3 α loop ran across the α 1 and α 2 helices of HLA B*3508, flanking the N-terminal end of peptide that bulges out from the Ag-binding cleft. α Ser⁹³ is located directly above, and contacted P7-Gln; α Phe⁹⁵ and α Tyr⁹⁶ contacted the α 2-helix of HLA B*3508 (spanning between Gln¹⁵⁵ and Leu¹⁶³) as well as the peptide (between P4 to P7) via VDW and H-bond interactions; and α Asn⁹⁷ H-bonded to Gln⁶⁵ and interacted with P5 to P7 of the peptide. Given the extent of

TABLE 1

Surface plasmon resonance analysis on SB27 TCR mutations

$t_{1/2} = 0.693/K_{d,eq}$, $\Delta\Delta G = RT\ln(K_{d,mut}/K_{d,WT})$, where R is the gas constant, T represents temperature in Kelvin, mut is the mutant studied and WT for the wild type SB27 TCR. *, less than 3-fold decrease difference compared to wild type affinity; **, between 3- and 5-fold decrease; ***, greater than 5-fold decrease. NB for non-binding observed at a maximum concentration of 200 μ M HLA B*3508^{LPEP}, and ND, not determined.

SB27 residues	K _{d,eq} (μM)	K _{on} (x10 ⁴ Ms ⁻¹)	K _{off} (s ⁻¹)	t _{1/2} (s)	ΔΔG _{eq} (kcal/mol)	Contact	Effects on affinity
Wild type	18.7 ± 0.4	6.56 ± 0.68	0.12 ± 0.01	8.42 ± 0.35			
CDR1α							
T29A	15.1 ± 1.3	5.91 ± 0.68	0.21 ± 0.01	4.78 ± 0.24	-0.13 ± 0.05	HLA	*
Y31A	22.1 ± 2.7	5.58 ± 0.01	0.18 ± 0.02	5.58 ± 0.51	0.10 ± 0.07	Peptide	*
CDR2α							
N50A	>200	ND	ND	ND	>1.40	HLA	***
F52A	NB	ND	ND	ND	>1.40	HLA	***
CDR3α							
S93A	>200	ND	ND	ND	>1.40	Peptide	***
F95A	NB	ND	ND	ND	>1.40	pHLA	***
Y96A	>200	ND	ND	ND	>1.40	pHLA	***
N97A	>200	ND	ND	ND	>1.40	pHLA	***
CDR1β							
N28A	26.6 ± 1.8	4.76 ± 0.14	0.16 ± 0.01	6.46 ± 0.25	0.21 ± 0.04	Peptide	*
H29A	NB	ND	ND	ND	>1.40	Peptide	***
N30A	75.0 ± 0.1	ND	ND	ND	0.82 ± 0.00	pHLA	**
S31G	>200	ND	ND	ND	>1.40	Peptide	***
Y33A	NB	ND	ND	ND	>1.40	Peptide	***
CDR2β							
S51A	11.0 ± 0.9	7.09 ± 0.25	0.09 ± 0.01	10.91 ± 0.23	-0.32 ± 0.05	HLA	*
Framework							
N66A	17.4 ± 0.2	7.04 ± 0.54	0.13 ± 0.01	7.67 ± 0.03	-0.04 ± 0.01	None	*
CDR3β							
P95A	NB	ND	ND	ND	>1.40	Peptide	***
L98A	77.0 ± 1.0	ND	ND	ND	0.84 ± 0.01	HLA	**
E101A	20.3 ± 1.4	5.89 ± 0.44	0.16 ± 0.01	6.37 ± 0.34	0.05 ± 0.04	HLA	*

these contacts, the corresponding mutations, unsurprisingly, all had a critical effect on the affinity of the interaction (Table 1). This highlights the important role the CDR3α loop played in contacting the peptide and the HLA B*3508 molecule.

CDR1β Loop—Five HLA B*3508^{LPEP} residues within the CDR1β loop were mutated, where all but one residue (βAsn³⁰) exclusively contacted the peptide (between P5 and P10) (Fig. 3c, Table 1). The βH29A, βS31G, and βY33A mutants were judged to be critical for the interaction, whereas βN30A and βN28A had a moderate and negligible effect, respectively. Accordingly, the germline-encoded CDR1β loop was observed to play a critical role in the energetics of the interaction, principally by interacting with the bulged peptide.

CDR2β and CDR3β Loops—The CDR2β loop contributes minimally to the SB27 TCR-HLA B*3508^{LPEP} interface, and mutation of the sole CDR2β contacting residue, βSer⁵¹, did not impact on the affinity of the interaction (Table 1). The CDR3β loop contains three residues that contact HLA B*3508^{LPEP}, the βPro⁹⁵ sat above P7-Gln, whereas the βLeu⁹⁸ and βGlu¹⁰¹ contact HLA B*3508. The βE101A mutant did not impact on the affinity of the interaction, indicating that the salt bridge between βGlu¹⁰¹ and Arg¹⁵¹ was not energetically important for SB27 TCR binding (Fig. 3d, Table 1). Furthermore, whereas βLeu⁹⁸ formed VDW contacts with numerous HLA B*3508 residues, the βL98A mutation only resulted in a moderate impact on the binding affinity (Table 1). In contrast, the βP95A mutant significantly impacted on the affinity of the interaction, thereby highlighting the importance of this peptide-mediated contact.

Next, we mapped the impact of the mutated SB27 TCR residues onto its structure to evaluate the location and size of the energetically important residues (the hot spot). The substitutions that had a marked effect on the affinity of the interaction formed a central strip on the surface of the Ag-binding domain of the SB27 TCR (Fig. 4a). Collectively, of the six CDR loops mutated in the SB27 TCR, the sum energetic contributions indicated that CDR3α ≈ CDR1β > CDR2α > CDR3β >> CDR1α ≈ CDR2β.

Energetic Landscape on HLA B*3508^{LPEP} Surface—To assess how HLA B*3508 contributes energetically toward SB27 TCR recognition, based on the crystal structure of the ternary complex, we substituted 10 HLA B*3508 residues to alanine, which included one control mutation (Gln⁷²) that was not involved in the interaction with the SB27 TCR. Additionally, one HLA B*3508 residue was mutated to glycine (A158G). HLA B*3508^{LPEP} mutations that caused less than a 3-fold loss in the affinity of the interaction with SB27 TCR compared with WT HLA B*3508^{LPEP} were considered to have no major effect; a 3–5-fold effect as moderate, and anything greater than 5-fold as critical to the energetic of the interaction.

Of the 10 selected and refolded single-site HLA B*3508 mutants, three and seven were located on the α1 helix (Gln⁶⁵, Thr⁶⁹, and Gln⁷²) and α2-helix (Arg¹⁵¹, Glu¹⁵⁴, Gln¹⁵⁵, Arg¹⁵⁷, Ala¹⁵⁸, Glu¹⁶¹, and Glu¹⁶³), respectively. We used SPR to measure the effect of the mutations, and established that the Q72A mutant did not affect the binding affinity. Of the two TCR-contacting residues located on the α1-helix (Q65A and T69A), neither of the corresponding mutations affected the binding

Peptide Focused TCR Recognition

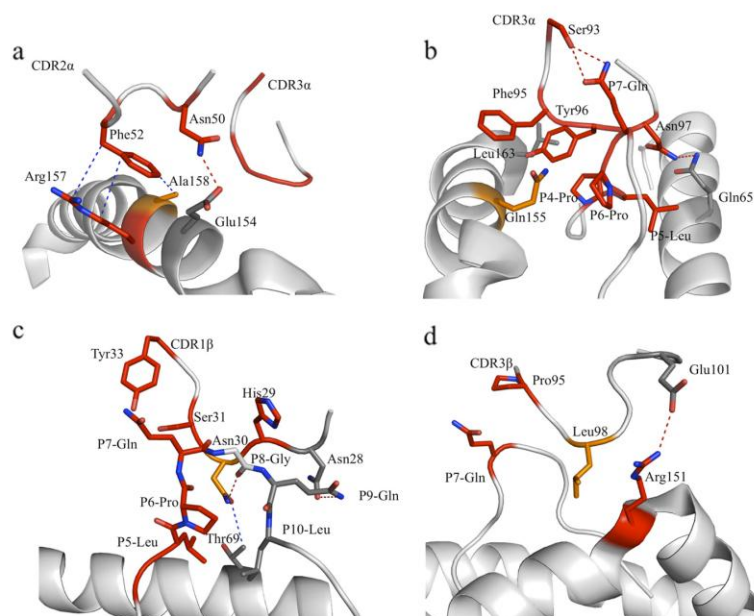


FIGURE 3. Interaction of the SB27 TCR with the HLA B*3508^{LPEP} complex. The residues on the four panels are colored according to the mutagenesis study, *red* are critical, *orange* moderately important, *gray*, did not affect the interaction, and *white* were not mutated. *a*, the CDR2 α loop interacts with the HLA B*3508 residues, Arg¹⁵⁷ (*red*), Glu¹⁵⁴ (*gray*), and Ala¹⁵⁸ (*orange*) and makes contacts with the CDR3 α loop. *b*, the CDR3 α spanning across both HLA helices, represented in *white schematic*, mediating critical contacts (*red* residues) with the peptide and the HLA residues. *c*, the CDR1 β loop "walls" the bulged peptide, forming an extensive bonding network primarily with the antigen. *d*, the CDR3 β contacts P7-Gln of the peptide and the Arg¹⁵¹ of the HLA B*3508 by VDW interaction and a salt bridge, respectively. H-bonds are represented with *red dashed line*, VDW in *blue dashed lines*. (PDB access code 2AK4).

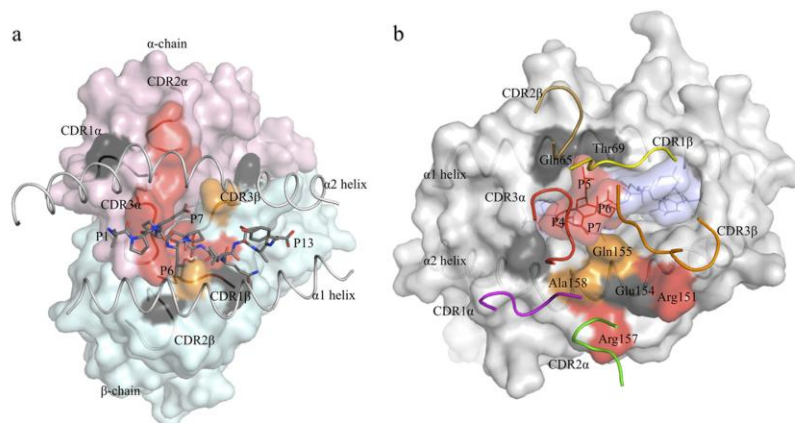


FIGURE 4. Energetic hot spots of the SB27-HLA B*3508^{LPEP} complex. *a*, surface representation of the SB27 TCR, with the α -chain in cyan; β -chain in pink; six CDR loops and the HLA B*3508^{LPEP} helices are shown as schematic representation; P4-P7 of the peptide are shown in green sticks. The critical residues are in red; the residues of moderate importance for the interaction are in orange; and the residue in dark gray were not important for the interaction. *b*, surface representation of the HLA B*3508 (*white*) bound to the LPEP peptide (*light blue*). SB27 CDR loops and the HLA B*3508 helices are shown as schematic representations. The CDR loops are colored in pink, green, and red for the CDR1, -2, and -3 β , respectively. The critical residues are colored in red, the residues of moderate importance for the interaction are in orange, and the residues in dark gray were not important for the interaction. PDB access code 2AK4.

affinity, thereby indicating that residues within the α 1-helix were dispensable for the interaction with the SB27 TCR. Of the six α 2-helix residues that were involved in contacts with the SB27 TCR, the mutational SPR analyses indicated that Glu¹⁵⁴ and Leu¹⁶³ were not required for the interaction. Interestingly α Asn⁵⁰, which contacted Glu¹⁵⁴, was shown to be critical for

the interaction. However, the TCR residue α Asn⁵⁰ also made intra-TCR contacts with the CDR3 α loop, and thus the role of the α Asn⁵⁰ side chain appears to be in maintaining the structural integrity of the SB27 TCR binding site. Indeed, the energetic hot spot on the HLA B*3508 surface was narrowed down to only two critically important residues (Arg¹⁵¹ and Arg¹⁵⁷)

TABLE 2

Surface plasmon resonance analysis on HLA-B*3508^{LPEP} mutations

$t_{1/2} = 0.693/K_{d,eq}$, $\Delta\Delta G = RT \ln(K_{d,mut}/K_{d,WT})$, where R is the gas constant, T represents temperature in Kelvin, mut is the mutant studied and WT for the wild-type HLA or peptide. *, less than 3-fold decrease difference compared to wild type affinity; **, between 3- and 5-fold decrease; ***, greater than 5-fold decrease, ND, not determined.

Residue	K _{d,eq} (μM)	K _{on} (x10 ⁴ Ms ⁻¹)	K _{off} (s ⁻¹)	t _{1/2} (s)	ΔΔG _{eq} (kcal/mol)	Contact	Effects on affinity
Wild type	18.7 ± 0.4	6.56 ± 0.68	0.12 ± 0.005	8.42 ± 0.35			
						Peptide contacted	
Q65A	12.1 ± 0.6	9.85 ± 1.86	0.135 ± 0.002	7.43 ± 0.14	-0.26 ± 0.03	N	*
T69A	10.5 ± 2.1	9.79 ± 1.11	0.094 ± 0.009	10.59 ± 0.97	-0.35 ± 0.12	Y	*
Q72A	28.0 ± 1.6	3.57 ± 0.48	0.125 ± 0.010	8.00 ± 0.06	-0.06 ± 0.08	N	*
R151A	188 ± 11.0	ND	ND	ND	-1.36 ± 0.03	N	***
E154A	27.8 ± 1.8	4.93 ± 0.01	0.082 ± 0.005	12.14 ± 0.72	0.35 ± 0.15	N	*
Q155A	89.8 ± 5.3	ND	ND	ND	1.04 ± 0.15	Y	**
R157A	>200	ND	ND	ND	>1.40	N	***
A158G	81.7 ± 3.0	ND	ND	ND	0.87 ± 0.02	N	**
E161A	41.0 ± 3.0	ND	ND	ND	0.72 ± 0.07	N	*
L163A	23.7 ± 1.1	3.23 ± 0.09	0.0785 ± 0.001	12.74 ± 0.23	0.14 ± 0.03	Y	*
						TCR contacted	
P4	119.0 ± 1.0	ND	ND	ND	1.09 ± 0.005	Y	***
P5	>200	ND	ND	ND	>1.40	Y	***
P6	>200	ND	ND	ND	>1.40	Y	***
P7	>200	ND	ND	ND	>1.40	Y	***
P9	20.9 ± 0.4	4.47 ± 0.01	0.093 ± 0.018	10.74 ± 2.14	0.06 ± 0.01	Y	*
P10	44.5 ± 1.5	ND	ND	ND	0.51 ± 0.02	Y	*

and two moderately important residues (Gln¹⁵⁵ and Ala¹⁵⁸), all located near the hinge region of the α2-helix (Fig. 4b, Table 2). Although Gln¹⁵⁵ H-bonded to the SB27 TCR and participated in stabilizing the peptide conformation, Arg¹⁵¹, Arg¹⁵⁷, and Ala¹⁵⁸ pointed away from the Ag-binding cleft, and contacted the TCR mainly via VDW contacts and one salt bridge (Arg¹⁵¹ and βGlu¹⁰¹ from the CDR3β loop), although the corresponding βE101A mutation indicated that the salt bridge was not energetically important.

To address if any of these four mutants (Arg¹⁵¹, Gln¹⁵⁵, Ala¹⁵⁸, and Arg¹⁵⁷) indirectly impacted on HLA B*3508^{LPEP} stability or peptide conformation, we undertook thermal stability assays, control SPR experiments, as well as structural studies. The thermal stability assay showed that all four HLA B*3508^{LPEP} mutants exhibit comparable melting temperature (T_m) to the wild type HLA B*3508 (supplemental Table S1). Arg¹⁵¹ and Arg¹⁵⁷ form intra-chain salt bridges (with HLA B*3508 Glu¹⁵⁴ and Glu¹⁶¹, respectively), and thus we considered that the Arg¹⁵¹ and Arg¹⁵⁷ mutants may have impacted on the local conformation of HLA B*3508, thereby indirectly impacting on SB27 TCR recognition. Thus we conducted the reciprocal mutagenesis experiments, and demonstrated that the E154A and E161A mutations did not impact the binding affinity (Table 2). Furthermore, to ascertain whether the mutations caused conformation shifts in the peptide itself, we determined the structures of the four HLA B*3508^{LPEP} mutants (supplemental Fig. 1a and supplemental Table S2). We showed that the peptide structure remains intact regardless of the HLA mutation introduced (root mean square deviation on the Ag-binding cleft range between 0.22 and 0.32 Å). As such, we concluded that the four HLA B*3508 hot spots were acting directly on SB27 TCR binding.

Significant Peptide Contribution to SB27 TCR Binding—To compare the relative energetic contribution of the peptide as opposed to the HLA B*3508 molecule toward SB27 TCR recog-

nition, we next mutated the six peptide positions that contacted SB27 TCR and undertook SPR-based affinity measurements. The peptide residues included P4-Pro, P5-Leu, P6-Pro, P7-Gln, P9-Gln, and P10-Leu-residues that spanned the bulged region of the peptide (Fig. 3c). First we assessed the thermal stability and structural impact of these introduced peptide mutations. The thermal stability assays demonstrated that only the P4-Pro to Ala mutant decreased the stability of the HLA B*3508^{LPEP} complex appreciably (by 9 °C) (supplemental Table S1). Furthermore, the crystal structure of the various HLA B*3508^{LPEP} peptide mutants showed that the conformation of the bulged peptide was not impacted significantly for five of them (supplemental Fig. S1b and Table S2). The P5-Leu mutation to alanine increased the mobility of the peptide, which leaned more toward the α1-helix of the HLA B*3508. This highlighted the importance of the P5-Leu residue for the peptide structure and so its recognition by the TCR. Thus, with the exception of P5-Leu mutant, any potential effect of peptide mutants could be attributable to directly impacting on SB27 TCR recognition. Although mutation of the two residues at the C-terminal end of the peptide (Pro⁹–Pro¹⁰) did not affect the affinity of the interaction, mutation of the Pro⁴–Pro⁷ positions resulted in marked reduction in binding affinity. Accordingly, the ascending and central region of the peptide bulge was critical for SB27 TCR recognition (Fig. 3c, Table 2). The ΔΔG analysis showed that, whereas the peptide only represents a small component of the solvent accessible HLA B*3508^{LPEP} interface, it contributes 56% to the overall energetics of the interaction with the SB27 TCR (Table 2).

The reciprocal mutagenesis on HLA B*3508^{LPEP} allowed us to determine the importance of the peptide and the HLA heavy chain on the TCR-contacting residues. The SB27 TCR utilized only one critical (αPhe⁵²) and three moderately (βLeu⁹⁸, αPhe⁹⁵, and αTyr⁹⁶) important residues to contact HLA B*3508. This is in marked contrast with the eight critical res-

Peptide Focused TCR Recognition

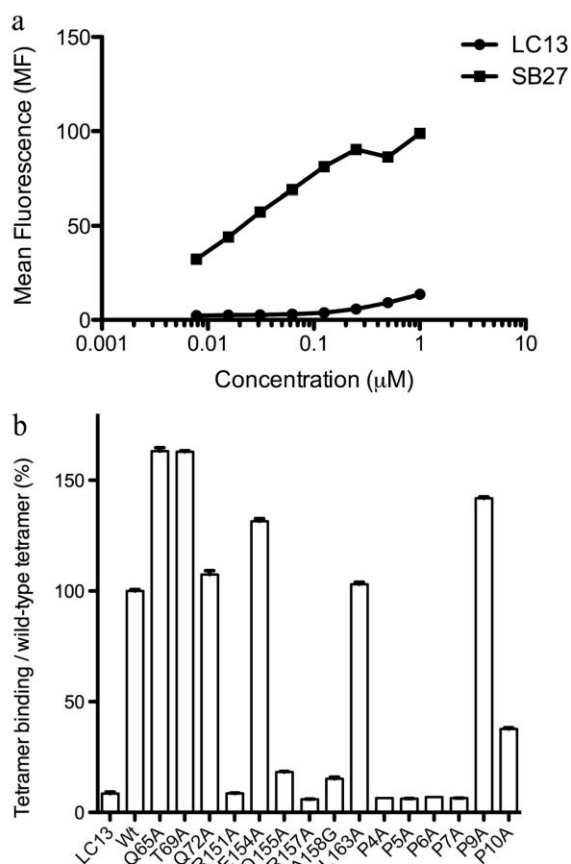


FIGURE 5. Fluorescence-activated cell sorting experiments. *a*, titration of SKW3-SB27 and SKW3-LC13 cells with different concentrations of wild type HLA B*3508^{LPEP} multimer. The MF of HLA B*3508^{LPEP} multimer staining is shown on the y axis and the final concentration of the multimer is shown on the x axis. *b*, the impact of HLA B*3508^{LPEP} variants were measured by tetramer staining (single concentration representing 50% of the maximum binding for the WT tetramer) and the percentage of binding is calculated by comparing with the wild type tetramer staining. The experiments on both panels have been carried in triplicate and the error bars show the mean \pm S.E.

dues (α His²⁹, α Ser³¹, α Tyr³³, α Ser⁹³, α Phe⁹⁵, α Tyr⁹⁶, α Asn⁹⁷, and β Pro⁹⁵) and one moderately (α Asn³⁰) important residue used to contact the peptide.

Cellular Assays—Next we established whether the peptide-centric nature of the SB27 TCR, as judged by SPR analysis, was also observed at the cellular level. We transduced the SB27 TCR and LC13 TCR (as a negative control) into the $\alpha\beta$ TCR negative SKW3 cell line and titrated these cells with different concentrations of wild-type HLA B*3508^{LPEP} tetramer (Fig. 5*a*). This allowed us to determine the HLA B*3508^{LPEP} tetramer concentration at which half of the maximum staining level was reached, as well as establishing the background MF. Using this value, we assessed the multimer staining level achieved using the HLA B*3508^{LPEP} mutants and compared these values to wild type staining.

Of the nine HLA B*3508 mutants tested (Glu¹⁶¹ excluded), five mutant multimers (Q65A, T69A, R72A, E154A, and L163A) stain comparably to the wild-type tetramer (Fig. 5*b*). For the Q155A and A158G mutants, low levels of tetramer staining were observed with an MF of 18.2 and 15.2%, respectively, compared with the WT tetramer. Furthermore, when R151A and R157A multimers were tested, very low MF levels were observed, values that were similar the negative control (SKW3-LC13) background level. Last, in the context of various peptide mutants, the tetramer binding results showed that P4 to P7 of the peptide were critically important for T cell binding. Accordingly, there was a strong correlation between the SPR data and the cellular staining data, which collectively demonstrated that the SB27 TCR-HLA B*3508^{LPEP} interaction was dependent on a few HLA B*3508 residues and was largely focused on a number of peptide-mediated contacts.

DISCUSSION

Structural and associated biophysical investigations of TCR-pMHC-I interactions have primarily focused on peptides of canonical length (8–10 amino acids), in which the peptide sits flush with the Ag-binding cleft, thereby making it challenging, *a priori*, to ascertain the relative roles of the peptide *versus* the MHC molecule in “driving” the interaction with the TCR. Some studies have indicated that the conserved TCR-pMHC docking topology is dictated by TCR-MHC contacts (9), whereas other studies have shown the peptide-centricity of the interaction (37). Indeed, it has recently been shown that energetic importance of V β -MHC contacts can be modified by the V α chain of the TCR (10, 11). Moreover, the absolute importance of TCR-MHC contact points can be dictated by the fine specificity that the TCR exhibits toward a viral epitope (14, 38, 39). However, as observed in viral immunity and autoimmunity, lengthy peptides can sit high above the Ag-binding cleft, thereby making their role in enabling the TCR-pMHC interaction intuitively clearer (29, 40). However, very little is known regarding how longer MHC-I restricted peptides determine the selection of the TCR repertoire as well as how TCRs recognize such featured landscapes. To address this, previously we investigated the biased T-cell repertoire selection against HLA B*3508^{LPEP}, and determined how the prototypical TCR (SB27) engaged HLA B*3508^{LPEP}. The SB27 TCR had a finger grip hold on the MHC while forming numerous contacts with the bulged viral determinant. However, it was unclear whether the limited TCR-MHC contact points represented the key energetic contributors to the interaction, or whether the TCR-peptide interactions played the prominent role. Guided by the SB27 TCR-HLA B*3508^{LPEP} crystal structure, using a mutagenesis, SPR, and cellular approach, we demonstrate that the SB27 TCR-MHC structural footprint is small, the corresponding energetic footprint is smaller still, with no residues on the α 1-helix of HLA B*3508 being required for the interaction. The MHC residues that contribute to the interaction were limited to two key residues (Arg¹⁵¹ and Arg¹⁵⁷) and two residues that played a moderate role (Gln¹⁵⁵ and Ala¹⁵⁸) that were located at the “elbow” region of the α 2-helix. Notably, the SB27 TCR, despite the limited involvement of MHC residues, is restricted to HLA B*3508, and does not cross-react to the closely related allo-

morph (HLA B*3501). HLA B*3501 is distinguished from HLA B*3508 by a single buried polymorphism at position 156 (Arg¹⁵⁶ in HLA B*3508; Leu¹⁵⁶ in HLA B*3501). The effect of this polymorphism is to cause a rigid body shift in the region of the α 2-helix (27) (residues 145–158) that overlaps with the MHC energetic hot spot. This highlights how the SB27 TCR shows remarkable fine specificity toward HLA B*3508.

We show that of the six peptide residues contacted by the SB27 TCR, four are critical to the interaction, thereby showing, in relative and absolute terms, that the LPEP peptide contributes markedly more toward the energetic landscape of the interaction than the HLA B*3508 molecule. Thus, the peptide centrality observed in the crystal structure is mirrored by the peptide-centric energetic landscape. A previous study has suggested that a two-step binding mechanism underpins the TCR-pMHC interaction whereby the germline-encoded loops engage the MHC initially, followed by the molding of the CDR3 loops around the peptide Ag (41). This model is hard to reconcile in the recognition of lengthy MHC-I restricted peptides, where it is more likely that the peptide-centric focus of the TCR dictates the initial interaction, and TCR-MHC interactions are subsequently formed that collectively enable productive TCR-pMHC-I engagement.

Given that the super-bulged peptide plays a central role in contributing to the energetic landscape, the question arises whether the responding TCR repertoire has been shaped primarily based on its ability to primarily recognize the peptide. The TCR repertoire directed toward HLA B*3508^{LPEP} in unrelated individuals exhibits a public α -chain (*TRAV19*01*, *TRAJ34*01*) and a highly conserved β chain (*TRBV6-1*01*), which differs only in the CDR3 β loop sequences. Our data demonstrated that CDR2 α and CDR3 α loops play an important energetic role in interacting with the HLA and pHLA, respectively, thereby explaining the strong selective pressure for *TRAV19* and *TRAJ34* gene usage. The energetic landscape of the SB27 β -chain rests heavily within the germline-encoded CDR1 β loop that interacts predominantly with the peptide Ag. Accordingly, the biased *TRBV6-1* gene usage was principally directed against the viral determinant. These observations have resonances with a germline-encoded TCR polymorphism, which determines the protective immune response to EBV, solely by contacting the viral determinant (8). The reduced energetic dependence of the CDR3 β loop was consistent with a lack of sequence conservation within this loop in unrelated individuals, and consistent with recent observations regarding how CDR3 β loop diversity can be tolerated in the anti-influenza response (36). Notably, whereas α Phe⁵² and β Leu⁹⁸ interact with the HLA B*3508 energetic hot spot (Arg¹⁵⁷ and Arg¹⁵¹, respectively), the remainder of the TCR residues that defined the energetic landscape coincided with TCR residues that contacted the peptide. It will be interesting to establish how other HLA B*3508^{LPEP} restricted TCRs, which vary in V α and V β usage, interact with the same lengthy Ag.

The SB27 TCR-HLA B*3508^{LPEP} interaction was principally driven by peptide contacts. To illustrate, of the 10 mutants impacting pHLA binding, 50% of them contacted the bulged peptide exclusively, 30% of TCR residues contacted both the peptide and HLA hot spots, and only 20% solely bound to HLA

hot spots. Moreover, of the TCR residues that contact both the peptide and HLA surface, they appeared to have a greater focus on the peptide, rather than the HLA, as judged by the reciprocal HLA-based mutagenesis experiments. Collectively our findings highlight the peptide-focused property of the SB27 TCR as well as highlighting the selective pressure of longer peptides in driving the restricted TCR repertoire. This has significant implications for T cell selection and the diversity of anti-viral responses when longer epitopes are presented.

Acknowledgments—We thank the staff at the MX2 beamline of the Australian synchrotron for assistance in data collection and Hanim Halim for technical assistance.

REFERENCES

1. Arstila, T. P., Casrouge, A., Baron, V., Even, J., Kanellopoulos, J., and Kourilsky, P. (1999) A direct estimate of the human $\alpha\beta$ T cell receptor diversity. *Science* **286**, 958–961
2. Theodossis, A., Guillonneau, C., Welland, A., Ely, L. K., Clements, C. S., Williamson, N. A., Webb, A. L., Wilce, J. A., Mulder, R. J., Dunstone, M. A., Doherty, P. C., McCluskey, J., Purcell, A. W., Turner, S. J., and Rossjohn, J. (2010) Constraints within major histocompatibility complex class I restricted peptides. Presentation and consequences for T-cell recognition. *Proc. Natl. Acad. Sci. U.S.A.* **107**, 5534–5539
3. Godfrey, D. I., Rossjohn, J., and McCluskey, J. (2008) The fidelity, occasional promiscuity, and versatility of T-cell receptor recognition. *Immunity* **28**, 304–314
4. Rudolph, M. G., Stanfield, R. L., and Wilson, I. A. (2006) How TCRs bind MHCs, peptides, and coreceptors. *Annu. Rev. Immunol.* **24**, 419–466
5. Adams, J. J., Narayanan, S., Liu, B., Birnbaum, M. E., Kruse, A. C., Bowerman, N. A., Chen, W., Levin, A. M., Connolly, J. M., Zhu, C., Kranz, D. M., and Garcia, K. C. (2011) T cell receptor signaling is limited by docking geometry to peptide-major histocompatibility complex. *Immunity* **35**, 681–693
6. Beddoe, T., Chen, Z., Clements, C. S., Ely, L. K., Bushell, S. R., Vivian, J. P., Kjer-Nielsen, L., Pang, S. S., Dunstone, M. A., Liu, Y. C., Macdonald, W. A., Perugini, M. A., Wilce, M. C., Burrows, S. R., Purcell, A. W., Tiganis, T., Bottomley, S. P., McCluskey, J., and Rossjohn, J. (2009) Antigen ligation triggers a conformational change within the constant domain of the $\alpha\beta$ T cell receptor. *Immunity* **30**, 777–788
7. Burrows, S. R., Chen, Z., Archbold, J. K., Tynan, F. E., Beddoe, T., Kjer-Nielsen, L., Miles, J. J., Khanna, R., Moss, D. J., Liu, Y. C., Gras, S., Kostenko, L., Brennan, R. M., Clements, C. S., Brooks, A. G., Purcell, A. W., McCluskey, J., and Rossjohn, J. (2010) Hard wiring of T cell receptor specificity for the major histocompatibility complex is underpinned by TCR adaptability. *Proc. Natl. Acad. Sci. U.S.A.* **107**, 10608–10613
8. Gras, S., Chen, Z., Miles, J. J., Liu, Y. C., Bell, M. J., Sullivan, L. C., Kjer-Nielsen, L., Brennan, R. M., Burrows, J. M., Neller, M. A., Khanna, R., Purcell, A. W., Brooks, A. G., McCluskey, J., Rossjohn, J., and Burrows, S. R. (2010) Allelic polymorphism in the T cell receptor and its impact on immune responses. *J. Exp. Med.* **207**, 1555–1567
9. Feng, D., Bond, C. J., Ely, L. K., Maynard, J., and Garcia, K. C. (2007) Structural evidence for a germline-encoded T cell receptor-major histocompatibility complex interaction “codon.” *Nat. Immunol.* **8**, 975–983
10. Stadianski, B. D., Trenth, P., Smith, R. L., Bautista, B., Huseby, P. G., Li, G., Stern, L. J., and Huseby, E. S. (2011) A role for differential variable gene pairing in creating T cell receptors specific for unique major histocompatibility ligands. *Immunity* **35**, 694–704
11. Turner, S. J., Doherty, P. C., McCluskey, J., and Rossjohn, J. (2006) Structural determinants of T-cell receptor bias in immunity. *Nat. Rev.* **6**, 883–894
12. Borg, N. A., Ely, L. K., Beddoe, T., Macdonald, W. A., Reid, H. H., Clements, C. S., Purcell, A. W., Kjer-Nielsen, L., Miles, J. J., Burrows, S. R., McCluskey, J., and Rossjohn, J. (2005) The CDR3 regions of an immunodominant T cell receptor dictate the “energetic landscape” of peptide-

Peptide Focused TCR Recognition

- MHC recognition. *Nat. Immunol.* **6**, 171–180
13. Ishizuka, J., Stewart-Jones, G. B., van der Merwe, A., Bell, J. I., McMichael, A. J., and Jones, E. Y. (2008) The structural dynamics and energetics of an immunodominant T cell receptor are programmed by its V β domain. *Immunity* **28**, 171–182
 14. Gras, S., Wilmann, P. G., Chen, Z., Halim, H., Liu, Y. C., Kjer-Nielsen, L., Purcell, A. W., Burrows, S. R., McCluskey, J., and Rossjohn, J. (2012) A structural basis for varied $\alpha\beta$ TCR usage against an immunodominant EBV antigen restricted to a HLA-B8 molecule. *J. Immunol.* **188**, 311–321
 15. Manning, T. C., Schlueter, C. J., Brodnicki, T. C., Parke, E. A., Speir, J. A., Garcia, K. C., Teyton, L., Wilson, I. A., and Kranz, D. M. (1998) Alanine scanning mutagenesis of an $\alpha\beta$ T cell receptor. Mapping the energy of antigen recognition. *Immunity* **8**, 413–425
 16. Ely, L. K., Beddoe, T., Clements, C. S., Matthews, J. M., Purcell, A. W., Kjer-Nielsen, L., McCluskey, J., and Rossjohn, J. (2006) Disparate thermodynamics governing T cell receptor-MHC-I interactions implicate intrinsic factors in guiding MHC restriction. *Proc. Natl. Acad. Sci. U.S.A.* **103**, 6641–6646
 17. Willcox, B. E., Gao, G. F., Weyer, J. R., Ladbury, J. E., Bell, J. I., Jakobsen, B. K., and van der Merwe, P. A. (1999) TCR binding to peptide-MHC stabilizes a flexible recognition interface. *Immunity* **10**, 357–365
 18. Baker, B. M., Turner, R. V., Gagnon, S. J., Wiley, D. C., and Biddison, W. E. (2001) Identification of a crucial energetic footprint on the alpha 1 helix of human histocompatibility leukocyte antigen (HLA)-A2 that provides functional interactions for recognition by tax peptide/HLA-A2-specific T cell receptors. *J. Exp. Med.* **193**, 551–562
 19. Jones, L. L., Colf, L. A., Bankovich, A. J., Stone, J. D., Gao, Y. G., Chan, C. M., Huang, R. H., Garcia, K. C., and Kranz, D. M. (2008) Different thermodynamic binding mechanisms and peptide fine specificities associated with a panel of structurally similar high-affinity T cell receptors. *Biochemistry* **47**, 12398–12408
 20. Burrows, S. R., Rossjohn, J., and McCluskey, J. (2006) Have we cut ourselves too short in mapping CTL epitopes? *Trends Immunol.* **27**, 11–16
 21. Hickman, H. D., Luis, A. D., Buchli, R., Few, S. R., Sathiamurthy, M., VanGundy, R. S., Giberson, C. F., and Hildebrand, W. H. (2004) Toward a definition of self. Proteomic evaluation of the class I peptide repertoire. *J. Immunol.* **172**, 2944–2952
 22. Ebert, L. M., Liu, Y. C., Clements, C. S., Robson, N. C., Jackson, H. M., Markby, J. L., Dimopoulos, N., Tan, B. S., Luescher, I. F., Davis, I. D., Rossjohn, J., Cebon, J., Purcell, A. W., and Chen, W. (2009) A long, naturally presented immunodominant epitope from NY-ESO-1 tumor antigen. Implications for cancer vaccine design. *Cancer Res.* **69**, 1046–1054
 23. Speir, J. A., Stevens, J., Joly, E., Butcher, G. W., and Wilson, I. A. (2001) Two different, highly exposed, bulged structures for an unusually long peptide bound to rat MHC class I RT1-Aa. *Immunity* **14**, 81–92
 24. Bade-Döding, C., Theodossis, A., Gras, S., Kjer-Nielsen, L., Eiz-Vesper, B., Seltsam, A., Huyton, T., Rossjohn, J., McCluskey, J., and Blaszczyk, R. (2011) The impact of human leukocyte antigen (HLA) micropolymorphism on ligand specificity within the HLA-B*41 allotypic family. *Haematologica* **96**, 110–118
 25. Gras, S., Kjer-Nielsen, L., Burrows, S. R., McCluskey, J., and Rossjohn, J. (2008) T-cell receptor bias and immunity. *Curr. Opin. Immunol.* **20**, 119–125
 26. Miles, J. J., Borg, N. A., Brennan, R. M., Tynan, F. E., Kjer-Nielsen, L., Silins, S. L., Bell, M. J., Burrows, J. M., McCluskey, J., Rossjohn, J., and Burrows, S. R. (2006) TCR α genes direct MHC restriction in the potent human T cell response to a class I-bound viral epitope. *J. Immunol.* **177**, 6804–6814
 27. Tynan, F. E., Borg, N. A., Miles, J. J., Beddoe, T., El-Hassen, D., Silins, S. L., van Zuylen, W. J., Purcell, A. W., Kjer-Nielsen, L., McCluskey, J., Burrows, S. R., and Rossjohn, J. (2005) High resolution structures of highly bulged viral epitopes bound to major histocompatibility complex class I. Implications for T-cell receptor engagement and T-cell immunodominance. *J. Biol. Chem.* **280**, 23900–23909
 28. Tynan, F. E., Reid, H. H., Kjer-Nielsen, L., Miles, J. J., Wilce, M. C., Kostenko, L., Borg, N. A., Williamson, N. A., Beddoe, T., Purcell, A. W., Burrows, S. R., McCluskey, J., and Rossjohn, J. (2007) A T cell receptor flattens a bulged antigenic peptide presented by a major histocompatibility complex class I molecule. *Nat. Immunol.* **8**, 268–276
 29. Tynan, F. E., Burrows, S. R., Buckle, A. M., Clements, C. S., Borg, N. A., Miles, J. J., Beddoe, T., Whisstock, J. C., Wilce, M. C., Silins, S. L., Burrows, J. M., Kjer-Nielsen, L., Kostenko, L., Purcell, A. W., McCluskey, J., and Rossjohn, J. (2005) T cell receptor recognition of a “super-bulged” major histocompatibility complex class I-bound peptide. *Nat. Immunol.* **6**, 1114–1122
 30. Kabsch, W. (2010) XDS. *Acta Crystallogr. D Biol. Crystallogr.* **66**, 125–132
 31. McCoy, A. J., Grosse-Kunstleve, R. W., Adams, P. D., Winn, M. D., Storoni, L. C., and Read, R. J. (2007) Phaser crystallographic software. *J. Appl. Crystallogr.* **40**, 658–674
 32. Emsley, P., Lohkamp, B., Scott, W. G., and Cowtan, K. (2010) Features and development of COOT. *Acta Crystallogr. D Biol. Crystallogr.* **66**, 486–501
 33. Adams, P. D., Afonine, P. V., Bunkóczi, G., Chen, V. B., Davis, I. W., Echols, N., Headd, J. J., Hung, L. W., Kapral, G. J., Grosse-Kunstleve, R. W., McCoy, A. J., Moriarty, N. W., Oeffner, R., Read, R. J., Richardson, D. C., Richardson, J. S., Terwilliger, T. C., and Zwart, P. H. (2010) PHENIX, a comprehensive Python-based system for macromolecular structure solution. *Acta Crystallogr. D Biol. Crystallogr.* **66**, 213–221
 34. Miles, J. J., Elhassen, D., Borg, N. A., Silins, S. L., Tynan, F. E., Burrows, J. M., Purcell, A. W., Kjer-Nielsen, L., Rossjohn, J., Burrows, S. R., and McCluskey, J. (2005) CTL recognition of a bulged viral peptide involves biased TCR selection. *J. Immunol.* **175**, 3826–3834
 35. Lefranc, M. P., Giudicelli, V., Ginestoux, C., Jabado-Michaloud, J., Folch, G., Bellahcene, F., Wu, Y., Gemrot, E., Brochet, X., Lane, J., Regnier, L., Ehrenmann, F., Lefranc, G., and Duroux, P. (2009) IMGT, the international ImMunoGeneTics information system. *Nucleic Acids Res.* **37**, D1006–1012
 36. Day, E. B., Guillonneau, C., Gras, S., La Gruta, N. L., Vignali, D. A., Doherty, P. C., Purcell, A. W., Rossjohn, J., and Turner, S. J. (2011) Structural basis for enabling T-cell receptor diversity within biased virus-specific CD8+ T-cell responses. *Proc. Natl. Acad. Sci. U.S.A.* **108**, 9536–9541
 37. Macdonald, W. A., Chen, Z., Gras, S., Archbold, J. K., Tynan, F. E., Clements, C. S., Bharadwaj, M., Kjer-Nielsen, L., Saunders, P. M., Wilce, M. C., Crawford, F., Stadinsky, B., Jackson, D., Brooks, A. G., Purcell, A. W., Kappler, J. W., Burrows, S. R., Rossjohn, J., and McCluskey, J. (2009) T cell allorecognition via molecular mimicry. *Immunity* **31**, 897–908
 38. Gras, S., Burrows, S. R., Kjer-Nielsen, L., Clements, C. S., Liu, Y. C., Sullivan, L. C., Bell, M. J., Brooks, A. G., Purcell, A. W., McCluskey, J., and Rossjohn, J. (2009) The shaping of T cell receptor recognition by self-tolerance. *Immunity* **30**, 193–203
 39. Kjer-Nielsen, L., Clements, C. S., Purcell, A. W., Brooks, A. G., Whisstock, J. C., Burrows, S. R., McCluskey, J., and Rossjohn, J. (2003) A structural basis for the selection of dominant $\alpha\beta$ T cell receptors in antiviral immunity. *Immunity* **18**, 53–64
 40. Bulek, A. M., Cole, D. K., Skowera, A., Dolton, G., Gras, S., Madura, F., Fuller, A., Miles, J. J., Gostick, E., Price, D. A., Drijfhout, J. W., Knight, R. R., Huang, G. C., Lissin, N., Molloy, P. E., Wooldridge, L., Jakobsen, B. K., Rossjohn, J., Peakman, M., Rizkallah, P. J., and Sewell, A. K. (2012) Structural basis for the killing of human beta cells by CD8(+) T cells in type 1 diabetes. *Nat. Immunol.* **13**, 283
 41. Wu, L. C., Tuot, D. S., Lyons, D. S., Garcia, K. C., and Davis, M. M. (2002) Two-step binding mechanism for T-cell receptor recognition of peptide MHC. *Nature* **418**, 552–556

Supplementary Figure 1. Crystal structures of the HLA and peptide mutants.

(a) Cartoon representation of the HLA B*3508 wt (blue) superposed with the HLA B*3508 mutants Ala151 (orange), Ala155 (green), Gly158 (grey) and Ala157 (pink) with their LPEP epitope represented in ribbon.

(b) Cartoon representation of the HLA B*3508 with the wt LPEP epitope (blue) superposed with the LPEP mutant structures: P4 (cyan), P5 (grey), P6 (brown), P7 (cyan), P9 (red) and P10 (green), with the peptides represented in ribbon.

Supplementary Table 1. Thermal stability assay of HLA B*3508^{LPEP} mutants.

HLA B*3508 mutant	T_m (°C)
Wild type	62.1 ± 0.6
Q65A	59.0 ± 0.7
T69A	61.1 ± 0.9
Q72A	63.1 ± 0.6
R151	59.0 ± 0.6
E154A	59.0 ± 0.6
Q155A	61.1 ± 0.7
R157A	60.5 ± 0.4
A158G	60.8 ± 0.8
E161A	60.3 ± 0.8
L163A	56.0 ± 0.5
Peptide mutants	T_m (°C)
P4A	52.9 ± 0.1
L5A	61.3 ± 0.6
P6A	62.8 ± 0.6
Q7A	59.9 ± 1.0
Q9A	59.0 ± 0.6
L10A	59.9 ± 0.6

T_m is the temperature required to reach 50% of unfolded protein.

Supplementary Table 2. Data collection and refinement statistics on HLA-B*3508^{LPEP} mutants.

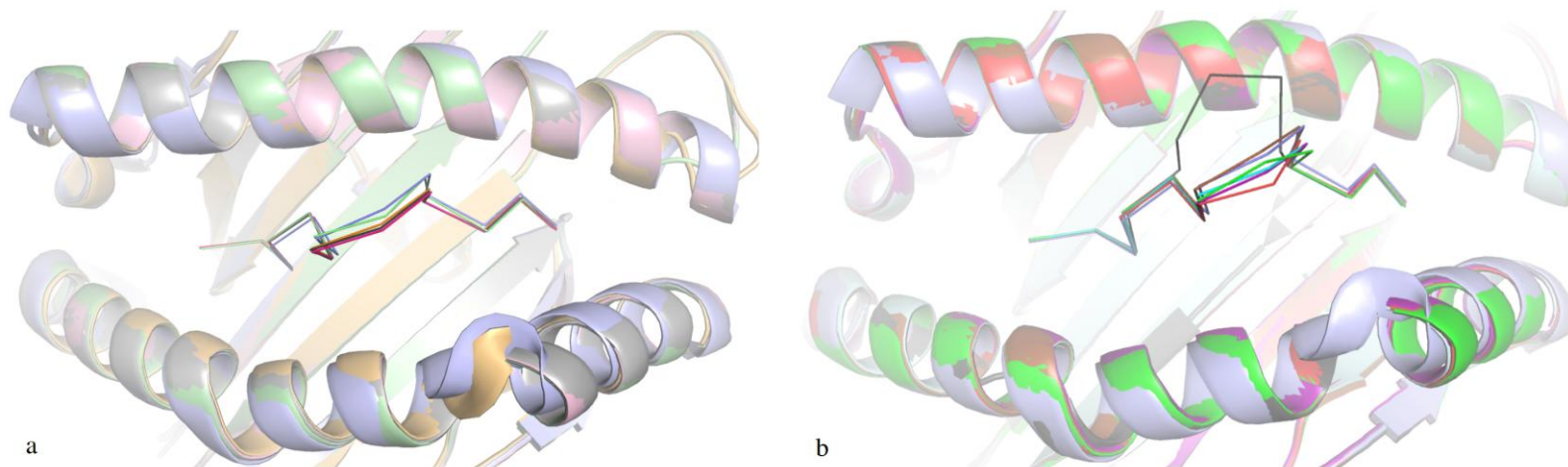
Structures	HLA B*3508 ^{LPEP} 151A	HLA B*3508 ^{LPEP} 155A	HLA B*3508 ^{LPEP} 157A	HLA B*3508 ^{LPEP} 158G	HLA B*3508 ^{LPEP} P4Ala
Resolution (Å)	19.4-1.5 (1.58-1.50)	19.7-1.90 (2.00-1.90)	19.7-1.70 (1.80-1.70)	19.6-1.85 (1.95-1.85)	20-1.85 (1.95-1.85)
Space group	<i>P2₁2₁2₁</i>	<i>P2₁2₁2₁</i>	<i>P2₁2₁2₁</i>	<i>P2₁2₁2₁</i>	<i>P2₁2₁2₁</i>
Unit cell parameters (a, b, c) (Å)	50.44, 80.63, 109.07	50.38, 81.91, 112.26	50.99, 81.52, 110.98	50.99, 81.51, 110.90	50.34, 80.66, 109.66
Temperature	100	100	100	100	100
Total number of observations	522683 (75294)	267243 (37328)	307782 (47321)	281757 (39679)	280600 (40323)
Number of unique reflections	72028 (10410)	37187 (5216)	47342 (7925)	39129 (5424)	38917 (5601)
Data Completeness (%)	100 (100)	99.4 (99.3)	91.6 (99.4)	97.3 (94.0)	99.9 (100)
R _{merge} (%)	6.9 (38.9)	9.1 (45)	5.8 (25.2)	8.2 (34.9)	9.5 (44.4)
I/σ _I	18.9 (5.3)	17.6 (4.7)	20.3 (5.6)	18.0 (6.19)	17.6 (4.7)
Multiplicity	7.3 (6.8)	7.2 (7.1)	6.5 (5.9)	7.2 (7.3)	7.2 (7.2)
R _{free} (%)	21.1	24.1	27.9	26.6	23.2
R _{work} (%)	18.2	19.1	24.6	20.7	17.5
PDB accession code	3VFN	3VFM	3VFO	3VFP	3VFR
Structures	HLA B*3508 ^{LPEP} P5Ala	HLA B*3508 ^{LPEP} P6Ala	HLA B*3508 ^{LPEP} P7Ala	HLA B*3508 ^{LPEP} P9Ala	HLA B*3508 ^{LPEP} P10Ala
Resolution (Å)	20-1.85 (1.95-1.85)	20-1.95 (2.05-1.95)	19.9-1.65 (1.74-1.65)	20-1.55 (1.65-1.55)	19.8-2.3 (2.40-2.30)
Space group	<i>P2₁2₁2₁</i>	<i>P2₁2₁2₁</i>	<i>P2₁2₁2₁</i>	<i>P2₁2₁2₁</i>	<i>P2₁2₁2₁</i>
Unit cell parameters (a, b, c) (Å)	50.77, 81.53, 111.45	50.77, 81.50, 111.30	50.32, 80.58, 109.54	50.8, 81.5, 110.6	50.88 81.56 111.24
Temperature (K)	100	100	100	100	100
Total number of observations	291329 (42196)	250052 (34445)	387310 (53712)	485952 (82794)	143352 (18326)
Number of unique reflections	40200 (5788)	34385 (4702)	54048 (7700)	66782 (11170)	20807 (2495)
Data Completeness (%)	99.8 (99.8)	99.8 (100)	99.4 (98.1)	99.1 (98.2)	98.0 (100)
R _{merge} (%)	12.0 (46.3)	14.1 (45.4)	7.8 (47.8)	4.9 (23.4)	6.3 (10.6)
I/σ _I	15.1 (5.07)	17.17 (6.17)	19.1 (4.2)	24 (8)	24.0 (15.87)
Multiplicity	7.2 (7.2)	7.3 (7.3)	7.2 (7.0)	7.3 (7.4)	6.9 (7.3)
R _{free} (%)	21.6	22.3	22.5	20.4	27.9
R _{work} (%)	17.1	17.2	19.0	17.0	21.4
PDB accession code	3VFS	3VFT	3VFU	3VFW	3VFW

^a R_{merge} = $\sum |I_{hkl} - \langle I_{hkl} \rangle| / \sum I_{hkl}$

^b R_{factor} = $\sum_{hkl} ||F_o| - |F_c|| / \sum_{hkl} |F_o|$ for all data except $\approx 5\%$ which were used for R_{free} calculation

*Values in parentheses are for highest-resolution shell.

Supplementary Figure 1.



4 Results: Divergent T cell receptor recognition modes towards a bulged epitope presented by a HLA molecule

Whilst it has been established that how an immuno-dominant CTL (termed SB27) recognises a super-bulged viral determinant (LPEP) that is central for the viral control in HLA-B*35:08+ individuals (Tynan et al., 2005a; Tynan et al., 2005b), it is unclear however, how other CTLs bearing various TCR architectures, can overcome this structurally challenging pHLA landscape whilst maintain the co-recognition of the peptide and HLA. To address this, this result chapter, which was published in *Journal of Biological Chemistry* (Liu et al., 2013), investigated the structures and functions of two distinct HLA-B*35:08-LPEP restricted T cell receptors derived from unrelated HLA-B*35:08+ individuals. Namely, the CA5 TCR was selected as it shared the repetitive selection of TRAV/TRBV gene usage compared to the SB27 TCR whilst expressing an alternate TRABJ segment that resulted in variation in the CDR3 β loop. Additionally, the SB47 TCR, which derived from the same individual as the SB27 TCR, was also examined as it encompassed a unique TRAV/TRBV combination and therefore, a completely different set of CDR loops compared to that of the SB27 and CA5 TCRs. As such, studying the interactions between these two TCRs and HLA-B*35:08-LPEP would allow us to examine the role of CDR3 β loop as well as alternative TCR architecture in enabling lengthy antigen recognition.

Using biophysical (surface plasmon resonance), cell-based and crystallographic approaches, this following chapter demonstrated two distinctive modes of TCR recognition towards a “featured” pHLA landscape. Notably, similar to the previously established SB27 TCR, the CA5 TCR docked centrally onto the bulged antigen while contacting minimally to the α 2-helix of HLA-B*35:08. The role of CDR3 β appeared to contribute towards antigen-specificity due to its close proximity with the bulged antigen. In contrast, the SB47 TCR, with its unique TRAV/TRBV composition, was able to engage N-terminally onto HLA-B*35:08 and essentially “by-passed” the bulged antigen landscape. This unique docking orientation also allowed the SB47 TCR to contact novel region of the HLA surface and ignored some of the TCR-contacting residues that are frequently observed in TCR-pMHC-I complex structures determined to date. Accordingly, these divergent TCR docking modes not only

provide novel structural insights into lengthy antigen detection by CD8⁺ T cells, but also shape our understanding towards the fine-specificity of MHC-restricted TCR recognition.

Highly Divergent T-cell Receptor Binding Modes Underlie Specific Recognition of a Bulged Viral Peptide bound to a Human Leukocyte Antigen Class I Molecule^{*S}

Received for publication, December 19, 2012, and in revised form, March 24, 2013. Published, JBC Papers in Press, April 8, 2013, DOI 10.1074/jbc.M112.447185

Yu Chih Liu[†], John J. Miles^{§¶1}, Michelle A. Neller[§], Emma Gostick[¶], David A. Price^{¶||2}, Anthony W. Purcell^{†‡3}, James McCluskey^{**}, Scott R. Burrows^{§4}, Jamie Rossjohn^{†¶5,6}, and Stephanie Gras^{†5,7}

From the [†]Department of Biochemistry and Molecular Biology, School of Biomedical Sciences, Monash University, Clayton 3800, Australia, the [§]Queensland Institute of Medical Research and Australian Centre for Vaccine Development, Brisbane 4006, Australia, the [¶]Institute of Infection and Immunity, Cardiff University School of Medicine, Heath Park, Cardiff CF14 4XN, Wales, United Kingdom, the ^{||}Human Immunology Section, Vaccine Research Center, NIADD, National Institutes of Health, Bethesda, Maryland 20892, and the ^{**}Department of Microbiology and Immunology, University of Melbourne, Parkville 3010, Australia

Background: The mechanisms by which T cell receptors (TCRs) engage lengthy peptides bound to human leukocyte antigens (HLA) is unclear.

Results: We have determined the structures of two TCRs binding to a 13-residue bulged peptide presented by HLA-B*35:08.

Conclusion: TCRs can adopt markedly differing docking strategies upon engaging lengthy bulged peptides.

Significance: The human T-cell repertoire is sufficiently robust to deal with viral determinants of atypical length.

Human leukocyte antigen (HLA)-I molecules can present long peptides, yet the mechanisms by which T-cell receptors (TCRs) recognize featured pHLA-I landscapes are unclear. We compared the binding modes of three distinct human TCRs, CA5, SB27, and SB47, complexed with a “super-bulged” viral peptide (LPEPLPQGQLTAY) restricted by HLA-B*35:08. The CA5 and SB27 TCRs engaged HLA-B*35:08^{LPEP} similarly, straddling the central region of the peptide but making limited contacts with HLA-B*35:08. Remarkably, the CA5 TCR did not contact the α 1-helix of HLA-B*35:08. Differences in the CDR3 β loop between the CA5 and SB27 TCRs caused altered fine specificities. Surprisingly, the SB47 TCR engaged HLA-B*35:08^{LPEP} using a completely distinct binding mechanism, namely “bypassing” the bulged peptide and making extensive contacts with the extreme N-terminal end of HLA-B*35:08. This docking footprint included HLA-I residues not observed previously as TCR contact sites. The three TCRs exhibited differing patterns of alloreactivity toward closely related or distinct HLA-I allotypes. Thus, the human T-cell repertoire comprises a range of

TCRs that can interact with “bulged” pHLA-I epitopes using unpredictable strategies, including the adoption of atypical footprints on the MHC-I.

Clonally distributed $\alpha\beta$ T-cell receptors (TCRs)⁸ on CD8⁺ cytotoxic T lymphocytes (CTLs) specifically recognize peptide (p) fragments, generally between 8 and 10 amino acids in length, presented by major histocompatibility complex class I (MHC-I) molecules expressed on the surface of all nucleated cells (1). TCR recognition of pMHC-I complexes is a key event in cellular immunity that is central to thymic selection (2), the lysis of pathogen-infected cells and the eradication of cancerous tissue. In general, TCR recognition is genetically restricted to self-MHC molecules, although the underlying basis of MHC restriction remains unclear (3–5). Puzzlingly, a relatively high frequency of T-cells break the “MHC restriction code” and recognize non-self (“allo”) human leukocyte antigen class I (HLA-I) molecules (6). The molecular mechanisms underpinning T-cell alloreactivity, a cause of T-cell-mediated transplant rejection, are beginning to emerge (7–9).

Structural studies have shed insight on the nature of the TCR-pMHC-I interaction (for recent reviews, see Refs. 3–5, 10, and 11). The TCR comprises six complementarity-determining regions (CDRs), whereby the germline-encoded CDR1/2 loops arise from the *TRAV* or *TRBV* genes (12), whereas the CDR3 loops lie at the V, (D), and J region junction, from which greater diversity is generated by random nucleotide (N) deletions and non-templated additions. TCRs can bind differing and identical pMHC-I epitopes using a range of docking modes (5, 7, 13). Within such TCR-pMHC-I complexes, the CDR loops of the TCR engage pMHC-I to varying extents (14). Despite these

* This work was supported by the Australian Research Council (ARC) Grant DP110102078 and the National Health and Medical Research Council of Australia (NHMRC) Grant APP1009326.

[¶] Author's Choice—Final version full access.

^S This article contains supplemental Tables S1–S4 and Figs. S1–S6.

The atomic coordinates and structure factors (codes 4JRX and 4JRY) have been deposited in the Protein Data Bank (<http://www.pdb.org/>).

[†] NHMRC Career Development Fellow.

[‡] Wellcome Trust Senior Investigator.

[§] NHMRC Senior Research Fellow.

^{||} NHMRC Principal Research Fellow.

[¶] Joint senior and corresponding authors.

¹ NHMRC Australia Fellow. To whom correspondence may be addressed: Dept. of Biochemistry and Molecular Biology, School of Biomedical Sciences, Monash University, Clayton, Vic 3800, Australia. Tel.: 613-99029236; Fax: 613-9902500; E-mail: jamie.rossjohn@monash.edu.

² ARC Future Fellow. To whom correspondence may be addressed: Dept. of Biochemistry & Molecular Biology, School of Biomedical Sciences, Monash University, Clayton, Vic 3800, Australia. Tel.: 613-99050254; Fax: 613-9902500; E-mail: stephanie.gras@monash.edu.

⁸ The abbreviations used are: TCR, T-cell receptor; BSA, buried surface area; CDR, complementarity-determining region; pMHC, peptide-major histocompatibility complex; CTL, cytotoxic T lymphocyte; HLA, human leukocyte antigen.

variations on a theme, a broad consensus TCR-pMHC-I footprint is conserved in which the V α and V β domains of the TCR sit over the MHC-I α 2- and α 1-helices, respectively. The short antigenic peptide fragments generally protrude minimally from the MHC-I cleft, such that the TCR mostly contacts the MHC-I molecule. Nevertheless, associated mutagenesis studies in a number of TCR-pMHC-I systems have shown that generally only a few residues of the MHC-I (termed the "hot spots") contribute significantly to the energetics of the TCR-pMHC-I interaction; moreover, such hot spots can vary between different TCR-pMHC-I systems (15–21). Such investigations highlight the peptide-centric nature of the TCR-pMHC-I interaction.

Although the N- and C-terminal ends of the MHC-I binding cleft constrain the majority of peptides to 8–10 amino acids in length, longer peptides are known to bind MHC-I (22–28). Indeed, such "atypically" long peptides can represent up to 10% of the peptide repertoire bound to MHC-I (29), and are known to play important roles in aberrant and protective immunity (30). Such peptides frequently bulge away from the antigen (Ag)-binding cleft, and can either exhibit substantial flexibility (23–25, 28) or adopt a more fixed conformation (25, 27, 31). The extent to which TCRs can accommodate such featured pMHC-I landscapes is unclear. Presently, TCRs have been shown to adopt two distinct strategies to ligate bulged pMHC-I epitopes. Namely, some TCRs can "flatten" the flexible and bulged peptide to enable an MHC-I-restricted response (32), whereas others form a more peptide-centric view and make very limited contacts with the MHC-I molecule (33). It is unclear whether other mechanisms might enable productive TCR recognition of atypical pMHC-I landscapes.

The recognition of a 13-amino acid (aa) determinant (LPEP-LPQGQLTAY, termed "LPEP") from Epstein-Barr virus, restricted by HLA-B*35:08, represents a well described example of how the T-cell repertoire, isolated from Epstein-Barr virus⁺ individuals (22), responds to a bulged pHLA-I epitope. Namely, the immune response to HLA-B*35:08^{LPEP} is underpinned by biased TCR usage in which the cognate repertoire is characterized by the dominant selection of TRBV5–6, 6–1, or 7–2 in distinct HLA-B*35:08 donors (33). In addition, the TCR α -chain is highly restricted, with TRAV19*01 and TRAJ34 found in nearly all HLA-B*35:08^{LPEP}-specific TCRs. Previously, we determined the structure of one prototypical TCR, termed SB27 (TRAV19*01-TRAJ34*01-TRBV6–1*01) in complex with HLA-B*35:08^{LPEP} (33). Here, the SB27 TCR made a limited footprint on HLA-B*35:08, yet contacted the peptide extensively. The peptide centrality of the interaction was further emphasized by an alanine-scanning mutagenesis study at the SB27 TCR-HLA-B*35:08^{LPEP} interface (15). Although the SB27 TCR cross-reacted poorly with the closely related HLA allomorph, HLA-B*35:01, it nevertheless, alloreacted with HLA-B*44:02 (33), which differs from HLA-B*35:08 by 16 amino acids (supplemental Fig. 1). The TCR α - and β -chains of the SB27 TCR mediated many contacts with the bulged viral peptide. How different TCRs with different gene architecture bind the same HLA-B*35:08^{LPEP} epitope, and how these binding modes impact their alloreactivity profiles, is unknown.

Here, we assessed the impact of TCR α - and β -chain usage on the recognition of an atypical pHLA-I landscape. We show that alternate TCR architecture modifies the fine specificity toward the viral peptide and the pattern of alloreactivity, and can markedly alter the mode of cognate recognition. Notably, a unique docking mode was observed, in which the TCR does not contact the prominently exposed region of the viral peptide. Instead, contacts with HLA-I are maximized via an extreme N-terminal footprint, which enables the TCR to recognize a distinct feature of the MHC that has not been observed in previous TCR-pMHC-I structures.

EXPERIMENTAL PROCEDURES

Analysis of TCR Gene Expression—Unbiased amplification of all expressed *TRB* or *TRA* gene products from T-cell clones was conducted using template-switch anchored RT-PCRs incorporating a 3' *TRB* constant region primer (5'-TGCTTCGATG-GCTCAAACACAGCGACCT-3') or a 3' *TRA* constant region primer (5'-AATAGGCAGACAGACTTGTCACTGGA-3'), respectively. Amplicons were subcloned, sampled, Sanger sequenced, and analyzed as described previously (34).

Cytotoxicity Assay—CTL clones were assayed in duplicate over a period of 5 h against peptide-pulsed ⁵¹Cr-labeled target cells. The target cells used to generate the data shown in Fig. 1 were HLA-B*35:08⁺ peripheral blood mononuclear cells expanded with phytohemagglutinin and propagated in IL-2-containing medium for up to 8 weeks. Percentage of specific lysis was calculated, and the peptide concentration required for half-maximum lysis was determined from dose-response curves. Peptides were synthesized by Mimotopes. A β scintillation counter (Topcount Microplate; Packard Instrument) was used to measure ⁵¹Cr levels in assay supernatant samples. The mean spontaneous lysis for targets in culture medium was always <20% and variation around the mean specific lysis was <10%. Normal lymphoblastoid cell lines and the C1R HLA-deficient mutant lymphoblastoid cell line were also used as targets, with or without transfection of the gene encoding HLA-B*44:02 (33).

Intracellular IFN- γ Staining—CTL clones were tested against a range of antigen-presenting cells and assayed for intracellular expression of IFN- γ by flow cytometry using the BD Cytotfix/Cytoperm kit (BD Biosciences) according to standard protocols. Briefly, clones were incubated with antigen-presenting cells at a stimulator to responder ratio of 1:2 for 4 h in the presence of brefeldin A (BioLegend). For peptide titration experiments, T2 cells were incubated with various concentrations of LPEP peptide for 1 h and then washed thoroughly prior to incubation with CTL clones. After stimulation, cells were stained with Live/Dead Fixable Aqua Dead Cell Stain (Invitrogen) and anti-CD8-Cy5.5-PerCP mAb (BioLegend) for 30 min at 4 °C. Cells were then washed, fixed, permeabilized, and labeled with anti-IFN- γ -antigen-presenting cell mAb (BioLegend) for 30 min at 4 °C. After a further wash, samples were collected using a FACSCanto II flow cytometer (BD Biosciences). Data were analyzed with FlowJo software (Tree Star). Lymphocytes were identified based on light scatter, then live CD8⁺ T-cells were selected and IFN- γ ⁺ gates were drawn based on unstimulated controls.

T-cell Receptor Recognition of an Atypical pMHC

Protein Expression, Refolding, and Purification—The production of TCRs and pHLA-I molecules was performed as described previously (15). Briefly, individual chains of the CA5 and SB47 TCR genes were codon optimized for bacterial expression and cloned into the pET30 vector. Plasmids containing TCR chains were transformed into *Escherichia coli* BL21 cells for expression. Inclusion bodies were isolated and solubilized in urea buffer (8 M urea, 20 mM Tris-HCl, pH 8, and 1 mM DTT) before injecting into refolding buffer. The refolding procedure lasted 2 days before the samples were dialyzed against 10 mM Tris buffer (pH 8) three times daily at 4 °C. Dialyzed samples were loaded sequentially onto DEAE cellulose, size-exclusion, hydrophobic interaction, and anion exchange columns to obtain pure proteins. Protein size and purity were assessed by SDS-PAGE.

Thermal Stability Assay—Thermal stability assays of HLA-B*35:08 mutants in complex with the LPEP peptide were performed with the Real Time Detection instrument (Corbett RotorGene 300) as described previously (22). The results are summarized in supplemental Table S1.

Crystallization, Data Collection, and Structure Determination—TCR-pHLA-I ternary complexes were obtained by mixing the purified TCR and pHLA-I proteins at a 1:1 molar ratio. Initial crystallization trials were performed using the Monash Macromolecular Crystallization Facility Platform. Optimization trials were conducted via the hanging-drop vapor diffusion method whereby 1 μ l of protein and 1 μ l of the reservoir solutions were mixed accordingly. The CA5 TCR-HLA-B*35:08^{LPEP} complex crystals were obtained at 20 °C, using a protein concentration of 10 mg/ml in a reservoir solution containing 0.1 M sodium cacodylate (pH 6.7), 0.2 M potassium iodide, and 16% PEG 3350, with crystals of SB27 TCR-HLA-B*35:08^{LPEP} as cross-seeds. Crystals of SB47 TCR-HLA-B*35:08^{LPEP} were produced at 20 °C, using a protein concentration of 9 mg/ml in a reservoir solution containing 10 mM HEPES (pH 7.5), 0.2 M sodium tartrate, and 12% PEG 10K. Crystals of the TCR-pHLA-I complexes were soaked with the reservoir solution with increased percentages of PEG before being flash-frozen in liquid nitrogen. Frozen crystals were taken to the Australia Synchrotron, Melbourne, and datasets were collected with an ADSC-Quantum 315r CCD detector on the MX2 beamline at 100 K. Both datasets were processed and scaled with the XDS program (35). The structures were determined by molecular replacement (36) using the published SB27 TCR (PDB code 2AK4 (33)) and HLA-B*35:08 minus the peptide (PDB code 1ZHK (22)) as starting search models, whereby the HLA-I was located initially within the asymmetric unit, followed by the TCR. Manual building of the models was conducted with the COOT program (37) and structural refinements were conducted via Phenix (38) and Buster (39) with maximum-likelihood refinement. The TCRs were numbered according to the International Immunogenetics Information System unique numbering system (12), whereby the CDR1 loops start at residue 27, the CDR2 loops start at residue 56, and the CDR3 loops start at residue 105. The final models were validated using the Protein Data Bank validation Web site, and submitted to the Protein Data Bank database. All molecular graphic representations were created using PyMol (40).

Surface Plasmon Resonance—Surface plasmon resonance experiments were conducted using a BIAcore 3000 instrument at 25 °C with HBS-EP buffer (10 mM HEPES, pH 7.4, and 150 mM NaCl) containing 0.005% surfactant P20 and 1% bovine serum albumin to prevent nonspecific binding. The conformation-specific antibody 12H8 (17), which recognizes a conformational epitope within the TCR constant domain, was coupled to the surface of a research grade CM5 sensorchip using a standard amine-coupling protocol. Approximately 200–400 response units of each TCR (SB27, CA5 and SB47) was coated onto independent flow cells; the first flow cell was left empty as a negative control. Various concentrations (0.78–200 μ M) of the analytes (either HLA-B*35:01^{LPEP} or HLA-B*35:08^{LPEP}) were passed over all flow cells. Experimental data were analyzed using the BIAevaluation program (version 3.1) assuming the 1:1 Langmuir binding model with drifting baseline to determine the kinetic constants (Table 1). Using the same protocol, the HLA-B*35:08^{LPEP} mutants were flowed over the SB47 and SB27 TCRs at various concentrations (0.78–200 μ M), and the equilibrium constant (K_{deq}) was determined (supplemental Table S2). All experiments were performed at least twice ($n = 2$) in duplicate.

RESULTS

Fine Specificity of the CA5 and SB47 CTL Clones for the LPEP Peptide—The T-cell repertoire directed against the HLA-B*35:08-restricted ⁵²LPEPLPQGQLTAY⁶⁴ (“LPEP”) peptide derived from the Epstein-Barr virus lytic Ag BZLF1 exhibits biased TCR α -chain usage (TRAV19*01-TRAJ34*01), in which the α -chain is largely germline-encoded, possessing a small N-region that encodes a highly conserved ⁹⁴Gly-Phe⁹⁵ motif (33). In contrast, the TCR β -chain shows greater genetic variability (TRBV5–6, TRBV6–1, or TRBV 7–2) as well as differing CDR3 β usage. For example, one HLA-B*35:08⁺ CTL clone, termed CA5, uses the same TCR α -chain and TRBV6–1*01 gene segment as the SB27 TCR, but a different J β gene segment (TRBJ1–1) (33). Consequently, their respective CDR3 β loops differ markedly, whereby the CDR3 β loop of the CA5 TCR (CASPGETEAF) is shorter than that of the SB27 TCR (CASPLGAGEYEYQ). Interestingly, whereas the TRAV19*01-TRAJ34 α -chain dominated the CTL response to HLA-B*35:08^{LPEP}, one CTL clone (termed SB47) exhibited a completely unique TCR architecture (TRAV39*01-TRAJ33-TRBV5–6*01-TRBJ2–7) (33). Accordingly, the SB27, CA5, and SB47 CTL clones enabled us to examine the impact of CDR3 β variability and TCR gene usage on the response to HLA-B*35:08^{LPEP}.

Previously, we demonstrated that the central region of the LPEP peptide (P4–P8) is critical for SB27 TCR recognition (33). To gain a detailed understanding of the fine specificity requirements of the CA5 and SB47 clones toward HLA-B*35:08^{LPEP}, we performed cytotoxicity assays with single site substitutions along the solvent exposed residues of the LPEP peptide, using the SB27 clone as a control (Fig. 1). Each solvent-exposed position along the length of the peptide was mutated to one of 6 residues (Gly/Ala, Ser, Val, Lys, Asp, and Tyr). As expected from the crystal structure of the SB27 TCR-HLA-B*35:08^{LPEP} complex and previous fine specificity analyses (33), the SB27 clone showed negligible sensitivity toward substitutions at

T-cell Receptor Recognition of an Atypical pMHC

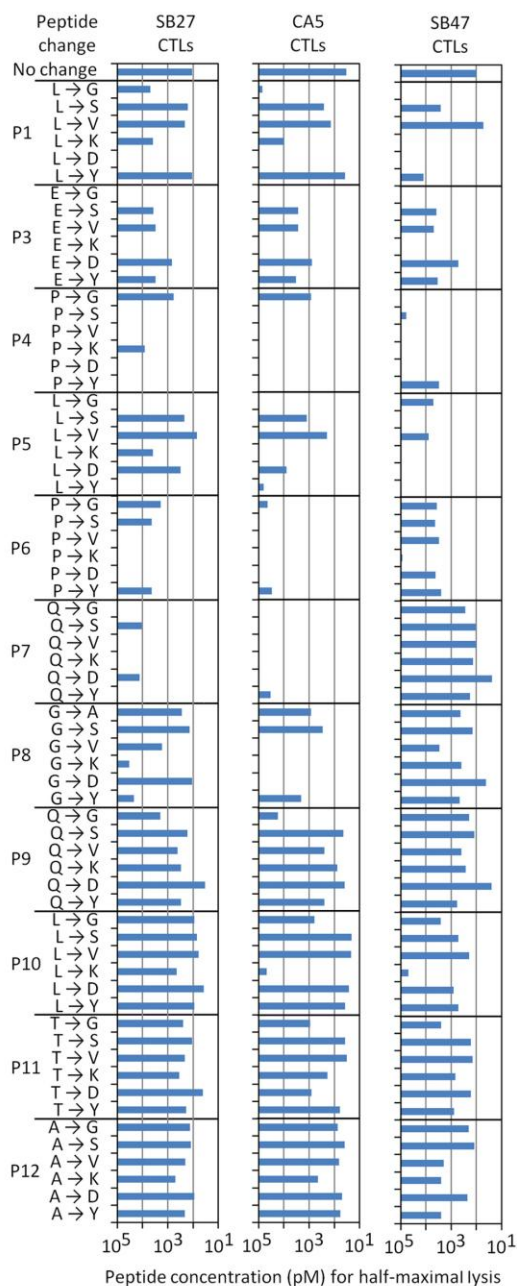


FIGURE 1. Antigen specificity of the SB27, CA5, and SB47 TCRs. Dose-response analysis of LPEP peptide analogues carrying single amino acid substitutions was conducted using chromium release assays to assess recognition by the SB27, CA5, and SB47 CTL clones. Peptide concentrations required to reach half-maximal lysis are shown. Some of the experiments with the SB27 clone were published previously and are shown here for comparison (33).

positions P9–P12, some sensitivity toward substitutions at P1, P3, P5, and P8, and substantial sensitivity toward substitutions at P4, P6, and P7. Overall, the fine specificity of the CA5 clone

mirrored that of the SB27 clone, with substitutions at the N-terminal region of the epitope exhibiting a greater effect. Nevertheless, differences in the fine specificity patterns were observed. Namely, whereas the SB27 clone tolerated the substitution of P8-Gly to Val or Asp, these replacements were not tolerated by the CA5 clone (Fig. 1). In addition, the CA5 clone showed a heightened sensitivity at P4–P7 in comparison to the SB27 clone. Accordingly, differing CDR3 β usage subtly affects the fine specificity profiles of the SB27 and CA5 clones.

Next, we examined the fine specificity of the SB47 clone toward the LPEP peptide. Substitutions at P7–P12 did not greatly impact on SB47 recognition, and a number of substitutions at P6 were also tolerated (Fig. 1). Thus, the SB47 clone was more tolerant to P6–P7 substitutions compared with the SB27 and CA5 clones. Additionally, the SB47 clone was considerably more sensitive at P1 and P5 compared with the SB27 and CA5 clones. These observations suggest that the fine specificity profile of the SB47 clone for the LPEP peptide is more N terminally focused than that of the SB27 and CA5 clones, in turn suggesting fundamentally different docking modes.

The Impact of HLA Polymorphism on T-cell Specificity—The HLA-B*35:01/08 molecules differ only by a single residue, which is buried inside the Ag-binding cleft (Arg¹⁵⁶ and Leu¹⁵⁶ in HLA-B*35:08 and HLA-B*35:01, respectively (supplemental Fig. S1)). To dissect the fine preferences for MHC restriction exhibited by the CA5 and SB47 TCRs, we compared reactivity of the CA5 and SB47 CTL clones toward HLA-B*35:08 and HLA-B*35:01 targets presenting the LPEP peptide (Fig. 2). Although the CA5 CTL clone recognized both HLA allomorphs when high peptide concentrations were added, it preferentially recognized HLA-B*35:08^{LPEP} when the peptide was limited (Fig. 2A), in a similar manner to the SB27 clone. Next, we undertook surface plasmon resonance analysis of the recombinant CA5 and SB27 TCRs to establish their affinities for HLA-B*35:08^{LPEP} and HLA-B*35:01^{LPEP} (Fig. 2B and supplemental Fig. S2). The affinity values obtained for the SB27 TCR were consistent with those published previously (Table 1) (33), with a 4-fold decrease in the affinity for HLA-B*35:01^{LPEP} ($K_{\text{deq}} = 52.25 \pm 4.88 \mu\text{M}$) compared with the HLA-B*35:08^{LPEP} complex ($K_{\text{deq}} = 12.15 \pm 0.35 \mu\text{M}$). The affinity of the CA5 TCR toward HLA-B*35:08^{LPEP} ($K_{\text{deq}} = 3.75 \pm 0.01 \mu\text{M}$) was ~4-fold higher than that of the SB27 TCR ($K_{\text{deq}} = 12.15 \pm 0.35 \mu\text{M}$), which was attributable to faster association and slower dissociation constants (CA5: $k_{\text{on}} = 50.80 \pm 8.06 \times 10^4 \text{ M}^{-1} \text{ s}^{-1}$, $k_{\text{off}} = 0.19 \pm 0.02 \text{ s}^{-1}$; SB27: $k_{\text{on}} = 10.05 \pm 0.92 \times 10^4 \text{ M}^{-1} \text{ s}^{-1}$, $k_{\text{off}} = 0.11 \pm 0.01 \text{ s}^{-1}$) (Table 1). In agreement with the cytotoxicity data, the affinity of the CA5 TCR toward HLA-B*35:01^{LPEP} ($K_{\text{deq}} = 27.10 \pm 0.42 \mu\text{M}$) was notably weaker compared with HLA-B*35:08^{LPEP}, which was due to slower association and faster dissociation rates upon HLA-B*35:01^{LPEP} binding (Fig. 2B, supplemental Fig. S2, and Table 1). Accordingly, the SB27 and CA5 TCRs exhibited similar patterns of cross-reactivity between HLA-B*35:01/08^{LPEP}, although the CA5 TCR bound with higher affinity to these HLA allomorphs.

In contrast to the SB27 and CA5 CTLs, the SB47 clone recognized the LPEP peptide presented by HLA-B*35:08 and HLA-B*35:01 equally well (Fig. 2C). To assess whether the

T-cell Receptor Recognition of an Atypical pMHC

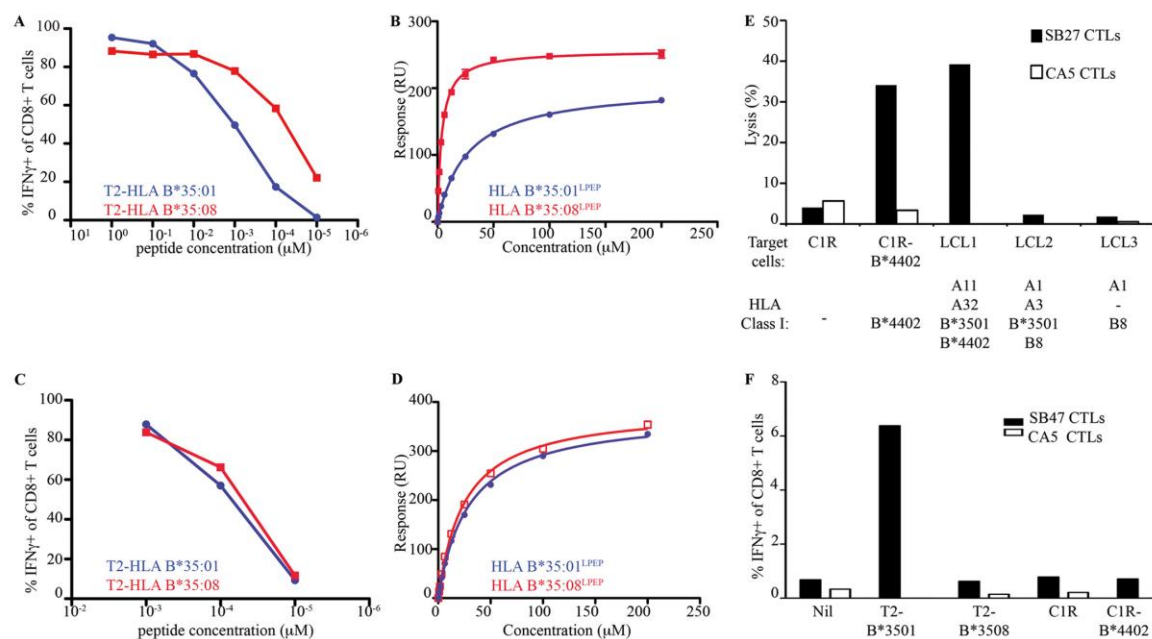


FIGURE 2. Cross-reactivity of the SB27, CA5, and SB47 TCRs. A and C, CD8⁺ T-cell activation was measured by intracellular cytokine staining for IFN γ after stimulation with peptide-pulsed T2 cells expressing either HLA-B*35:08 or HLA-B*35:01 as indicated. Experiments were performed twice with similar results. B and D, surface plasmon resonance experiments showing CA5 (B) and SB47 (D) TCR binding to HLA-B*35:08 and HLA-B*35:01 presenting the LPEP peptide. Data represent the concentration versus response unit curve derived from two experiments. E and F, HLA-restricted recognition and alloreactivity of the SB27, CA5, and SB47 CTL clones. E, specific lysis of target cells expressing different HLA molecules by SB27 and CA5 CTLs. The HLA⁻ cell line C1R was included as a control. F, activation of CA5 and SB47 CTLs after stimulation with T2 cells expressing HLA-B*35 allomorphs, parental C1R cells, or C1R cells expressing HLA-B*44:02.

TABLE 1

Surface plasmon resonance experiments for HLA-B35^{LPEP} and the CA5, SB27, and SB47 TCRs

The experiments were conducted at least twice ($n = 2$) in duplicate and the values represent the mean \pm S.E.

Immobilized TCR	Analyte	K_{deq}	K_{on}	K_{off}	$t_{1/2}^a$	K_{dcatc}
		μM	$\times 10^4 \text{ M}^{-1} \text{ s}^{-1}$	s^{-1}	s	μM
CA5	HLA-B*35:08 ^{LPEP}	3.75 ± 0.01	50.80 ± 8.06	0.19 ± 0.02	3.62 ± 0.32	3.78 ± 0.95
SB27	HLA-B*35:08 ^{LPEP}	12.15 ± 0.35	10.05 ± 0.92	0.11 ± 0.01	6.21 ± 0.55	11.14 ± 0.03
SB47	HLA-B*35:08 ^{LPEP}	25.00 ± 0.28	15.05 ± 5.16	0.30 ± 0.01	2.33 ± 0.05	19.77 ± 6.75
CA5	HLA-B*35:01 ^{LPEP}	27.10 ± 0.42	34.45 ± 6.01	0.67 ± 0.16	1.07 ± 0.26	19.38 ± 1.34
SB27	HLA-B*35:01 ^{LPEP}	52.25 ± 4.88	ND ^b	ND ^b	ND ^b	ND ^b
SB47	HLA-B*35:01 ^{LPEP}	29.25 ± 0.07	15.50 ± 0.03	0.33 ± 0.04	2.15 ± 0.24	20.9 ± 1.99

^a $t_{1/2} = 0.693/K_{\text{off}}$.

^b ND, not determined.

affinity of the SB47 TCR was affected by the HLA-B*35:01/08 polymorphism, we quantified SB47 TCR binding to HLA-B*35:08^{LPEP} and HLA-B*35:01^{LPEP}. The affinity of the SB47 TCR for HLA-B*35:08^{LPEP} ($K_{\text{deq}} = 25.00 \pm 0.28 \mu\text{M}$) was lower compared with the CA5 and SB27 TCRs, which was due to a faster dissociation rate ($k_{\text{off}} = 0.30 \pm 0.01 \text{ s}^{-1}$) (Table 1). Furthermore, in contrast to the SB27 and CA5 TCRs, the SB47 TCR bound the HLA-B*35:08^{LPEP} and HLA-B*35:01^{LPEP} ($K_{\text{deq}} = 29.25 \pm 0.07 \mu\text{M}$) complexes with similar affinities (Fig. 2D, supplemental Fig. S2, and Table 1). These findings are consistent with the functional data indicating that the SB47 TCR could not discriminate between the two closely related HLA-B35 allomorphs when bound to the LPEP peptide.

Unique Alloreactivity Footprints Across Clonotypes—The SB27 CTL clone alloreacts with HLA-B*44:02 presenting one or more unknown self-peptide(s) (Fig. 2E)(33). HLA-B*35:08 and HLA-B*44:02 differ by 16 residues, three of which (positions 80,

83, and 167) are solvent exposed (supplemental Fig. S1), yet are not involved in the SB27 TCR-HLA-B*35:08^{LPEP} interaction. Moreover, HLA-B*35:08 and HLA-B*44:02 are structurally very similar (root mean square deviation of the Ag-binding cleft is 0.4 Å), suggesting that the SB27 TCR could potentially bind both pHLA-I molecules with a similar docking mode. Next, we assessed whether the CA5 and SB47 clones could alloreact with HLA-B*44:02, using a CTL lysis assay against allogeneic cells in the absence of exogenous peptide. Surprisingly, the CA5 CTL clone did not alloreact with HLA-B*44:02 (Fig. 2E). Given that the CA5 and SB27 TCRs differ only in the CDR3 β loop, which forms dominant interactions with peptide in the SB27 TCR-HLA-B*35:08^{LPEP} complex, this indicates that the observed differences in alloreactivity patterns are driven by peptide-centric interactions.

Similarly the SB47 clone did not alloreact with HLA-B*44:02 presenting self-peptides (Fig. 2F). However, the SB47 CTL

T-cell Receptor Recognition of an Atypical pMHC

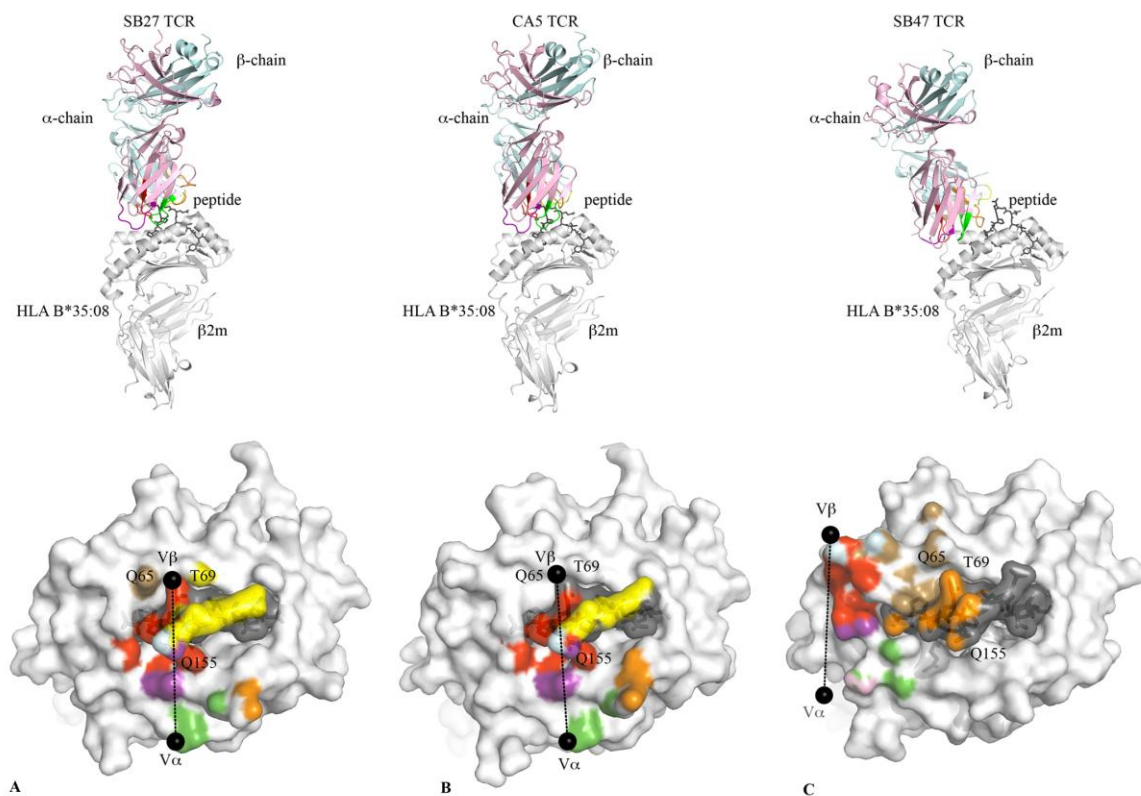


FIGURE 3. Overview and structural footprints of the SB27, CA5, and SB47 TCRs. Overview (upper panels) of the SB27 (A), CA5 (B), and SB47 (C) TCRs bound to HLA-B*35:08 (white) presenting the LPEP peptide (black). The color scheme is consistent across all panels and the orientation of HLA-B*35:08 is identical. TCR α - and β -chain framework residues are colored in pale pink and cyan, respectively. CDR1 α , purple; CDR2 α , green; CDR3 α , red; CDR1 β , yellow; CDR2 β , sand; CDR3 β , orange. The structural footprints (lower panels) of the SB27 (A), CA5 (B), and SB47 (C) TCRs onto HLA-B*35:08^{LPEP} are shown as surface representation with atoms colored based on the corresponding CDR loops that mediate the contacts. The black spheres represent the center of mass for the V α and V β domains.

clone did alloreact with HLA-B*35:01. This alloreactivity appeared to be dependent on one or more self-peptide(s) processed and presented independently of the transporter associated with antigen processing because the transporter associated with the antigen processing-deficient T2 cell line, transfected to express HLA-B*35:01, was recognized. In contrast, SB47 failed to recognize T2 cells transfected to express self-HLA-B*35:08. Given that the SB47 CTL clone did not distinguish between HLA-B*35:08 and B*35:01 presenting the LPEP viral peptide, this indicates that the nature of the self-peptide(s) dictates the HLA-B*35:01 alloreactivity. Accordingly, similar to the cognate interaction, the extent of alloreactivity across the three CTL clones is determined via a peptide-centric mechanism.

Structure of the CA5 TCR-HLA-B*35:08^{LPEP} Complex—To understand how the CA5 TCR ligated to HLA-B*35:08^{LPEP}, we determined its ternary complex and compared it to the SB27 TCR-HLA-B*35:08^{LPEP} complex (Fig. 3). The structure of the CA5 TCR-HLA-B*35:08^{LPEP} complex was solved at 2.3-Å resolution and refined to $R_{\text{factor}}/R_{\text{free}}$ values of 20.5 and 25.7%, respectively (Table 2). Unambiguous electron density was observed at the CA5 TCR-HLA-B*35:08^{LPEP} interface

(supplemental Fig. S3, A and B). In contrast to the SB27 TCR-HLA-B*35:08^{LPEP} structure, in which two different orientations of the SB27 TCR were observed in the crystal lattice, the CA5 TCR-HLA-B*35:08^{LPEP} complex crystallized in a different space group, and only one ternary complex was present in the asymmetric unit.

The CA5 TCR-HLA-B*35:08^{LPEP} complex overlaid closely with the SB27 TCR-HLA-B*35:08^{LPEP} complex (root mean square deviation of 1.65 Å over the entire complex) (Fig. 3, A and B). As such, the CA5 TCR docked orthogonally (93°) to the long axis of the binding cleft of HLA-B*35:08 (Fig. 3B). The total buried surface area (BSA) at the CA5 TCR-HLA-B*35:08^{LPEP} interface ($\approx 1800 \text{ \AA}^2$) was similar to that of the SB27 TCR-HLA-B*35:08^{LPEP} interface ($\approx 1900 \text{ \AA}^2$), and the total number of contacts at the respective interfaces was similar (CA5 TCR: 142 van der Waals, 13 hydrogen bonds; SB27 TCR: 137 van der Waals, 16 hydrogen bonds, and 1 salt bridge). Moreover, the contributions from each of the CDR loops at the respective interfaces were similar, with the CDR1 α , -2 α , and -3 α loops of the CA5 TCR contributing 13.0, 18.4, and 32.9% of the total BSA, respectively, and the CDR1 β , -2 β , and -3 β loops of the CA5 TCR contributing 17.5, 1.7, and 15.6% of the total BSA,

T-cell Receptor Recognition of an Atypical pMHC

TABLE 2
Data collection and refinement statistics

Structure	CA5 TCR-HLA-B*35:08 ^{LPEP}	SB47 TCR-HLA-B*35:08 ^{LPEP}
Resolution (Å) ^a	19.8-2.3 (2.5-2.3)	168-2.8 (2.9-2.8)
Space group	<i>P</i> ₂	<i>I</i> ₄
Temperature	100 K	100 K
Unit-cell parameters (Å)	55.10, 78.41, 105.34	237.60, 237.60, 61.20
(°)	$\beta = 93.06$	
No. observations	253,487 (56298)	299,703 (31899)
No. unique reflections	39,873 (8770)	42,851 (4208)
Completeness (%)	99.8 (100)	99.9 (100)
<i>R</i> _{merge} ^b (%)	10.0 (42.5)	14.5 (47.6)
$\langle I/\sigma(I) \rangle$	13.2 (3.98)	9.59 (3.45)
Multiplicity	6.3 (6.4)	7.0 (7.5)
Refinement statistics		
Non-hydrogen atoms		
Protein	6727	6707
Water	132	124
<i>R</i> _{factor} ^c (%)	20.5	20.0
<i>R</i> _{free} ^c (%)	25.7	23.3
Root mean square deviations from ideality		
Bond lengths (Å)	0.008	0.012
Bond angles (°)	1.08	1.21
Ramachandran plot (%)		
Most-favored region	91.2	91.4
Allowed region	8.2	8.4
Generously allowed region	0.4	0.2

^a Values in parentheses represent the highest-resolution shell.

^b $R_{\text{merge}} = \sum |I_{hkl} - \langle I_{hkl} \rangle| / \sum I_{hkl}$

^c $R_{\text{factor}} = \sum |F_o - F_c| / \sum |F_o|$ for all data except 5%, which were used to calculate *R*_{free}.

respectively. Accordingly, consistent with the biased TRAV19*01-TRAJ34*01 usage, the α -chain of the CA5 TCR dominated the interface (BSA 64.3%).

Akin to the SB27 TCR, the CA5 TCR adopted the same “peptide-centric” docking onto the HLA-B*35:08^{LPEP} complex, with ~50% of the BSA at the interface arising from the bulged peptide (Fig. 3B), which markedly contrasts with typical TCR-pMHC interactions involving peptides of canonical length (BSA 20%) (41). Furthermore, similar to the SB27 TCR interaction, the CA5 TCR did not deform the bulged peptide upon ligation, and the conformation of the peptide in the SB27 TCR and CA5 TCR ternary complexes was very similar. Within the CA5 and SB27 TCR complexes, the TCR-peptide interaction was mediated primarily via the CDR3 α and CDR1 β loops (15) (Fig. 4A). Specifically, the CDR1 β loop of the CA5 and SB27 TCRs ran parallel to the bulged Ag, forming extensive interactions with residues from P6 to P9 of the peptide, whereas the CDR3 α loops flanked primarily the ascending region of the LPEP peptide between residues P4 to P7 (Fig. 4A).

Despite the overall similarities between the CA5 TCR-HLA-B*35:08^{LPEP} and SB27 TCR-HLA-B*35:08^{LPEP} complexes, differences within the interfaces were apparent. First, the shape complementarity (42) at the CA5 TCR-HLA-B*35:08^{LPEP} interface (shape complementarity = 0.77) was moderately higher than that of the corresponding SB27 TCR interface (shape complementarity = 0.71), which correlated with the higher affinity of the CA5 TCR toward HLA-B*35:08^{LPEP}. Second, in comparison to the SB27 TCR footprint, the CA5 TCR docked slightly differently onto HLA-B*35:08^{LPEP}, with the most notable consequence being that the CA5 TCR did not directly contact any residues from the α 1-helix of HLA-B*35:08 (Fig. 3B). Although the SB27 TCR contacts two positions on the α 1-helix (65 and 69) (Fig. 3A), previous mutagenesis studies on the SB27 TCR-HLA-B*35:08^{LPEP} complex underscore the observation that the α 1-helix of HLA-B*35:08 does not appreciably contribute to

the TCR-HLA-B*35:08^{LPEP} interface of either the SB27 or CA5 TCRs (Fig. 3B). Conversely, residues within the α 2-helix of HLA-B*35:08 define an energetic hot spot that underpins SB27 TCR recognition (15). Given that these residues, namely Arg¹⁵¹, Gln¹⁵⁵, Arg¹⁵⁷, and Ala¹⁵⁸, are also contacted by the CA5 TCR, this suggests that a common hot spot within the α 2-helix of HLA-B*35:08 drives the association with the SB27 and CA5 TCRs (supplemental Table S3, Fig. 4C).

CDR3 β Loop-mediated Interactions—The SB27 and CA5 TCRs differ in their CDR3 β loops (CA5 TCR, CASPGETEAF; SB27 TCR, CASPGLAGEYEYQY), and the interactions mediated by this loop varied accordingly between the two ternary complexes. Within the SB27 TCR-HLA-B*35:08^{LPEP} complex, the CDR3 β loop contacted the peptide and the α 2-helix of HLA-B*35:08. Pro⁶⁹⁵ solely interacted with the peptide, contacting the P7-Gln and P8-Gly residues located at the top of the bulged peptide (Fig. 4B). The SB27 CDR3 β -HLA-B*35:08 interactions principally arose from Leu⁶⁹⁸ forming a large number of van der Waals contacts with HLA-B*35:08 and Glu⁶¹⁰¹ salt bridging to Arg¹⁵¹. Although the conformation of the N-terminal region (¹⁰⁴CASPG¹⁰⁸) in the CA5 TCR CDR3 β loop overlaid closely with the corresponding region of the SB27 CDR3 β loop, the remainder of the CDR3 β loop adopted a markedly different conformation and, as a consequence, the CDR3 β -HLA-B*35:08 interactions differed (Fig. 4B). Namely, the salt bridge with Arg¹⁵¹ was absent in the CA5 TCR ternary complex; instead, Arg¹⁵¹ formed van der Waals contacts with Thr⁶¹¹⁰ (Fig. 4C). Additionally, Leu⁶⁹⁸ in the SB27 TCR was replaced by Glu⁶¹⁰⁹ in the CA5 TCR, whose side chain orientated away from the interface (Fig. 4D), with its aliphatic moiety packing against Ala¹⁵⁰ and Arg¹⁵¹ (Fig. 4, B and C). As a consequence, although the CA5 Glu⁶¹⁰⁹ did not directly contact the bulged peptide, its close proximity with P8-Gly (Fig. 4D) may explain why the CA5 CTL clone was more sensitive to P8 substitutions than the SB27 CTL clone (Fig. 1).

T-cell Receptor Recognition of an Atypical pMHC

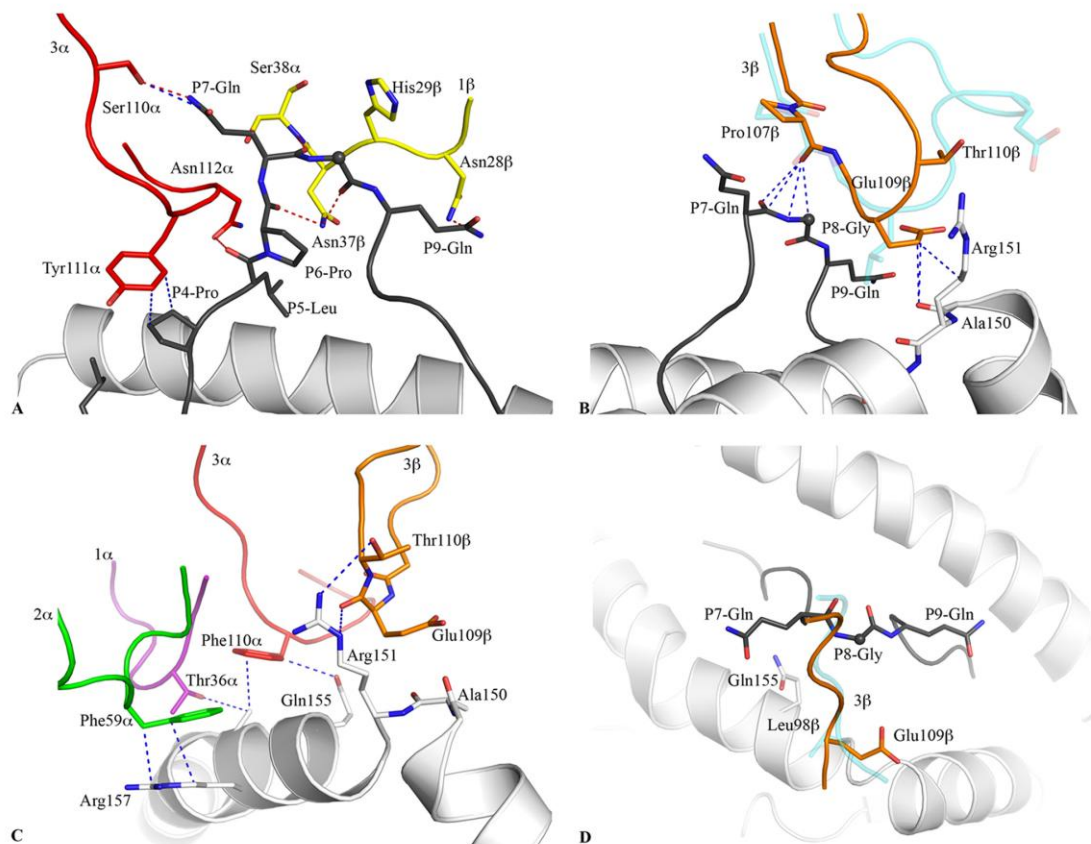


FIGURE 4. Contacts between the CA5 TCR and the HLA-B*35:08^{LPEP} complex. *A*, CA5 TCR-peptide interactions were mediated primarily via the CDR3 α (red) and CDR1 β (yellow) loops. *B*, structural superposition of the CDR3 β loops of the CA5 TCR (orange) and SB27 TCR (transparent cyan) in the corresponding ternary complexes. The conserved TCR-peptide interaction, with the peptide in black stick, is highlighted and the specific TCR-HLA interaction mediated by the CA5 TCR is compared with the SB27 TCR. *C*, conserved TCR-HLA interactions observed in the CA5 and SB27 ternary complex structures. *D*, top view of the CDR3 β loop interaction with the HLA-B*35:08^{LPEP} complex for the CA5 TCR (orange) superposed with the SB27 TCR (transparent cyan). This view shows the difference in orientation between the Glu¹⁰⁹ and Leu⁹⁸ side chains in the CA5 and SB27 TCRs, respectively. All structural representations follow the color scheme depicted in Fig. 3. Blue dashed lines represent van der Waals interactions; red dashed lines represent hydrogen-bond contacts; spheres represent the C α atom of glycine residues.

Overview of the SB47 TCR-HLA-B*35:08^{LPEP} Complex—To understand the shifted fine specificity profile of the SB47 TCR (Fig. 1), we determined the crystal structure of the SB47 TCR-HLA-B*35:08^{LPEP} complex. The structure was solved to 2.8-Å resolution and refined to $R_{\text{factor}}/R_{\text{free}}$ values of 20.0 and 23.3%, respectively (Table 2). Unambiguous electron density was observed at the SB47 TCR-HLA-B*35:08^{LPEP} interface (supplemental Fig. S3, C and D).

The SB47 TCR bound orthogonally onto HLA-B*35:08^{LPEP} with a docking angle of $\sim 87^\circ$ (Fig. 3C), similar to the orientation of the CA5 and SB27 TCRs ligated to HLA-B*35:08^{LPEP} (Fig. 3). However, in stark contrast to the CA5 and SB27 TCRs docking modes, the SB47 TCR was positioned toward the very N-terminal end of the HLA-B*35:08 Ag-binding cleft, thereby essentially not contacting the prominent apex of the super-bulged peptide.

The total BSA at the SB47 TCR-HLA-B*35:08^{LPEP} interface was ≈ 2000 Å, moderately higher than the BSA of the SB27 and

CA5 TCR-HLA-B*35:08^{LPEP} complexes, yet nevertheless, within the range of TCR-pMHC-I interactions determined to date (5). The greater BSA was consistent with an increased number of interactions observed at the SB47 TCR-HLA-B*35:08^{LPEP} interface (168 van der Waals, 16 H-bonds, and 3 salt bridges) compared with the respective CA5 and SB27 TCR-HLA-B*35:08^{LPEP} interfaces. However, unlike the centrally docked SB27 and CA5 TCRs, which made limited contacts with HLA-B*35:08, the extreme N-terminal positioning of the SB47 TCR allowed extensive interactions with the HLA-I molecule itself. Indeed, at this interface, the SB47 TCR interacted with the $\alpha 1$ - and $\alpha 2$ -helices (spanning residues 55–68 and 162–170, respectively). Consequently, the SB47 TCR-HLA-B*35:08 interactions (BSA 83%) were more prominent than the SB47 TCR-peptide contacts (BSA 17%) (Fig. 3C). Nevertheless, despite this more extensive HLA footprint, the affinity of the SB47 TCR for HLA-B*35:08^{LPEP} was weaker than that of the CA5 and SB27 TCRs (Table 1).

T-cell Receptor Recognition of an Atypical pMHC

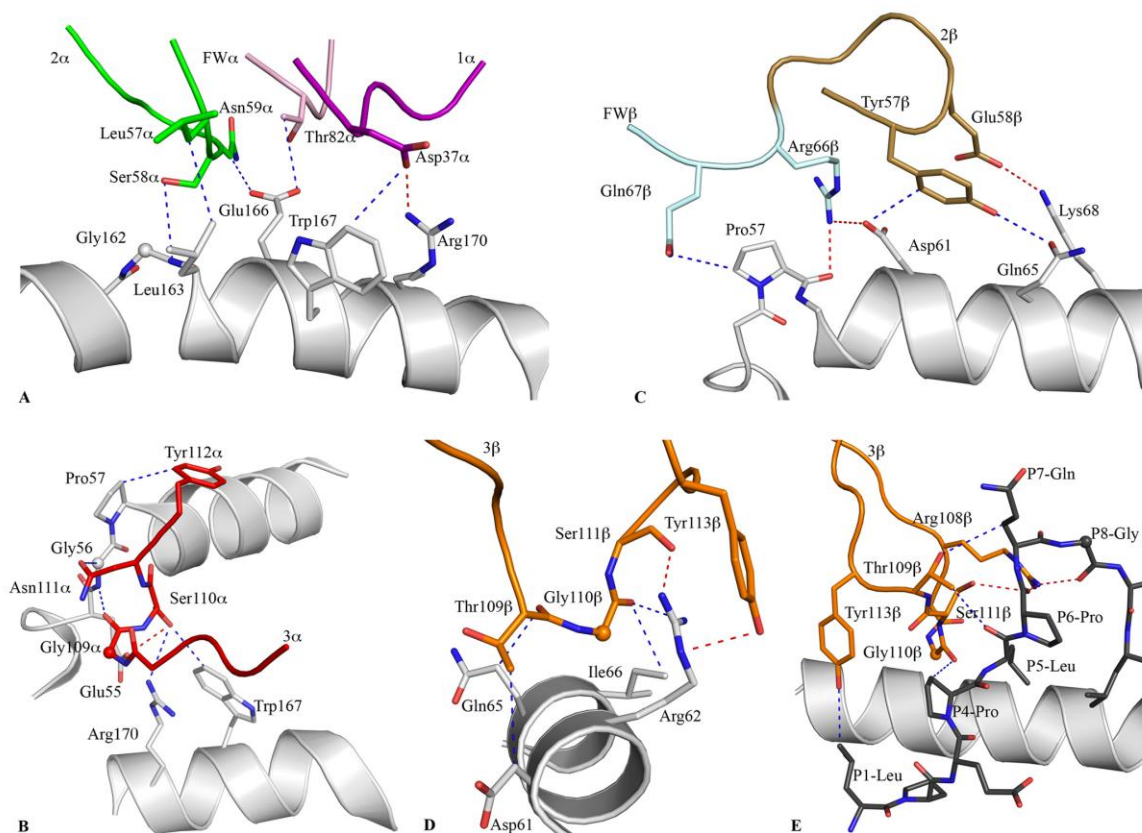


FIGURE 5. Contacts between the SB47 TCR and the HLA-B*35:08^{LPEP} complex. *A*, the germline-encoded SB47 V α chain, including CDR1 α , CDR2 α , and framework residues, interacted extensively with the α 2-helix of HLA-B*35:08. *B*, the CDR3 α loop bridged between the α 1- and α 2-helices, contacting a loop region from Glu⁵⁵ to Pro⁵⁷ of HLA-B*35:08. *C*, the CDR2 β loop and its neighboring framework residues sat directly above the N-terminal part of the α 1-helix of HLA-B*35:08, making contacts between Pro⁵⁷ and Lys⁶⁸. *D*, the CDR3 β loop contacted a small stretch of the α 1-helix of HLA-B*35:08, including Gln⁶⁵. *E*, the SB47 TCR interacted with the N-terminal region of the peptide, including P1-Leu and P4-Pro to P8-Gly, exclusively via the CDR3 β loop. All structural representations follow the color scheme depicted in Fig. 3. *Blue dashed lines* represent van der Waals interactions; *red dashed lines* represent hydrogen-bond contacts; *spheres* represent the C α atom of glycine residues.

A New Footprint on HLA-I—As exemplified by the SB27 and CA5 TCR-HLA-B*35:08^{LPEP} complexes, a bulged and rigid peptide bound within the Ag-binding cleft acts a “hurdle” for the TCR to dock extensively onto the HLA itself. However, the SB47 TCR overcomes this hurdle by adopting a markedly shifted N-terminal footprint, whose center of gravity differs markedly (by 18 Å) compared with that of the SB27 TCR. Indeed, due to its extreme N-terminal footprint, the SB47 TCR did not contact position 155 of HLA-B*35:08 (Fig. 3C), a position that represents a TCR contact point in all TCR-pMHC-I structures determined to date (5, 14).

Five of six SB47 CDR loops contacted HLA-B*35:08 (Fig. 3C, supplemental Table S4), with the CDR3 α and CDR3 β loops contributing most extensively to the interface (19.5 and 39.7% of the total BSA, respectively). Remarkably, only one HLA-B*35:08 contact point was shared between the SB47 and CA5 TCRs (Gly¹⁶²), and the SB47 and SB27 TCRs (Gln⁶⁵); moreover, different CDR loops were involved in these contacts (supplemental Table S4). The SB47 α -chain (BSA 44%) contacted both helices of HLA-B*35:08 (Fig. 3C).

The role of the CDR1 α loop (BSA 8.7%) was limited to Asp³⁷ salt bridging to Arg¹⁷⁰, and forming van der Waals contacts with Trp¹⁶⁷ (Fig. 5A). A stretch of residues, ⁵⁷LSN⁵⁹, from the CDR2 α loop (BSA 12.2%), contacted Gly¹⁶², Leu¹⁶³, and Glu¹⁶⁶, the latter of which interacted with the framework residue, Thr⁸² (Fig. 5A). The CDR3 α loop formed an extended network of interactions with HLA-B*35:08, with its loop positioned orthogonally to the main axis of the α 1-helix, contacting residues spanning positions 55 to 61, as well as interacting with Trp¹⁶⁷ and Arg¹⁷⁰ of the α 2-helix (Fig. 5B). Of note, residues 55–57 of HLA-B*35:08 form a turn before the start of the α 1-helix, and this region of the HLA-I has not been contacted by any TCR determined to date (Fig. 5B).

The SB47 β -chain (BSA 56%) exclusively contacted the α 1-helix via its CDR2 β (BSA 8.6%) and CDR3 β loops (supplemental Table S4). The interactions mediated via the CDR2 β loop involved Tyr⁵⁷ and Glu⁵⁸, as well as two framework (FW) residues upstream of CDR2 β , namely Arg⁶⁶ and Gln⁶⁷ (Fig. 5C). The CDR2 β /FW β interaction spanned from Pro⁵⁷ to Lys⁶⁸ and involved a number of van der Waals interactions and

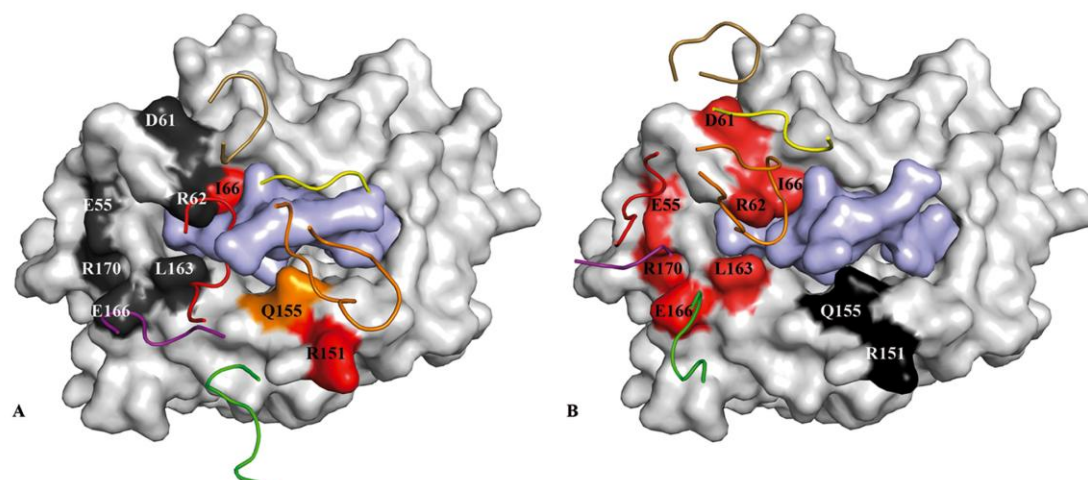


FIGURE 6. Energetic footprints of the SB27 and SB47 TCRs on the HLA-B*35:08^{LPEP} complex. *A* and *B*, surface representation of HLA-B*35:08 (white) with the LPEP peptide (pale purple). The energetic footprint is colored accordingly to the importance of each residue, with critical residues in red (K_{deg} decrease > 5-fold); important residue in orange (5-fold > K_{deg} decrease > 3-fold); dark gray indicates residues that were not important for the interaction. *Panel A* shows the SB27 TCR energetic footprint, and *panel B* shows the SB47 TCR energetic footprint. The CDR loops are represented in schematic format and colored according to the scheme used in Fig. 3.

two salt bridges (Lys⁶⁸ with Glu⁵⁸ and Asp⁶¹ with Arg⁶⁶) (Fig. 5C). The CDR3 β loop was wedged between the ascending part of the bulged peptide (P4–P7) and Arg⁶² of the α 1-helix. The non-germline-encoded residues Thr¹⁰⁹ and Gly¹¹⁰ made van der Waals contacts with Gln⁶⁵/Asp⁶¹ and Arg⁶²/Ile⁶⁶, respectively (Fig. 5D). The majority of the interactions between the CDR3 β loop and the α 1-helix were focused around Arg⁶², whose side chain was flanked by the main chain of the CDR3 β loop and Tyr¹¹³ (Fig. 5D). Collectively, the SB47 TCR adopted a markedly contrasting footprint onto HLA-B*35:08 compared with the SB27 and CA5 TCRs. This extreme N-terminal footprint is reminiscent of the way in which some autoreactive TCRs dock onto MHC-II (supplemental Fig. S2) (43–45), although N-terminal docking footprints have also been observed for antimicrobial TCR-pMHC-I complexes (13).

To investigate further the importance of the N-terminal region of HLA-B*35:08 for SB47 TCR recognition, we performed alanine scanning mutagenesis in conjunction with surface plasmon resonance analyses. Of the N-terminal HLA-B*35:08 residues involved in the interaction with SB47 TCR, we mutated the following to alanine: Glu⁵⁵, Asp⁶¹, Arg⁶², Ile⁶⁶, Leu¹⁶³, Glu¹⁶⁶, and Arg¹⁷⁰. We also included two control residues, namely Arg¹⁵¹ and Gln¹⁵⁵, as they are not contacted by the SB47 TCR, yet they are important for SB27 TCR recognition (15). First, we tested the stability of each mutant via a thermal shift assay; only the I66A mutant decreased the stability of the pHLA-I complex significantly (by more than 10 °C) (supplemental Table S1) (22). Next, we performed surface plasmon resonance analyses against the panel of HLA-B*35:08^{LPEP} mutants (supplemental Table S2). The I66A mutant impacted on SB47 and SB27 TCR recognition, despite the absence of direct contacts with the SB27 TCR. This effect is most likely indirect, with Ile⁶⁶ being important for maintaining pMHC structural integrity. The control mutations, including Arg¹⁵¹

and Gln¹⁵⁵, both exhibited decreased affinities with the SB27 TCR yet had minimal impact on SB47 TCR recognition (supplemental Table 2A). The six other HLA-B*35:08 mutants all decreased SB47 TCR binding affinity by more than 7-fold, with minimal effects on SB27 TCR affinity (supplemental Table S2, Fig. 6). The energetic footprint of the SB47 TCR is in marked contrast to the corresponding energetic footprint for the SB27 TCR (15) (Fig. 6). Collectively, the mutagenesis data not only highlight the N terminally focused nature of the SB47 TCR but also, for the first time, illustrate the importance of the Glu⁵⁵ and Asp⁶¹ HLA residues in enabling TCR recognition.

New TCR Footprint on the Bulged Peptide—Due to the distinct SB47 TCR footprint, its interaction with the bulged peptide differed from that of the SB27 and CA5 TCRs. Namely, the SB47 TCR formed limited contacts with the LPEP peptide, mediated exclusively via the CDR3 β loop (Fig. 5E). The CDR3 β loop sequence, ¹⁰⁸RTGSTYE¹¹⁴, contacted the N-terminal part of the peptide, P1-Leu and P4-Pro, as well as the ascending part of the super-bulge, from P5-Leu to P8-Gly (Fig. 5E). The P1-Leu residue interacted with Tyr¹¹³, and P4-Pro contacted the main chain of Gly¹¹⁰-Ser¹¹¹, thereby providing a basis for the decreased CTL activity observed when these two positions were substituted in the LPEP peptide (Fig. 1). The interactions spanning P5-Leu to P8-Gly were mostly featured by main chain interactions arising either from the peptide or the CDR3 β loop, with three H-bonds (Arg¹⁰⁸NH₂ to P6-Pro^O, P7-Gln^O, P8-Gly; Gly¹¹⁰CO to P5-Leu^N; Ser¹¹¹CO γ to P5-Leu^O, P6-Pro^O) helping to drive the specificity of this interaction. Additionally, the P5-Leu side chain packed against Arg¹⁰⁸ and the main chain of the CDR3 β loop. The P7-Gln and P8-Gly residues were mostly solvent exposed (Fig. 5E), thereby providing a basis for understanding why the SB47 TCR was tolerant to substitutions at these positions. Thus, by adopting an extreme N-terminal

T-cell Receptor Recognition of an Atypical pMHC

docking mode on HLA-B*35:08, the SB47 TCR does not contact the most prominent feature of the bulged peptide.

DISCUSSION

The circulating TCR repertoire encompasses enormous diversity and enables adaptive immune responses to a universe of different pMHC complex antigens. For peptides of canonical length (8–10 residues) presented by MHC-I, a portrait of how closely related and distinct TCRs can interact with the same pMHC epitope has been established (5). In particular, for V β 8.2⁺ TCRs, which are arguably the most intensively investigated (4), approximate common TCR-pMHC docking modes have prevailed, thereby suggesting a basis for MHC bias that largely arises from conserved germline-encoded interactions between the CDR2 β loop and a given region of the MHC (46, 47). A wider range of docking footprints atop the same pMHC landscape is apparent when distinct TCR α - and/or β -chain usage is considered (13, 16, 48). Previously, we provided insight into how the T-cell repertoire can accommodate atypical peptides (>10 amino acids in length) bound to the MHC-I (32, 33). Two divergent TCR recognition modes were apparent. In one mode, the bulged peptide was flattened to enable a large and “standard” MHC footprint (32). In the other mode, a predominantly peptide-centric interaction with a rigid bulged peptide resulted in a very limited MHC-I footprint (33). Here, we provide structural and mechanistic data to explain how both closely related and distinct TCRs can interact with a “super-bulged” peptide presented by HLA-I.

The CA5 TCR is encoded by the same *TRAV-TRAJ-TRBV* gene combination as the archetypal SB27 TCR, with the differences being confined to their respective CDR3 β loops. Accordingly, the overall TCR-HLA-B*35:08^{LPEP} footprints were similar. The SB27 TCR made limited contacts with the α 1- and α 2-helices of HLA-B*35:08. Nonetheless, the footprint was even more restricted with the CA5 TCR, which does not contact the α 1-helix. Accordingly, despite a consensus docking mode between these two TCRs, the non-germline-encoded CDR3 β loop affected MHC-driven contacts, whereas essentially preserving the extent of the peptide-TCR interactions. This highlights the peptide-centricity of this particular TCR-pMHC-I interaction and makes generalizations, such as two-step binding modes and exclusive germline-encoded MHC bias, difficult to reconcile in this system (49). Intriguingly, whereas the SB27 and CA5 TCRs both preferentially recognized HLA-B*35:08^{LPEP} over HLA-B*35:01^{LPEP}, they nevertheless, showed different patterns of alloreactivity. Indeed, only the SB27 TCR alloreacted with HLA-B*44:02. Given the close structural homology between HLA-B*35:08 and HLA-B*44:02, and the peptide-centric focus of these TCRs, these data suggest that peptide-centric molecular mimicry defines HLA-B*44:02 alloreactivity for the SB27 TCR and that the nature of the HLA-B*44:02-restricted self-peptide is non-permissive for CA5 TCR binding. In line with this view, fine specificity differences between SB27 TCR and the CA5 TCR with regard to the cognate LPEP peptide were also apparent.

Additionally, we determined the structure of a TCR that possessed markedly different *TRAV-TRAJ-TRBV* gene usage in comparison to the SB27 and CA5 TCRs, yet nevertheless, rec-

ognized the same HLA-B*35:08^{LPEP} complex. Remarkably, the SB47 TCR employed a peculiar and unprecedented binding mechanism to accommodate the bulged LPEP epitope. Namely, by establishing an extensive footprint on the extreme N-terminal end of HLA-B*35:08, the SB47 TCR essentially circumvented the most prominent feature of the bulged epitope. The CDR3 β loop and, to a lesser extent, the CDR3 α loop, dominated contacts with HLA-B*35:08^{LPEP}, with the docking mode enabling a more HLA-centric view in comparison to the SB27 and CA5 TCRs. Moreover, the markedly shifted N-terminal footprint enabled the TCR to contact a region of MHC-I that had not been observed previously to mediate contacts with a TCR. Notably, this docking strategy also obviated TCR contacts with Gln¹⁵⁵ from HLA-B*35:08, which is surprising given that position 155 has been contacted in every TCR-pMHC-I complex reported to date (5). The N-terminal docking mode explains why the SB47 TCR was able to bind both HLA-B*35:08^{LPEP} and HLA-B*35:01^{LPEP}, as the point of difference between these two allomorphs resides within the α 2-helical hinge, a region that is not contacted in the corresponding ternary complex. Although the SB47 TCR did not alloreact with HLA-B*44:02 and was not activated by HLA-B*35:08 presenting self-peptides, it nevertheless, alloreacted with HLA-B*35:01. Intriguingly, this implicates differences in the repertoire or conformation of self-peptides bound to HLA-B*35:01 versus HLA-B*35:08 in the HLA-B*35:01 alloreactivity of this TCR.

In summary, our data demonstrate that alternative TCR structures with unanticipated docking modes can contribute to T-cell-mediated immune recognition of a lengthy and rigid viral peptide bound to MHC-I. These unusual strategies not only illustrate the versatility of the T-cell repertoire, but also shape our understanding of MHC restriction and TCR alloreactivity.

Acknowledgments—We thank Hanim Halim and the staff at the Monash Crystallization Facility and the Australian Synchrotron for assistance.

REFERENCES

1. Townsend, A., and Bodmer, H. (1989) Antigen recognition by class I-restricted T lymphocytes. *Annu. Rev. Immunol.* **7**, 601–624
2. Viret, C., and Janeway, C. A., Jr. (1999) MHC and T cell development. *Rev. Immunogenet.* **1**, 91–104
3. Yin, Y., Li, Y., and Mariuzza, R. A. (2012) Structural basis for self-recognition by autoimmune T-cell receptors. *Immunol. Rev.* **250**, 32–48
4. Yin, L., Scott-Browne, J., Kappler, J. W., Gapin, L., and Marrack, P. (2012) T cells and their eons-old obsession with MHC. *Immunol. Rev.* **250**, 49–60
5. Gras, S., Burrows, S. R., Turner, S. J., Sewell, A. K., McCluskey, J., and Rossjohn, J. (2012) A structural voyage toward an understanding of the MHC-I-restricted immune response. Lessons learned and much to be learned. *Immunol. Rev.* **250**, 61–81
6. Gras, S., Kjer-Nielsen, L., Chen, Z., Rossjohn, J., and McCluskey, J. (2011) The structural bases of direct T-cell allorecognition. Implications for T-cell-mediated transplant rejection. *Immunol. Cell Biol.* **89**, 388–395
7. Macdonald, W. A., Chen, Z., Gras, S., Archbold, J. K., Tynan, F. E., Clements, C. S., Bharadwaj, M., Kjer-Nielsen, L., Saunders, P. M., Wilce, M. C., Crawford, F., Stadinsky, B., Jackson, D., Brooks, A. G., Purcell, A. W., Kappler, J. W., Burrows, S. R., Rossjohn, J., and McCluskey, J. (2009) T cell allorecognition via molecular mimicry. *Immunity* **31**, 897–908

T-cell Receptor Recognition of an Atypical pMHC

8. Archbold, J. K., Ely, L. K., Kjer-Nielsen, L., Burrows, S. R., Rossjohn, J., McCluskey, J., and Macdonald, W. A. (2008) T cell allorecognition and MHC restriction. A case of Jekyll and Hyde? *Mol. Immunol.* **45**, 583–598
9. Colf, L. A., Bankovich, A. J., Hanick, N. A., Bowerman, N. A., Jones, L. L., Kranz, D. M., and Garcia, K. C. (2007) How a single T cell receptor recognizes both self and foreign MHC. *Cell* **129**, 135–146
10. Birnbaum, M. E., Dong, S., and Garcia, K. C. (2012) Diversity-oriented approaches for interrogating T-cell receptor repertoire, ligand recognition, and function. *Immunol. Rev.* **250**, 82–101
11. Baker, B. M., Scott, D. R., Blevins, S. J., and Hawse, W. F. (2012) Structural and dynamic control of T-cell receptor specificity, cross-reactivity, and binding mechanism. *Immunol. Rev.* **250**, 10–31
12. Lefranc, M.-P., Giudicelli, V., Kaas, Q., Duprat, E., Jabado-Michaloud, J., Scaviner, D., Ginestoux, C., Clément, O., Chaume, D., and Lefranc, G. (2005) IMGT, the international IMMunoGeneTics information system. *Nucleic Acids Res.* **33**, D593–597
13. Gras, S., Burrows, S. R., Kjer-Nielsen, L., Clements, C. S., Liu, Y. C., Sullivan, L. C., Bell, M. J., Brooks, A. G., Purcell, A. W., McCluskey, J., and Rossjohn, J. (2009) The shaping of T cell receptor recognition by self-tolerance. *Immunity* **30**, 193–203
14. Burrows, S. R., Chen, Z., Archbold, J. K., Tynan, F. E., Beddoe, T., Kjer-Nielsen, L., Miles, J. J., Khanna, R., Moss, D. J., Liu, Y. C., Gras, S., Kostenko, L., Brennan, R. M., Clements, C. S., Brooks, A. G., Purcell, A. W., McCluskey, J., and Rossjohn, J. (2010) Hard wiring of T cell receptor specificity for the major histocompatibility complex is underpinned by TCR adaptability. *Proc. Natl. Acad. Sci. U.S.A.* **107**, 10608–10613
15. Liu, Y. C., Chen, Z., Burrows, S. R., Purcell, A. W., McCluskey, J., Rossjohn, J., and Gras, S. (2012) The energetic basis underpinning T-cell receptor recognition of a super-bulged peptide bound to a major histocompatibility complex class I molecule. *J. Biol. Chem.* **287**, 12267–12276
16. Gras, S., Wilmann, P. G., Chen, Z., Halim, H., Liu, Y. C., Kjer-Nielsen, L., Purcell, A. W., Burrows, S. R., McCluskey, J., and Rossjohn, J. (2012) A structural basis for varied $\alpha\beta$ TCR usage against an immunodominant EBV antigen restricted to a HLA-B8 molecule. *J. Immunol.* **188**, 311–321
17. Borg, N. A., Ely, L. K., Beddoe, T., Macdonald, W. A., Reid, H. H., Clements, C. S., Purcell, A. W., Kjer-Nielsen, L., Miles, J. J., Burrows, S. R., McCluskey, J., and Rossjohn, J. (2005) The CDR3 regions of an immunodominant T cell receptor dictate the "energetic landscape" of peptide-MHC recognition. *Nat. Immunol.* **6**, 171–180
18. Ishizuka, J., Stewart-Jones, G. B., van der Merwe, A., Bell, J. I., McMichael, A. J., and Jones, E. Y. (2008) The structural dynamics and energetics of an immunodominant T cell receptor are programmed by its V β domain. *Immunity* **28**, 171–182
19. Manning, T. C., Schlueter, C. J., Brodnicki, T. C., Parke, E. A., Speir, J. A., Garcia, K. C., Teyton, L., Wilson, I. A., and Kranz, D. M. (1998) Alanine scanning mutagenesis of an $\alpha\beta$ T cell receptor. Mapping the energy of antigen recognition. *Immunity* **8**, 413–425
20. Willcox, B. E., Gao, G. F., Weyer, J. R., Ladbury, J. E., Bell, J. I., Jakobsen, B. K., and van der Merwe, P. A. (1999) TCR binding to peptide-MHC stabilizes a flexible recognition interface. *Immunity* **10**, 357–365
21. Baker, B. M., Turner, R. V., Gagnon, S. J., Wiley, D. C., and Biddison, W. E. (2001) Identification of a crucial energetic footprint on the $\alpha 1$ helix of human histocompatibility leukocyte antigen (HLA)-A2 that provides functional interactions for recognition by tax peptide/HLA-A2-specific T cell receptors. *J. Exp. Med.* **193**, 551–562
22. Tynan, F. E., Borg, N. A., Miles, J. J., Beddoe, T., El-Hassen, D., Silins, S. L., van Zuylen, W. J., Purcell, A. W., Kjer-Nielsen, L., McCluskey, J., Burrows, S. R., and Rossjohn, J. (2005) High resolution structures of highly bulged viral epitopes bound to major histocompatibility complex class I. Implications for T-cell receptor engagement and T-cell immunodominance. *J. Biol. Chem.* **280**, 23900–23909
23. Bade-Döding, C., Theodossis, A., Gras, S., Kjer-Nielsen, L., Eiz-Vesper, B., Seltam, A., Huyton, T., Rossjohn, J., McCluskey, J., and Blaszczyk, R. (2011) The impact of human leukocyte antigen (HLA) micropolymorphism on ligand specificity within the HLA-B*41 allotypic family. *Haematologica* **96**, 110–118
24. Probst-Keppler, M., Hecht, H. J., Herrmann, H., Janke, V., Ockenburg, F., Klempner, J., van den Eynde, B. J., and Weiss, S. (2004) Conformational restraints and flexibility of 14-meric peptides in complex with HLA-B*3501. *J. Immunol.* **173**, 5610–5616
25. Speir, J. A., Stevens, J., Joly, E., Butcher, G. W., and Wilson, I. A. (2001) Two different, highly exposed, bulged structures for an unusually long peptide bound to rat MHC class I RT1-Aa. *Immunity* **14**, 81–92
26. Ebert, L. M., Liu, Y. C., Clements, C. S., Robson, N. C., Jackson, H. M., Markby, J. L., Dimopoulos, N., Tan, B. S., Luescher, I. F., Davis, I. D., Rossjohn, J., Cebon, J., Purcell, A. W., and Chen, W. (2009) A long, naturally presented immunodominant epitope from NY-ESO-1 tumor antigen. Implications for cancer vaccine design. *Cancer Res.* **69**, 1046–1054
27. Wynn, K. K., Fulton, Z., Cooper, L., Silins, S. L., Gras, S., Archbold, J. K., Tynan, F. E., Miles, J. J., McCluskey, J., Burrows, S. R., Rossjohn, J., and Khanna, R. (2008) Impact of clonal competition for peptide-MHC complexes on the CD8⁺ T-cell repertoire selection in a persistent viral infection. *Blood* **111**, 4283–4292
28. Miles, J. J., Borg, N. A., Brennan, R. M., Tynan, F. E., Kjer-Nielsen, L., Silins, S. L., Bell, M. J., Burrows, J. M., McCluskey, J., Rossjohn, J., and Burrows, S. R. (2006) TCR α genes direct MHC restriction in the potent human T cell response to a class I-bound viral epitope. *J. Immunol.* **177**, 6804–6814
29. Burrows, S. R., Rossjohn, J., and McCluskey, J. (2006) Have we cut ourselves too short in mapping CTL epitopes? *Trends Immunol.* **27**, 11–16
30. Green, K. J., Miles, J. J., Tellam, J., van Zuylen, W. J., Connolly, G., and Burrows, S. R. (2004) Potent T cell response to a class I-binding 13-mer viral epitope and the influence of HLA micropolymorphism in controlling epitope length. *Eur. J. Immunol.* **34**, 2510–2519
31. Tynan, F. E., Elhassen, D., Purcell, A. W., Burrows, J. M., Borg, N. A., Miles, J. J., Williamson, N. A., Green, K. J., Tellam, J., Kjer-Nielsen, L., McCluskey, J., Rossjohn, J., and Burrows, S. R. (2005) The immunogenicity of a viral cytotoxic T cell epitope is controlled by its MHC-bound conformation. *J. Exp. Med.* **202**, 1249–1260
32. Tynan, F. E., Reid, H. H., Kjer-Nielsen, L., Miles, J. J., Wilce, M. C., Kostenko, L., Borg, N. A., Williamson, N. A., Beddoe, T., Purcell, A. W., Burrows, S. R., McCluskey, J., and Rossjohn, J. (2007) A T cell receptor flattens a bulged antigenic peptide presented by a major histocompatibility complex class I molecule. *Nat. Immunol.* **8**, 268–276
33. Tynan, F. E., Burrows, S. R., Buckle, A. M., Clements, C. S., Borg, N. A., Miles, J. J., Beddoe, T., Whistock, J. C., Wilce, M. C., Silins, S. L., Burrows, J. M., Kjer-Nielsen, L., Kostenko, L., Purcell, A. W., McCluskey, J., and Rossjohn, J. (2005) T cell receptor recognition of a "super-bulged" major histocompatibility complex class I-bound peptide. *Nat. Immunol.* **6**, 1114–1122
34. Quigley, M. F., Almeida, J. R., Price, D. A., and Douek, D. C. (2011) Unbiased molecular analysis of T cell receptor expression using template-switch anchored RT-PCR. *Curr. Protoc. Immunol.* **94**, 10.33.1–10.33.16
35. Kabsch, W. (2010) Integration, scaling, space-group assignment and post-refinement. *Acta Crystallogr. D Biol. Crystallogr.* **66**, 133–144
36. Read, R. J. (2001) Pushing the boundaries of molecular replacement with maximum likelihood. *Acta Crystallogr. D Biol. Crystallogr.* **57**, 1373–1382
37. Emsley, P., and Cowtan, K. (2004) Coot. Model-building tools for molecular graphics. *Acta Crystallogr. D Biol. Crystallogr.* **60**, 2126–2132
38. Adams, P. D., Grosse-Kunstleve, R. W., Hung, L.-W., Ioerger, T. R., McCoy, A. J., Moriarty, N. W., Read, R. J., Sacchettini, J. C., Sauter, N. K., and Terwilliger, T. C. (2002) PHENIX. Building new software for automated crystallographic structure determination. *Acta Crystallogr. D Biol. Crystallogr.* **58**, 1948–1954
39. Bricogne, G., Blanc, E., Brandl, M., Flensburg, C., Keller, P., Paciorek, W., Roversi, P., Sharff, A., Smart, O. S., Vornrhein, C., and Womack, T. O. (2011) *Buster, Version 2.10*, Global Phasing Ltd., Cambridge, United Kingdom
40. DeLano, W. L. (2002) *The PyMOL Molecular Graphics System*, Schrödinger, LLC, New York
41. Godfrey, D. I., Rossjohn, J., and McCluskey, J. (2008) The fidelity, occasional promiscuity, and versatility of T cell receptor recognition. *Immunity* **28**, 304–314
42. Lawrence, M. C., and Colman, P. M. (1993) Shape complementarity at protein/protein interfaces. *J. Mol. Biol.* **234**, 946–950
43. Deng, L., and Mariuzza, R. A. (2007) Recognition of self-peptide-MHC complexes by autoimmune T-cell receptors. *Trends Biochem. Sci.* **32**,

T-cell Receptor Recognition of an Atypical pMHC

- 500–508
44. Hahn, M., Nicholson, M. J., Pyrdol, J., and Wucherpfennig, K. W. (2005) Unconventional topology of self peptide-major histocompatibility complex binding by a human autoimmune T cell receptor. *Nat. Immunol.* **6**, 490–496
45. Li, Y., Huang, Y., Lue, J., Quandt, J. A., Martin, R., and Mariuzza, R. A. (2005) Structure of a human autoimmune TCR bound to a myelin basic protein self-peptide and a multiple sclerosis-associated MHC class II molecule. *EMBO J.* **24**, 2968–2979
46. Dai, S., Huseby, E. S., Rubtsova, K., Scott-Browne, J., Crawford, F., Macdonald, W. A., Marrack, P., and Kappler, J. W. (2008) Crossreactive T cells spotlight the germline rules for $\alpha\beta$ T cell-receptor interactions with MHC molecules. *Immunity* **28**, 324–334
47. Feng, D., Bond, C. J., Ely, L. K., Maynard, J., and Garcia, K. C. (2007) Structural evidence for a germline-encoded T cell receptor-major histocompatibility complex interaction "codon." *Nat. Immunol.* **8**, 975–983
48. Gras, S., Chen, Z., Miles, J. J., Liu, Y. C., Bell, M. J., Sullivan, L. C., Kjer-Nielsen, L., Brennan, R. M., Burrows, J. M., Neller, M. A., Khanna, R., Purcell, A. W., Brooks, A. G., McCluskey, J., Rossjohn, J., and Burrows, S. R. (2010) Allelic polymorphism in the T cell receptor and its impact on immune responses. *J. Exp. Med.* **207**, 1555–1567
49. Wu, L. C., Tuot, D. S., Lyons, D. S., Garcia, K. C., and Davis, M. M. (2002) Two-step binding mechanism for T-cell receptor recognition of peptide MHC. *Nature* **418**, 552–556

Supplementary Data

Figure S1. Polymorphic residues. (A) The HLA-B*35:08 molecule is represented in green cartoon, with HLA-B*35:01 in orange cartoon. The unique polymorphic residue at position 156 is represented in stick. (B) The graphic represents the surface of the HLA-B*35:08 molecule in white, with the LPEP peptide in cyan. The polymorphic residues are coloured in pink; A41, N80, R82, G83 and W167 in the HLA-B*35:08 molecule, correspond to T41, T80, L82, R83 and S167 in the HLA-B*44:02 molecule.

Figure S2. Analysis of SB27, CA5 and SB47 TCR binding to HLA-B35:08^{LPEP} and HLA-B*35:01^{LPEP}. The left and middle panels show the binding curves of immobilized SB27 (A), CA5 (B) and SB47 (C) TCRs with serial dilutions of HLA-B35:08^{LPEP} and HLA-B*35:01^{LPEP} in the fluid phase, respectively. The right panels show kinetic fits for the binding of SB27 (A), CA5 (B) and SB47 (C) TCRs with serial dilutions of HLA-B*35:08^{LPEP}.

Figure S3. Unbiased and refined density around the LPEP peptide. Unbiased (A and C) and refined (B and D) electron densities for the CA5 (A and B) and SB47 (C and D) ternary complexes. The unbiased electron density maps were generated via mFo-Fc maps at 3 sigma (green); refined density maps are contoured at 1 sigma with 2Fo-DFc maps (blue). The peptide is represented in black stick format.

Figure S4. Structural comparison of the SB47 TCR-pMHC-I complex. The N-terminally focused docking topology of the SB47 TCR (A) was structurally similar to the MHC-II-restricted autoimmune 3A6 TCR (B), the OB.1A12 TCR (C), and the E8 TCR (D). All MHC antigen binding clefts are coloured in white cartoon, with peptides shown as black sticks. CDR1 α , purple; CDR2 α , green; CDR3 α , red; CDR1 β yellow; CDR2 β , sand; CDR3 β , orange.

Table S1. Thermal stability assays of HLA B*35:08 mutants bound to the LPEP peptide.

Table S2. Surface plasmon resonance experiments for HLA-B*35:08^{LPEP} mutants and the SB27 and SB47 TCRs.

Table S3. Contact table for the CA5 TCR with the HLA-B*35:08^{LPEP} complex.

Table S4. Contact table for the SB47 TCR with the HLA-B*35:08^{LPEP} complex.

Table S1. Thermal stability assays of HLA B*35:08 mutants bound to the LPEP peptide.

HLA B*35:08 mutant-LPEP	T_m (°C)
B*35:08 wild-type-LPEP	60.3 ± 1.0
B*35:08-E55A-LPEP	57.3 ± 1.0
B*35:08-D61A-LPEP	59.0 ± 1.7
B*35:08-R62A-LPEP	59.8 ± 1.0
B*35:08-I66A-LPEP	48.5 ± 0.4
B*35:08-L163A-LPEP	57.0 ± 0.6
B*35:08-E166A-LPEP	57.6 ± 1.6
B*35:08-R170A-LPEP	57.1 ± 1.4

T_m, or thermal melt, is the temperature required to reach 50% unfolded protein.

Table S2. Surface plasmon resonance experiments for HLA-B*35:08^{LPEP} mutants and the SB27 and SB47 TCRs.

HLA-B*35:08 mutant-LPEP	SB27 TCR K_{d,eq} (μM)	SB47 TCR K_{d,eq} (μM)
B*35:08 wild-type-LPEP	10.4 ± 1.6	22.3 ± 1.6
B*35:08-E55A-LPEP	12.6 ± 0.6	NB
B*35:08-D61A-LPEP	11.7 ± 0.1	NB
B*35:08-R62A-LPEP	17.5 ± 7.3	NB
B*35:08-I66A-LPEP	60.8 ± 10.0	160.6 ± 24.7
B*35:08-R151A-LPEP	87.1 ± 6.2	28.9 ± 2.4
B*35:08-Q155A-LPEP	48.1 ± 5.6	25.7 ± 0.7
B*35:08-L163A-LPEP	16.1 ± 3.4	>200
B*35:08-E166A-LPEP	18.5 ± 0.5	162 ± 5.7
B*35:08-R170A-LPEP	5.4 ± 0.4	NB

Equilibrium dissociation constants (K_{d,eq}) were determined from duplicate measurements for SB27 and SB47 TCR binding to HLA-B*35:08 wild-type and mutants bound to the LPEP peptide. The K_{d,eq} values represent the mean ± standard error of the mean (sem).

Table S3. Contact table for the CA5 TCR with the HLA-B*35:08^{LPEP} complex.

TCR gene segment	CA5 TCR	HLA-B*35:08	Type of bond
CDR1 α	Thr ³⁶	Ala ¹⁵⁸ , Gly ¹⁶²	VDW
CDR1 α	Thr ³⁶ O- γ 1	Ala ¹⁵⁸ O	H-bond
CDR2 α	Asn ⁵⁷	Glu ¹⁵⁴	VDW
CDR2 α	Asn ⁵⁷ N- δ 2	Glu ¹⁵⁴ O- ϵ 1	H-bond
CDR2 α	Phe ⁵⁹	Glu ¹⁵⁴ , Arg ¹⁵⁷ , Ala ¹⁵⁸ , Glu ¹⁶¹	VDW
CDR3 α -N	Phe ¹¹⁰	Gln ¹⁵⁵ , Ala ¹⁵⁸ ,	VDW
CDR3 α -N	Phe ¹¹⁰ O	Gln ¹⁵⁵ N- ϵ 2	H-bond
CDR3 α -J	Tyr ¹¹¹	Gln ¹⁵⁵ , Ala ¹⁵⁸ , Tyr ¹⁵⁹ , Leu ¹⁶³	VDW
CDR3 β -N	Glu ¹⁰⁹	Ala ¹⁵⁰ , Arg ¹⁵¹	VDW
CDR3 β -J	Thr ¹¹⁰	Arg ¹⁵¹	VDW
TCR gene segment	CA5 TCR	LPEP peptide	Type of bond
CDR1 α	Tyr ³⁸	Gln ⁷	VDW
CDR1 α	Tyr ³⁸ OH	Gln ⁷ N ϵ 1	H-bond
CDR3 α -V	Ser ¹⁰⁸	Gln ⁷	VDW
CDR3 α -V	Ser ¹⁰⁸ O- γ	Gln ⁷ N- ϵ 2	H-bond
CDR3 α -N	Gly ¹⁰⁹	Gln ⁷	VDW
CDR3 α -N	Phe ¹¹⁰	Pro ⁶ , Gln ⁷	VDW
CDR3 α -J	Tyr ¹¹¹	Pro ⁴ , Leu ⁵ , Gln ⁷	VDW
CDR3 α -J	Asn ¹¹²	Leu ⁵ , Pro ⁶ , Gln ⁷	VDW
CDR3 α -J	Asn ¹¹² N	Leu ⁵ O	H-bond
CDR3 α -J	Asp ¹¹⁴	Gln ⁷	VDW
CDR1 β	Met ²⁷	Gln ⁹	VDW
CDR1 β	Asn ²⁸	Gln ⁹	VDW
CDR1 β	Asn ²⁸ N- δ 2	Gln ⁹ N- ϵ 2	H-bond
CDR1 β	His ²⁹	Gln ⁷ , Gly ⁸ , Gln ⁹	VDW
CDR1 β	Asn ³⁷	Pro ⁶ , Gln ⁷ , Gly ⁸	VDW
CDR1 β	Asn ³⁷ N	Gln ⁷ O, Gly ⁸ O	H-bond
CDR1 β	Asn ³⁷ N- δ 2	Pro ⁶ O, Gly ⁸ O	H-bond
CDR1 β	Ser ³⁸	Gln ⁷	VDW
CDR1 β	Ser ³⁸ N	Gly ⁷ O	H-bond
FW β	Tyr ⁴⁰	Gln ⁷	VDW
FW β	Tyr ⁴⁰ OH	Gln ⁷ N- ϵ 2	H-bond
CDR3 β -N	Pro ¹⁰⁷	Gln ⁷ , Gly ⁸	VDW

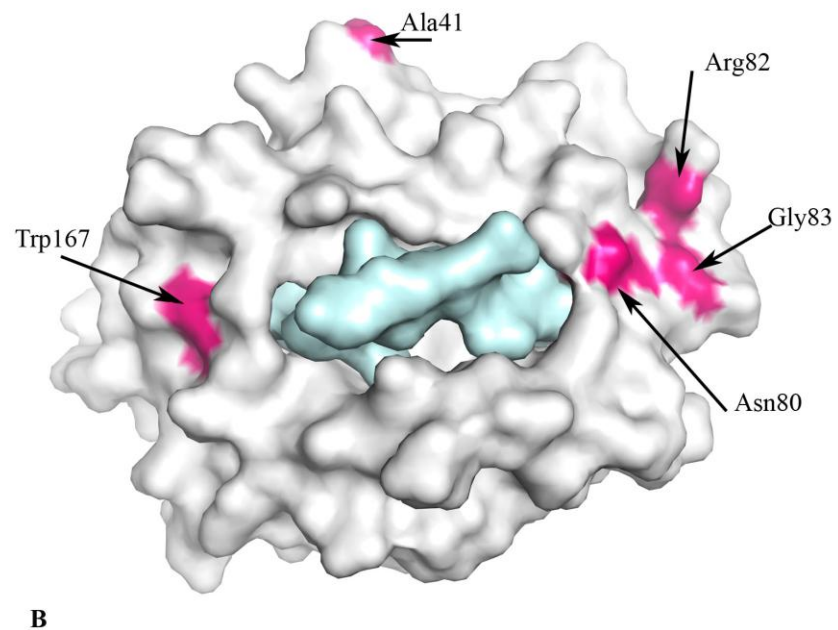
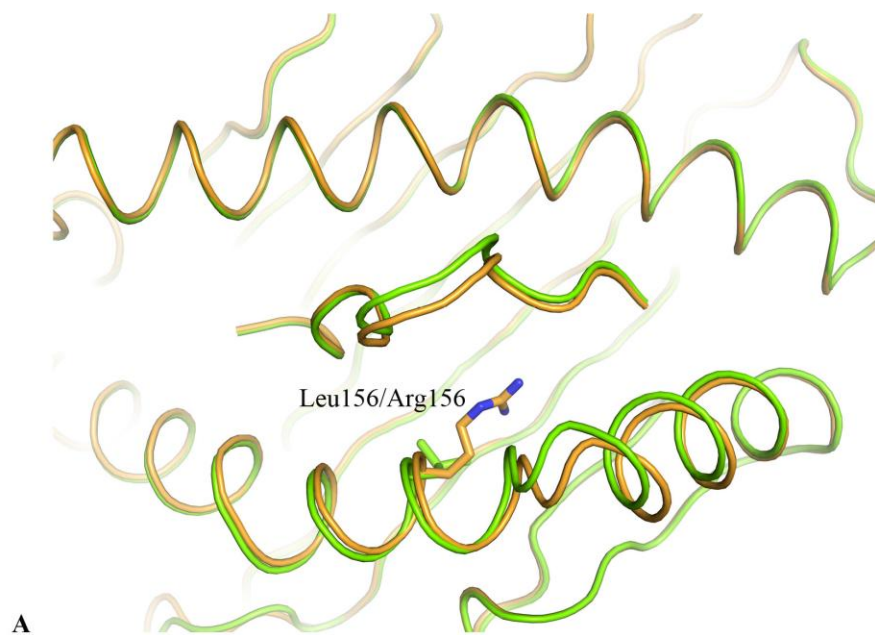
CDR: complementarity-determining region; FW: framework; V: variable; J: junction;
N: non-germline; VDW: van der Waals; H-bond: hydrogen bond.

Table S4. Contact table for the SB47 TCR with the HLA-B*35:08^{LPEP} complex.

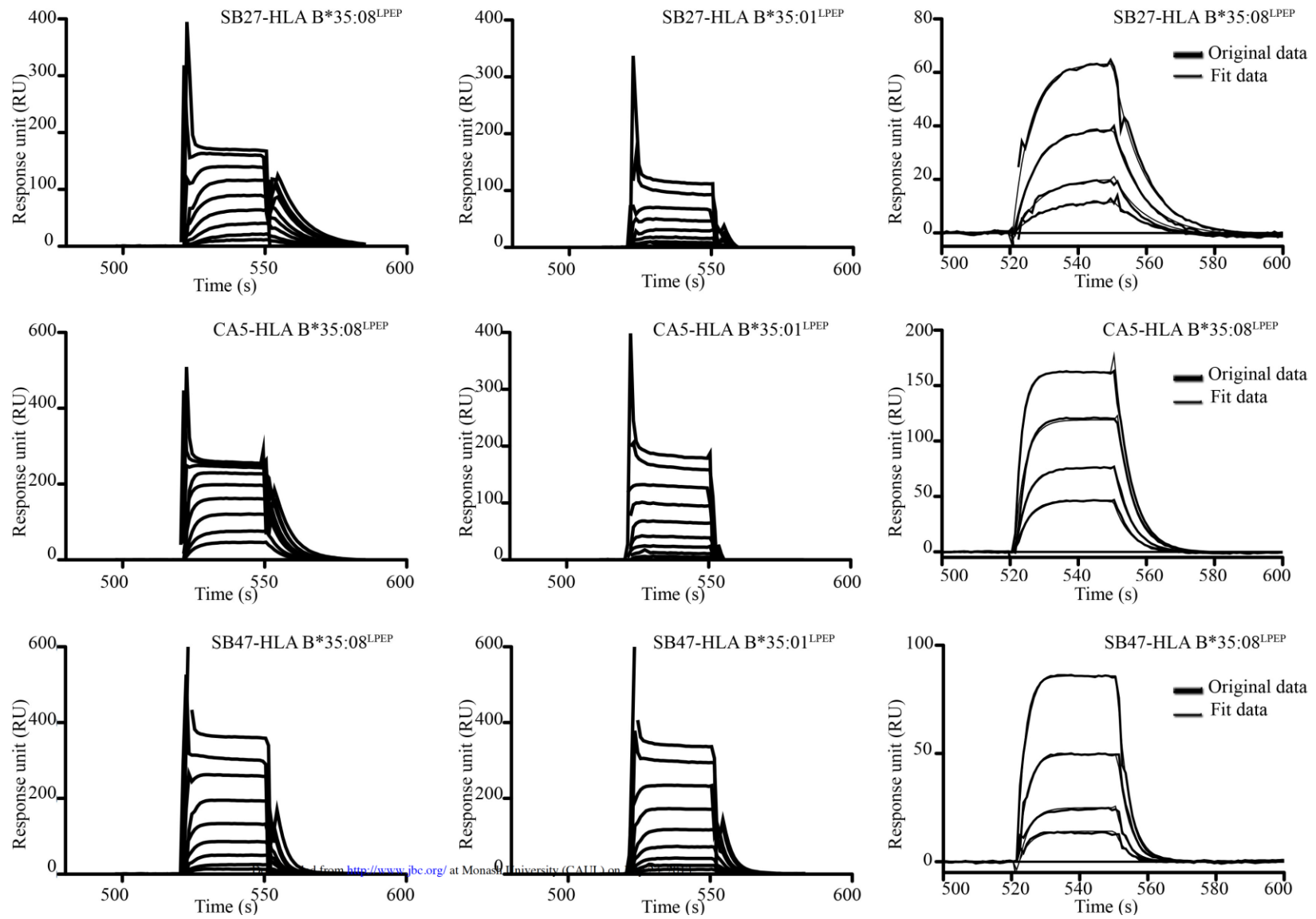
TCR gene segment	SB47 TCR	HLA-B*35:08	Type of bond
CDR1 α	Asp ³⁷	Trp ¹⁶⁷ , Arg ¹⁷⁰	VDW
CDR1 α	Asp ³⁷ O- δ 1, δ 2	Arg ¹⁷⁰ NH1, NH2	Salt bridge
CDR2 α	Leu ⁵⁷	Leu ¹⁶³	VDW
CDR2 α	Ser ⁵⁸	Gly ¹⁶² , Glu ¹⁶⁶	VDW
CDR2 α	Asn ⁵⁹	Glu ¹⁶⁶	VDW
CDR2 α	Asn ⁵⁹ N	Glu ¹⁶⁶ O- ϵ 1	H-bond
FW α	Thr ⁸²	Glu ¹⁶⁶	VDW
CDR3 α -N	Gly ¹⁰⁹	Glu ⁵⁵ , Gly ⁵⁶ , Arg ¹⁷⁰	VDW
CDR3 α -N	Gly ¹⁰⁹ O	Gly ⁵⁶ N	H-bond
CDR3 α -J	Ser ¹¹⁰	Gly ⁵⁶ , Pro ⁵⁷ , Glu ⁵⁸ , Tyr ⁵⁹ , Trp ¹⁶⁷ , Arg ¹⁷⁰	VDW
CDR3 α -J	Ser ¹¹⁰ O	Glu ⁵⁸ N	H-bond
CDR3 α -J	Ser ¹¹⁰ O- γ	Glu ⁵⁵ O- ϵ 1	H-bond
CDR3 α -J	Asn ¹¹¹	Pro ⁵⁷ , Glu ⁵⁸	VDW
CDR3 α -J	Tyr ¹¹²	Pro ⁵⁷ , Glu ⁵⁸ , Asp ⁶¹	VDW
CDR3 α -J	Tyr ¹¹² OH	Asp ⁶¹ O- δ 2	H-bond
CDR2 β	Tyr ⁵⁷	Asp ⁶¹ , Gln ⁶⁵	VDW
CDR2 β	Glu ⁵⁸ O- ϵ 1	Lys ⁶⁸ N ζ	Salt bridge
FW β	Arg ⁶⁶	Pro ⁵⁷ , Asp ⁶¹	VDW
FW β	Arg ⁶⁶ N- ϵ	Asp ⁶¹ O- δ 1, δ 2	H-bond
FW β	Arg ⁶⁶ NH2	Pro ⁵⁷ O	H-bond
FW β	Arg ⁶⁶ NH1, NH2	Asp ⁶¹ O- δ 1, δ 2	Salt bridge
FW β	Gln ⁶⁷	Pro ⁵⁷	VDW
CDR3 β -N	Thr ¹⁰⁹	Gln ⁶⁵ , Asp ⁶¹	VDW
CDR3 β -N	Gly ¹¹⁰	Arg ⁶² , Ile ⁶⁶	VDW
CDR3 β -N	Gly ¹¹⁰ O	Arg ⁶² NH1	H-bond
CDR3 β -J	Ser ¹¹¹	Arg ⁶²	VDW
CDR3 β -J	Ser ¹¹¹ O	Arg ⁶² NH1, NH2	H-bond
CDR3 β -J	Tyr ¹¹³	Arg ⁶²	VDW
CDR3 β -J	Tyr ¹¹³ OH	Arg ⁶² NH1	H-bond
TCR gene segment	SB47 TCR	LPEP peptide	Type of bond
CDR3 β -N	Arg ¹⁰⁸	Leu ⁵ , Pro ⁶ , Gln ⁷	VDW
CDR3 β -N	Arg ¹⁰⁸ NH2	Pro ⁶ O, Gln ⁷ O, Gly ⁸ O	H-bond
CDR3 β -N	Thr ¹⁰⁹	Leu ⁵	VDW
CDR3 β -N	Gly ¹¹⁰	Pro ⁴ , Leu ⁵	VDW
CDR3 β -N	Gly ¹¹⁰ O	Leu ⁵ N	H-bond
CDR3 β -J	Ser ¹¹¹	Pro ⁴ , Leu ⁵ , Pro ⁶ , Gln ⁷	VDW
CDR3 β -J	Ser ¹¹¹ O- γ	Leu ⁵ O, Pro ⁶ O	H-bond
CDR3 β -J	Thr ¹¹²	Leu ⁵ , Gln ⁷	VDW
CDR3 β -J	Tyr ¹¹³	Leu ¹	VDW
CDR3 β -J	Glu ¹¹⁴	Gln ⁷	VDW

CDR: complementarity-determining region; FW: framework; V: variable; J: junction; N: non-germline; VDW: van der Waals; H-bond: hydrogen bond.

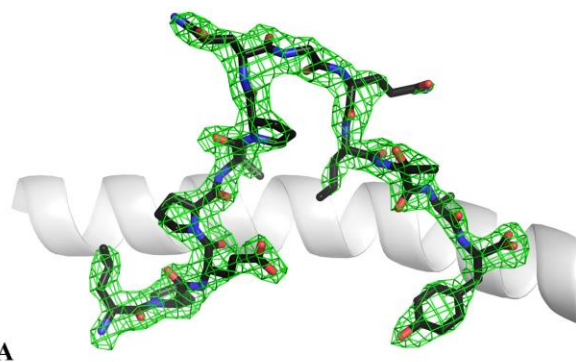
Supplementary Figure 1.



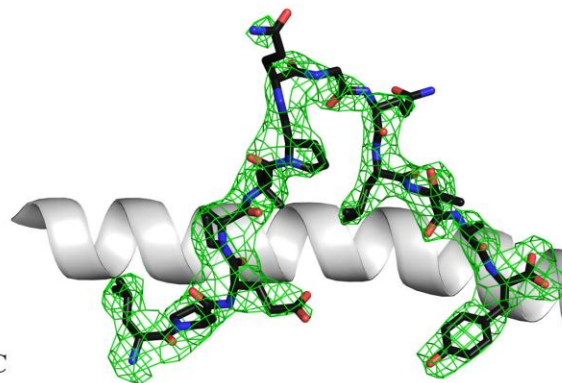
Supplementary Figure 2.



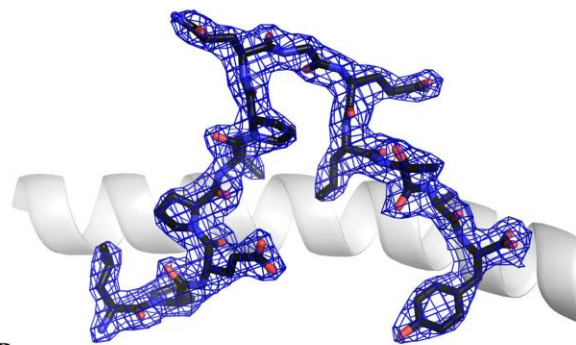
Supplementary Figure 3.



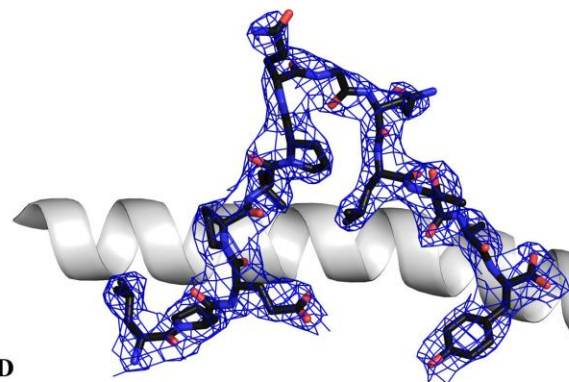
A



C

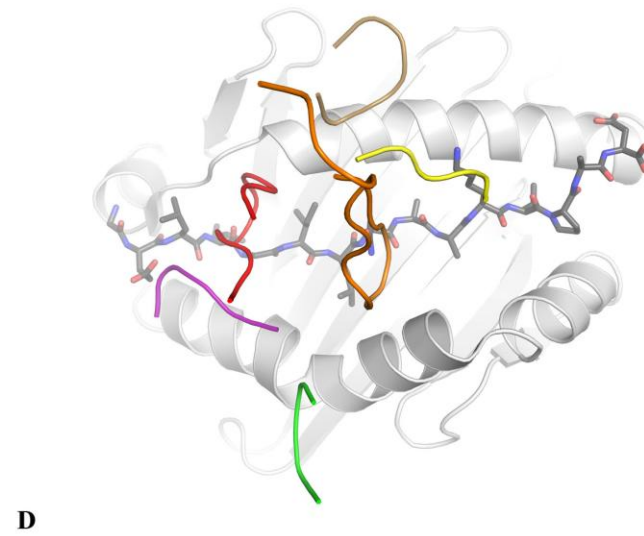
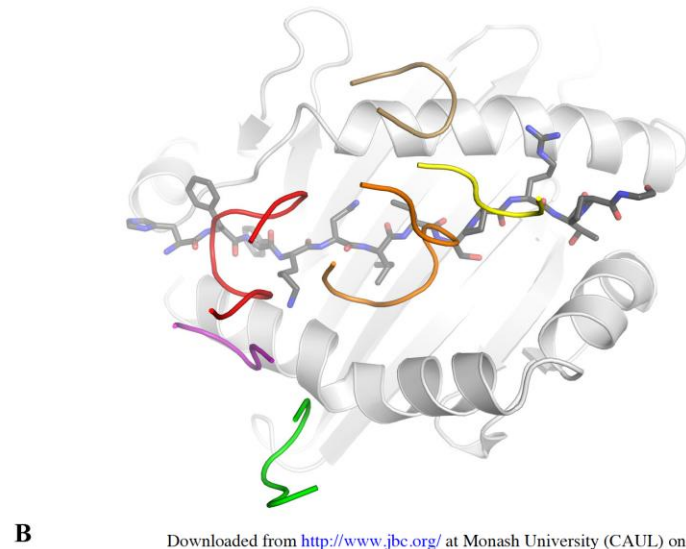
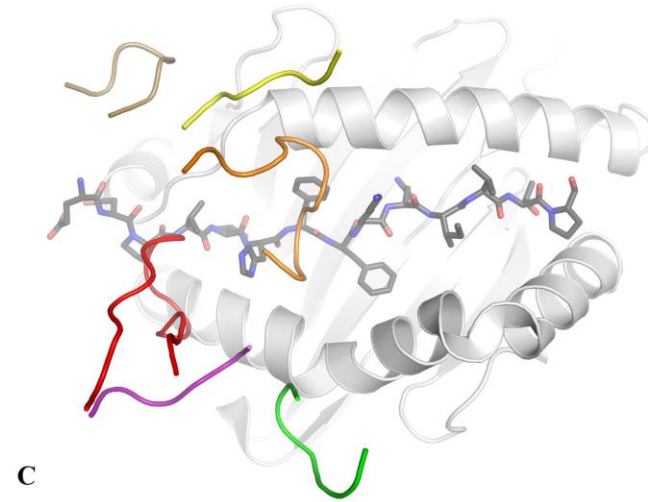
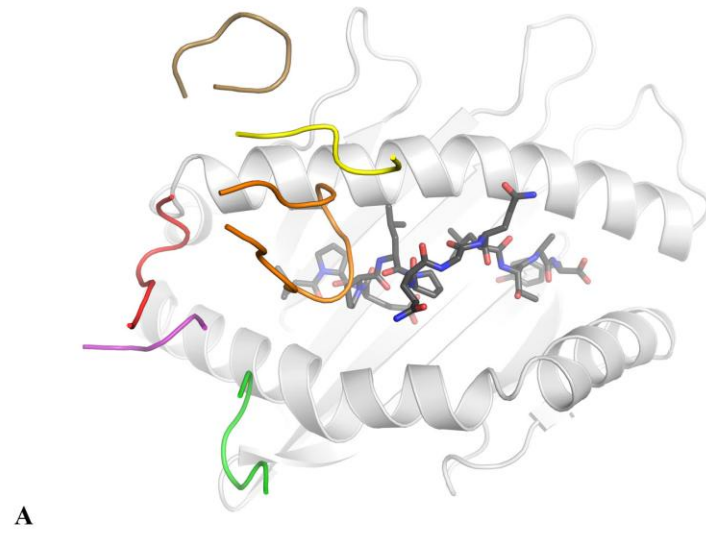


B



D

Supplementary Figure 4.



5 Results: A molecular basis for the interplay between T cells, viral mutants and HLA micropolymorphism

To evade from the host immune surveillance, viruses frequently adapt by mutating T cell epitopes, altering their presentation as a viral escape mechanism. As a consequence, the maintenance of Human Leukocyte Antigen (HLA) polymorphism at the population level became an important component to the host antiviral immunity. This is further assisted by the inherent binding degeneracy of the T cell receptors, allowing them to simultaneously interact and recognise diverse antigens bound to HLA molecules. However, the molecular basis dictating the interplay between HLA polymorphism, viral mutations, and the associated impacts on the T cell recognition is not completely understood, especially in the context of lengthy antigens that often display unusual structural features restricted to HLA class I molecules.

Using the immunodominant TK3 TCR that directed towards a 11mer EBV viral epitope (⁴⁰⁷HPVGEADYFEY⁴¹⁷, HPVVG for short, derived from the EBNA-1 epitope) from HLA-B*35:01+ individual as an example, this following chapter published in the *Journal of Biological Chemistry* (Liu et al., 2014), investigated the structural and functional basis of TK3 recognition towards four naturally occurring and HPVVG variants (HPVVG, HPVVG-A4, HPVVG-D5 and HPVVG-Q5) from different EBV strains, bound to two polymorphic HLA molecules (HLA-B*35:08 and HLA-B*35:01). Based on the structural approach, my results demonstrated that the interplay between buried HLA polymorphism (Leu156 in HLA-B*35:01 and Arg156 in HLA-B*35:08) and antigen variations significantly impacted on both the rigidity and conformation of the epitopes. For instance, Leu156 in HLA-B*35:01 and Arg156 in HLA-B*35:08 manipulated mainly the flexibility of the HPVVG-A4 presentation, whereas their interplay with the HPVVG-D5 and HPVVG-Q5 variants resulted in profound conformational rearrangements of the respective antigens. In particular, the P5-E to P5-Q substitution caused this secondary anchor residue to be structurally replaced by the P7-D, allowing the peptide to form a helical turn within the HLA antigen-binding clefts. Surprisingly, despite these remarkable differences between pHLA conformations, the TK3 TCR interacted with HLA-B*35:08-HPVVG, HLA-B*35:01-HPVVG-Q5 and HLA-B*35:08-HPVVG-D5 complexes via a highly conserved mode of

interaction, similar to that of the cognate ternary complex with minimal CDR loops rearrangement. Instead, the degree of antigen malleability appeared to play a pivotal role in enabling and fine-tuning of the TK3 TCR recognition, which further correlated with the associated biophysical (surface plasmon resonance) and functional data (cellular experiment). Collectively, results summarized in this chapter illustrate the structural and functional interplays between HLA polymorphism, antigen variation, presentation, and the subsequent T cell recognition in the context of unusually long EBV viral determinants.

A molecular basis for the interplay between T cells, viral mutants and human leukocyte antigen polymorphism

Yu Chih Liu¹, Zhenjun Chen², Michelle A. Neller³, John J. Miles³, Anthony W. Purcell¹, James McCluskey², Scott R. Burrows³, Jamie Rossjohn^{1,4,5,*} & Stephanie Gras^{1,5,*}

¹The Department of Biochemistry and Molecular Biology, School of Biomedical Sciences, Monash University, Clayton, 3800, Australia.

²Department of Microbiology & Immunology, Peter Doherty Institute for Infection and Immunity, University of Melbourne, Parkville, Victoria 3010, Australia

³QIMR Berghofer Medical Research Institute and QIMR Berghofer Centre for Immunotherapy and Vaccine Development, Brisbane, 4006, Australia.

⁴Institute of Infection and Immunity, Cardiff University School of Medicine, Heath Park, Cardiff CF14 4XN, Wales, UK.

⁵ARC Centre of Excellence in Advanced Molecular Imaging

* Joint senior and corresponding authors

Running title: *HLA polymorphism and viral escape*

To whom correspondence should be addressed: Stephanie Gras, stephanie.gras@monash.edu Dept. of Biochemistry & Molecular Biology, School of Biomedical Sciences, Monash University, Clayton, Vic 3800, Australia, Tel: (613) 99050254 Fax: (613) 9902500; and Jamie Rossjohn, jamie.rossjohn@monash.edu Dept. of Biochemistry & Molecular Biology, School of Biomedical Sciences, Monash University, Clayton, Vic 3800, Australia, Tel: (613) 99029236 Fax: (613) 9902500

Keywords: human leukocyte antigen class I, Epstein-Barr virus, viral escape, T cell receptor, viral immunity, structural biology.

Background. The impact of EBV variation on T-cell immunity is unclear.

Results. We determined the structures of EBV epitopes bound to HLA-B*35:01/08 and examined the associated T-cell responses.

Conclusion. Viral mutants and HLA polymorphism interplay causes changes in epitope conformation.

Significance. We provide a basis for the impact of EBV strain variation on cellular immunity in humans.

ABSTRACT

Mutations within T cell epitopes represent a common mechanism of viral escape from the host's protective immune response. The diverse T cell repertoire and the extensive *human leukocyte antigen* (HLA) polymorphism across populations is the evolutionary response to viral mutation. However, the molecular basis underpinning the interplay between HLA polymorphism, the T cell repertoire and viral escape is unclear. Here, we investigate the T cell response to a HLA-B*35:01 and HLA-B*35:08 restricted ⁴⁰⁷HPVGEADYFEY⁴¹⁷ epitope

(HPVG) from Epstein-Barr virus (EBV), and naturally occurring variants at positions 4 and 5 thereof. Each viral variant differently impacted on the epitope's flexibility and conformation when bound to HLA-B*35:08 or HLA-B*35:01. We provide a molecular basis for understanding how the single residue polymorphism that discriminates between HLA-B*35:01/08 profoundly impacts on T cell receptor recognition. Surprisingly, one viral variant (P5-Glu to P5-Asp) effectively changed restriction preference from HLA-B*35:01 to HLA-B*35:08. Collectively, our study portrays the interplay between the T cell response, viral escape and HLA polymorphism, whereby HLA polymorphism enables altered presentation of epitopes from different strains of EBV.

INTRODUCTION

The human leukocyte antigen (HLA) complex is the most polymorphic region of the human genome, with over 10,500 HLA alleles documented presently. The maintenance of this diversity reflects the need, at a population level, to present a wide array of pathogen-derived antigens (Ags) to enable

sufficient and protective immunity by the host (1). Each HLA allomorph can bind a large repertoire of peptides (p), with peptide specificity being determined via six pockets (A-F) within the Ag-binding cleft of the molecule (2). Typically, two HLA pockets represent the main peptide anchor, with neighbouring HLA residues also impacting on peptide binding. For example, within the HLA-B*35 family, the B- and F-pockets preferentially bind P2-Pro and P Ω -Phe respectively, with residues lining the D/E pockets (3,4), especially position 156, also impacting on peptide binding (5-7). HLA polymorphism can also exert more subtle effects on the bound peptide repertoire, such as influencing peptide loading and extent of tapasin dependence, and/or altering epitope conformation and flexibility (8,9). However, the full extent of the impact of HLA polymorphism on the responding T cell repertoire remains to be elucidated.

The T cell repertoire comprises a vast array of $\alpha\beta$ T cell receptors (TCRs) that can cope with the challenge of the myriad of potential peptide (p) HLA landscapes (10,11). Despite this diversity, T cells are, for the most part, genetically restricted to interacting with foreign peptide bound to an individual's self-HLA molecules (12). Thus, the HLA-restriction paradigm states that T cells from an HLA-B*35:08⁺/HLA-B*35:01⁻ individual should not cross react with HLA-B*35:01⁺ antigen presenting cells, despite HLA-B*35:08 and HLA-B*35:01 differing by only one residue at position 156 (HLA-B*35:08, Arg; HLA-B*35:01, Leu).

In the periphery, self-HLA molecules bound to processed viral antigens are sensed as foreign, thereby leading to T cell activation and lysis of the virally infected cell. However, to escape immune surveillance, viruses have deployed a wide range of strategies; including interfering with the Ag-processing machinery, and mutating T cell epitopes (13,14). Mutations within major histocompatibility complex (MHC)-bound peptides can potentially impact MHC binding or TCR recognition, which can subsequently lead to immune escape. However, the interplay characterising the molecular arms race between viral escape, HLA polymorphism and the ensuing adaptive immune response is not fully understood.

To understand the impact of HLA polymorphism on anti-viral immunity, we have investigated the protective immune response to Epstein-Barr virus

(EBV), a ubiquitous human pathogen. EBV is controlled by a robust cellular immune response that is directed against a defined number of EBV antigens. There are two distinct strains of EBV, type 1 and type 2, which are primarily divergent within the genes EBNA-2 and EBNA-3 (15,16). In addition, variation in EBNA-1, BZLF1, and LMP1 has been identified, which has led to a greater diversity of known epitope mutations (17). Indeed, it has been suggested that variation in the latent nuclear protein EBNA-1 is linked to the development of EBV associated diseases (18). One EBNA-1 epitope that contains known mutations is HPVG (HPVG^{EADYFEY}), which has been identified in EBV strains infecting Caucasians (19,20). The EBV strains infecting Chinese individuals (21,22) encode a variation at position 5 of this epitope, with an Asp replacing the Glu (HPVG-D5), while in some type 1 EBV isolates (19,23) a glutamine is encoded at position 5 (HPVG-Q5). In addition, the Ag876 EBV strain (type 2 EBV) is prevalent in Africa and encodes a Gly to Ala variation at position 4 of the HPVG epitope (HPVG-A4) (24).

The HPVG epitope is restricted to two closely related allomorphs, HLA-B*35:01 and HLA-B*35:08. The cytotoxic T cell (CTL) response towards this epitope is biased with preferential use of the TRBV9, which pairs with two different TCR α -chains (TRAV20 or TRAV29) based on the HLA restriction element required (25). Previously, we investigated the CTL response to the HPVG determinant in HLA-B*35:01⁺ individuals, and the mode of recognition by a prototypic TRBV9⁺ public TCR, termed TK3. While the TK3 clone could recognise both HLA-B*35:01 and HLA-B*35:08 presenting the HPVG peptide, it exhibited much higher reactivity towards HLA-B*35:01 (20). However, the molecular basis of the TK3 HLA allomorph specificity was unclear. As the TK3 TCR directly contacted P5-Glu of the HPVG epitope, we asked whether the different EBV strains harbouring mutations surrounding P5 could impact on HLA-B*35:01-restricted recognition by the TK3 TCR. Here we report the cellular, biophysical and structural analysis comparing the TK3 clone response in the context of the two HLA allomorphs presenting the HPVG epitope and three naturally occurring EBV strain variants.

EXPERIMENTAL PROCEDURES

Expression, refolding and purification of recombinant TCR and pHLA

The production of the TK3 TCR, HLA-B*35 allomorphs in complex with HPV-G and its variants, were from protocols that were previously described (20). Briefly, individual components of the TCR and HLA molecules were expressed in BL21 *E. coli* cells as inclusion bodies and solubilised in 8 M urea buffer containing 10 mM Tris-pH8, 0.5 mM Na-EDTA, and 1 mM dithiothreitol. TCR and pHLA proteins were then refolded separately in refolding buffer containing 3 M or 5 M urea, 100 mM Tris-HCl pH 8, 2 mM Na-EDTA, 400 mM L-Arg-HCl, 0.5 mM oxidized glutathione and 5 mM reduced glutathione. The refolded solution was dialysed twice against 10 mM Tris-HCl pH 8 overnight to allow sufficient buffer exchange. The dialysed samples were then purified through diethylaminoethanol cellulose, size-exclusion and anion exchange chromatography columns. The quality and purity of the proteins were analysed via SDS-PAGE gel.

Surface Plasmon Resonance Measurement and Analysis

All surface plasmon resonance (SPR) experiments were conducted at 25 °C on the BIAcore 3000 instrument using HBS buffer (10 mM HEPES pH 7.4, 150 mM NaCl, and 0.005% surfactant P20) with 1% BSA to prevent nonspecific binding. The human TCR-specific monoclonal antibody 12H8 (26) was coupled to research grade CM5 chips with standard amine coupling. The experiment was conducted as previously described (27), with a concentration range of 0.78 to 200 µM of the pHLA complexes. BIAevaluation Version 3.1 was used for data analysis with the 1:1 Langmuir binding model.

Thermal melting experiment

Thermal stability experiments of HLA-B*35:01 or HLA-B*35:08 bound to the HPV-G epitope and its variants, were carried out using a Real Time PCR instrument (Corbett RotorGene 300). Purified pHLA samples were concentrated to 5 and 10 µM in TBS buffer (10 mM Tris-HCl pH 8 and 150 mM NaCl) and the experiment was conducted as previously described (28).

Crystallisation of pHLA and TK3 TCR-pHLA complexes

Using hanging drop vapour diffusion techniques, large rod-shape crystals of pHLA were obtained at 20°C with 5mg/ml protein concentration, mixing

with reservoir solutions containing 0.1 M tri-Na-Citrate pH 5.6, 16% PEG 4K and 0.2 M Ammonium Acetate at 1:1 ratio. Plate-like crystals of TK3 TCR-pHLA complexes were obtained at 6 mg/ml protein concentration in reservoir solution consist of 0.2 M LiSO₄, 0.1 M tri-Na-Citrate pH 5.6 and 18% PEG 3350.

Data collection and structure determination

All crystals were soaked in the reservoir solutions with 30% PEG concentration before being flash-frozen in liquid nitrogen. Datasets were collected at the Australian synchrotron (Clayton) with an ADSC-Quantum 210 CCD on MX1 and an ADSC-Quantum 315r CCD on MX2 detector at 100 K. All data were processed and scaled with the XDS program (29) and Scala from the CCP4 suite program respectively (30). The structures were solved using the molecular replacement program, PHASER (31), with the published structure of HLA-B*35:01 (PDB code 2FYU) (25) and TK3 TCR-HLA-B*35:01 (PDB code 3MV7) (20) minus the peptide as models. Structural refinements were performed with PHENIX (32) and BUSTER (33) programs and manual building of the models were carried out with Coot (34). The TCR was numbered according to the IMGT unique numbering system (35) whereby the CDR1 loops start at residue number 27, the CDR2 loops start at number 56, and the CDR3 loops start at residue number 105. The final models have been validated using the Protein Data Base validation web site and the final refinement statistics are summarized in Tables 2&3. Coordinates submitted to PDB database, HLA-B*35:08-HPV-G-A4 (4PRB), HLA-B*35:08-HPV-G-D5 (4PRD), HLA-B*35:08-HPV-G-Q5 (4PRE), HLA-B*35:01-HPV-G-A4 (4PRN), HLA-B*35:01-HPV-G-D5 (4PR5), HLA-B*35:01-HPV-G-Q5 (4PRA), TK3 TCR-HLA-B*35:08-HPV-G (4PRI), TK3 TCR-HLA-B*35:08-HPV-G-D5 (4PRH) and TK3 TCR-HLA-B*35:01-HPV-G-Q5 (4PRP). All molecular graphic representations were created using PyMol (36).

Cellular assays

The TK3 CTLs clone was tested in duplicate for cytotoxicity in standard 5-h chromium release assays. In brief, CTLs were assayed against ⁵¹Cr-labeled lymphoblastoid cell line (LCL) targets (E:T ratios = 4:1, 2:1, 1:1, 0.5:1) or an EBV-negative PHA-stimulated T cell line that was pre-treated with various concentrations of synthetic peptide or left untreated (E:T ratio = 1:1). Toxicity testing of all

peptides was performed before use by adding peptide to ⁵¹Cr-labeled PHA blasts in the absence of CTL effectors. The mean spontaneous lysis for target cells in the culture medium was always <20%, and the variation from the mean specific lysis was <10%.

The ability of TK3 CTLs to secrete IFN- γ , TNF, granzyme A, granzyme B, MIP-1 β and FasL in response to HPV-G and its variants was assessed using a CBA Flex Set (BD Biosciences, San Diego, CA). First, the T2 cell line, transfected with HLA-B*35:01 or T2-HLA-B*35:08, were incubated individually for 1 h with various concentrations of HPV-G, HPV-G-A4, HPV-G-D5, and HPV-G-Q5. After washing these peptide-coated stimulator cells to remove unbound peptide, they were combined with TK3 cells at a 1:20 stimulator to responder ratio. The cells were incubated at 37 °C for 20 h, before supernatants were removed for CBA analysis, according to the manufacturer's protocol. Briefly, CBA capture bead pools were incubated with culture supernatants for 1 h at room temperature, after which a pool of phycoerythrin-conjugated detection reagents was added and incubated for 2 h at room temperature. The capture bead pools were then washed and analysed on a FACSCanto II (BD Biosciences). Analyte production was calculated by comparing test samples to standard curves using FCAP Array Software (Soft Flow Hungary, Pécs, Hungary).

RESULTS

HLA polymorphism affects epitope recognition by the TK3 T cell clone

The TK3 T cell clone, isolated from a HLA-B*35:01⁺ EBV seropositive individual (25), preferentially lysed HLA-B*35:01⁺ EBV-infected target cells presenting the HPV-G epitope over HLA-B*35:08⁺ targets. This was despite these two allomorphs differing by only one residue at position 156 (**Figure 1A**). We next asked whether the three HPV-G variants (HPV-G-A4, HPV-G-Q5, HPV-G-D5) were equivalently recognised by the TK3 clone when presented by HLA-B*35:01 or HLA-B*35:08.

As previously observed the TK3 CTL clone recognised the HPV-G-A4 variant comparably to the wild type (wt) HPV-G epitope in the context of self-HLA-B*35:01, whereas the HPV-G-Q5 and HPV-G-D5 variants showed markedly diminished TK3 recognition (20). Next, we performed a cytotoxicity assay using HLA-B*35:08⁺ target cells in the

presence of the HPV-G peptide and its three variants. Surprisingly, the effects of some of the EBV variants on TK3 activation in the context of HLA-B*35:08 were markedly different compare with presentation by HLA-B*35:01 (**Figure 1B**). Namely, the HPV-G-A4 and HPV-G-Q5 variants, that bound to HLA-B*35:08, poorly stimulated the TK3 clone compared with the wt HPV-G epitope. Moreover, while the HPV-G-D5 epitope markedly diminished TK3 activation when presented by HLA-B*35:01, this variant markedly improved TK3 CTL recognition when presented by HLA-B*35:08 (**Figure 1B**).

This data suggested that HLA polymorphism changes the immunogenicity hierarchy of the TK3 CTL clone towards the HPV-G variant epitopes, with the wt HPV-G epitope being preferentially being recognised by HLA-B*35:01 target cells, whereas the HPV-G-D5 variant is preferentially recognised in the context of HLA-B*35:08.

Difference in cytokine production due to EBV polymorphism

In order to further assess the impact of HLA polymorphism and Ag variation on TK3 CTL activation and polyfunctionality, we used a bead-based multianalyte flow immunoassay (37). This assay enabled the simultaneous detection of the cytokines IL-2, TNF, IFN- γ , and MIP-1 β , in addition to FasL and granzymes A and B. These analytes were all detected in culture supernatants following TK3 CTL activation and, as expected, this clone was best stimulated by HPV-G presented by HLA-B*35:01 (**Figure 2**). While the levels of released analytes were moderately lower in the presence of the HPV-G-A4 peptide (**Figure 2**), the absolute cytokine/granzyme A levels (**Figure 2**) enabled efficient killing of the HLA-B*35:01 target cells presenting the HPV-G-A4 peptide (20). However, the concentrations of these analytes produced by TK3 in the presence of the HPV-G-D5 and HPV-G-Q5 variants and HLA-B*35:01⁺-target cells were markedly diminished. In contrast, the HPV-G-D5 peptide presented by the HLA-B*35:08⁺ target cells was able to stimulate the TK3 clone at a greater level than the wt HPV-G epitope (**Figure 2**). As such, the EBV variant HPV-G-D5 has a variable impact on T cell recognition depending on whether it is presented by HLA-B*35:01 (negative impact) or HLA-B*35:08 (positive impact). Collectively, the analyte production (**Figure 2**) and cytotoxicity data (**Figure 1**) indicate that, while HPV-G

represents the most immunogenic peptide when presented by HLA-B*35:01, the variant HPV-G-D5 is the most immunogenic epitope when presented by HLA-B*35:08 for the TK3 clonotype.

pHLA complex stability and HPV-G polymorphism

To understand the effect of EBV polymorphism on HPV-G epitope presentation, we questioned whether mutation within this epitope could impact the stability of the HLA-B*35:01 and HLA-B*35:08 complexes. Although the HPV-G peptide exhibited greater flexibility when bound to HLA-B*35:01 than HLA-B*35:08 (25), this did not affect pHLA stability (T_m was 67.3 °C for HLA-B*35:01-HPV-G and 64.3 °C for HLA-B*35:08-HPV-G). While the HLA-B*35:08-HPV-G-Q5 complex showed reduced stability (T_m of 56.9 °C), the HPV-G-A4 and HPV-G-D5 variants did not significantly affect the T_m for either HLA-B*35:08 or HLA-B*35:01 (Table 1). Thus, the impact of the EBV variants on TK3 CTL clone activation is not attributable to differential impact on pHLA stability.

TK3 TCR binding affinity

To better understand the basis of the HLA restriction and epitope specificity of TK3, we undertook SPR-based measurements of the TK3 TCR and HLA-B*35:08 bound to HPV-G and its variant epitopes. The affinity (K_d) of the TK3 TCR for the HLA-B*35:01-HPV-G complex was 2.2 μ M (20), while its affinity for HLA-B*35:08-HPV-G was lower, at 93.2 μ M (Figure 3A). The affinities of the TK3 TCR for HPV-G-A4 and HPV-G-Q5 bound to HLA-B*35:08 were approximately 100 μ M (Figures 3 B&C), while for HLA-B*35:08-HPV-G-D5 the K_d was 25.4 μ M with a k_{on} of $1.087 \pm 0.302 \times 10^4$ /Ms and k_{off} of 0.389 ± 0.047 /s (Figure 3D). Thus, consistent with the functional assays, the TK3 TCR preferentially recognises the HPV-G-D5 variant over the HPV-G epitope when bound to HLA-B*35:08.

HLA structural changes induced by HPV-G variants

To determine the structural basis for the differential immunogenicity profiles of the HPV-G variants, we solved the high-resolution crystal structures of HPV-G-A4, HPV-G-D5 and HPV-G-Q5 complexed with HLA-B*35:01 and HLA-B*35:08 (Table 2), and compared them with the respective HLA-B*35:01/08-HPV-G complexes.

As shown previously, the HPV-G peptide bound to HLA-B*35:08 was fully resolved (Figure 4A), and indicated a rigid peptide, while the central part of the peptide was mobile when bound to HLA-B*35:01 (Figure 4B) (25). P4-Gly of the HPV-G epitope points towards solvent, and thus the HPV-G-A4 variant was readily accommodated within HLA-B*35:08 and HLA-B*35:01 (Figures 4 C&D). Both structures adopt a similar conformation, comparable to the HLA-B*35:08-HPV-G structure (root mean square deviation (r.m.s.d.) < 0.25 Å). Curiously, the HPV-G-A4 variant was better resolved in the Ag-binding cleft in comparison to the HPV-G peptide when presented by HLA-B*35:01.

P5-Glu of the HPV-G epitope was found to act as a secondary anchor residue in the HLA-B*35:08 cleft (Figure 4A). The HLA-B*35:08-HPV-G-D5 complex was similar to HLA-B*35:08-HPV-G, displaying an r.m.s.d. of 0.13 Å for the Ag-binding cleft and 0.29 Å for the peptide (Figures 4 A&E). The differences between these two pHLA complexes lay primarily at the P5-D replacement. The shorter P5-D side chain was further away from Arg97 than the corresponding P5-Glu (Figure 4E), and as a result the HPV-G-D5 epitope showed greater flexibility (poor electron density) within HLA-B*35:08 compared to the wt HPV-G epitope, due to the lack of salt-bridge with the Arg97. The structure of HPV-G-D5 bound to HLA-B*35:01 was more surprising (Figure 4F), as it adopted a different conformation compared to the HLA-B*35:08-HPV-G-D5 and caused rearrangements within the HLA-B*35:01 cleft itself. The HPV-G-D5 conformation was constrained within the HLA-B*35:01 Ag-binding cleft, whereby the central region of HPV-G peptide (P5–P8) formed one helical turn and was stabilised by intra-peptide contacts. The helical turn enabled the P5-D to salt bridge with Arg97, the conformation of which was also impacted by the insertion of P9-Phe into the Ag-binding cleft. Moreover, P8-Y also inserted its aromatic ring between the helical turn of the peptide and the HLA α 2-helix. Accordingly, within HLA-B*35:01, structural rearrangements compensate for the shorter side chain of the P5-D to improve peptide-HLA interactions and internal peptide constraints.

The HPV-G-Q5 peptide did not markedly affect the overall antigen-binding cleft conformation of either HLA-B*35:01 (r.m.s.d. of 0.11 Å) or HLA-B*35:08

(r.m.s.d. of 0.22 Å). However, the P5-Gln mutation causes a complete rearrangement of the peptide in both HLA allomorphs (**Figures 4 G&H**). Namely, the P5-Gln flipped outward and became solvent-exposed and thus no longer contacted Arg97 at the base of the Ag-binding cleft. To compensate, P7-Asp reorients from its surface-exposed position within the HLA-B*3:08-HPVG complex to act as a secondary anchor and salt bridge with Arg97 (**Figure 4G**). While the HPVG-Q5 structure was similar between the two HLA molecules (r.m.s.d. of 0.29 Å), conformational differences were observed around position 156. Namely, the Leu156 of HLA-B*35:01 allowed the P7-D to be 1Å deeper in the binding cleft compared to the HLA-B*35:08 structure, in which the large Arg156 occupied this region (**Figures 4 G&H**).

Together, our data show that the HPVG variants exists in dramatically different structural states when bound to the highly homologous allomorphs HLA-B*35:01 and HLA-B*35:08.

The TK3 TCR 'untangles' the HPVG-Q5 epitope

Whilst the HPVG-Q5 variant exhibited a unique peptide conformation when presented by HLA-B*35:01, the TK3 TCR nevertheless exhibited an affinity of 52 μM towards this epitope (20). To understand how the TK3 TCR could accommodate these differences, we solved the structure of the TK3 TCR in complex with HLA-B*35:01-HPVG-Q5 (**Figure 5 and Table 3**).

The TK3 TCR docked onto HLA-B*35:01-HPVG-Q5 comparably to the HLA-B*35:01-HPVG complex (overall r.m.s.d. of 0.29 Å; **Figures 5 A&B**). However, the total buried surface area (BSA) was moderately smaller (~1960 Å²) in the HPVG-Q5 complex compared with the HPVG complex (~2050 Å²), and this also correlated with a reduced number of contacts in the HPVG-Q5 ternary complex (154 contacts compared to 193 contact observed in TK3-HLA-B*35:01-HPVG complex). Despite the striking structural differences observed between the two peptides in the HLA-B*35:01 cleft, upon the TK3 TCR binding, both peptides adopted the same conformation (r.m.s.d. of 0.08 Å; **Figure 6A**). Thus, the TK3 TCR 'untangled' one helical turn within the central region of HPVG-Q5 peptide, in the cleft of HLA-B*35:01, which moulded the peptide into a structure that mimicked the TK3-ligated HPVG conformation. This peptide untangling correlated

with a 27-fold slower on-rate for TK3 TCR when recognising HLA-B*35:01-HPVG-Q5 ($K_{on} = 0.15 \times 10^4 / \text{Ms}$) compared to HLA-B*35:01-HPVG ($K_{on} = 4.0 \times 10^4 / \text{Ms}$) (20). Thus, an induced form of molecular mimicry enables the TK3 TCR to recognise HPVG variants that adopt differing conformations in the binary pHLA-B*35:01 complexes.

*The TK3 TCR-HLA-B*35:08-HPVG ternary complex*

The TRBV9⁺ TK3 TCR preferentially recognised the HLA-B*35:01-HPVG complex over the HLA-B*35:08-HPVG complex. To understand the basis of this finely tuned HLA restricted response, we determined the structure of the TK3 TCR-HLA-B*35:08-HPVG complex. This complex was crystallised in the same space group as the TK3 TCR-HLA-B*35:01-HPVG complex, and determined to 2.4 Å resolution (**Table 3**). The TK3 TCR docked diagonally (66°) onto the HLA-B*35:08-HPVG complex and aligned similarly to that of the cognate TK3 TCR-HLA-B*35:01-HPVG complex ($\alpha 1$ - $\alpha 2$ domains r.m.s.d. value of 0.24 Å) (**Figure 5C**). The total buried surface area (BSA) of the TK3 TCR-HLA-B*35:08-HPVG interface is 2040 Å², which was comprised of 150 van der Waals (vdw) contacts, 14 H-bonds (Hb) and 1 salt bridge (sb) interactions, and exhibited fewer contacts than the TK3 TCR-HLA-B*35:01-HPVG complex (BSA of 2050 Å², 172 vdw, 18 Hb, 3 sb).

The structures of the HLA-B*35:08-HPVG free and in complex with the TK3 TCR provided an opportunity to analyse the conformational changes of the HPVG epitope upon complexation. The central region of the HPVG epitope was disordered in the HLA-B*35:01 binary complex, yet fully resolved and more rigid in the HLA-B*35:08 complex. Comparison of the HLA-B*35:08-HPVG structures in its free and TK3 TCR bound forms revealed that the HPVG peptide changed conformation markedly upon TCR ligation. In the binary HLA-B*35:08-HPVG complex, the HPVG peptide leant towards the $\alpha 1$ -helix of HLA-B*35:08, and upon TK3 TCR binding, the central region (P7-D to P9-F) of the peptide was pushed towards the $\alpha 2$ -helix, with a maximal displacement of 3.5 Å of the P8-Y C α atom (**Figure 6B**). The CDR3 α loop of the TK3 TCR pushed the P7-D to avoid steric clashes, allowing the P8-Y aromatic ring to be enveloped by the three CDR β loops. A notable feature of the TK3 TCR-HLA-B*35:08-

6

HPVG complex is that the peptide adopted the same conformation as that observed in the TK3 TCR-HLA-B*35:01-HPVG complex (r.m.s.d. of 0.18 Å) (**Figure 6C**), despite marked differences observed in their binary complexes (**Figures 4 A&B**). The TK3 TCR-induced structural changes observed in the HPVG peptide when bound by the HLA-B*35:08 are consistent with the lower affinity and reduced activity of the TK3 TCR towards the HLA-B*35:08-HPVG complex (**Figures 1A&2**) in comparison to the HLA-B*35:01-HPVG complex (20). Accordingly, the micro-polymorphism between HLA-B*35:01/08 plays a pivotal role in fine-tuning the dynamics of antigen flexibility, which subsequently impacts on TK3 TCR recognition and ultimately immunogenicity.

A HPV variant changes HLA restriction

While the TK3 TCR affinity was low for HLA-B*35:08 presenting the wt HPVG peptide from the most frequent Caucasian EBV strain ($K_d = 93.2 \mu\text{M}$) it was improved by almost four-fold with the HPVG-D5 variant from the Chinese EBV strain ($K_d = 25.4 \mu\text{M}$) (**Figure 2**). To understand the mechanism driving the higher affinity of the TK3 TCR towards HPVG-D5, we solved the structure of the TK3 TCR-HLA-B*35:08-HPVG-D5 complex (**Figure 5D**). The overall structure was similar to the TK3 TCR-HLA-B*35:08-HPVG ternary complexes. Namely, the TK3 TCR adopted a diagonal docking mode onto HLA-B*35:08-HPVG-D5 (66°), with a BSA of 2020 \AA^2 . The main differences between the two ternary complexes were centred on the P5 position of the peptide. In HLA-B*35:08-HPVG, Arg156 is part of a polar network that includes Arg97 and P5-E (**Figure 4A**), whereas in HLA-B*35:08-HPVG-D5, this polar network is weakened due to the shorter side chain of P5-D (**Figure 4E**). Upon TK3 TCR binding, the HPVG-D5, was pushed towards the $\alpha 2$ -helix of HLA-B*35:08 by the CDR3 α loop (**Figure 6D**) in a manner similar to the TK3 TCR-induced HPVG peptide movement. In comparison to the P5-E residue, the shorter P5-D residue was positioned 1 Å deeper into the cleft upon TK3 TCR ligation, which caused Arg97 to shift away from the peptide and interact with the Asp114 and Tyr74. However, the longer P5-E residue does not allow these conformational readjustments in HLA-B*35:08 upon TK3 engagement. Accordingly, the HLA-B*35:08-HPVG-D5 complex appeared intrinsically more malleable than the HLA-B*35:08-HPVG

complex, which resulted in improved recognition by the TK3 TCR.

DISCUSSION

Viral mutations are well known to subvert the antiviral T cell mediated response by impacting HLA binding, the Ag-presentation machinery, and T cell receptor recognition. Here we show how naturally occurring EBV variants affect the flexibility and conformation of a T cell epitope, which directly subsequently impacts TCR recognition. We also show how a single HLA micropolymorphism within the HLA-B*35 family alters the conformation, and hence immunogenicity, of the wt viral epitope and variants. Moreover, our findings demonstrate the functional benefit of maintaining HLA micropolymorphism, as one viral variant effectively caused the switching of the HLA restriction element.

The HPV epitope is restricted to HLA-B*35:01 and HLA-B*35:08, two HLA allomorphs that differ by one residue at position 156, with this polymorphism also dictating the nature of the responding T-cell repertoire (25). Namely, in HLA-B*35:01⁺ individuals the CTL response is characterised by biased TRAV20-TRBV9 usage, while in HLA-B*35:08⁺ individuals it is underpinned by TRAV29-TRBV9 usage (20,25). Previously, we characterised the molecular basis of recognition by the prototypical TCR TK3 that responds to the HPVG epitope from HLA-B*35:01⁺ individuals, and also showed how TCR polymorphism within the TRBV9 gene impacted this protective immune response (20). We also demonstrated how the viral mutants HPVG-A4, HPVG-D5, and HPVG-Q5 impacted this HLA-B*35:01-restricted response.

In this study, we aimed to address the basis of the finely balanced HLA-B*35:01/08 restriction. The single residue polymorphism (HLA-B*35:01, Leu 156; HLA-B*35:08, Arg 156) is located at the base of the Ag-binding cleft, so *a priori* it was unclear how such a buried polymorphism could impact TCR recognition in this system. Previously, the mechanisms for this HLA-B*35:01/08 polymorphism's impacts on the conformation and immunogenicity have been determined for another 10mer and 11mer (6,38) as well as 13mer EBV determinants (39). More broadly, buried polymorphisms within the HLA-B*44 (40-42) and HLA-B*57 families (43) can impact epitope

7

flexibility and TCR recognition in antiviral responses and, in the context of HLA-B*44, in an alloreactive T cell response (42). Here we show that the HPV-G epitope is directly impacted by this polymorphic position, with the magnitude of the effect being dependent on the nature of the naturally occurring viral variants of the HPV-G epitope. The impact of these viral mutants was dramatic and unpredictable. For example, the HPV-G-Q5 variant caused a large reorientation of the epitope within HLA-B*35:01/08 such that the P5-Q residue was pointing out of the cleft, whereas the P5-Glu residue represented a middle anchor residue in HLA-B*35:01. Despite this difference, the TK3 TCR was still able to ligate to the HLA-B*35:01-HPV-G-Q5 epitope, albeit more weakly. The TK3 TCR was able to achieve this recognition by flattening the HPV-G-Q5 determinant in a manner analogous to how TCRs have been shown to ‘bulldoze’ bulged antigenic determinants (38). Here, the HPV-G-Q5 peptide adopted the same conformation as the HPV-G determinant in its TCR-ligated state, thereby indicating that the TK3 TCR can accommodate differing HPV-G landscapes via an induced-fit mechanism.

The TK3 TCR was able to cope well with the HPV-G-A4 variant when presented by HLA-B*35:01, whereas the HPV-G-D5 variant was very poorly recognised. Surprisingly, however, the HPV-G-D5 variant was recognised better by TK3 when presented by HLA-B*35:08 than the wt-HPV-G epitope. The ability of the TK3 clone to preferentially recognise the HPV-G-D5 determinant is due to the greater capacity of this epitope to enable conformational changes within HLA-B*35:08 upon TCR ligation. It is likely that the T cell repertoire in HLA-B*35:01⁺ individuals, harbouring the EBV strain containing the HPV-G-D5 variant, will differ from the classical TK3 gene usage (TRAV20/TRBV9) to maintain optimal viral suppression. Our findings highlight the sensitive and unpredictable interplay between T cell repertoire usage, HLA polymorphism, and viral escape.

REFERENCES

1. Parham, P. (1996) *Nature* **384**, 109-110
2. Rammensee, H. G., Falk, K., and Rotzschke, O. (1993) *Annual review of immunology* **11**, 213-244
3. Falk, K., Rotzschke, O., Grahovac, B., Schendel, D., Stevanovic, S., Jung, G., and Rammensee, H. G. (1993) *Immunogenetics* **38**, 161-162
4. Smith, K. J., Reid, S. W., Stuart, D. I., McMichael, A. J., Jones, E. Y., and Bell, J. I. (1996) *Immunity* **4**, 203-213
5. Burrows, J. M., Wynn, K. K., Tynan, F. E., Archbold, J., Miles, J. J., Bell, M. J., Brennan, R. M., Walker, S., McCluskey, J., Rossjohn, J., Khanna, R., and Burrows, S. R. (2007) *Eur J Immunol* **37**, 946-953
6. Tynan, F. E., Elhassen, D., Purcell, A. W., Burrows, J. M., Borg, N. A., Miles, J. J., Williamson, N. A., Green, K. J., Tellam, J., Kjer-Nielsen, L., McCluskey, J., Rossjohn, J., and Burrows, S. R. (2005) *J Exp Med* **202**, 1249-1260
7. Tynan, F. E., Borg, N. A., Miles, J. J., Beddoe, T., El-Hassen, D., Silins, S. L., van Zuylen, W. J., Purcell, A. W., Kjer-Nielsen, L., McCluskey, J., Burrows, S. R., and Rossjohn, J. (2005) *J Biol Chem* **280**, 23900-23909
8. Zernich, D., Purcell, A. W., Macdonald, W. A., Kjer-Nielsen, L., Ely, L. K., Laham, N., Crockford, T., Mifsud, N. A., Bharadwaj, M., Chang, L., Tait, B. D., Holdsworth, R., Brooks, A. G., Bottomley, S. P., Beddoe, T., Peh, C. A., Rossjohn, J., and McCluskey, J. (2004) *J Exp Med* **200**, 13-24
9. Hulsmeyer, M., Hillig, R. C., Volz, A., Ruhl, M., Schroder, W., Saenger, W., Ziegler, A., and Uchanska-Ziegler, B. (2002) *J Biol Chem* **277**, 47844-47853
10. Davis, M. M., and Bjorkman, P. J. (1988) *Nature* **334**, 395-402

11. Turner, S. J., Doherty, P. C., McCluskey, J., and Rossjohn, J. (2006) *Nat Rev Immunol* **6**, 883-894
12. Doherty, P. C., and Zinkernagel, R. M. (1975) *Nature* **256**, 50-52
13. Fruh, K., Ahn, K., Djaballah, H., Sempe, P., van Endert, P. M., Tampe, R., Peterson, P. A., and Yang, Y. (1995) *Nature* **375**, 415-418
14. Ladell, K., Hashimoto, M., Iglesias, M. C., Wilmann, P. G., McLaren, J. E., Gras, S., Chikata, T., Kuse, N., Fastenackels, S., Gostick, E., Bridgeman, J. S., Venturi, V., Arkoub, Z. A., Agut, H., van†Bockel, D. J., Almeida, J. R., Douek, D. C., Meyer, L., Venet, A., Takiguchi, M., Rossjohn, J., Price, D. A., and Appay, V. (2013) *Immunity* **38**, 425-436
15. Dambaugh, T., Hennessy, K., Chamnankit, L., and Kieff, E. (1984) *Proceedings of the National Academy of Sciences of the United States of America* **81**, 7632-7636
16. Sample, J., Young, L., Martin, B., Chatman, T., Kieff, E., and Rickinson, A. (1990) *Journal of virology* **64**, 4084-4092
17. Sitki-Green, D., Edwards, R. H., Webster-Cyriaque, J., and Raab-Traub, N. (2002) *Journal of virology* **76**, 9645-9656
18. Wang, J. T., Sheeng, T. S., Su, I. J., Chen, J. Y., and Chen, M. R. (2003) *Journal of medical virology* **69**, 417-425
19. Bell, M. J., Brennan, R., Miles, J. J., Moss, D. J., Burrows, J. M., and Burrows, S. R. (2008) *The Journal of infectious diseases* **197**, 1594-1597
20. Gras, S., Chen, Z., Miles, J. J., Liu, Y. C., Bell, M. J., Sullivan, L. C., Kjer-Nielsen, L., Brennan, R. M., Burrows, J. M., Neller, M. A., Khanna, R., Purcell, A. W., Brooks, A. G., McCluskey, J., Rossjohn, J., and Burrows, S. R. (2010) *The Journal of Experimental Medicine* **207**, 1555-1567
21. Wang, W. Y., Chien, Y. C., Jan, J. S., Chueh, C. M., and Lin, J. C. (2002) *Clinical cancer research : an official journal of the American Association for Cancer Research* **8**, 2586-2590
22. Zhang, X. S., Wang, H. H., Hu, L. F., Li, A., Zhang, R. H., Mai, H. Q., Xia, J. C., Chen, L. Z., and Zeng, Y. X. (2004) *Cancer letters* **211**, 11-18
23. Snudden, D. K., Smith, P. R., Lai, D., Ng, M. H., and Griffin, B. E. (1995) *Oncogene* **10**, 1545-1552
24. Dolan, A., Addison, C., Gatherer, D., Davison, A. J., and McGeoch, D. J. (2006) *Virology* **350**, 164-170
25. Miles, J. J., Borg, N. A., Brennan, R. M., Tynan, F. E., Kjer-Nielsen, L., Silins, S. L., Bell, M. J., Burrows, J. M., McCluskey, J., Rossjohn, J., and Burrows, S. R. (2006) *Journal of immunology* **177**, 6804-6814
26. Borg, N. A., Ely, L. K., Beddoe, T., Macdonald, W. A., Reid, H. H., Clements, C. S., Purcell, A. W., Kjer-Nielsen, L., Miles, J. J., Burrows, S. R., McCluskey, J., and Rossjohn, J. (2005) *Nat Immunol* **6**, 171-180
27. Gras, S., Burrows, S. R., Kjer-Nielsen, L., Clements, C. S., Liu, Y. C., Sullivan, L. C., Bell, M. J., Brooks, A. G., Purcell, A. W., McCluskey, J., and Rossjohn, J. (2009) *Immunity* **30**, 193-203
28. Gras, S., Wilmann, P. G., Chen, Z., Halim, H., Liu, Y. C., Kjer-Nielsen, L., Purcell, A. W., Burrows, S. R., McCluskey, J., and Rossjohn, J. (2012) *Journal of immunology* **188**, 311-321
29. Kabsch, W. (2010) *Acta Crystallogr D Biol Crystallogr* **66**, 125-132
30. (1994) *Acta crystallographica. Section D, Biological crystallography* **50**, 760-763
31. McCoy, A. J., Grosse-Kunstleve, R. W., Adams, P. D., Winn, M. D., Storoni, L. C., and Read, R. J. (2007) *J Appl Crystallogr* **40**, 658-674
32. Adams, P. D., Afonine, P. V., Bunkoczi, G., Chen, V. B., Davis, I. W., Echols, N., Headd, J. J., Hung, L. W., Kapral, G. J., Grosse-Kunstleve, R. W., McCoy, A. J., Moriarty, N. W., Oeffner, R., Read, R. J., Richardson, D. C., Richardson, J. S., Terwilliger, T. C., and Zwart, P. H. (2010) *Acta Crystallogr D Biol Crystallogr* **66**, 213-221

33. Smart, O. S., Womack, T. O., Flensburg, C., Keller, P., Paciorek, W., Sharff, A., Vornrhein, C., and Bricogne, G. (2012) *Acta crystallographica. Section D, Biological crystallography* **68**, 368-380
34. Emsley, P., Lohkamp, B., Scott, W. G., and Cowtan, K. (2010) *Acta Crystallogr D Biol Crystallogr* **66**, 486-501
35. Lefranc, M.-P., Giudicelli, V., Kaas, Q., Duprat, E., Jabado-Michaloud, J., Scaviner, D., Ginestoux, C., Clement, O., Chaume, D., and Lefranc, G. (2005) *Nucl. Acids Res.* **33**, D593-597
36. DeLano, W. L. (2002) The PyMOL Molecular Graphics System. DeLano Scientific, San Carlos, CA, USA
37. Varro, R., Chen, R., Sepulveda, H., and Apgar, J. (2007) *Methods in molecular biology* **378**, 125-152
38. Tynan, F. E., Reid, H. H., Kjer-Nielsen, L., Miles, J. J., Wilce, M. C. J., Kostenko, L., Borg, N. A., Williamson, N. A., Beddoe, T., Purcell, A. W., Burrows, S. R., McCluskey, J., and Rossjohn, J. (2007) *Nat Immunol* **8**, 268-276
39. Tynan, F. E., Burrows, S. R., Buckle, A. M., Clements, C. S., Borg, N. A., Miles, J. J., Beddoe, T., Whisstock, J. C., Wilce, M. C., Silins, S. L., Burrows, J. M., Kjer-Nielsen, L., Kostenko, L., Purcell, A. W., McCluskey, J., and Rossjohn, J. (2005) *Nat Immunol* **6**, 1114-1122
40. Macdonald, W. A., Purcell, A. W., Mifsud, N. A., Ely, L. K., Williams, D. S., Chang, L., Gorman, J. J., Clements, C. S., Kjer-Nielsen, L., Koelle, D. M., Burrows, S. R., Tait, B. D., Holdsworth, R., Brooks, A. G., Lovrecz, G. O., Lu, L., Rossjohn, J., and McCluskey, J. (2003) *J Exp Med* **198**, 679-691
41. Archbold, J. K., Macdonald, W. A., Gras, S., Ely, L. K., Miles, J. J., Bell, M. J., Brennan, R. M., Beddoe, T., Wilce, M. C., Clements, C. S., Purcell, A. W., McCluskey, J., Burrows, S. R., and Rossjohn, J. (2009) *J Exp Med* **206**, 209-219
42. Macdonald, W. A., Chen, Z., Gras, S., Archbold, J. K., Tynan, F. E., Clements, C. S., Bharadwaj, M., Kjer-Nielsen, L., Saunders, P. M., Wilce, M. C. J., Crawford, F., Stadinsky, B., Jackson, D., Brooks, A. G., Purcell, A. W., Kappler, J. W., Burrows, S. R., Rossjohn, J., and McCluskey, J. (2009) *Immunity* **31**, 897-908
43. Stewart-Jones, G. B., Simpson, P., van der Merwe, P. A., Easterbrook, P., McMichael, A. J., Rowland-Jones, S. L., Jones, E. Y., and Gillespie, G. M. (2012) *Proceedings of the National Academy of Sciences of the United States of America* **109**, E3483-3492

ACKNOWLEDGMENTS

We thank the staff at the Australian Synchrotron for assistance with data collection. This work was supported by the Australian Research Council (ARC, www.arc.gov.au) and the National Health and Medical Research Council of Australia (NHMRC, www.nhmrc.gov.au; Grant number APP1067374). JJM by an NHMRC Career Development Fellowship, AWP by a NHMRC Senior Research Fellowship, SRB by an NHMRC Principal Research Fellowship and JR by a NHMRC Australia Fellowship and SG by an ARC Future Fellowship. Abbreviations: BSA, buried surface area; CDR, complementarity-determining region; pHLA, peptide-Human Leukocyte Antigen complex; SPR, surface plasmon resonance.

FIGURE LEGENDS

Figure 1. TK3 clone reactivity.

(A) Preferential recognition of HLA-B*35:01⁺ LCLs cells by the TK3 CTL clone compare to HLA-B*35:08⁺ LCLs cells presenting the HPV peptide. (B) Recognition of HPV and three EBV variants of the epitopes by the TK3 clone using a cytotoxicity assay with HLA-B*35:08⁺-PHA blasts as target cells.

Figure 2. Analyte production by TK3.

Analytes released by TK3 following stimulation with HPV-G peptide or one of its three variants, presented either by T2-HLA-B*35:01 (full line) or T2-HLA-B*35:08 APCs (dashed lines) are shown. The culture supernatants of stimulated TK3 cells were assessed by CBA, and analyte production in response to HPV-G (blue), HPV-G-A4 (green), HPV-G-D5 (red), and HPV-G-Q5 (purple) stimulation is shown, at a range of peptide concentrations.

Figure 3. Surface Plasmon resonance sensograms of the TK3 TCR with HLA-B*35:08 bound to HPV-G and its variants.

A range of concentrations (0.78 to 200 μ M) of the HLA-B*35:08 in complex with either HPV-G (A); HPV-G-A4 (B); HPV-G-Q5 (C) or HPV-G-D5 (D) were used for SPR response analysis with the TK3 TCR. The experiments have been conducted in duplicate and the values represent the mean \pm standard error of the mean (sem).

Figure 4. Binary structures of pHLA complexes.

Structures of four HPV-G epitopes (stick) bound to HLA-B*35:08 (pale blue cartoon) or HLA-B*35:01 (pale pink cartoon) (25). The HPV-G peptide is in cyan and pink on panels A and B; HPV-G-A4 is in dark blue and magenta on panels C and D; the HPV-G-D5 is in blue and purple on panels E and F and the HPV-G-Q5 is in pale blue and pale pink on panels G and H bound to HLA-B*35:08 and HLA-B*35:01 respectively. The Arg97 from the cleft and the polymorphic residue 156 (Arg in HLA-B*35:08 and Leu in HLA-B*35:01) of the antigen-binding cleft are represented in stick and coloured accordingly to the HLA. The variations in the HPV-G peptide are highlighted in yellow at position 4 and 5. The red dashed lines represent the salt-bridges between the P5 or P7 of the peptide with the Arg97 and Arg156.

Figure 5. Ternary structures of TK3 TCR-pHLA complexes.

The top panels show an overview of the TK3 TCR in complex with either HLA-B*35:01-HPV-G (A), HLA-B*35:01-HPV-G-Q5 (B); HLA-B*35:08-HPV-G (C) or HLA-B*35:08-HPV-G-D5 (D). The TK3 TCR is represented in cartoon with the α -chain in pale pink, the β -chain in pale blue and the CDR loops colour in yellow, magenta and marine for the CDR1, 2 and 3 α ; in orange, red and green for the CDR1, 2 and 3 β respectively. The HLA and β 2m are represented in cartoon and coloured in white (HLA-B*35:01 and β 2m) or grey (HLA-B*35:08). The peptides are represented in stick and coloured in pale purple for HPV-G, green for HPV-G-D5 and brown for the HPV-G-Q5. The bottom panels show the footprint of the TK3 TCR on the surface of the pHLA complexes, namely HLA-B*35:01-HPV-G (A), HLA-B*35:01-HPV-G-Q5 (B), HLA-B*35:08-HPV-G (C) or HLA-B*35:08-HPV-G-D5 (D). The atomic contact are coloured accordingly to the CDR loop and follow the same colour scheme that the top panel. The black spheres represent the centre of mass of the V α and V β domains of the TK3 TCR.

Figure 6. Peptide flexibility enhances the TK3 TCR recognition.

(A) Superposition of the TK3 TCR-HLA-B*35:01-HPV-G-Q5 complex (yellow) with the TK3 TCR-HLA-B*35:01-HPV-G complex (pink), with the TCR and HLA in cartoon and the peptide in stick representation. (B) Superposition of the HLA-B*35:08-HPV-G free (orange) and bound to the TK3 TCR (green). The peptide is represented in cartoon with the C α of the P8-Tyr residue show in sphere. (C) Superposition of the TK3 TCR in complex with the HLA-B*35:01-HPV-G (pink) and HLA-B*35:08-HPV-G (green), with the TCR and HLA in cartoon representation and the peptide in stick representation. (D) Superposition of the HLA-B*35:08-HPV-G-D5 free (red) and bound to the TK3 TCR (blue). The spheres represent the C α atom of the P8-Tyr from the HPV-G-D5 peptide, the red dash lines represent the hydrogen bonds form by the Arg97 with the Asp114 and Tyr74 in the TK3 TCR-HLA-B*35:08-HPV-G-D5 structure.

Table 1. Thermal stability measurement of HLA-B*35:01 or HLA-B*35:08 in complex with the HPV G peptide and its variants. T_m is the thermal melt point of each protein, representing the temperature required to unfold 50% of the sample.

Proteins	T_m (°C)
B*35:01-HPVG	67.3 ± 0.3
B*35:01-HPVG-A4	68.6 ± 0.2
B*35:01-HPVG-D5	68.0 ± 0.4
B*35:01-HPVG-Q5	65.0 ± 0.6
B*35:08-HPVG	64.3 ± 1.4
B*35:08-HPVG-A4	67.3 ± 0.9
B*35:08-HPVG-D5	61.0 ± 1.7
B*35:08-HPVG-Q5	56.9 ± 0.7

Table 2. Data collection and refinement statistics of pHLA structures.

Structures	B*35:01-HPVG-A4	B*35:01-HPVG-D5	B*35:01-HPVG-Q5
Resolution (Å)	1.65 (1.75-1.65)	1.8 (1.9-1.8)	1.85 (1.95-1.85)
Space group	P2₁2₁2₁	P2₁2₁2₁	P2₁2₁2₁
Unit cell parameters (Å)	50.7, 81.3, 110.4	50.6, 81.2, 109.1	50.7, 81.4, 109.5
Temperature (K)	100	100	100
Total number of observations	400579 (61312)	311047 (46089)	289411 (42022)
Number of unique reflections	55695 (8882)	42487 (6249)	39526 (5701)
Completeness (%)	100 (100)	100 (100)	100 (99.9)
^a R _{merge} (%)	5.8 (40.5)	6.6 (44.7)	7.6 (42.7)
I/σI	20.7 (4.53)	26.2 (4.76)	21.6 (5.1)
Multiplicity	7.2 (6.9)	7.3 (7.3)	7.3 (7.3)
^b R _{factor} (%)	18.4	17.8	18.9
^b R _{free} (%)	22.1	21.3	22.4
Rmsd bond lengths (Å)	0.012	0.010	0.008
Rmsd bond angles (°)	1.234	1.097	1.074
<i>Ramachandran plot (%)</i>			
Favoured/Allowed	99.4	99.1	99.4
Generously allowed	0.6	0.9	0.6
Disallowed	0.0	0.0	0.0
Structures	B*35:08-HPVG-A4	B*35:08-HPVG-D5	B*35:08-HPVG-Q5
Resolution (Å)	1.75 (1.85-1.75)	1.75 (1.85-1.75)	1.65 (1.75-1.65)
Space group	P2₁2₁2₁	P2₁2₁2₁	P2₁2₁2₁
Unit-cell parameters (Å)	50.8, 82.1, 110.5	50.9, 82.0, 110.4	50.9, 81.7, 110.8
Temperature (K)	100	100	100
Total number of observations	344591 (51279)	345635 (51872)	403652 (61175)
Number of unique reflections	47355 (7124)	47357 (7124)	55751 (8726)
Completeness (%)	100 (100)	99.9 (99.7)	98.9 (96.8)
^a R _{merge} (%)	5.5 (48.9)	5.4 (32.0)	5.1 (35.2)
I/σI	25.6 (4.29)	24.1 (6.5)	26.9 (5.9)
Multiplicity	7.3 (7.3)	7.3 (7.3)	7.2 (7.0)
^b R _{factor} (%)	20.0	19.6	17.7
^b R _{free} (%)	23.3	23.4	20.3
Rmsd bond lengths (Å)	0.016	0.012	0.014
Rmsd bond angles (°)	1.201	1.172	1.255
<i>Ramachandran plot (%)</i>			
Favoured/Allowed	99.1	99.4	99.4
Generously allowed	0.9	0.6	0.6
Disallowed	0.0	0.0	0.0

^a R_{merge} = $\sum |I_{hkl} - \langle I_{hkl} \rangle| / \sum I_{hkl}$. ^b R_{factor} = $\sum_{hkl} ||F_o| - |F_c|| / \sum_{hkl} |F_o|$ for all data except $\approx 5\%$ which were used for R_{free} calculation. Values in parentheses are for the highest resolution-shell. Rmsd: root mean square deviation.

Table 3. Data collection and refinement statistics of the TK3 TCR-pHLA complexes.

Structures	TK3-B*35:08-HPVG	TK3- B*35:08-HPVG_D5	TK3- B*35:01-HPVG_Q5
Resolution (Å)	41.7-2.4 (2.5-2.4)	50-2.5 (2.6-2.5)	47.3-2.5 (2.64-2.5)
Space group	P1	P1	P1
Unit cell parameters (Å)	44.58, 62.37, 100.45	44.83, 62.08, 98.33	45.14, 62.60, 97.81
(°)	98.17, 94.59, 109.11	92.69, 101.92, 108.21	92.04, 102.53, 109.70
Temperature (K)	100	100	100
Total number of observations	142189 (16985)	125672 (14351)	125365 (18871)
Number of unique reflections	73467 (8684)	32833 (3671)	32843 (4832)
Completeness (%)	93.6 (96.2)	96.9 (98.2)	97.2 (98.0)
^a R _{merge} (%)	7.0 (32.3)	7.5 (44.5)	8.2 (49.0)
I/σI	10.77 (2.69)	11.79 (3.27)	11.9 (3.7)
Multiplicity	1.9 (1.9)	3.8 (3.9)	3.8 (3.9)
^b R _{factor} (%)	21.3	22.5	18.0
^b R _{free} (%)	26.1	26.5	22.8
Rmsd bond lengths (Å)	0.011	0.010	0.010
Rmsd bond angles (°)	1.17	1.13	1.07
<i>Ramachandran plot (%)</i>			
Favoured/Allowed	98.9	99.2	99.0
Generously allowed	0.7	0.6	0.6
Disallowed	0.4	0.2	0.4

^a $R_{\text{merge}} = \sum |I_{\text{hkl}} - \langle I_{\text{hkl}} \rangle| / \sum I_{\text{hkl}}$. ^b $R_{\text{factor}} = \sum_{\text{hkl}} ||F_o| - |F_c|| / \sum_{\text{hkl}} |F_o|$ for all data except $\approx 5\%$ which were used for R_{free} calculation. Values in parentheses are for the highest resolution-shell. Rmsd: root mean square deviation.

Figure 1.

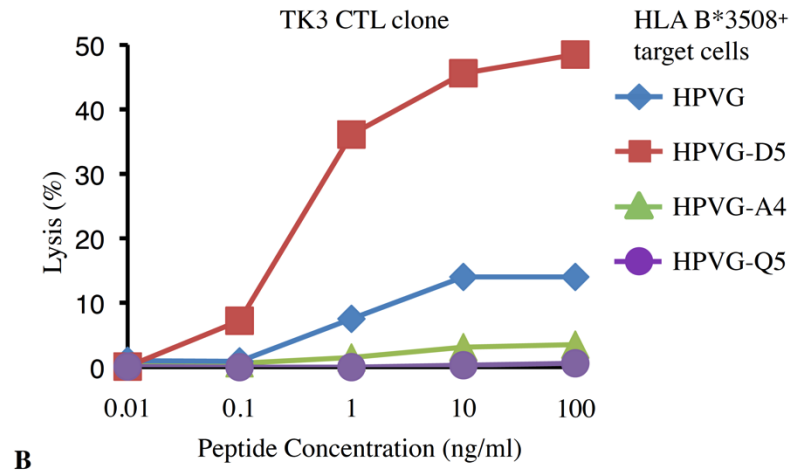
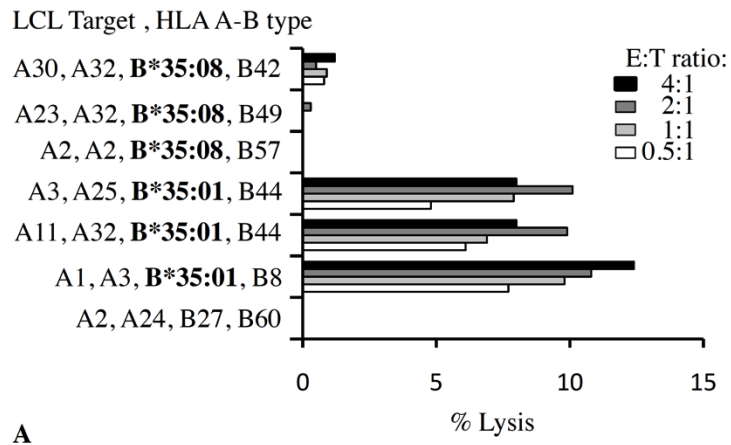


Figure 2.

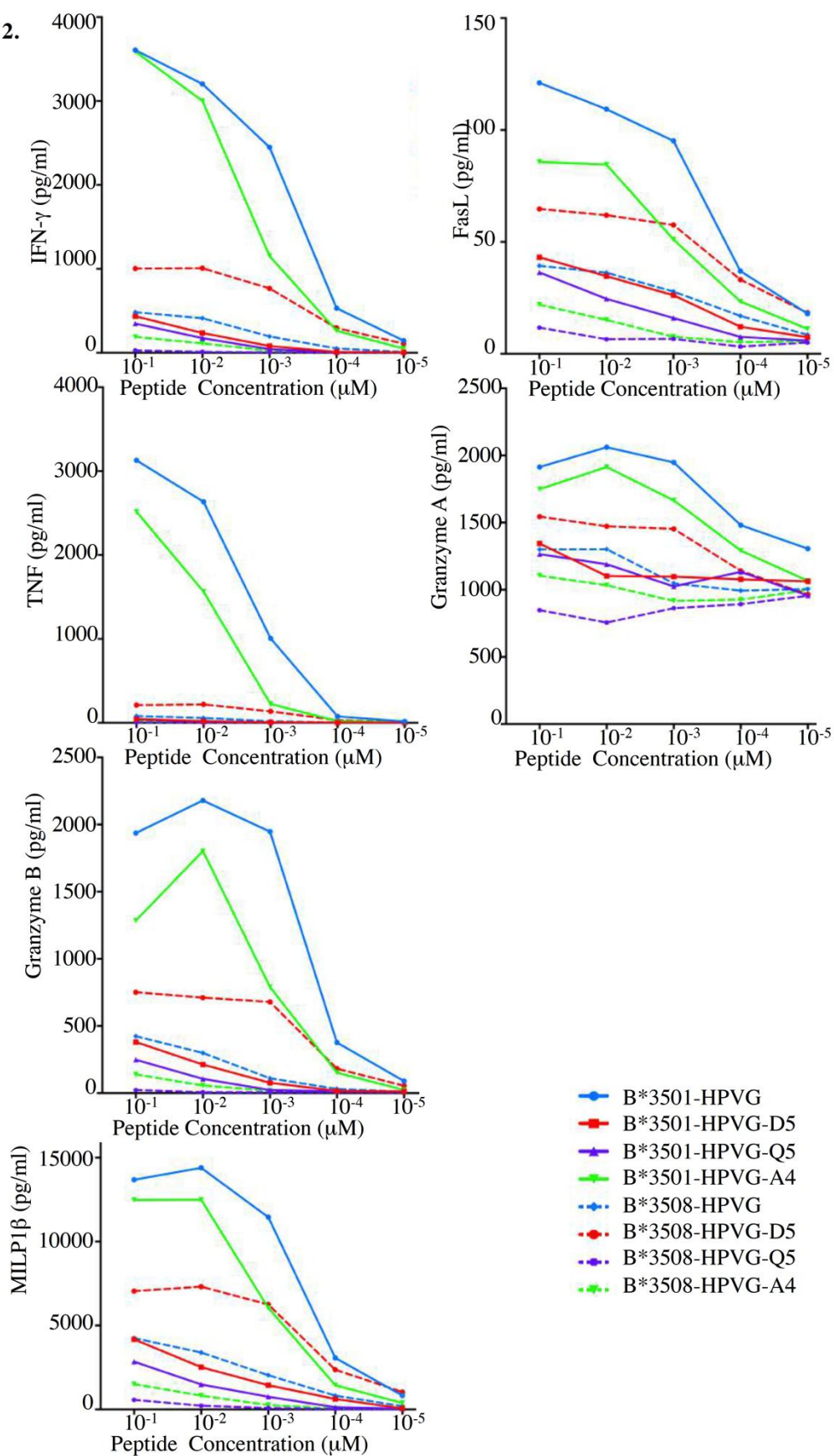


Figure 3.

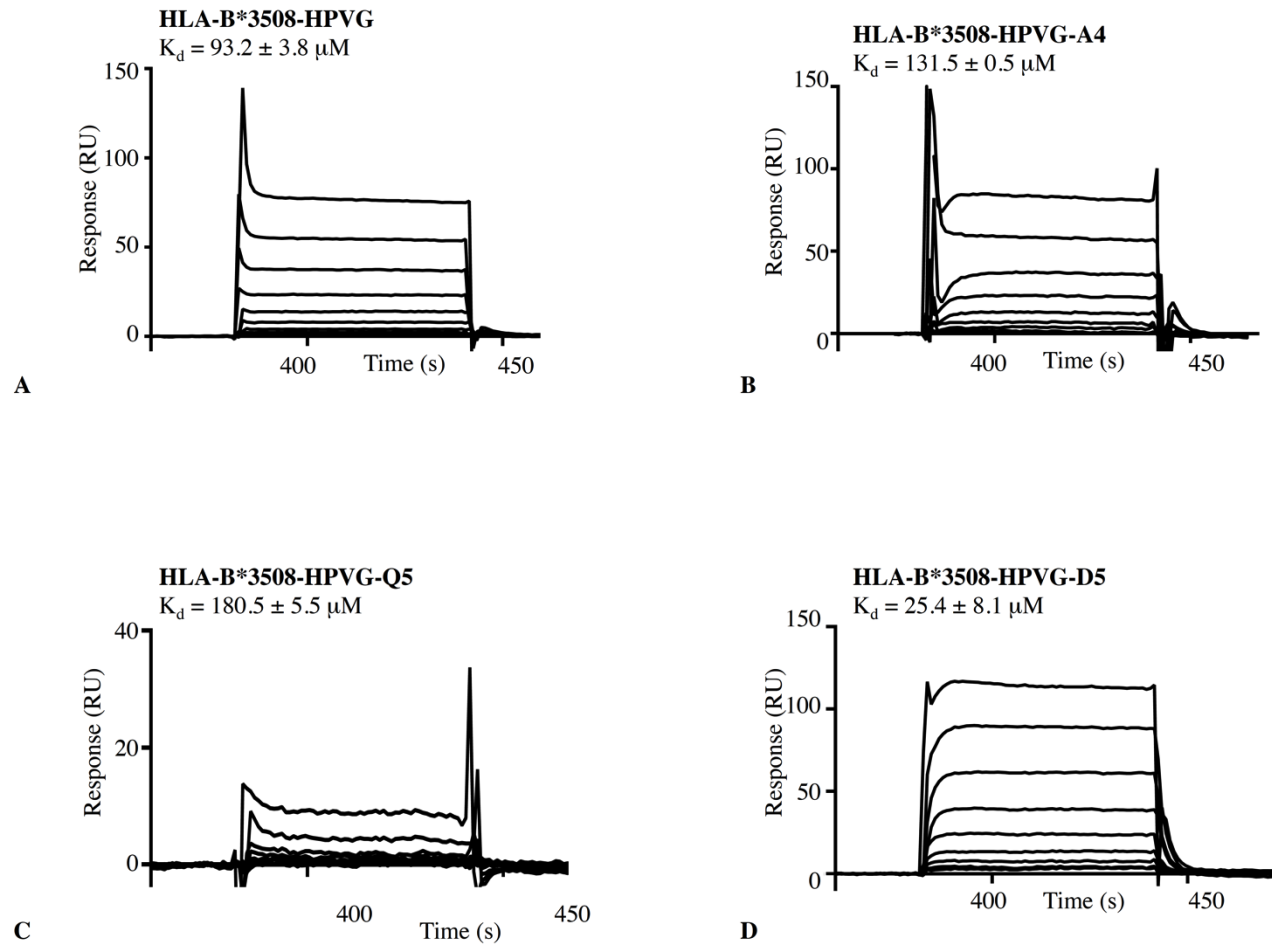
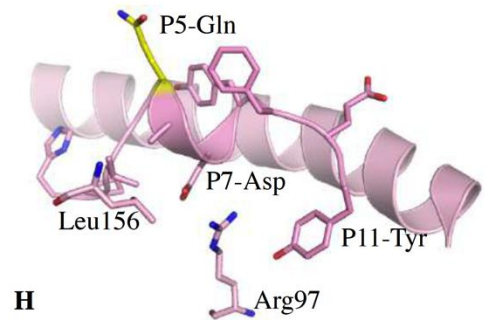
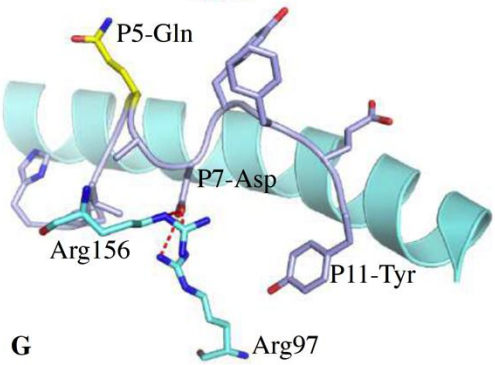
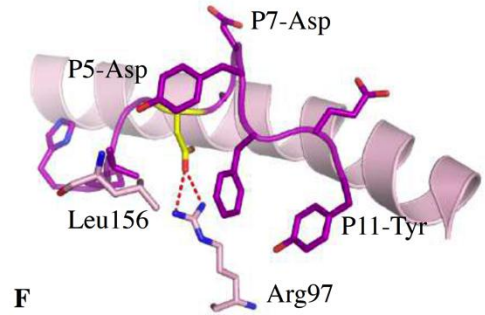
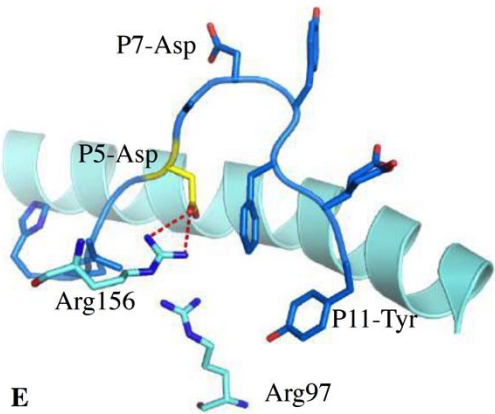
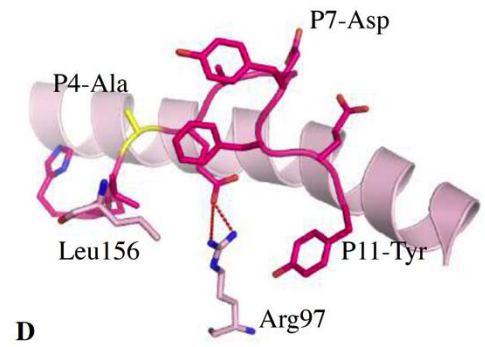
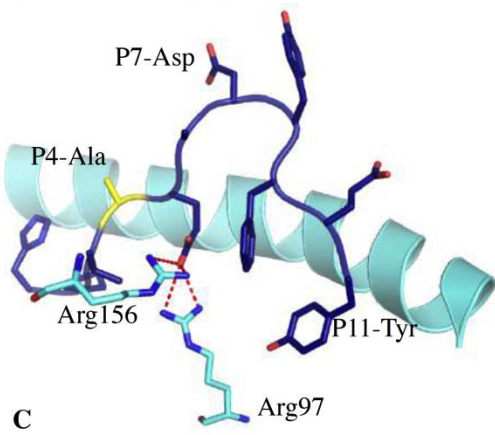
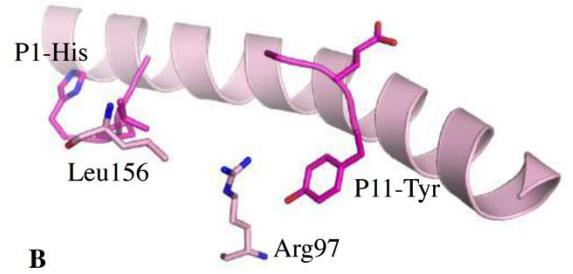
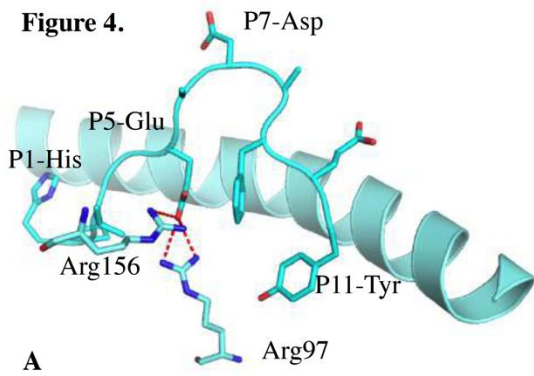
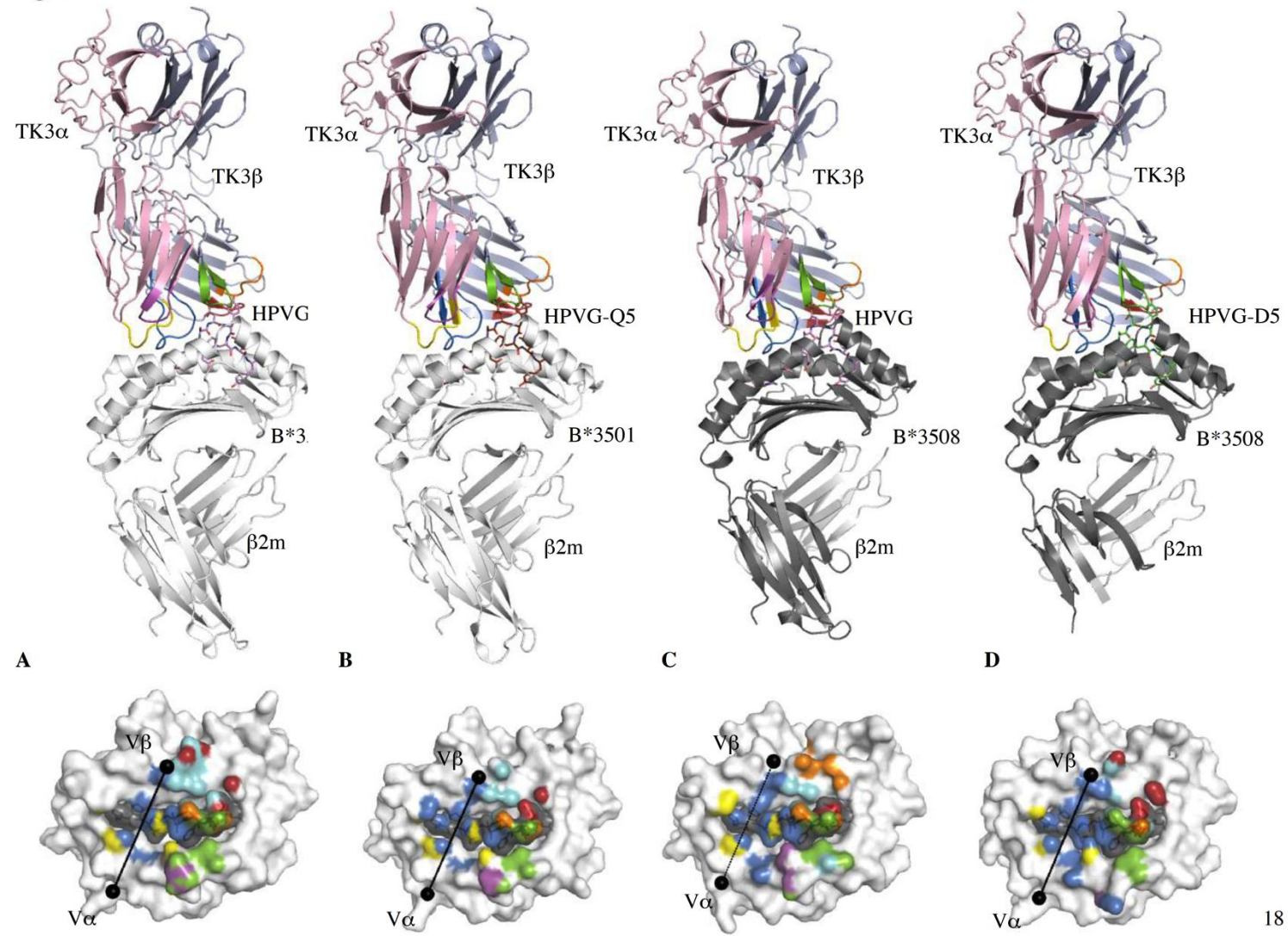


Figure 4.



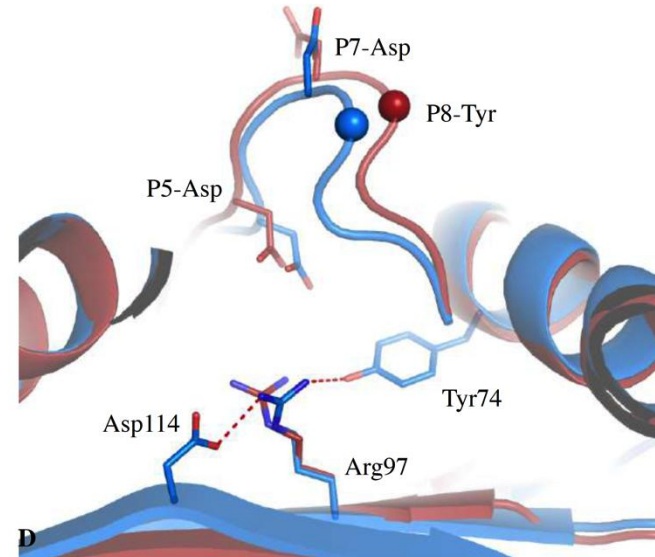
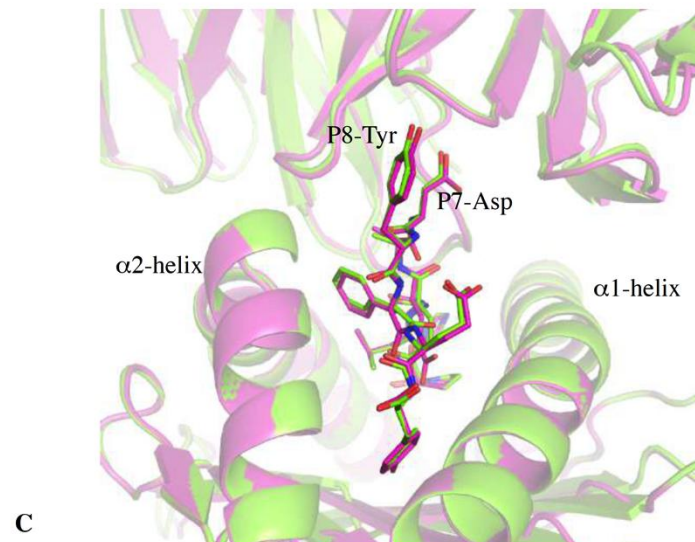
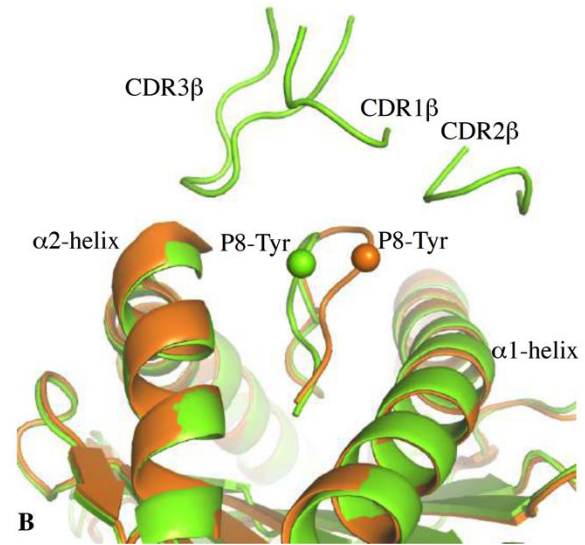
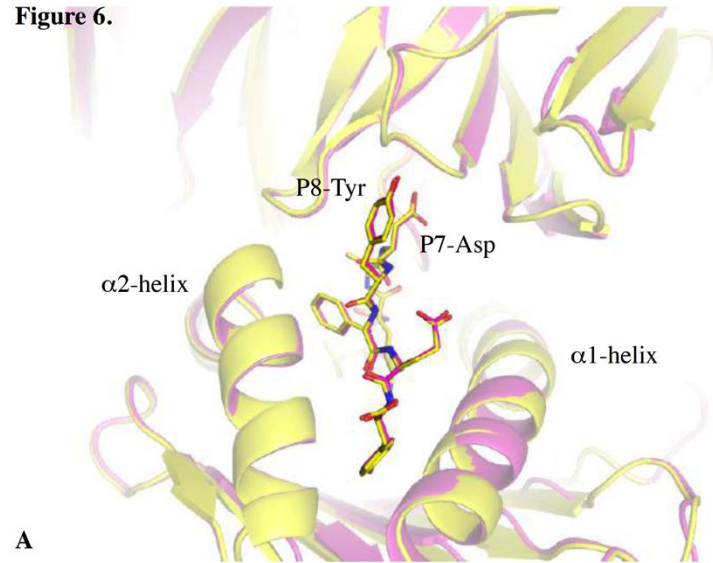
17

Figure 5.



18

Figure 6.



6 Discussion

Cytotoxic T cells represent a major line of defence in vertebrate to combat against foreign pathogens and control intracellular abnormality of the host such as microbial infections and cellular transformation. To effectively perform these functions, T cells undergo a two-step selection process in the thymus where they become “educated” to specifically recognise antigens presented by self-MHC molecules, a phenomenon known as MHC restriction (Zinkernagel and Doherty, 1974). Nevertheless, cytotoxic T cells also simultaneously exhibit remarkable binding degeneracy, allowing them to effectively recognise the vast number of antigens they might encounter. In fact, this multifaceted and paradoxical nature of T cells is important not only in the context of protective and aberrant immunity, but also manifest clinically in the setting of organ transplantation where T cells cross-react (alloreact) with foreign pMHC-I target and causes graft rejection and/or graft versus host diseases (Afzali et al., 2007; Brehm et al., 2010; Keever et al., 1994). Thus, understanding the fundamental basis of MHC-restricted recognition and T cell binding degeneracy is biomedically important as we constantly seek new ways to enhance protective immunity and alleviate unintended T-cell mediated immune responses such as T-cell mediated allorecognition.

This thesis examined the structural and biophysical basis of HLA-B*35-restricted recognition towards a common human pathogen, EBV, and investigated the dual specificity of various T cells in providing host protection. Particularly, the antigens that were investigated in this thesis exceeded the canonical length (8-10 amino acids) for MHC-I-bound antigens. It is unclear however, how cytotoxic T cells, via the use of varying T cell receptors, interact with lengthy antigens and recognise these unusually long antigens. Towards this end, using X-ray crystallography as a tool, along with associated biophysical and cellular approaches, the presented data here allowed me to depict the precise mechanisms by which T cells adopts, not only to overcome structurally distinct pHLA landscape but also maintaining simultaneous specificity and degeneracy. These results, which include five TCR-pMHC-I ternary structures, have shaped our understanding towards T-cell mediated immunoprotection.

6.1 TCR recognition towards lengthy antigen

Most of the structural and biophysical investigations into TCR-pMHC-I interaction have focused predominantly on short antigens with canonical length presented by MHC-I molecules (Gras et al., 2012a). In contrast, how lengthy antigens (>10 amino acids) are recognised by the immune system remains relatively under-appreciated. To address this, the prototypical TCR (term SB27) in complex with the 13mer LPEP peptide presented by HLA-B*35:08 have provided an interesting snapshot of how a TCR, via the use of novel structural solution, to “see” such atypically “featured” pMHC-I landscape (Tynan et al., 2005b). Namely, the SB27 TCR perched atop the LPEP antigen via an unconventional orthogonal docking orientation and enabled the SB27 TCR to form extensive contacts with the central region of the antigen. Furthermore, due to the “super-bulged” conformation of the LPEP antigen, the SB27 TCR struggled to contact the HLA surface, and only mediated limited contacts with HLA-B*35:08. In fact, the number of TCR-peptide contacts was significantly increased compared to other typical TCR-pMHC-I interactions (Rudolph et al., 2006), contributing to approximately 45% of the buried surface area (Tynan et al., 2005b). This observation prompts us to ask two questions: how does the energetic basis of this complex differ from other TCR-pMHC-I systems previously established? and what is the driving force behind this unique mode of TCR recognition? To answer these central questions, guided by the published SB27-HLA-B*35:08-LPEP structure, I performed an alanine scanning mutagenesis approach at the SB27 TCR-HLA-B*35:08-LPEP binding interface to survey key residues that govern the binding energetics of this interaction.

The mutagenesis results demonstrated that, whilst the structural footprint of SB27 TCR was small, the energetic landscape was even smaller. In particular, of the nine HLA residues that were contacted by the TCR, only four were defined either critical or intermediately important for SB27 recognition. These residues included Arg151, Gln155, Arg157 and Ala158 that are located around the hinge region of the α 2-helix. Residues on the α 1-helix on the other hand, appeared to be energetically dispensable, as mutations in this region did not appreciably impact on TCR recognition. In stark contrast to the limited role of HLA residues in “driving” this interaction, four out of six peptide residues were shown to abrogate TCR binding when mutated. These

residues covered the ascending region of the LPEP antigen and are critical for the functional recognition of SB27 CTL as previously outlined. As such, similar to the peptide-focused structural profile, the bulged LPEP antigen plays a dominant role in “driving” the recognition by the SB27 TCR. These findings contrast to the MHC-centric view of TCR recognition observed originally by the murine 2C TCR system (Lee et al., 2000; Manning et al., 1998), but is consistent with the peptide-centric mode that is observed in the human A6 TCR system, although the energetic hot spots in the A6 systems locates exclusively on the α 1- instead of α 2-helix (Baker et al., 2001; Hausmann et al., 1999). More recently, I determined the structure of the SB47 TCR that also interact with HLA-B*35:08-LPEP (**Chapter 4**). This structure allows me to further investigate, if the peptide-focused mode of recognition is maintained across different CTLs towards the lengthy epitope. Via mutation on the selected HLA residues, alongside with supplemented peptide substitution data, it is apparent that HLA residues contribute more significantly in the SB47 binding interface compared to that of the SB27. Specifically, of the seven SB47-contacting HLA residues, mutations have invariably abrogated TCR recognition, as judged by the associated SPR results. This is in contrast to the peptide substitution experiment, which illustrated that only four solvent-exposed antigen residues impacted on TCR recognition (P1 and P4-P6). This observation is in agreement with the structural footprint of the SB47 TCR that contacts extensively onto the HLA-B*35:08 via an N-terminally focused docking orientation.

Accordingly, although it is logical to consider that TCR-peptide interaction may be more important in driving lengthy antigen recognition by TCRs given the prominent structural feature of the lengthy antigen presentation by the MHC-I molecules (such as the HLA-B*35:08-LPEP described in this thesis), the relative energetic contribution between the HLA and peptide can actually vary significantly depending on the specific TCR that is examined (peptide-focused versus HLA-focused). Firstly, in the case of the SB27 TCR, the peptide-centric view of lengthy epitope recognition is apparent. This argues against the two-step model where TCR-MHC interactions are considered to initiate the complex formation, whilst TCR-peptide interactions only participate during the second binding phase to allow optimal antigen recognition (Wu et al., 2002). In fact, due to the central docking orientation of the SB27 TCR, peptide residues are most likely to represent the first point of contacts. In marked contrast, the

energetic basis of the SB47 complex appears to be more MHC-focused, although it may be important to fully explore the energetic basis governing the SB47 TCR-pHLA-I complex. Regardless, results arising from this thesis represent the first energetic mapping of TCR-pHLA interactions in the context of non-canonical peptide length, and have provided alternative views that shape our understanding towards MHC-restricted TCR recognition (discussed in section 6.5).

6.2 The energetic basis of biased TCR repertoire

Given the vast number of potential naïve T cell receptors that arises from the V(D)J gene recombination event, it is perplexing that CTL responses towards many viruses such as CMV (Trautmann et al., 2005), EBV (Argaet et al., 1994), HIV (Price et al., 2004) and Influenza (Gillespie et al., 2006; Turner et al., 2003) are often controlled via biased TCR usage. Such TCR immunodominance is observed in both human and mice systems, and implies that particular TCR motifs might be important in enabling ligand binding. In this regard, TCR repertoire towards the lengthy LPEP antigen in unrelated HLA-B*35:08+ individual represents an example of TCR immunodominance, characterized by the public selection of a V α chain (TRAV19*01, TRAJ34) along with a preferred V β (TRBV6-1*01) chain that was found in approximately 60% and of the CTL clones from unrelated individuals, despite variations in the CDR3 β loop was evidenced (Tynan et al., 2005a). To investigate the underlying basis of this TCR bias, results in Chapter 2 extended the alanine mutagenesis scanning approaches to residues in the SB27 CDR loops. The SPR data illustrated that, the energetic landscape of SB27 was contributed by both the V α and V β chains, which contrasts to V β focused-energetic profile seen in the JM22 system (Ishizuka et al., 2008), but analogous to other murine and human TCR systems previously reported (Borg et al., 2005; Manning et al., 1998). Specifically, CDR2 α and CDR3 α loops govern the energetic landscape of the SB27 V α chain, and interacted with the HLA and peptide residues respectively. These observations provide the underlying basis dictating the public V α gene usage as the energetically important residues are found exclusively in TRAV19*01 (Asn50, Phe52 and Ser93). Similarly, the energetic landscape of the V β chain was investigated, highlighting the role of CDR1 β loop in driving peptide recognition, whilst the CDR3 β loop only contributed intermediately to TCR recognition. This observation coincides with the

fact that sequence variation in the CDR3 β region is tolerated between HLA-B*35:08-LPEP restricted CTLs (such as the CA5 TCR that exhibits a similar docking orientation) and is reminiscent to that of the murine CTL responses towards an anti-influenza epitope recently reported (Day et al., 2011).

Another interesting fact arises from studying the TCR repertoire in this system is that whilst TRAV19*01 can pair up with a range of differing TRBV chains (TRBV6-1*01, TRBV5-6*01 and TRBV7-2*01), the TRBV6-1*01 usage, which comprises an unique ²⁸NHNSMY³³ motif in the CDR1 β loop, is nevertheless preferred (>60% of the CTLs) (Tynan et al., 2005a). A number of different factors can contribute towards this preference, such as naive T cell frequency, preferential TCR pairing as a structural constraint, or affinity / avidity. Structurally, the use of TRBV6-1*01 genes enabled the CDR1 β chain to mediate contacts with the peptide. The CDR1 β -peptide interaction is conserved in both the SB27 and CA5 TCR, and has been shown to govern the binding energetic of SB27 V β chain. It is therefore possible that, this “innate-like” antigen recognition mode is preferentially selected as a result of a co-evolutionary event between this ancient viral infection and the host defense system. As such, TRBV6-1*01-bearing TCRs are “hardwired” towards this prominent epitope to provide effective control over EBV in HLA-B*35:08+ individual. Indeed, this germline-encoded antigen recognition has also been proposed to govern the public CTL responses towards an HCMV epitope (Gras et al., 2009b). Nevertheless, it will be interesting to investigate the difference in other TRAV19*01-bearing TCRs, kinetically, structurally and functionally in complex with the HLA-B*35:08-LPEP to further examine the hierarchy of the CTL responses.

6.3 TCR binding strategies towards super-bulged pMHC landscapes

Whilst it has been established that how different TCRs can interact with the same pMHC-I targets via alternative binding strategies, how such genetic variations can contribute towards lengthy antigen recognition remains unclear. In particular, lengthy antigens typically form a super-bulged peptide landscape when bound to MHC-I molecules, and can exhibit either defined or flexible conformations. In one example demonstrated by Speir and et al, a single lengthy antigen can even adopt two distinct conformations simultaneously (Speir et al., 2001). These factors make it difficult to

conceive, how TCRs can cope with such structurally challenging landscapes, whilst maintaining contacts with both MHC helices to achieve pMHC specificity.

Given the role and prevalence of lengthy antigen in cellular immunity (up to 10%) (Hickman et al., 2004), the results described in Chapter 3 involved in the structural examination of two distinct TCRs (CA5 and SB47) in complex with the HLA-B*35:08 presenting the 13mer LPEP antigen, in comparison to the SB27-HLA-B*35:08-LPEP complex that was previously established (Tynan et al., 2005b). The structure of the CA5 ternary complex demonstrated that, analogous to the SB27 ternary complex, the CA5 TCR “perched” atop the pHLA centrally and focused on the most prominent feature of the pHLA landscape, the bulged antigen. This docking mechanism allowed the formation of extensive TCR-peptide contacts, similar to that of the SB27 complex (Tynan et al., 2005b). Nevertheless, the CA5 TCR was tilted slightly further towards the $\alpha 2$ -helix, allowing it to “ignore” residues presented on the HLA $\alpha 1$ -helix (Liu et al., 2013). This observation is interesting as all TCR-pMHC-I complexes determined to date involved in TCR-MHC interactions on both helices (Rudolph et al., 2006). This also raises the question as to what drives the selection of the V β chain that sits on top the $\alpha 2$ -helix yet not making any contact with the HLA? Whilst the answer is unclear without knowing exactly what ligand the CA5 TCR “sees” during thymic selection, the structural role of the CA5 V β chain contributes significantly towards antigen recognition via its germ-line encoded CDR1 β loop. This feature certainly contrasts to the MHC-centric view in predicting TCR docking orientation (Garcia et al., 2009), and highlights the role of antigen in driving TCR recognition and possibly TCR repertoire selection. Indeed, both CA5 and SB27 exhibit a shared peptide-focused structural profile, where TCR-peptide interactions are largely conserved, contributing approximately 50% and 45% of the BSA respectively. This observation also coincides with a recent finding, demonstrating that conserved peptide motifs govern TCR binding specificity (Birnbaum et al., 2014).

Despite limited TCR-MHC interactions were observed in both CA5 and SB27 ternary complexes, the associated binding affinities were within the typical range of TCR-pMHC interactions (Gras et al., 2012a). In particular, the CA5 TCR, which exhibits a different and shortened CDR3 β , interacted with the pHLA approximately three-fold stronger than that of the SB27 TCR. This kinetic difference was attributed primarily

to the faster on rate, which implies that the CA5 TCR is in a more ready-to-go conformation for pHLA recognition, whilst the lengthier SB27 CDR3 β loop might be associated with a greater extent of conformational rearrangement before optimal binding is achieved. This hypothesis could be tested directly by determining the unliganded structure of the respective TCRs, yet crystallisation of the CA5 or SB27 has been so far unsuccessful.

To further explore how differing TCR architectures allow them to recognise a featured pHLA landscape, we examined the structure of the SB47 TCR (TRAV39*01 and TRBV5-6*01) that comprises a completely different set of CDR loops compared to the CA5 and SB27 TCRs, in complex with the HLA-B*35:08-LPEP. Strikingly, unlike the central docking mode observed in the CA5 and SB27 complexes, the SB47 TCR was positioned towards the N-terminal end of the antigen-binding cleft with a conserved orthogonal docking orientation. This N-terminal docking allowed the SB47 TCR to essentially “by-pass” the apex of the bulged LPEP antigen, and is reminiscent to another MHC-I restricted anti-EBV viral CTL response previously described (Gras et al., 2009a). However, this extreme TCR docking mode is more prominent in the context of the SB47 ternary complex, and it is even more analogous to some of the MHC-II restricted autoreactive TCR-pMHC-II complexes (Deng and Mariuzza, 2007; Hahn et al., 2005; Li et al., 2005). Interestingly, unlike the SB27 and CA5 TCRs that struggled to interact with the HLA landscape, this shifted TCR docking mode allowed the SB47 TCR to contact the MHC surface extensively via the use of five out of six CDR loops (~85% BSA), whilst TCR-peptide contacts were mediated marginally and exclusively via the CDR3 β loop (~15% BSA). Furthermore, this unique structural footprint of SB47 also enabled the TCR to contact HLA residues 55-57, which represents a novel TCR-MHC contacting region for TCR-pMHC-I structures determined to date. Collectively, the structures of the CA5 and SB47 ternary complexes have provided distinctive mechanisms that TCR adopt to productively circumvent a rigid and super-bulged pHLA landscape. These differences in docking mechanisms also explain the shifted antigen specificity observed in the functional experiments.

Unlike the SB27 and CA5 CTLs, which represents the immunodominant CTLs found in unrelated HLA-B*35:08+ individuals, the SB47 CTL that was investigated

accounts for only approximately 10% of the circulating CTLs (Tynan et al., 2005a). Whilst structurally it is unclear if the peptide-focused (SB27/CA5) versus MHC-focused (SB47) mode of interaction is responsible for the different hierarchy, there were clear kinetic differences between these CTLs whereby the SB47 TCR exhibited the weakest affinity compared to the CA5 and SB27 TCRs. Furthermore, differences between the TCR docking orientation were apparent, which has been suggested to associate with the recruitment of co-receptor as well as impacting T cell signalling outcome (Adams et al., 2011; Buslepp et al., 2003). Thus, it is possible that, due to the combination of a relatively weak binding affinity, along with an unfavourable TCR docking geometry for the recruitment of co-receptor, the SB47 CTL response is out-competed. It is unclear however, at this stage, how such steric requirement constraints this process and contributes to the hierarchy of TCR repertoires. Perhaps it will be interesting to examine the dependency of CD8 binding for the SB27, CA5 and SB47 system, to start exploring such correlations.

In addition to the 13mer LPEP epitope, this thesis also investigated TCR mechanisms towards a 11mer HPV antigens bound to HLA-B*35:01/08. Namely, results summarized in Chapter 4 involved the determination of TK3 TCR structure in complex with three different pHLA-I, including HLA-B*35:01-HPVG-Q5, HLA-B*35:08-HPVG and HLA-B*35:08-D5 (Liu et al., 2014). Despite sequence variations between these pHLA ligands were limited to 1 or 2 amino acids compared to the cognate HLA-B*35:01-HPVG previously shown, the respective binary structures have revealed unexpected changes not only in the context of peptide conformation, but also their associated mobility. Surprisingly, upon TK3 TCR binding, all antigens were reshaped, and the TK3 TCR contacted all pHLA landscapes via a highly conserved binding mode. Thus, TK3 recognition of lengthy antigen is associated with structural reconfigurations on the peptide itself, which is facilitated by the inherent flexibility of the MHC-I bound antigen. This mechanism is reminiscent of the “bulldozing” effect of the ELS4 TCR (Tynan et al., 2007), and the peptide malleability of DM1 (Archbold et al., 2009) and LC13 (Macdonald et al., 2009) TCRs, but in contrast to the rigid LPEP system whereby different TCRs overcome the steric challenge by alternative docking mechanisms (Liu et al., 2013; Tynan et al., 2005b).

Collectively, this thesis has highlighted the versatility of TCR recognition in providing unpredictable yet effective solutions over lengthy antigens derived from an ancient human pathogen, the EBV. Whether or not we have fully explored TCR strategies is unclear, nevertheless, results presented here certainly extended our current knowledge on some of the many ways TCR diversity offered in achieving productive antigen recognition.

6.4 TCR recognition of altered pHLA landscape

A key feature for T-cell mediated immunity is the multifaceted nature of TCR that allows it to finely discriminate between self, altered self and foreign antigens, whilst at the same time being remarkable cross-reactive in order to combat against the indefinite number of foreign invasion one might encounter. To explore the underlying basis of TCR recognition, early structural studies into the murine 2C and human A6 system indicated that TCR binding degeneracy arises from the structural plasticity of the CDR loops, which enables TCR binding towards various altered peptide ligands (APLs) (Degano et al., 2000; Ding et al., 1999; Gagnon et al., 2006; Garcia et al., 1998). These studies demonstrated the importance of CDR loops flexibility in enabling cross-recognition, and highlighted the role of TCR induced-fit in enabling antigen recognition. In contrast, it has also been shown that, via comparing the structural footprints of the 2C TCR bound to H-2K^b and H-2L^d, TCR binding degeneracy can also be achieved via alternative docking mechanisms (Colf et al., 2007; Garcia et al., 1998). More recently, there is also a growing appreciation on the role of the antigen flexibility in contributing such adaptability. For instance, the LC13 TCR that recognises both HLA-B*8 and HLA-B*44 is underpinned by a molecular mimicry event, associated with significant reconfiguration of the peptide conformation (Macdonald et al., 2009). Moreover, the A6 TCR that recognises HLA-A*2-Tax has recently been solved in complex with another peptide ligand, Telp1 (Borbulevych et al., 2009). Comparison of these two complexes revealed that, the shape of the respective peptide antigens diverged only post A6 TCR ligation, further highlighting the role of antigen adaptability in enabling TCR cross-recognition.

6.4.1 TCR recognition of polymorphic HLA landscapes

This thesis also explored how TCRs cross-react or discriminate different pHLA ligands carrying substitutions either via HLA polymorphisms and/or antigen variants derived from a range of different viral strains. Firstly, in the context of the LPEP antigen, the impact of micropolymorphism on HLA landscape was investigated using HLA-B*35:01 as an example that differs from HLA-B*35:08 by one buried amino acids at position 156 (Arg in HLA-B*35:08 compared to Leu in HLA-B*35:01). This difference within the binary structures causes a rigid body shift in the hinge region of the respective α 2-helices, which acted as a contacting point for TCR discrimination (Liu et al., 2012; Tynan et al., 2005a; Tynan et al., 2005b). Indeed, both SB27 and CA5 TCRs exhibited the ability to differentiate HLA-B*35:08/01 as illustrated by the functional and SPR data outlined in Chapter 3. Structurally, both SB27 and CA5 TCRs contacted the α 2-helix extensively, especially around the hinge region where HLA-B*35:08 and HLA-B*35:01 structurally varied, providing immediate structural explanation for the HLA-B*35:08-restricted recognition of the LPEP peptide. Moreover, the mutagenesis results from Chapter 2 further support this idea as mutations within this hinge region result in a significant reduction of the SB27 binding. In addition, we also investigated the specificity of SB47 TCR in discriminating altered MHC landscape using HLA-B*35:01/08 via SPR and functional assay. Surprisingly, the SB47 TCR is unable to distinguish HLA-B*35:01 from HLA-B*35:08 as judged by the similarity in kinetic constants and T cell functions. Indeed, due to the N-terminal docking orientation of the SB47 TCR onto HLA-B*35:08-LPEP, this TCR did not contact the hinge region of the α 2-helix, therefore providing direct insights into the cross-reactive and allo-reactive nature of HLA-B*35:01 recognition. Accordingly, the ability for TCRs to subtly differentiate or cross-react with HLA polymorphism in the LPEP system is directly mirrored by TCR docking footprints, which allows them to “see” or “ignore” altered pHLA landscapes arising from buried polymorphism.

In addition, this thesis explored the impact of micropolymorphism (HLA-B*35:08/01) in the context of the 11mer HPVG epitope. Unlike the HLA-B*35:01/08-LPEP system described in Chapters 2 and 3, there is no significant difference between the HLA landscapes in the respective HLA structures. Instead, the conformation and

flexibility of HPVVG differed remarkably when presented by these two allomorphs (Miles et al., 2006). Given that the HLA-B*35:01-restricted TK3 TCR interacted only weakly to the HLA-B*35:08-HPVG, both kinetically and functionally, I determined the structure of the TK3-B*35:08-HPVG and compared that to the cognate TK3-HLA-B*35:01-HPVG complex. Surprisingly, the TK3 TCR adopted a conserved docking orientation onto the HLA-B*35:08 with minimal structural rearrangements in the CDR loops compared to the cognate ternary complex. In contrast, the rigid and bulged HPVVG peptide presented by HLA-B*35:08 was bent upon TCR ligation, to form an identical peptide conformation observed in the TK3-HLA-B*35:01-HPVG complex. These changes allowed the TK3 TCR to mediate contacts with both the MHC and peptide, and it resembles the “antigen-flattening” mechanisms utilized by the ELS4 TCR previously described (Tynan et al., 2007). Nevertheless, unlike the ELS4 TCR that preferably recognised a rigid antigen conformation, the TK3 TCR interacted much stronger with the flexible HPVVG bound to HLA-B*35:01. As such, the ability for TK3 to discriminate the two allomorphs arises indirectly from the fine-tuning of antigen flexibility, which is controlled, at least in our current system, by the polymorphic residue of the HLA. Accordingly, this study highlights the fact that mobile antigens are not necessarily “challenging” for TCR recognition. Instead, some TCR (such as TK3) are “designed” to preferentially see this flexible nature of the MHC-I bound peptide. It will be also interesting however, to test if TCR flexibility and pHLA mobility is presented at the same time to yield TCR specificity. This can be examined directly by solving the structure of the TK3 TCR on its own.

6.4.2 Impacts of altered peptide ligand (APL) presentation

In addition to HLA polymorphism, we also tested, both structurally and biophysically, how TK3 TCR cross-reacts with three peptide variants presented by both HLA-B*35:08 and HLA-B*35:01 molecules. Unexpectedly, when structures of the binary complexes were determined, we observed remarkable variability between the respective pHLA variants, attributed to only single amino acid substitution compared to the cognate pHLA complex. In particular, the HPVVG-Q5 variant that bound to HLA-B*35:01/08, formed a helical turn within the antigen-binding cleft, thereby exhibiting a flatter peptide landscape. These unique peptide conformations contrast to the typical super-bulge conformation exhibited by lengthy epitopes, and was unexpectedly associated with the switch of peptide register in the C pocket of the

HLA where P5 of the HPV-G antigen typically sits. Instead, the P7D of the HPV-G-Q5 variant pointed into the C pocket of the HLA whereas the P5Q flipped and was solvent exposed. Whilst the helical peptide conformation has also been previously shown in the HLA-B*35 (Wynn et al., 2008) and HLA-B*41 (Bade-Doding et al., 2011) systems, how TCR can interact with such unique pHLA landscape remains to be further investigated. Of note, the unpredictability of these antigen conformation observed, has prompted us to reconsider some of the algorithms used in antigen-binding prediction, which focuses primarily on the peptide anchoring position P2 and P Ω (Milik et al., 1998; Singh and Raghava, 2001; Sturniolo et al., 1999). Alternatively, the results highlighted here showed how subtle variations in non-anchoring peptide could also have profound impact on the antigen conformation, which impacts on subsequent TCR recognition.

6.4.3 TCR recognition of APL

Given the structural differences between the HLA-B*35:01-HPV-G-Q5 and HLA-B*35:01-HPV-G pHLAs and the observation that the TK3 TCR was able to cross-react with both pHLA with reasonable binding affinity. The TK3 system provides us with an ideal system to examine the mechanism of TCR binding degeneracy. In this regard, we determined the structure of the TK3 TCR bound to HLA-B*35:01-HPV-G-Q5 and compared that to the TK3-B*35:01-HPV-G complex. Intriguingly, despite the divergent pHLA landscapes associated with the two variants, both ternary complexes were highly similar not only in terms of the respective TCR docking orientation, but also surprisingly, the antigen conformation. Indeed, the helical conformation of the HPV-G-Q5 that was found in the binary structure, became “untangled” and bulged away from the antigen-binding cleft post TK3 TCR binding; a structural feature that has not been reported to date. This prominent antigen reconfiguration was associated with the conformational switches between P5 and P7 of the peptide whereby the buried P7 side chain flips out of the Ag-binding cleft, and act as a direct contacting point for TK3 recognition. Similarly, TK3 cross-recognition towards the HPV-G and HPV-G-D5 variant bound to HLA-B*35:08 was also investigated, demonstrating a comparable TCR-pHLA binding mode. This is perhaps not surprising given that the binary structures of HLA-B*35:08-HPV-G and HLA-B*35:08-HPV-G-D5 were also similar. Nevertheless, the TK3 TCR interacted approximately 3 times stronger to the

HLA-B*35:08-HPVG-D5, presumably due to the loosely anchored P5D peptide side chain that facilitates antigen rearrangement that is required for TK3 TCR binding. Thus, whilst TK3 cross-recognition is depicted via a molecular mimicry mechanism that arises primarily from the induced-fit of the antigen itself, differences in the conformation and dynamic of the presented peptide, can finely impact on the strength of TCR recognition.

6.4.4 Insights into TCR allorecognition

Another interesting observation arising from the LPEP study is that I have identified unexpected allorecognition profiles associated with the SB47 CTL, but not with the CA5 CTL that is similar to the alloreactive SB27 CTL (Tynan et al., 2005b). Understanding the fundamental basis of allorecognition is important as such undesired CTL cross-recognition can contribute clinically towards graft rejection and graft-versus-host diseases (Brehm et al., 2010; Jurcevic et al., 2001; Sayegh, 1999). Structurally, examples of allorecognition have been illustrated previously in both murine and human TCR systems. In the murine systems, ternary structures of the 2C TCR bound to self H-2K^b-dEV8 and foreign H-2L^d-QL9 ligands have revealed distinct docking modes in enabling TCR allorecognition (Colf et al., 2007; Garcia et al., 1998; Lee et al., 2000). Alongside with mutagenesis data on the 2C TCR, allorecognition in this system appears to be driven heavily by TCR-MHC interaction (Manning et al., 1998), which favours the MHC-centric view of allorecognition. Similarly, the mechanism of a MHC-II restricted TCR (YAe62) that alloreacts towards the H-2K^b molecule has been recently reported (Yin et al., 2011). In this system, the YAe62 TCR docked towards both MHC-I and MHC-II ligands in a highly similar mode, and the germline-encoded amino acids from both TCR chains were also found to mediate similar contacts to both IA^b and H-2K^b. The conformation of the CDR3 loops on the other hand, varied substantially between the two complexes in order to cope with the different ligands. In marked contrast to the murine system, the human LC13 TCR bound to the cognate HLA-B*8-FLR and foreign HLA-B*44:05-EEYL is depicted by a molecular mimicry mechanism, whereby the TCR interacts with both pHLA complexes via a shared docking orientation (Macdonald et al., 2009). Nevertheless, due to the limited allo-TCR-pMHC-I complex structures, what governs T cell allorecognition in general awaits further experimental insights.

Although the allo-ligand(s) responsible for SB27 allorecognition is/are unidentified, HLA-B*35:08 residues contacted by the SB27 TCR are conserved in HLA-B*44:02. This observation has led to the speculation that allorecognition of the SB27 might be depicted via a conserved docking strategy in this system (Tynan et al., 2005b). However, due to the uncertainty of the self antigen that leads to allorecognition, it is still possible that SB27 and CA5 TCR might engage the self pHLA target via an alternative docking mechanism. Based on the structure of the CA5 and SB27 TCR-pHLA complexes, works arising from this thesis favour the peptide-centric view that dictates SB27 allorecognition. Firstly, we showed that the CA5 TCR, which differs from the SB27 TCR only in its CDR3 β loop, is not alloreactive onto HLA-B*44:02 (Liu et al., 2013). This finding demonstrates the role of CDR3 β in enabling pHLA discrimination. Structurally, the CA5 TCR engaged the HLA-B*35:08 landscape similarly to that of the SB27 TCR, and placed its CDR3 β loop directly above the bulged peptide antigen. Whilst the differences between the two CDR3 β loops (SB27 and CA5 TCR) did not form direct contact with the peptide, its close proximity to the P8 position of the LPEP antigen was able to cause a shift in peptide specificity. As such, whilst both SB27 and CA5 TCR might potentially dock onto HLA-B*44:02 via conserved TCR-HLA contacts, the shortened CA5 CDR3 β loop may serve to enable differential recognition towards the self peptide.

In addition to the SB27/CA5 system, I also observed unexpected allorecognition profile associated with the SB47 CTL (Liu et al., 2013). Structurally, the SB47 TCR docks N-terminally onto the HLA-B*35:08-LPEP landscape, and is unable to differentiate between HLA-B*35:08 and HLA-B*35:01. This implies that a shared docking orientation could also be highly feasible in the setting of the allo-pHLA ligand. However, the observation that SB47 was alloreactive onto HLA-B*35:01 but not HLA-B*35:08 (since SB47 derived from HLA-B*35:08+ individual), suggests that differences in the peptide repertoire, or the shape of the presented antigen, is responsible for the alloresponse observed in HLA-B*35:01. As polymorphism between HLA-B*35:08 and HLA-B*35:01 does not involve in the primarily antigen-anchoring sites, and is located centrally where antigens typically bulged away from the peptide-binding cleft, structural differences between the HLA-B*35:01 and HLA-B*35:08 presenting the same self-peptide are likely be responsible for SB47 allorecognition. Indeed, as evidenced from the HPVG system described in Chapter 5,

it is apparent how such micropolymorphisms can have remarkable impact on the conformation and dynamic of the bound antigen, which indirectly alters the outcome of CTL responses. Thus, whilst the identity of the self-antigens that are responsible for the allorecognition of SB27 and SB47 remains unclear, our findings favour the peptide-centric view in triggering T cell mediated allorecognition.

6.5 Insights into the paradigm of MHC restriction

One of the hallmarks for T-cell mediated immunity is that antigen recognition is restricted to presentation by host MHC molecules, a phenomenon known as MHC restriction (Zinkernagel and Doherty, 1974). Studying the key elements governing MHC restriction will not only help to identify the structural requirements that enable TCR-pMHC-I interaction, but also allowing us to potentially predict TCR docking orientation. However, of the 30 unique TCR-pMHC-I structures observed to date, the “rule of engagement” is not completely understood as variability between the ternary structures is often observed. Structurally, the observation that TCR V α and V β chains always docks onto α 2- and α 1-helices respectively, hints that this docking geometry is constrained. It is however, important to note that no conserved TCR-MHC interaction has been identified to date to explain such restriction.

In 2005, Tynan and colleagues determined the structure of the SB27 TCR in complex with the super-bulged HLA-B*35:08-LPEP (Tynan et al., 2005b). Due to the super-bulged peptide conformation, the SB27 TCR only mediated limited contacts with the HLA. Some of these HLA residues, which were consistently contacted by TCRs in other ternary complexes determined at the time, were hypothesized to represent the minimal elements governing MHC restriction. These residues, which are termed the “restriction triad”, include position 65 and 69 from the α 1 as well as position 155 from the α 2-helix. In particular, residue 155 has also been proposed to function as a “gatekeeper”, changing its conformation from stabilizing the peptide to form TCR contacts upon complex formation (Tynan et al., 2005b). However, the structure of the CA5 TCR has illustrated incompatible features with this concept as it did not contact any residue on the α 1-helix and hence bypass 65 and 69 of the triad residues. Moreover, mutagenesis study arising from this thesis also demonstrated that HLA-B*35:08 positions 65 and 69 did not contribute appreciably towards SB27 recognition

(Liu et al., 2012). Furthermore, the SB47 TCR that showed extreme N-terminal docking orientation did not contact HLA residues 155 and 69. As such, it is obvious that TCR recognition of MHC, in our tested system at least, is not fully dependent on the restriction triad. This observation is also evident in the murine 6218 system as well as the AS01 TCR system where not all triad residues were contacted by respective TCRs (Day et al., 2011; Miles et al., 2010). Indeed, via mutagenesis scanning and functional experiments, Burrows and colleagues have also tested and shown that the dependency of the triad residues in enabling TCR recognition can vary significantly between TCR systems (Burrows et al., 2010). This is perhaps not surprising given that T cells inherited with strong MHC binding affinity would be removed from the periphery as a result of the negative selection (Rammensee and Bevan, 1984; Viret and Janeway, 1999). Perhaps it will be more interesting to investigate the role of triad residues in the context of self-ligands (positive selecting ligands for example) as the restriction triad residues might be playing more important role in T cell selection.

In order to explain TCR bias towards MHC molecules, Garcia and colleagues proposed that the germline-encoded region of the $V\alpha$ and $V\beta$ chains (CDR1/2 loops) are co-evolved with the $\alpha 2$ - and $\alpha 1$ -helices in a pairwise manner (Garcia et al., 2009; Marrack et al., 2008). In this model, TCRs are “hardwired” to recognise specific motifs or “codons” that are present on the MHC surface. Thus, the docking orientation of any given TCR is therefore determined and varied depending on the specific of $V\alpha$ - $V\beta$ chains pairing as well as the specific MHC allele. Experimentally, this MHC centric view of TCR recognition is supported by the identification of conserved contacts between $V\beta 8$ -bearing TCRs that interact with the MHC molecule, I-A^b (Feng et al., 2007). However, this concept is incompatible with both the SB27 and CA5 TCR-pHLA-I complexes as a peptide-focused mode of recognition is evident. Namely, via structural and biophysical investigations into the SB27 and CA5 ternary complexes summarized in chapter 3 and 4, it is clear that, the CDR1 β loop, which governs the binding energetic of the SB27 $V\beta$ chain, is primarily responsible for the recognition of the peptide antigen. Indeed, this germline-encoded antigen recognition mode is even more exaggerated in the CA5 complex as its $V\beta$ chain did not even contact the $\alpha 1$ -helix of HLA-B*35:08 which strongly argue against the

“codon” theory and potentially highlight the role of peptide in determining TCR docking orientation. Accordingly, identifying the elements of MHC restriction remains a key challenge to the field, using lengthy antigens as examples, studies arising from this thesis, have provided interesting insights into the paradigm of MHC restriction. To understand the rule of MHC restriction will certainly require more studies of TCR-pMHC interaction, kinetically, functionally and structurally.

6.6 Future directions

Although my thesis has provided some insights governing TCR specificity and degeneracy in the context of lengthy antigens, a huge amount of work remains to be examined in order to fully explore the paradigm of this central immunological event. Firstly, the structures of the SB27, CA5 and SB47 ternary complexes certainly have provided good examples of how TCRs can interact with a “feature” pHLA landscape, there are other available CTLs that might be worth investigating both kinetically and structurally. For instance, studying the SB9 TCR that comprises the public TRAV19-1*01 chain and the alternative TRBV7-2*01 would ultimately allow us to investigate the structural impact on TCR chain pairing. This would also provide an opportunity to potentially explore the underlying basis of the preferential TRBV5-6*01 usage as seen in the CA5 and SB27 TCR. Perhaps it would be also valuable is to study the SB32 TCR, which is essentially a “hybrid” between the TRAV19-1*01 of SB27 and TRBV5-6*01 of SB47 TCR. Given that it has been proposed that TCR-MHC interaction dictates TCR docking orientations (Garcia et al., 2009), it is possible to predict, and test by structural determination of the SB32 ternary complexes, the germline-encoded theory of MHC-restricted TCR recognition as the docking of the SB27 and SB47 on the HLA-B*35:08 are available. Moreover, it will also be important explore, kinetically and functionally, if these TCRs can discriminate differences in HLA micropolymorphism and how this correlates with structural findings to further understand the fine-specificity of MHC-restricted recognition. Lastly, given that remarkable differences in TCR docking modes were observed for lengthy antigen detection, this structural information has also provided a great opportunity to investigate the correlations between the positioning of the TCR chains and their ability to effectively recruit co-receptors such as CD8. This can be tested

using specific TCR transfected cells (such as SKW3) with / without CD8 expression, or via anti-CD8 blocking antibody, to determine the associated CTL functions.

In addition, the fact that SB27 and CA5 TCRs both have minimal MHC contacts is intriguing. This observation makes it entirely possible that, from the structural and energetic perspectives, peptide-focused TCRs are more likely to cross-react with different HLA targets compare to the MHC-focused TCR such as the SB47. Whilst the impact of polymorphism has been examined using HLA-B*35:08/01 as an example, it might be important to address how other polymorphism, which differs at other HLA positions, impacts on TCR recognition as it might be potentially useful to stimulate a peptide-focused CTL response and thereby circumvent the complexity of MHC polymorphism when considering T-cell-based therapies.

Similarly, the allorecognition profiles observed in both SB27 and SB47 should be explored further. The fact that these two TCRs appear to focus on different features of the pHLA landscapes (peptide and the HLA respectively) raise an intriguing question whether T cell allorecognition is driven by the MHC-centric or peptide-centric view as previously proposed. This question cannot be addressed without identifying the self-antigen in the context of allogeneic MHC, which represents a longstanding challenge in the immunology field. However, recent innovations including the use of baculovirus display library to study allo-ligands (Macdonald et al., 2009), as well as mass spectrometry to study self-peptide repertoire (Illing et al., 2012), have provided different solutions to overcome this problem. These advancements would allow us not only to address how TCRs interact with foreign MHC landscapes (allorecognition) in the context of self-antigens, but also potentially enable us to visualize TCR recognition that are essential for the process of thymic selection. It will be interesting to compare, in terms of structures, what T cells are “educated” to see during the positive selection and what they actually recognise in the periphery as the positive selection has recently been shown to play a role in optimizing cognate recognition (Mandl et al., 2013). Moreover, it might be also important to compare these results with the negative selecting ligand to provide further insights into the maintenance of self-tolerance.

To further examine CTL responses towards lengthy antigens, the HPVG system can be further studied. For instance, in contrast to the HLA-B*35:01-HPVG restricted

TK3 CTL, HLA-B*35:08+ individuals use an alternative TCR, termed MB4 to recognise the HPV8 epitope, characterized by the TRBV9*01 gene usage similar to the TK3 TCR, along with an alternative TRAV29*01 (instead of TRAV20*01 in TK3) chain (Miles et al., 2005). It would be therefore valuable, given the differences between HLA-B*35:01-HPV8 and HLA-B*35:08-HPV8 that have been demonstrated, to investigate how buried polymorphism drives the selection of differing TCR repertoires. Furthermore, the specificity of the MB4 TCR can also be further examined as it has been shown that MB4 CTL was unable to respond to HLA-B*35:08-HPV8, contrasting to the weakly cross-reactive nature of the TK3 CTL (Miles et al., 2005). As such, it would be important to investigate the MB4 TCR both structurally and kinetically, in order to understand the contribution of the TRAV chain in contributing MHC restriction. Lastly, given the conserved TRBV9*01 chain that is used in both MB4 and TK3 TCR, the MB4 TCR-pHLA-I complex structure would also provide interesting insights to test if any germline-encoded TCR-MHC interaction is present, that is, conserved TRAV-HLA-B*35 interaction. This study would also address the impact of TCR pairing in editing the docking orientation as recently illustrated by the MHC-II restricted TCR system (Stadinski et al., 2011).

Moreover, as evidenced in the TK3 system, it might be also valuable to explore the binding degeneracy of the MB4 TCR in conferring protective immunity against some of the viral variants established. This will potentially provide alternative mechanisms into governing TCR cross-reactivity, given that MB4 prefers and rigid HPV8 HLA-B*35:08 instead of the flexible HPV8 presented by HLA-B*35:01. Last but not least, what is the underlying basis of the bias TRBV selection in both TK3 and MB4 system? And what governs the binding energetic for these two complexes? Is the concept of peptide-centricity still valid among these TCR-pHLA-I systems? To address these central immunological questions, alanine mutagenesis scanning approaches on the HLA or the TCR residues will certainly provide stimulating insights that further shape our understanding into TCR bias.

6.7 Conclusions

This thesis examines the structural mechanisms underpinning CTL responses towards lengthy EBV-pHLA-I complexes, and explores the simultaneous binding specificity and degeneracy of the respective TCRs. In this regards, results outlined here

described three distinct TCR solutions in response to structurally “featured” pHLA landscapes. Namely, both the SB27 and CA5 TCRs perched atop the rigid bulged antigen whilst making limited contacts with the HLA landscape. In contrast, the SB47 TCR was able to “bypass” the super-bulged antigen conformation via an extreme docking orientation that involves in novel TCR-MHC-I contacts. Lastly, the TK3 TCR that bound to HPVG variants has illustrated the role of antigen mobility in fine-tuning TCR recognition.

In addition, this thesis also explores the fundamental basis of MHC-restricted recognition for the respective TCR systems described. Specifically, the results revealed that buried micropolymorphisms between the MHC molecules, such as observed in HLA-B*35:01 and HLA-B*35:08, can impact either on the MHC landscape or altering the structural dynamic of the presented antigen. These differences, which are potentially “detectable” via the TCR structural footprint, finely impacts on the binding specificity / degeneracy of immuno-recognition. More interestingly, contrast to our current understanding of MHC restriction that focuses on conserved TCR-MHC contacts, either directly or in a pairwise manner, findings arising from this thesis have provided an alternative view that challenges some of these concepts. Instead, MHC restriction is governed by the ability to “see” differences in the pHLA landscape. This is evident in the SB27 and CA5 TCR that subtly discriminate HLA-B*35:01/08 yet struggle to contact the MHC surface, and further illustrated by the cross-reactive SB47 TCR that formed extensive MHC contact and bypassed key features between HLA-B*35:08/01.

In conclusion, findings arising from the thesis have provided significant insights into lengthy antigen detection by the cellular immune system, and address key questions how TCR maintain specificity and cross-reactivity simultaneously in responses to structurally challenging pHLA landscapes. Understanding the molecular basis of this process will certainly benefit as we constantly seek biomedical and therapeutic interventions towards the advancement of anti-viral and anti-cancer immunity as well as ways to alleviate unintended immunity such as allorecognition in organ transplantation.

7 References

- Acha-Orbea, H., Mitchell, D.J., Timmermann, L., Wraith, D.C., Tausch, G.S., Waldor, M.K., Zamvil, S.S., McDevitt, H.O., and Steinman, L. (1988). Limited heterogeneity of T cell receptors from lymphocytes mediating autoimmune encephalomyelitis allows specific immune intervention. *Cell* 54, 263-273.
- Adams, J.J., Narayanan, S., Liu, B., Birnbaum, M.E., Kruse, A.C., Bowerman, N.A., Chen, W., Levin, A.M., Connolly, J.M., Zhu, C., *et al.* (2011). T cell receptor signaling is limited by docking geometry to peptide-major histocompatibility complex. *Immunity* 35, 681-693.
- Adams, P.D., Grosse-Kunstleve, R.W., Hung, L.W., Ioerger, T.R., McCoy, A.J., Moriarty, N.W., Read, R.J., Sacchettini, J.C., Sauter, N.K., and Terwilliger, T.C. (2002). PHENIX: building new software for automated crystallographic structure determination. *Acta Crystallogr D Biol Crystallogr* 58, 1948-1954.
- Afzali, B., Lechler, R.I., and Hernandez-Fuentes, M.P. (2007). Allorecognition and the alloresponse: clinical implications. *Tissue Antigens* 69, 545-556.
- Al-Lazikani, B., Lesk, A.M., and Chothia, C. (2000). Canonical structures for the hypervariable regions of T cell alphabeta receptors. *J Mol Biol* 295, 979-995.
- Ambrus, M., Hernadi, E., and Bajtai, G. (1977). Prevalence of HLA-A1 and HLA-B8 antigens in selective IgA deficiency. *Clin Immunol Immunopathol* 7, 311-314.
- Androlewicz, M.J., and Cresswell, P. (1996). How selective is the transporter associated with antigen processing? *Immunity* 5, 1-5.
- Appay, V., and Rowland-Jones, S.L. (2004). Lessons from the study of T-cell differentiation in persistent human virus infection. *Semin Immunol* 16, 205-212.
- Archbold, J.K., Macdonald, W.A., Burrows, S.R., Rossjohn, J., and McCluskey, J. (2008). T-cell allorecognition: a case of mistaken identity or déjà vu? *Trends in immunology* 29, 220-226.
- Archbold, J.K., Macdonald, W.A., Gras, S., Ely, L.K., Miles, J.J., Bell, M.J., Brennan, R.M., Beddoe, T., Wilce, M.C., Clements, C.S., *et al.* (2009). Natural micropolymorphism in human leukocyte antigens provides a basis for genetic control of antigen recognition. *J Exp Med* 206, 209-219.
- Archbold, J.K., Macdonald, W.A., Miles, J.J., Brennan, R.M., Kjer-Nielsen, L., McCluskey, J., Burrows, S.R., and Rossjohn, J. (2006). Alloreactivity between disparate cognate and allogeneic pMHC-I complexes is the result of highly focused, peptide-dependent structural mimicry. *The Journal of biological chemistry* 281, 34324-34332.
- Argaet, V.P., Schmidt, C.W., Burrows, S.R., Silins, S.L., Kurilla, M.G., Doolan, D.L., Suhrbier, A., Moss, D.J., Kieff, E., Sculley, T.B., and Misko, I.S. (1994). Dominant selection of an invariant T cell antigen receptor in response to persistent infection by Epstein-Barr virus. *J Exp Med* 180, 2335-2340.
- Arstila, T.P., Casrouge, A., Baron, V., Even, J., Kanellopoulos, J., and Kourilsky, P. (1999). A direct estimate of the human alphabeta T cell receptor diversity. *Science* 286, 958-961.
- Babbe, H., Roers, A., Waisman, A., Lassmann, H., Goebels, N., Hohlfeld, R., Friese, M., Schroder, R., Deckert, M., Schmidt, S., *et al.* (2000). Clonal expansions of CD8(+) T cells dominate the T cell infiltrate in active multiple sclerosis lesions as shown by micromanipulation and single cell polymerase chain reaction. *J Exp Med* 192, 393-404.

- Bade-Doding, C., Theodossis, A., Gras, S., Kjer-Nielsen, L., Eiz-Vesper, B., Seltsam, A., Huyton, T., Rossjohn, J., McCluskey, J., and Blasczyk, R. (2011). The impact of human leukocyte antigen (HLA) micropolymorphism on ligand specificity within the HLA-B*41 allotypic family. *Haematologica* 96, 110-118.
- Baker, B.M., Turner, R.V., Gagnon, S.J., Wiley, D.C., and Biddison, W.E. (2001). Identification of a crucial energetic footprint on the alpha1 helix of human histocompatibility leukocyte antigen (HLA)-A2 that provides functional interactions for recognition by tax peptide/HLA-A2-specific T cell receptors. *J Exp Med* 193, 551-562.
- Baker, F.J., Lee, M., Chien, Y.H., and Davis, M.M. (2002). Restricted islet-cell reactive T cell repertoire of early pancreatic islet infiltrates in NOD mice. *Proc Natl Acad Sci U S A* 99, 9374-9379.
- Ballerini, C., Nacmias, B., Rombola, G., Marcon, G., Massacesi, L., and Sorbi, S. (1999). HLA A2 allele is associated with age at onset of Alzheimer's disease. *Ann Neurol* 45, 397-400.
- Bavan, M.J. (1984). High determinant density may explain the phenomenon of alloreactivity. *Trends in immunology* 5, 128-130.
- Beck, S., and Trowsdale, J. (2000). The human major histocompatibility complex: lessons from the DNA sequence. *Annu Rev Genomics Hum Genet* 1, 117-137.
- Bell, M.J., Brennan, R., Miles, J.J., Moss, D.J., Burrows, J.M., and Burrows, S.R. (2008). Widespread sequence variation in Epstein-Barr virus nuclear antigen 1 influences the antiviral T cell response. *J Infect Dis* 197, 1594-1597.
- Bentley, G.A., Boulot, G., Karjalainen, K., and Mariuzza, R.A. (1995). Crystal structure of the beta chain of a T cell antigen receptor. *Science* 267, 1984-1987.
- Birnbaum, M.E., Mendoza, J.L., Sethi, D.K., Dong, S., Glanville, J., Dobbins, J., Ozkan, E., Davis, M.M., Wucherpfennig, K.W., and Garcia, K.C. (2014). Deconstructing the peptide-MHC specificity of T cell recognition. *Cell* 157, 1073-1087.
- Bjorkman, P.J., Saper, M.A., Samraoui, B., Bennett, W.S., Strominger, J.L., and Wiley, D.C. (1987a). The foreign antigen binding site and T cell recognition regions of class I histocompatibility antigens. *Nature* 329, 512-518.
- Bjorkman, P.J., Saper, M.A., Samraoui, B., Bennett, W.S., Strominger, J.L., and Wiley, D.C. (1987b). Structure of the human class I histocompatibility antigen, HLA-A2. *Nature* 329, 506-512.
- Bjorkman, P.J., Strominger, J.L., and Wiley, D.C. (1985). Crystallization and X-ray diffraction studies on the histocompatibility antigens HLA-A2 and HLA-A28 from human cell membranes. *J Mol Biol* 186, 205-210.
- Blake, N., Lee, S., Redchenko, I., Thomas, W., Steven, N., Leese, A., Steigerwald-Mullen, P., Kurilla, M.G., Frappier, L., and Rickinson, A. (1997). Human CD8+ T cell responses to EBV EBNA1: HLA class I presentation of the (Gly-Ala)-containing protein requires exogenous processing. *Immunity* 7, 791-802.
- Blum, J.S., Wearsch, P.A., and Cresswell, P. (2013). Pathways of antigen processing. *Annu Rev Immunol* 31, 443-473.
- Boniface, J.J., Reich, Z., Lyons, D.S., and Davis, M.M. (1999). Thermodynamics of T cell receptor binding to peptide-MHC: evidence for a general mechanism of molecular scanning. *Proc Natl Acad Sci U S A* 96, 11446-11451.
- Borbulevych, O.Y., Insaiddo, F.K., Baxter, T.K., Powell, D.J., Jr., Johnson, L.A., Restifo, N.P., and Baker, B.M. (2007). Structures of MART-126/27-35 Peptide/HLA-A2 complexes reveal a remarkable disconnect between antigen structural homology and T cell recognition. *J Mol Biol* 372, 1123-1136.

- Borbulevych, O.Y., Piepenbrink, K.H., Gloor, B.E., Scott, D.R., Sommese, R.F., Cole, D.K., Sewell, A.K., and Baker, B.M. (2009). T cell receptor cross-reactivity directed by antigen-dependent tuning of peptide-MHC molecular flexibility. *Immunity* *31*, 885-896.
- Borbulevych, O.Y., Santhanagopalan, S.M., Hossain, M., and Baker, B.M. (2011). TCRs used in cancer gene therapy cross-react with MART-1/Melan-A tumor antigens via distinct mechanisms. *Journal of immunology* *187*, 2453-2463.
- Borg, N.A., Ely, L.K., Beddoe, T., Macdonald, W.A., Reid, H.H., Clements, C.S., Purcell, A.W., Kjer-Nielsen, L., Miles, J.J., Burrows, S.R., *et al.* (2005). The CDR3 regions of an immunodominant T cell receptor dictate the 'energetic landscape' of peptide-MHC recognition. *Nat Immunol* *6*, 171-180.
- Boulter, J.M., Glick, M., Todorov, P.T., Baston, E., Sami, M., Rizkallah, P., and Jakobsen, B.K. (2003). Stable, soluble T-cell receptor molecules for crystallization and therapeutics. *Protein Eng* *16*, 707-711.
- Brehm, M.A., Daniels, K.A., Priyadarshini, B., Thornley, T.B., Greiner, D.L., Rossini, A.A., and Welsh, R.M. (2010). Allografts stimulate cross-reactive virus-specific memory CD8 T cells with private specificity. *Am J Transplant* *10*, 1738-1748.
- Brennan, R.M., Petersen, J., Neller, M.A., Miles, J.J., Burrows, J.M., Smith, C., McCluskey, J., Khanna, R., Rossjohn, J., and Burrows, S.R. (2012). The impact of a large and frequent deletion in the human TCR beta locus on antiviral immunity. *Journal of immunology* *188*, 2742-2748.
- Breur-Vriesendorp, B.S., Dekker-Saeys, A.J., and Ivanyi, P. (1987). Distribution of HLA-B27 subtypes in patients with ankylosing spondylitis: the disease is associated with a common determinant of the various B27 molecules. *Ann Rheum Dis* *46*, 353-356.
- Bricogne G., B.E., Brandl M., Flensburg C., Keller P., Paciorek W., Roversi P, Sharff A., Smart O.S., Vonnrhein C., Womack T.O. (2011). BUSTER version 1.6.0. Global Phasing Ltd, Cambridge, United Kingdom.
- Brodsky, F.M., Bodmer, W.F., and Parham, P. (1979a). Characterization of a monoclonal anti-beta 2-microglobulin antibody and its use in the genetic and biochemical analysis of major histocompatibility antigens. *Eur J Immunol* *9*, 536-545.
- Brodsky, F.M., Parham, P., Barnstable, C.J., Crumpton, M.J., and Bodmer, W.F. (1979b). Monoclonal antibodies for analysis of the HLA system. *Immunol Rev* *47*, 3-61.
- Brusic, V., Petrovsky, N., Zhang, G., and Bajic, V.B. (2002). Prediction of promiscuous peptides that bind HLA class I molecules. *Immunol Cell Biol* *80*, 280-285.
- Bulek, A.M., Cole, D.K., Skowera, A., Dolton, G., Gras, S., Madura, F., Fuller, A., Miles, J.J., Gostick, E., Price, D.A., *et al.* (2012). Structural basis for the killing of human beta cells by CD8(+) T cells in type 1 diabetes. *Nat Immunol* *13*, 283-289.
- Burrows, S.R., Chen, Z., Archbold, J.K., Tynan, F.E., Beddoe, T., Kjer-Nielsen, L., Miles, J.J., Khanna, R., Moss, D.J., Liu, Y.C., *et al.* (2010). Hard wiring of T cell receptor specificity for the major histocompatibility complex is underpinned by TCR adaptability. *Proc Natl Acad Sci U S A* *107*, 10608-10613.
- Burrows, S.R., Rossjohn, J., and McCluskey, J. (2006). Have we cut ourselves too short in mapping CTL epitopes? *Trends in immunology* *27*, 11-16.
- Burrows, S.R., Silins, S.L., Cross, S.M., Peh, C.A., Rischmueller, M., Burrows, J.M., Elliott, S.L., and McCluskey, J. (1997). Human leukocyte antigen phenotype

- imposes complex constraints on the antigen-specific cytotoxic T lymphocyte repertoire. *Eur J Immunol* 27, 178-182.
- Burrows, S.R., Silins, S.L., Moss, D.J., Khanna, R., Misko, I.S., and Argat, V.P. (1995). T cell receptor repertoire for a viral epitope in humans is diversified by tolerance to a background major histocompatibility complex antigen. *J Exp Med* 182, 1703-1715.
- Buslepp, J., Wang, H., Biddison, W.E., Appella, E., and Collins, E.J. (2003). A correlation between TCR Valpha docking on MHC and CD8 dependence: implications for T cell selection. *Immunity* 19, 595-606.
- Cabaniols, J.P., Fazilleau, N., Casrouge, A., Kourilsky, P., and Kanellopoulos, J.M. (2001). Most alpha/beta T cell receptor diversity is due to terminal deoxynucleotidyl transferase. *J Exp Med* 194, 1385-1390.
- Callan, M.F., Annels, N., Steven, N., Tan, L., Wilson, J., McMichael, A.J., and Rickinson, A.B. (1998). T cell selection during the evolution of CD8+ T cell memory in vivo. *Eur J Immunol* 28, 4382-4390.
- Chen, J.L., Stewart-Jones, G., Bossi, G., Lissin, N.M., Wooldridge, L., Choi, E.M., Held, G., Dunbar, P.R., Esnouf, R.M., Sami, M., *et al.* (2005). Structural and kinetic basis for heightened immunogenicity of T cell vaccines. *J Exp Med* 201, 1243-1255.
- Chothia, C., Boswell, D.R., and Lesk, A.M. (1988). The outline structure of the T-cell alpha beta receptor. *EMBO J* 7, 3745-3755.
- Ciatto, C., Tissot, A.C., Tschopp, M., Capitani, G., Pecorari, F., Pluckthun, A., and Grutter, M.G. (2001). Zooming in on the hydrophobic ridge of H-2D(b): implications for the conformational variability of bound peptides. *J Mol Biol* 312, 1059-1071.
- Clements, C.S., Dunstone, M.A., Macdonald, W.A., McCluskey, J., and Rossjohn, J. (2006). Specificity on a knife-edge: the alphabeta T cell receptor. *Curr Opin Struct Biol* 16, 787-795.
- Cole, D.K., Yuan, F., Rizkallah, P.J., Miles, J.J., Gostick, E., Price, D.A., Gao, G.F., Jakobsen, B.K., and Sewell, A.K. (2009). Germ line-governed recognition of a cancer epitope by an immunodominant human T-cell receptor. *The Journal of biological chemistry* 284, 27281-27289.
- Colf, L.A., Bankovich, A.J., Hanick, N.A., Bowerman, N.A., Jones, L.L., Kranz, D.M., and Garcia, K.C. (2007). How a single T cell receptor recognizes both self and foreign MHC. *Cell* 129, 135-146.
- Combarros, O., Escribano, J., Sanchez-Velasco, P., Leyva-Cobian, F., Oterino, A., Leno, C., and Berciano, J. (1998). Association of the HLA-A2 allele with an earlier age of onset of Alzheimer's disease. *Acta Neurol Scand* 98, 140-141.
- Cresswell, P., Ackerman, A.L., Giodini, A., Peaper, D.R., and Wearsch, P.A. (2005). Mechanisms of MHC class I-restricted antigen processing and cross-presentation. *Immunol Rev* 207, 145-157.
- Dai, S., Huseby, E.S., Rubtsova, K., Scott-Browne, J., Crawford, F., Macdonald, W.A., Marrack, P., and Kappler, J.W. (2008). Crossreactive T Cells spotlight the germline rules for alphabeta T cell-receptor interactions with MHC molecules. *Immunity* 28, 324-334.
- Davis, M.M., and Bjorkman, P.J. (1988). T-cell antigen receptor genes and T-cell recognition. *Nature* 334, 395-402.
- Davis, M.M., Boniface, J.J., Reich, Z., Lyons, D., Hampl, J., Arden, B., and Chien, Y. (1998). Ligand recognition by alpha beta T cell receptors. *Annu Rev Immunol* 16, 523-544.

- Davis-Harrison, R.L., Insaïdoo, F.K., and Baker, B.M. (2007). T cell receptor binding transition states and recognition of peptide/MHC. *Biochemistry* 46, 1840-1850.
- Day, E.B., Guillonneau, C., Gras, S., La Gruta, N.L., Vignali, D.A., Doherty, P.C., Purcell, A.W., Rossjohn, J., and Turner, S.J. (2011). Structural basis for enabling T-cell receptor diversity within biased virus-specific CD8+ T-cell responses. *Proc Natl Acad Sci U S A* 108, 9536-9541.
- Degano, M., Garcia, K.C., Apostolopoulos, V., Rudolph, M.G., Teyton, L., and Wilson, I.A. (2000). A functional hot spot for antigen recognition in a superagonist TCR/MHC complex. *Immunity* 12, 251-261.
- Deng, L., and Mariuzza, R.A. (2007). Recognition of self-peptide-MHC complexes by autoimmune T-cell receptors. *Trends Biochem Sci* 32, 500-508.
- Diedrich, G., Bangia, N., Pan, M., and Cresswell, P. (2001). A role for calnexin in the assembly of the MHC class I loading complex in the endoplasmic reticulum. *Journal of immunology* 166, 1703-1709.
- Ding, Y.H., Baker, B.M., Garboczi, D.N., Biddison, W.E., and Wiley, D.C. (1999). Four A6-TCR/peptide/HLA-A2 structures that generate very different T cell signals are nearly identical. *Immunity* 11, 45-56.
- Ding, Y.H., Smith, K.J., Garboczi, D.N., Utz, U., Biddison, W.E., and Wiley, D.C. (1998). Two human T cell receptors bind in a similar diagonal mode to the HLA-A2/Tax peptide complex using different TCR amino acids. *Immunity* 8, 403-411.
- Doherty, P.C., and Zinkernagel, R.M. (1975). A biological role for the major histocompatibility antigens. *Lancet* 1, 1406-1409.
- Dolan, A., Addison, C., Gatherer, D., Davison, A.J., and McGeoch, D.J. (2006). The genome of Epstein-Barr virus type 2 strain AG876. *Virology* 350, 164-170.
- Dong, G., Wearsch, P.A., Peaper, D.R., Cresswell, P., and Reinisch, K.M. (2009). Insights into MHC class I peptide loading from the structure of the tapasin-ERp57 thiol oxidoreductase heterodimer. *Immunity* 30, 21-32.
- Elliott, T.J., and Eisen, H.N. (1990). Cytotoxic T lymphocytes recognize a reconstituted class I histocompatibility antigen (HLA-A2) as an allogeneic target molecule. *Proc Natl Acad Sci U S A* 87, 5213-5217.
- Ely, L.K., Beddoe, T., Clements, C.S., Matthews, J.M., Purcell, A.W., Kjer-Nielsen, L., McCluskey, J., and Rossjohn, J. (2006). Disparate thermodynamics governing T cell receptor-MHC-I interactions implicate extrinsic factors in guiding MHC restriction. *Proc Natl Acad Sci U S A* 103, 6641-6646.
- Ely, L.K., Burrows, S.R., Purcell, A.W., Rossjohn, J., and McCluskey, J. (2008). T-cells behaving badly: structural insights into alloreactivity and autoimmunity. *Curr Opin Immunol* 20, 575-580.
- Ely, L.K., Kjer-Nielsen, L., McCluskey, J., and Rossjohn, J. (2005). Structural studies on the alphabeta T-cell receptor. *IUBMB Life* 57, 575-582.
- Emsley, P., and Cowtan, K. (2004). Coot: model-building tools for molecular graphics. *Acta Crystallogr D Biol Crystallogr* 60, 2126-2132.
- Engelhard, V.H. (1994). Structure of peptides associated with class I and class II MHC molecules. *Annu Rev Immunol* 12, 181-207.
- Felix, N.J., Donermeyer, D.L., Horvath, S., Walters, J.J., Gross, M.L., Suri, A., and Allen, P.M. (2007). Alloreactive T cells respond specifically to multiple distinct peptide-MHC complexes. *Nat Immunol* 8, 388-397.
- Feng, D., Bond, C.J., Ely, L.K., Maynard, J., and Garcia, K.C. (2007). Structural evidence for a germline-encoded T cell receptor-major histocompatibility complex interaction 'codon'. *Nat Immunol* 8, 975-983.

- Fernandez-Sueiro, J.L., Alonso, C., Blanco, F.J., Rodriguez-Gomez, M., Galdo, F., and Gonzalez-Gay, M.A. (2004). Prevalence of HLA-B27 and subtypes of HLA-B27 associated with ankylosing spondylitis in Galicia, Spain. *Clin Exp Rheumatol* 22, 465-468.
- Fields, B.A., Ober, B., Malchiodi, E.L., Lebedeva, M.I., Braden, B.C., Ysern, X., Kim, J.K., Shao, X., Ward, E.S., and Mariuzza, R.A. (1995). Crystal structure of the V alpha domain of a T cell antigen receptor. *Science* 270, 1821-1824.
- Gagnon, S.J., Borbulevych, O.Y., Davis-Harrison, R.L., Turner, R.V., Damirjian, M., Wojnarowicz, A., Biddison, W.E., and Baker, B.M. (2006). T cell receptor recognition via cooperative conformational plasticity. *J Mol Biol* 363, 228-243.
- Garbi, N., Tan, P., Diehl, A.D., Chambers, B.J., Ljunggren, H.G., Momburg, F., and Hammerling, G.J. (2000). Impaired immune responses and altered peptide repertoire in tapasin-deficient mice. *Nat Immunol* 1, 234-238.
- Garboczi, D.N., Ghosh, P., Utz, U., Fan, Q.R., Biddison, W.E., and Wiley, D.C. (1996). Structure of the complex between human T-cell receptor, viral peptide and HLA-A2. *Nature* 384, 134-141.
- Garboczi, D.N., Hung, D.T., and Wiley, D.C. (1992). HLA-A2-peptide complexes: refolding and crystallization of molecules expressed in *Escherichia coli* and complexed with single antigenic peptides. *Proc Natl Acad Sci U S A* 89, 3429-3433.
- Garcia, K.C., Adams, J.J., Feng, D., and Ely, L.K. (2009). The molecular basis of TCR germline bias for MHC is surprisingly simple. *Nat Immunol* 10, 143-147.
- Garcia, K.C., Degano, M., Pease, L.R., Huang, M., Peterson, P.A., Teyton, L., and Wilson, I.A. (1998). Structural basis of plasticity in T cell receptor recognition of a self peptide-MHC antigen. *Science* 279, 1166-1172.
- Garcia, K.C., Degano, M., Stanfield, R.L., Brunmark, A., Jackson, M.R., Peterson, P.A., Teyton, L., and Wilson, I.A. (1996). An alphabeta T cell receptor structure at 2.5 Å and its orientation in the TCR-MHC complex. *Science* 274, 209-219.
- Garcia, K.C., Teyton, L., and Wilson, I.A. (1999). Structural basis of T cell recognition. *Annu Rev Immunol* 17, 369-397.
- Garrett, T.P., Saper, M.A., Bjorkman, P.J., Strominger, J.L., and Wiley, D.C. (1989). Specificity pockets for the side chains of peptide antigens in HLA-Aw68. *Nature* 342, 692-696.
- Gascoigne, N.R., Zal, T., and Alam, S.M. (2001). T-cell receptor binding kinetics in T-cell development and activation. *Expert Rev Mol Med* 2001, 1-17.
- Gillespie, G.M., Stewart-Jones, G., Rengasamy, J., Beattie, T., Bwayo, J.J., Plummer, F.A., Kaul, R., McMichael, A.J., Easterbrook, P., Dong, T., *et al.* (2006). Strong TCR conservation and altered T cell cross-reactivity characterize a B*57-restricted immune response in HIV-1 infection. *Journal of immunology* 177, 3893-3902.
- Godfrey, D.I., Rossjohn, J., and McCluskey, J. (2008). The fidelity, occasional promiscuity, and versatility of T cell receptor recognition. *Immunity* 28, 304-314.
- Gotch, F., Rothbard, J., Howland, K., Townsend, A., and McMichael, A. (1987). Cytotoxic T lymphocytes recognize a fragment of influenza virus matrix protein in association with HLA-A2. *Nature* 326, 881-882.
- Goulder, P.J., Phillips, R.E., Colbert, R.A., McAdam, S., Ogg, G., Nowak, M.A., Giangrande, P., Luzzi, G., Morgan, B., Edwards, A., *et al.* (1997). Late escape from an immunodominant cytotoxic T-lymphocyte response associated with progression to AIDS. *Nat Med* 3, 212-217.
- Gouveia, E.B., Elmann, D., and Morales, M.S. (2012). Ankylosing spondylitis and uveitis: overview. *Rev Bras Reumatol* 52, 742-756.

- Grakoui, A., Bromley, S.K., Sumen, C., Davis, M.M., Shaw, A.S., Allen, P.M., and Dustin, M.L. (1999). The immunological synapse: a molecular machine controlling T cell activation. *Science* 285, 221-227.
- Grande, A.G., 3rd, Golovina, T.N., Hamilton, S.E., Sriram, V., Spies, T., Brutkiewicz, R.R., Harty, J.T., Eisenlohr, L.C., and Van Kaer, L. (2000). Impaired assembly yet normal trafficking of MHC class I molecules in Tapasin mutant mice. *Immunity* 13, 213-222.
- Gras, S., Burrows, S.R., Kjer-Nielsen, L., Clements, C.S., Liu, Y.C., Sullivan, L.C., Bell, M.J., Brooks, A.G., Purcell, A.W., McCluskey, J., and Rossjohn, J. (2009a). The shaping of T cell receptor recognition by self-tolerance. *Immunity* 30, 193-203.
- Gras, S., Burrows, S.R., Turner, S.J., Sewell, A.K., McCluskey, J., and Rossjohn, J. (2012a). A structural voyage toward an understanding of the MHC-I-restricted immune response: lessons learned and much to be learned. *Immunol Rev* 250, 61-81.
- Gras, S., Chen, Z., Miles, J.J., Liu, Y.C., Bell, M.J., Sullivan, L.C., Kjer-Nielsen, L., Brennan, R.M., Burrows, J.M., Neller, M.A., *et al.* (2010). Allelic polymorphism in the T cell receptor and its impact on immune responses. *J Exp Med* 207, 1555-1567.
- Gras, S., Kjer-Nielsen, L., Chen, Z., Rossjohn, J., and McCluskey, J. (2011). The structural bases of direct T-cell allorecognition: implications for T-cell-mediated transplant rejection. *Immunol Cell Biol* 89, 388-395.
- Gras, S., Saulquin, X., Reiser, J.B., Debeauvais, E., Echasserieau, K., Kissenpfennig, A., Legoux, F., Chouquet, A., Le Gorrec, M., Machillot, P., *et al.* (2009b). Structural bases for the affinity-driven selection of a public TCR against a dominant human cytomegalovirus epitope. *Journal of immunology* 183, 430-437.
- Gras, S., Wilmann, P.G., Chen, Z., Halim, H., Liu, Y.C., Kjer-Nielsen, L., Purcell, A.W., Burrows, S.R., McCluskey, J., and Rossjohn, J. (2012b). A structural basis for varied alphabeta TCR usage against an immunodominant EBV antigen restricted to a HLA-B8 molecule. *Journal of immunology* 188, 311-321.
- Green, K.J., Miles, J.J., Tellam, J., van Zuylen, W.J., Connolly, G., and Burrows, S.R. (2004). Potent T cell response to a class I-binding 13-mer viral epitope and the influence of HLA micropolymorphism in controlling epitope length. *Eur J Immunol* 34, 2510-2519.
- Guan, P., Doytchinova, I.A., and Flower, D.R. (2003). HLA-A3 supermotif defined by quantitative structure-activity relationship analysis. *Protein Eng* 16, 11-18.
- Gunther, S., Schlundt, A., Sticht, J., Roske, Y., Heinemann, U., Wiesmuller, K.H., Jung, G., Falk, K., Rotzschke, O., and Freund, C. (2010). Bidirectional binding of invariant chain peptides to an MHC class II molecule. *Proc Natl Acad Sci U S A of the United States of America* 107, 22219-22224.
- Hahn, M., Nicholson, M.J., Pyrdol, J., and Wucherpfennig, K.W. (2005). Unconventional topology of self peptide-major histocompatibility complex binding by a human autoimmune T cell receptor. *Nat Immunol* 6, 490-496.
- Hausmann, S., Biddison, W.E., Smith, K.J., Ding, Y.H., Garboczi, D.N., Utz, U., Wiley, D.C., and Wucherpfennig, K.W. (1999). Peptide recognition by two HLA-A2/Tax11-19-specific T cell clones in relationship to their MHC/peptide/TCR crystal structures. *Journal of immunology* 162, 5389-5397.
- Hendel, H., Caillat-Zucman, S., Lebuane, H., Carrington, M., O'Brien, S., Andrieu, J.M., Schachter, F., Zagury, D., Rappaport, J., Winkler, C., *et al.* (1999). New class

- I and II HLA alleles strongly associated with opposite patterns of progression to AIDS. *Journal of immunology* *162*, 6942-6946.
- Hickman, H.D., Luis, A.D., Buchli, R., Few, S.R., Sathiamurthy, M., VanGundy, R.S., Giberson, C.F., and Hildebrand, W.H. (2004). Toward a definition of self: proteomic evaluation of the class I peptide repertoire. *Journal of immunology* *172*, 2944-2952.
- Hill, A.V., Elvin, J., Willis, A.C., Aidoo, M., Allsopp, C.E., Gotch, F.M., Gao, X.M., Takiguchi, M., Greenwood, B.M., Townsend, A.R., and et al. (1992). Molecular analysis of the association of HLA-B53 and resistance to severe malaria. *Nature* *360*, 434-439.
- Housset, D., Mazza, G., Gregoire, C., Piras, C., Malissen, B., and Fontecilla-Camps, J.C. (1997). The three-dimensional structure of a T-cell antigen receptor V alpha V beta heterodimer reveals a novel arrangement of the V beta domain. *The EMBO journal* *16*, 4205-4216.
- Howarth, M., Williams, A., Tolstrup, A.B., and Elliott, T. (2004). Tapasin enhances MHC class I peptide presentation according to peptide half-life. *Proc Natl Acad Sci U S A of the United States of America* *101*, 11737-11742.
- Huang, J., Zarnitsyna, V.I., Liu, B., Edwards, L.J., Jiang, N., Evavold, B.D., and Zhu, C. (2010). The kinetics of two-dimensional TCR and pMHC interactions determine T-cell responsiveness. *Nature* *464*, 932-936.
- Huppa, J.B., Axmann, M., Mortelmaier, M.A., Lillemeier, B.F., Newell, E.W., Brameshuber, M., Klein, L.O., Schutz, G.J., and Davis, M.M. (2010). TCR-peptide-MHC interactions in situ show accelerated kinetics and increased affinity. *Nature* *463*, 963-967.
- Illing, P.T., Vivian, J.P., Dudek, N.L., Kostenko, L., Chen, Z., Bharadwaj, M., Miles, J.J., Kjer-Nielsen, L., Gras, S., Williamson, N.A., et al. (2012). Immune self-reactivity triggered by drug-modified HLA-peptide repertoire. *Nature* *486*, 554-558.
- Ishizuka, J., Stewart-Jones, G.B., van der Merwe, A., Bell, J.I., McMichael, A.J., and Jones, E.Y. (2008). The structural dynamics and energetics of an immunodominant T cell receptor are programmed by its Vbeta domain. *Immunity* *28*, 171-182.
- Jones, L.L., Colf, L.A., Stone, J.D., Garcia, K.C., and Kranz, D.M. (2008). Distinct CDR3 conformations in TCRs determine the level of cross-reactivity for diverse antigens, but not the docking orientation. *Journal of immunology* *181*, 6255-6264.
- Jurcevic, S., Chandler, P., Sacks, S.H., and Simpson, E. (2001). Rapid rejection of HLA-A2 transgenic skin graft due to indirect allorecognition. *Transplantation* *72*, 994-997.
- Kabsch, W. (2010). Xds. *Acta Crystallogr D Biol Crystallogr* *66*, 125-132.
- Kaslow, R.A., Carrington, M., Apple, R., Park, L., Munoz, A., Saah, A.J., Goedert, J.J., Winkler, C., O'Brien, S.J., Rinaldo, C., et al. (1996). Influence of combinations of human major histocompatibility complex genes on the course of HIV-1 infection. *Nat Med* *2*, 405-411.
- Keever, C.A., Leong, N., Cunningham, I., Copelan, E.A., Avalos, B.R., Klein, J., Kapoor, N., Adams, P.W., Orosz, C.G., Tutschka, P.J., and et al. (1994). HLA-B44-directed cytotoxic T cells associated with acute graft-versus-host disease following unrelated bone marrow transplantation. *Bone Marrow Transplant* *14*, 137-145.
- Kjer-Nielsen, L., Clements, C.S., Brooks, A.G., Purcell, A.W., Fontes, M.R., McCluskey, J., and Rossjohn, J. (2002a). The structure of HLA-B8 complexed to

- an immunodominant viral determinant: peptide-induced conformational changes and a mode of MHC class I dimerization. *Journal of immunology* *169*, 5153-5160.
- Kjer-Nielsen, L., Clements, C.S., Brooks, A.G., Purcell, A.W., McCluskey, J., and Rossjohn, J. (2002b). The 1.5 Å crystal structure of a highly selected antiviral T cell receptor provides evidence for a structural basis of immunodominance. *Structure* *10*, 1521-1532.
- Kjer-Nielsen, L., Clements, C.S., Purcell, A.W., Brooks, A.G., Whisstock, J.C., Burrows, S.R., McCluskey, J., and Rossjohn, J. (2003). A structural basis for the selection of dominant alphabeta T cell receptors in antiviral immunity. *Immunity* *18*, 53-64.
- Koch, M., Camp, S., Collen, T., Avila, D., Salomonsen, J., Wallny, H.J., van Hateren, A., Hunt, L., Jacob, J.P., Johnston, F., *et al.* (2007). Structures of an MHC class I molecule from B21 chickens illustrate promiscuous peptide binding. *Immunity* *27*, 885-899.
- Krissinel, E., and Henrick, K. (2004). Secondary-structure matching (SSM), a new tool for fast protein structure alignment in three dimensions. *Acta Crystallogr D Biol Crystallogr* *60*, 2256-2268.
- Krogsgaard, M., and Davis, M.M. (2005). How T cells 'see' antigen. *Nat Immunol* *6*, 239-245.
- Krogsgaard, M., Prado, N., Adams, E.J., He, X.L., Chow, D.C., Wilson, D.B., Garcia, K.C., and Davis, M.M. (2003). Evidence that structural rearrangements and/or flexibility during TCR binding can contribute to T cell activation. *Mol Cell* *12*, 1367-1378.
- Ladell, K., Hashimoto, M., Iglesias, M.C., Wilmann, P.G., McLaren, J.E., Gras, S., Chikata, T., Kuse, N., Fastenackels, S., Gostick, E., *et al.* (2013). A molecular basis for the control of preimmune escape variants by HIV-specific CD8⁺ T cells. *Immunity* *38*, 425-436.
- Lancet, D., Parham, P., and Strominger, J.L. (1979). Heavy chain of HLA-A and HLA-B antigens is conformationally labile: a possible role for beta 2-microglobulin. *Proc Natl Acad Sci U S A of the United States of America* *76*, 3844-3848.
- Lawrence, M.C., and Colman, P.M. (1993). Shape complementarity at protein/protein interfaces. *J Mol Biol* *234*, 946-950.
- Lee, B., and Richards, F.M. (1971). The interpretation of protein structures: estimation of static accessibility. *J Mol Biol* *55*, 379-400.
- Lee, P.U., Churchill, H.R., Daniels, M., Jameson, S.C., and Kranz, D.M. (2000). Role of 2CT cell receptor residues in the binding of self- and allo-major histocompatibility complexes. *J Exp Med* *191*, 1355-1364.
- Lee, S.P., Brooks, J.M., Al-Jarrah, H., Thomas, W.A., Haigh, T.A., Taylor, G.S., Humme, S., Schepers, A., Hammerschmidt, W., Yates, J.L., *et al.* (2004). CD8 T cell recognition of endogenously expressed epstein-barr virus nuclear antigen 1. *J Exp Med* *199*, 1409-1420.
- Lefranc, M.P. (2011). IMGT, the International ImMunoGeneTics Information System. *Cold Spring Harb Protoc* *2011*, 595-603.
- Lehner, P.J., Wang, E.C., Moss, P.A., Williams, S., Platt, K., Friedman, S.M., Bell, J.I., and Borysiewicz, L.K. (1995). Human HLA-A0201-restricted cytotoxic T lymphocyte recognition of influenza A is dominated by T cells bearing the V beta 17 gene segment. *J Exp Med* *181*, 79-91.
- Li, L., and Bouvier, M. (2004). Structures of HLA-A*1101 complexed with immunodominant nonamer and decamer HIV-1 epitopes clearly reveal the

- presence of a middle, secondary anchor residue. *Journal of immunology* 172, 6175-6184.
- Li, Y., Huang, Y., Lue, J., Quandt, J.A., Martin, R., and Mariuzza, R.A. (2005). Structure of a human autoimmune TCR bound to a myelin basic protein self-peptide and a multiple sclerosis-associated MHC class II molecule. *EMBO J* 24, 2968-2979.
- Liu, Y.C., Chen, Z., Burrows, S.R., Purcell, A.W., McCluskey, J., Rossjohn, J., and Gras, S. (2012). The energetic basis underpinning T-cell receptor recognition of a super-bulged peptide bound to a major histocompatibility complex class I molecule. *The Journal of biological chemistry* 287, 12267-12276.
- Liu, Y.C., Chen, Z., Neller, M.A., Miles, J.J., Purcell, A.W., McCluskey, J., Burrows, S.R., Rossjohn, J., and Gras, S. (2014). A molecular basis for the interplay between T cells, viral mutants, and human leukocyte antigen micropolymorphism. *The Journal of biological chemistry* 289, 16688-16698.
- Liu, Y.C., Miles, J.J., Neller, M.A., Gostick, E., Price, D.A., Purcell, A.W., McCluskey, J., Burrows, S.R., Rossjohn, J., and Gras, S. (2013). Highly Divergent T-cell Receptor Binding Modes Underlie Specific Recognition of a Bulged Viral Peptide bound to a Human Leukocyte Antigen Class I Molecule. *The Journal of biological chemistry* 288, 15442-15454.
- Luz, J.G., Huang, M., Garcia, K.C., Rudolph, M.G., Apostolopoulos, V., Teyton, L., and Wilson, I.A. (2002). Structural comparison of allogeneic and syngeneic T cell receptor-peptide-major histocompatibility complex complexes: a buried alloreactive mutation subtly alters peptide presentation substantially increasing V(beta) Interactions. *J Exp Med* 195, 1175-1186.
- Macdonald, I.K., Harkiolaki, M., Hunt, L., Connelley, T., Carroll, A.V., MacHugh, N.D., Graham, S.P., Jones, E.Y., Morrison, W.I., Flower, D.R., and Ellis, S.A. (2010). MHC class I bound to an immunodominant *Theileria parva* epitope demonstrates unconventional presentation to T cell receptors. *PLoS Pathog* 6, e1001149.
- Macdonald, W.A., Chen, Z., Gras, S., Archbold, J.K., Tynan, F.E., Clements, C.S., Bharadwaj, M., Kjer-Nielsen, L., Saunders, P.M., Wilce, M.C., *et al.* (2009). T cell allorecognition via molecular mimicry. *Immunity* 31, 897-908.
- Madden, D.R., Garboczi, D.N., and Wiley, D.C. (1993). The antigenic identity of peptide-MHC complexes: a comparison of the conformations of five viral peptides presented by HLA-A2. *Cell* 75, 693-708.
- Madden, D.R., Gorga, J.C., Strominger, J.L., and Wiley, D.C. (1991). The structure of HLA-B27 reveals nonamer self-peptides bound in an extended conformation. *Nature* 353, 321-325.
- Madden, D.R., Gorga, J.C., Strominger, J.L., and Wiley, D.C. (1992). The three-dimensional structure of HLA-B27 at 2.1 Å resolution suggests a general mechanism for tight peptide binding to MHC. *Cell* 70, 1035-1048.
- Magierowska, M., Theodorou, I., Debre, P., Sanson, F., Autran, B., Riviere, Y., Charron, D., and Costagliola, D. (1999). Combined genotypes of CCR5, CCR2, SDF1, and HLA genes can predict the long-term nonprogressor status in human immunodeficiency virus-1-infected individuals. *Blood* 93, 936-941.
- Mandl, J.N., Monteiro, J.P., Vriskoop, N., and Germain, R.N. (2013). T cell-positive selection uses self-ligand binding strength to optimize repertoire recognition of foreign antigens. *Immunity* 38, 263-274.
- Manning, T.C., Schlueter, C.J., Brodnicki, T.C., Parke, E.A., Speir, J.A., Garcia, K.C., Teyton, L., Wilson, I.A., and Kranz, D.M. (1998). Alanine scanning

- mutagenesis of an alphabeta T cell receptor: mapping the energy of antigen recognition. *Immunity* 8, 413-425.
- Marrack, P., Scott-Browne, J.P., Dai, S., Gapin, L., and Kappler, J.W. (2008). Evolutionarily conserved amino acids that control TCR-MHC interaction. *Annu Rev Immunol* 26, 171-203.
- Matzinger, P., and Bevan, M.J. (1977). Hypothesis: why do so many lymphocytes respond to major histocompatibility antigens? *Cell Immunol* 29, 1-5.
- Mazza, C., Auphan-Anezin, N., Gregoire, C., Guimezanes, A., Kellenberger, C., Roussel, A., Kearney, A., van der Merwe, P.A., Schmitt-Verhulst, A.M., and Malissen, B. (2007). How much can a T-cell antigen receptor adapt to structurally distinct antigenic peptides? *EMBO J* 26, 1972-1983.
- McCoy, A.J., Grosse-Kunstleve, R.W., Adams, P.D., Winn, M.D., Storoni, L.C., and Read, R.J. (2007). Phaser crystallographic software. *J Appl Crystallogr* 40, 658-674.
- Miles, J.J., Borg, N.A., Brennan, R.M., Tynan, F.E., Kjer-Nielsen, L., Silins, S.L., Bell, M.J., Burrows, J.M., McCluskey, J., Rossjohn, J., and Burrows, S.R. (2006). TCR alpha genes direct MHC restriction in the potent human T cell response to a class I-bound viral epitope. *Journal of immunology* 177, 6804-6814.
- Miles, J.J., Bulek, A.M., Cole, D.K., Gostick, E., Schauenburg, A.J., Dolton, G., Venturi, V., Davenport, M.P., Tan, M.P., Burrows, S.R., *et al.* (2010). Genetic and structural basis for selection of a ubiquitous T cell receptor deployed in Epstein-Barr virus infection. *PLoS Pathog* 6, e1001198.
- Miles, J.J., Elhassen, D., Borg, N.A., Silins, S.L., Tynan, F.E., Burrows, J.M., Purcell, A.W., Kjer-Nielsen, L., Rossjohn, J., Burrows, S.R., and McCluskey, J. (2005). CTL recognition of a bulged viral peptide involves biased TCR selection. *Journal of immunology* 175, 3826-3834.
- Milik, M., Sauer, D., Brunmark, A.P., Yuan, L., Vitiello, A., Jackson, M.R., Peterson, P.A., Skolnick, J., and Glass, C.A. (1998). Application of an artificial neural network to predict specific class I MHC binding peptide sequences. *Nat Biotechnol* 16, 753-756.
- Mohammadi, J., Ramanujam, R., Jarefors, S., Rezaei, N., Aghamohammadi, A., Gregersen, P.K., and Hammarstrom, L. (2010). IgA deficiency and the MHC: assessment of relative risk and microheterogeneity within the HLA A1 B8, DR3 (8.1) haplotype. *J Clin Immunol* 30, 138-143.
- Momburg, F., Roelse, J., Hammerling, G.J., and Neefjes, J.J. (1994). Peptide size selection by the major histocompatibility complex-encoded peptide transporter. *J Exp Med* 179, 1613-1623.
- Monks, C.R., Freiberg, B.A., Kupfer, H., Sciaky, N., and Kupfer, A. (1998). Three-dimensional segregation of supramolecular activation clusters in T cells. *Nature* 395, 82-86.
- Morrison, J., Elvin, J., Latron, F., Gotch, F., Moots, R., Strominger, J.L., and McMichael, A. (1992). Identification of the nonamer peptide from influenza A matrix protein and the role of pockets of HLA-A2 in its recognition by cytotoxic T lymphocytes. *Eur J Immunol* 22, 903-907.
- Moss, P.A., Moots, R.J., Rosenberg, W.M., Rowland-Jones, S.J., Bodmer, H.C., McMichael, A.J., and Bell, J.I. (1991). Extensive conservation of alpha and beta chains of the human T-cell antigen receptor recognizing HLA-A2 and influenza A matrix peptide. *Proc Natl Acad Sci U S A* 88, 8987-8990.

- Mungall, A.J., Palmer, S.A., Sims, S.K., Edwards, C.A., Ashurst, J.L., Wilming, L., Jones, M.C., Horton, R., Hunt, S.E., Scott, C.E., *et al.* (2003). The DNA sequence and analysis of human chromosome 6. *Nature* *425*, 805-811.
- Munz, C., Holmes, N., King, A., Loke, Y.W., Colonna, M., Schild, H., and Rammensee, H.G. (1997). Human histocompatibility leukocyte antigen (HLA)-G molecules inhibit NKAT3 expressing natural killer cells. *J Exp Med* *185*, 385-391.
- Naeher, D., Daniels, M.A., Hausmann, B., Guillaume, P., Luescher, I., and Palmer, E. (2007). A constant affinity threshold for T cell tolerance. *J Exp Med* *204*, 2553-2559.
- Parham, P., Barnstable, C.J., and Bodmer, W.F. (1979a). Use of a monoclonal antibody (W6/32) in structural studies of HLA-A,B,C, antigens. *Journal of immunology* *123*, 342-349.
- Parham, P., and Ohta, T. (1996). Population biology of antigen presentation by MHC class I molecules. *Science* *272*, 67-74.
- Parham, P., Sehgal, P.K., and Brodsky, F.M. (1979b). Anti-HLA-A,B,C monoclonal antibodies with no alloantigenic specificity in humans define polymorphisms in other primate species. *Nature* *279*, 639-641.
- Payami, H., Schellenberg, G.D., Zarepari, S., Kaye, J., Sexton, G.J., Head, M.A., Matsuyama, S.S., Jarvik, L.F., Miller, B., McManus, D.Q., *et al.* (1997). Evidence for association of HLA-A2 allele with onset age of Alzheimer's disease. *Neurology* *49*, 512-518.
- Peh, C.A., Burrows, S.R., Barnden, M., Khanna, R., Cresswell, P., Moss, D.J., and McCluskey, J. (1998). HLA-B27-restricted antigen presentation in the absence of tapasin reveals polymorphism in mechanisms of HLA class I peptide loading. *Immunity* *8*, 531-542.
- Price, D.A., Brenchley, J.M., Ruff, L.E., Betts, M.R., Hill, B.J., Roederer, M., Koup, R.A., Migueles, S.A., Gostick, E., Wooldridge, L., *et al.* (2005). Avidity for antigen shapes clonal dominance in CD8+ T cell populations specific for persistent DNA viruses. *J Exp Med* *202*, 1349-1361.
- Price, D.A., West, S.M., Betts, M.R., Ruff, L.E., Brenchley, J.M., Ambrozak, D.R., Edghill-Smith, Y., Kuroda, M.J., Bogdan, D., Kunstman, K., *et al.* (2004). T cell receptor recognition motifs govern immune escape patterns in acute SIV infection. *Immunity* *21*, 793-803.
- Probst-Kepper, M., Hecht, H.J., Herrmann, H., Janke, V., Ocklenburg, F., Klempnauer, J., van den Eynde, B.J., and Weiss, S. (2004). Conformational restraints and flexibility of 14-meric peptides in complex with HLA-B*35:01. *Journal of immunology* *173*, 5610-5616.
- Purcell, A.W., McCluskey, J., and Rossjohn, J. (2007). More than one reason to rethink the use of peptides in vaccine design. *Nat Rev Drug Discov* *6*, 404-414.
- Rammensee, H.G., and Bevan, M.J. (1984). Evidence from in vitro studies that tolerance to self antigens is MHC-restricted. *Nature* *308*, 741-744.
- Reiser, J.B., Darnault, C., Gregoire, C., Mosser, T., Mazza, G., Kearney, A., van der Merwe, P.A., Fontecilla-Camps, J.C., Housset, D., and Malissen, B. (2003). CDR3 loop flexibility contributes to the degeneracy of TCR recognition. *Nat Immunol* *4*, 241-247.
- Reiser, J.B., Darnault, C., Guimezanes, A., Gregoire, C., Mosser, T., Schmitt-Verhulst, A.M., Fontecilla-Camps, J.C., Malissen, B., Housset, D., and Mazza, G. (2000). Crystal structure of a T cell receptor bound to an allogeneic MHC molecule. *Nat Immunol* *1*, 291-297.

- Reiser, J.B., Gregoire, C., Darnault, C., Mosser, T., Guimezanes, A., Schmitt-Verhulst, A.M., Fontecilla-Camps, J.C., Mazza, G., Malissen, B., and Housset, D. (2002). A T cell receptor CDR3beta loop undergoes conformational changes of unprecedented magnitude upon binding to a peptide/MHC class I complex. *Immunity* *16*, 345-354.
- Robinson, J., Halliwell, J.A., McWilliam, H., Lopez, R., Parham, P., and Marsh, S.G. (2013). The IMGT/HLA database. *Nucleic Acids Res* *41*, D1222-1227.
- Rodgers, J.R., and Cook, R.G. (2005). MHC class Ib molecules bridge innate and acquired immunity. *Nat Rev Immunol* *5*, 459-471.
- Rosenthal, A.S., and Shevach, E.M. (1973). Function of macrophages in antigen recognition by guinea pig T lymphocytes. I. Requirement for histocompatible macrophages and lymphocytes. *J Exp Med* *138*, 1194-1212.
- Rudolph, M.G., Stanfield, R.L., and Wilson, I.A. (2006). How TCRs bind MHCs, peptides, and coreceptors. *Annu Rev Immunol* *24*, 419-466.
- Rudolph, M.G., and Wilson, I.A. (2002). The specificity of TCR/pMHC interaction. *Curr Opin Immunol* *14*, 52-65.
- Sabatino, J.J., Jr., Huang, J., Zhu, C., and Evavold, B.D. (2011). High prevalence of low affinity peptide-MHC II tetramer-negative effectors during polyclonal CD4+ T cell responses. *J Exp Med* *208*, 81-90.
- Sadasivan, B., Lehner, P.J., Ortmann, B., Spies, T., and Cresswell, P. (1996). Roles for calreticulin and a novel glycoprotein, tapasin, in the interaction of MHC class I molecules with TAP. *Immunity* *5*, 103-114.
- Saper, M.A., Bjorkman, P.J., and Wiley, D.C. (1991). Refined structure of the human histocompatibility antigen HLA-A2 at 2.6 Å resolution. *J Mol Biol* *219*, 277-319.
- Saric, T., Chang, S.C., Hattori, A., York, I.A., Markant, S., Rock, K.L., Tsujimoto, M., and Goldberg, A.L. (2002). An IFN-gamma-induced aminopeptidase in the ER, ERAP1, trims precursors to MHC class I-presented peptides. *Nat Immunol* *3*, 1169-1176.
- Sayegh, M.H. (1999). Why do we reject a graft? Role of indirect allorecognition in graft rejection. *Kidney Int* *56*, 1967-1979.
- Schamel, W.W., and Reth, M. (2007). The TCR binding site does move. *Proc Natl Acad Sci U S A* *104*, 16398-16399.
- Sebzda, E., Mariathasan, S., Ohteki, T., Jones, R., Bachmann, M.F., and Ohashi, P.S. (1999). Selection of the T cell repertoire. *Annu Rev Immunol* *17*, 829-874.
- Serwold, T., Gonzalez, F., Kim, J., Jacob, R., and Shastri, N. (2002). ERAAP customizes peptides for MHC class I molecules in the endoplasmic reticulum. *Nature* *419*, 480-483.
- Sette, A., and Sidney, J. (1999). Nine major HLA class I supertypes account for the vast preponderance of HLA-A and -B polymorphism. *Immunogenetics* *50*, 201-212.
- Sha, W.C., Nelson, C.A., Newberry, R.D., Pullen, J.K., Pease, L.R., Russell, J.H., and Loh, D.Y. (1990). Positive selection of transgenic receptor-bearing thymocytes by Kb antigen is altered by Kb mutations that involve peptide binding. *Proc Natl Acad Sci U S A* *87*, 6186-6190.
- Sherman, L.A., and Chattopadhyay, S. (1993). The molecular basis of allorecognition. *Annu Rev Immunol* *11*, 385-402.
- Shimizu, A., Kawana-Tachikawa, A., Yamagata, A., Han, C., Zhu, D., Sato, Y., Nakamura, H., Koibuchi, T., Carlson, J., Martin, E., *et al.* (2013). Structure of TCR and antigen complexes at an immunodominant CTL epitope in HIV-1 infection. *Sci Rep* *3*, 3097.

- Sidney, J., Peters, B., Frahm, N., Brander, C., and Sette, A. (2008). HLA class I supertypes: a revised and updated classification. *BMC Immunol* 9, 1.
- Singh, H., and Raghava, G.P. (2001). ProPred: prediction of HLA-DR binding sites. *Bioinformatics* 17, 1236-1237.
- Smith, P.A., Brunmark, A., Jackson, M.R., and Potter, T.A. (1997). Peptide-independent recognition by alloreactive cytotoxic T lymphocytes (CTL). *J Exp Med* 185, 1023-1033.
- Snudden, D.K., Smith, P.R., Lai, D., Ng, M.H., and Griffin, B.E. (1995). Alterations in the structure of the EBV nuclear antigen, EBNA1, in epithelial cell tumours. *Oncogene* 10, 1545-1552.
- Speir, J.A., Stevens, J., Joly, E., Butcher, G.W., and Wilson, I.A. (2001). Two different, highly exposed, bulged structures for an unusually long peptide bound to rat MHC class I RT1-Aa. *Immunity* 14, 81-92.
- Stadinski, B.D., Trenh, P., Smith, R.L., Bautista, B., Huseby, P.G., Li, G., Stern, L.J., and Huseby, E.S. (2011). A role for differential variable gene pairing in creating T cell receptors specific for unique major histocompatibility ligands. *Immunity* 35, 694-704.
- Stevanovic, S. (2005). Antigen processing is predictable: From genes to T cell epitopes. *Transpl Immunol* 14, 171-174.
- Stewart-Jones, G.B., Gillespie, G., Overton, I.M., Kaul, R., Roche, P., McMichael, A.J., Rowland-Jones, S., and Jones, E.Y. (2005). Structures of three HIV-1 HLA-B*5703-peptide complexes and identification of related HLAs potentially associated with long-term nonprogression. *Journal of immunology* 175, 2459-2468.
- Stewart-Jones, G.B., McMichael, A.J., Bell, J.I., Stuart, D.I., and Jones, E.Y. (2003). A structural basis for immunodominant human T cell receptor recognition. *Nat Immunol* 4, 657-663.
- Stewart-Jones, G.B., Simpson, P., van der Merwe, P.A., Easterbrook, P., McMichael, A.J., Rowland-Jones, S.L., Jones, E.Y., and Gillespie, G.M. (2012). Structural features underlying T-cell receptor sensitivity to concealed MHC class I micropolymorphisms. *Proc Natl Acad Sci U S A of the United States of America* 109, E3483-3492.
- Strominger, J.L., Humphreys, R.E., McCune, J.M., Parham, P., Robb, R., Springer, T., and Terhorst, C. (1976). The immunoglobulin-like structure of human histocompatibility antigens. *Fed Proc* 35, 1177-1182.
- Strominger, J.L., Kabat, E.A., Bilofsky, H., Mann, D., Orr, H., Parham, P., Ploegh, H., Robb, R., Terhorst, C., and Wu, T.T. (1979). Structural and sequence homologies between HLA-A and HLA-B antigens and immunoglobulins. *Transplantation proceedings* 11, 1303.
- Sturniolo, T., Bono, E., Ding, J., Raddrizzani, L., Tuereci, O., Sahin, U., Braxenthaler, M., Gallazzi, F., Protti, M.P., Sinigaglia, F., and Hammer, J. (1999). Generation of tissue-specific and promiscuous HLA ligand databases using DNA microarrays and virtual HLA class II matrices. *Nat Biotechnol* 17, 555-561.
- Sullivan, L.C., Hoare, H.L., McCluskey, J., Rossjohn, J., and Brooks, A.G. (2006). A structural perspective on MHC class Ib molecules in adaptive immunity. *Trends in immunology* 27, 413-420.
- Tellam, J., Connolly, G., Green, K.J., Miles, J.J., Moss, D.J., Burrows, S.R., and Khanna, R. (2004). Endogenous presentation of CD8+ T cell epitopes from Epstein-Barr virus-encoded nuclear antigen 1. *J Exp Med* 199, 1421-1431.

- Theodossis, A., Guillonneau, C., Welland, A., Ely, L.K., Clements, C.S., Williamson, N.A., Webb, A.I., Wilce, J.A., Mulder, R.J., Dunstone, M.A., *et al.* (2010). Constraints within major histocompatibility complex class I restricted peptides: presentation and consequences for T-cell recognition. *Proc Natl Acad Sci U S A* *107*, 5534-5539.
- Tonegawa, S. (1983). Somatic generation of antibody diversity. *Nature* *302*, 575-581.
- Torres-Nagel, N., Deutschlander, A., Herrmann, T., Arden, B., and Hunig, T. (1997). Control of TCR V alpha-mediated positive repertoire selection and alloreactivity by differential J alpha usage and CDR3 alpha composition. *Int Immunol* *9*, 1441-1452.
- Trautmann, L., Rimbart, M., Echasserieau, K., Saulquin, X., Neveu, B., Dechanet, J., Cerundolo, V., and Bonneville, M. (2005). Selection of T cell clones expressing high-affinity public TCRs within Human cytomegalovirus-specific CD8 T cell responses. *Journal of immunology* *175*, 6123-6132.
- Turner, S.J., and Carbone, F.R. (1998). A dominant V beta bias in the CTL response after HSV-1 infection is determined by peptide residues predicted to also interact with the TCR beta-chain CDR3. *Molecular immunology* *35*, 307-316.
- Turner, S.J., Diaz, G., Cross, R., and Doherty, P.C. (2003). Analysis of clonotype distribution and persistence for an influenza virus-specific CD8+ T cell response. *Immunity* *18*, 549-559.
- Turner, S.J., Doherty, P.C., McCluskey, J., and Rossjohn, J. (2006). Structural determinants of T-cell receptor bias in immunity. *Nat Rev Immunol* *6*, 883-894.
- Tynan, F.E., Borg, N.A., Miles, J.J., Beddoe, T., El-Hassen, D., Silins, S.L., van Zuylen, W.J., Purcell, A.W., Kjer-Nielsen, L., McCluskey, J., *et al.* (2005a). High resolution structures of highly bulged viral epitopes bound to major histocompatibility complex class I. Implications for T-cell receptor engagement and T-cell immunodominance. *The Journal of biological chemistry* *280*, 23900-23909.
- Tynan, F.E., Burrows, S.R., Buckle, A.M., Clements, C.S., Borg, N.A., Miles, J.J., Beddoe, T., Whisstock, J.C., Wilce, M.C., Silins, S.L., *et al.* (2005b). T cell receptor recognition of a 'super-bulged' major histocompatibility complex class I-bound peptide. *Nat Immunol* *6*, 1114-1122.
- Tynan, F.E., Reid, H.H., Kjer-Nielsen, L., Miles, J.J., Wilce, M.C., Kostenko, L., Borg, N.A., Williamson, N.A., Beddoe, T., Purcell, A.W., *et al.* (2007). A T cell receptor flattens a bulged antigenic peptide presented by a major histocompatibility complex class I molecule. *Nat Immunol* *8*, 268-276.
- Viret, C., and Janeway, C.A., Jr. (1999). MHC and T cell development. *Rev Immunogenet* *1*, 91-104.
- Wang, W.Y., Chien, Y.C., Jan, J.S., Chueh, C.M., and Lin, J.C. (2002). Consistent sequence variation of Epstein-Barr virus nuclear antigen 1 in primary tumor and peripheral blood cells of patients with nasopharyngeal carcinoma. *Clin Cancer Res* *8*, 2586-2590.
- Watts, C. (1997). Capture and processing of exogenous antigens for presentation on MHC molecules. *Annu Rev Immunol* *15*, 821-850.
- Wearsch, P.A., and Cresswell, P. (2007). Selective loading of high-affinity peptides onto major histocompatibility complex class I molecules by the tapasin-ERp57 heterodimer. *Nat Immunol* *8*, 873-881.
- Wearsch, P.A., Peaper, D.R., and Cresswell, P. (2011). Essential glycan-dependent interactions optimize MHC class I peptide loading. *Proc Natl Acad Sci U S A of the United States of America* *108*, 4950-4955.

- Wenzel, T., Eckerskorn, C., Lottspeich, F., and Baumeister, W. (1994). Existence of a molecular ruler in proteasomes suggested by analysis of degradation products. *FEBS Lett* *349*, 205-209.
- Willcox, B.E., Gao, G.F., Wyer, J.R., Ladbury, J.E., Bell, J.I., Jakobsen, B.K., and van der Merwe, P.A. (1999). TCR binding to peptide-MHC stabilizes a flexible recognition interface. *Immunity* *10*, 357-365.
- Williams, A.P., Peh, C.A., Purcell, A.W., McCluskey, J., and Elliott, T. (2002). Optimization of the MHC class I peptide cargo is dependent on tapasin. *Immunity* *16*, 509-520.
- Winn, M.D., Ballard, C.C., Cowtan, K.D., Dodson, E.J., Emsley, P., Evans, P.R., Keegan, R.M., Krissinel, E.B., Leslie, A.G., McCoy, A., *et al.* (2011). Overview of the CCP4 suite and current developments. *Acta Crystallogr D Biol Crystallogr* *67*, 235-242.
- Wu, L.C., Tuot, D.S., Lyons, D.S., Garcia, K.C., and Davis, M.M. (2002). Two-step binding mechanism for T-cell receptor recognition of peptide MHC. *Nature* *418*, 552-556.
- Wu, Y., Gao, F., Liu, J., Qi, J., Gostick, E., Price, D.A., and Gao, G.F. (2011). Structural basis of diverse peptide accommodation by the rhesus macaque MHC class I molecule Mamu-B*17: insights into immune protection from simian immunodeficiency virus. *Journal of immunology* *187*, 6382-6392.
- Wynn, K.K., Fulton, Z., Cooper, L., Silins, S.L., Gras, S., Archbold, J.K., Tynan, F.E., Miles, J.J., McCluskey, J., Burrows, S.R., *et al.* (2008). Impact of clonal competition for peptide-MHC complexes on the CD8+ T-cell repertoire selection in a persistent viral infection. *Blood* *111*, 4283-4292.
- Yin, L., Huseby, E., Scott-Browne, J., Rubtsova, K., Pinilla, C., Crawford, F., Marrack, P., Dai, S., and Kappler, J.W. (2011). A single T cell receptor bound to major histocompatibility complex class I and class II glycoproteins reveals switchable TCR conformers. *Immunity* *35*, 23-33.
- York, I.A., and Rock, K.L. (1996). Antigen processing and presentation by the class I major histocompatibility complex. *Annu Rev Immunol* *14*, 369-396.
- Zarling, A.L., Luckey, C.J., Marto, J.A., White, F.M., Brame, C.J., Evans, A.M., Lehner, P.J., Cresswell, P., Shabanowitz, J., Hunt, D.F., and Engelhard, V.H. (2003). Tapasin is a facilitator, not an editor, of class I MHC peptide binding. *Journal of immunology* *171*, 5287-5295.
- Zhang, X.S., Wang, H.H., Hu, L.F., Li, A., Zhang, R.H., Mai, H.Q., Xia, J.C., Chen, L.Z., and Zeng, Y.X. (2004). V-val subtype of Epstein-Barr virus nuclear antigen 1 preferentially exists in biopsies of nasopharyngeal carcinoma. *Cancer Lett* *211*, 11-18.
- Zhu, C., Jiang, N., Huang, J., Zarnitsyna, V.I., and Evavold, B.D. (2013). Insights from in situ analysis of TCR-pMHC recognition: response of an interaction network. *Immunol Rev* *251*, 49-64.
- Zinkernagel, R.M., and Doherty, P.C. (1974). Restriction of in vitro T cell-mediated cytotoxicity in lymphocytic choriomeningitis within a syngeneic or semiallogeneic system. *Nature* *248*, 701-702.